COMPUTATIONAL MODELLING OF THE HUMAN MOTOR CONTROL SYSTEM

Nonlinear Enhancement of the Adaptive Model Theory through Simulation and Experiment

---

A thesis
submitted in partial fulfilment
of the requirements for the Degree
of
Doctor of Philosophy in Electrical and Electronic Engineering
in the
University of Canterbury

by

Paul R. Davidson B.E. (Hons)

University of Canterbury

2001

Contents

Abstract

Adaptive Model Theory (AMT) proposes that the brain forms and adaptively maintains inverse models of the world around it for adaptive feedforward control. This leading motor control theory unites principles of neurobiology, psychology and engineering. A modified version of AMT was developed with the capacity to control nonlinear systems, to predict signals with nonlinear statistical characteristics, and to perform simultaneous feedback and feedforward adaptive control. The modified version is called *nonlinear Adaptive Model Theory* or *nAMT*. An experimental study was also performed investigating inverse model formation in the human motor control system, the results of which were then compared with the nAMT model.

A nonlinear dynamic system identification method was developed for nAMT to replace the linear structures employed by AMT. This method employs a neurobiologically-inspired locally-recurrent neural-network structure. A multi-layer adaptation algorithm was also developed specifically for this structure. Nonlinear Auto-Regressive Moving-Average (NARMA) adaptive predictor structures replace the linear Moving Average (MA) predictor circuits used in AMT. Adaptive feedback control is augmented using a nonlinear dynamic forward model observer to improve the quality of the estimated response signal. Nonlinear dynamic inverse models are formed by placing the forward model in an internal feedback loop in which the gain function is adjusted to maintain stability.

The internal inverse model motor-control hypothesis was tested experimentally in a study looking at human open-loop performance in a tracking task. The study was aimed at directly demonstrating the formation of an internal inverse model of a novel visuomotor relationship for feedforward control in the brain. The study involved 20 normal adult subjects who performed a pursuit random tracking task with a steering wheel for input. During learning the response cursor was periodically blanked, removing all feedback about the external system (i.e., about the relationship between hand motion and response cursor motion). Results showed a transfer of learning from the unblanked runs to the blanked runs for a static nonlinear system (14% median improvement between first 4 and last 4 runs, $p = .001$) thereby demonstrating adaptive feedforward control in the nervous system. No such transfer was observed for a dynamic linear system, indicating a dominant adaptive feedback control component. The observed open-loop responses showed a high-pass frequency response which could not be explained using traditional control-systems motor control models.

Experimental results were compared with simulated results from the nAMT model. Results from the experimental study were used to verify and tune the computational model. The resulting simulations produced effects that mirrored the closed- and open-loop characteristics of the experimental response trajectories. This supports the claim that an internal feedback loop is used for the inversion of external systems in the human brain. Other control-systems models (both AMT and feedback-error learning) would require substantial ad hoc modification to reproduce the observed disparity between closed- and open-loop results. In contrast, nAMT naturally reproduced the effect as a consequence of its novel nonlinear inversion method. In nAMT an inverse model is formed by embedding a forward model in an internal feedback loop incorporating a low derivative gain. The derivative loop-gain caused the inverse model to be relatively inaccurate at low frequencies, for which the feedback control loop was adequate, but to be increasingly accurate at higher frequencies. Maintenance of the loop-gain at the lowest possible levels maximizes the internal stability of the inverse. The simulation work confirmed that the nAMT model is capable of reproducing human behaviour under a wide range of conditions.

Preface

This PhD research project has benefited from contributions from many individuals and organizations. In particular, the research was conducted at the Departments of Electrical and Electronic Engineering at the University of Canterbury, Medical Physics and Bioengineering at Christchurch Hospital and Systems and Control at the University of New South Wales, all of which have contributed immeasurably to the project.

Since this project began in 1998 I have been fortunate to be under the excellent supervision of Dr Richard Jones, Assoc. Prof Harsha Sirisena and Dr John Andreae. I would like to thank Richard for his constant dedication, encouragement and enthusiasm over the last three years, Harsha for his valuable insight and John for his guidance and tireless input to the project. My work has benefited enormously from their contributions. I would also like to thank everyone else who has contributed more indirectly over the past three years. Your assistance and support was equally valuable.

During my research I was fortunate to spend time working with Peter and Megan Neilson in the Neuroengineering Research Group in the Department of Systems and Control at the University of New South Wales. Peter Neilson was the originator of the Adaptive Model Theory, the human motor control model on which this research is based. This visit was an invaluable experience, broadening my understanding not only of AMT but of the wider implications of the human motor control field.

The computational simulation work described in this thesis was conducted using the Matlab® Simulink package. Standard AMT code, written in Basic in the 1980s and generously donated by Peter Neilson, was re-implemented in Matlab early in the project. Dr Neilson also provided optimum trajectory generation (OTG) code which aided in the initial implementation of the AMT model. All subsequent developments were written employing a combination of Simulink s-functions and blocks. C++ code was also utilized where necessary. This provided a flexible development environment in which a broad range of solutions could be tested quickly.

During my research I presented several academic papers, at both local and international conferences. In October 1999 I attended the First Joint Meeting of the Biomedical Engineering and IEEE Engineering in Medicine and Biology Societies in Atlanta, Georgia. At this meeting I presented two posters, both of which were well received.

This research project has produced the following publications :

Davidson, P. R., Jones, R. D., Andreae, J. H., & Sirisena, H. R. (submitted). Computational modeling of the human motor system: The nonlinear Adaptive Model Theory (nAMT). *IEEE Transactions on Biomedical Engineering.*

Davidson, P. R., Jones, R. D., Andreae, J. H., & Sirisena, H. R. (submitted). Simulating closed- and open-loop voluntary movement with nAMT. IEEE Transactions on Biomedical Engineering.

Davidson, P. R., Jones, R. D., Sirisena, H. R., & Andreae, J. H. (2001). Evidence for the formation of inverse motor models in the brain. International Journal of Neuroscience, 109, 221.

Davidson, P. R., Jones, R. D., Sirisena, H. R., & Andreae, J. H. (2000). Detection of adaptive inverse models in the human motor system. Human Movement Science, 19, 761-795.

Davidson, P. R., Jones, R. D., Sirisena, H. R., & Andreae, J. H. (2000). Understanding the role of sensory feedback in the human motor control system. Proceedings of the Christchurch Medical Research Society.

Davidson, P. R., Jones, R. D., Sirisena, H. R., Andreae, J. H., & Neilson, P. D. (1999). *Evaluation of a nonlinear generalization of the adaptive model theory.* Proceedings of the First Joint Meeting of the BMES/EMBS, Atlanta, GA, *1*, 392.

Davidson, P. R., Jones, R. D., Sirisena, H. R., Andreae, J. H., & Neilson, P. D. (1999). *A neurobiologically motivated generalization of the adaptive model theory of human voluntary movement to the control of nonlinear systems.* Proceedings of the First Joint Meeting of the BMES/EMBS, Atlanta, *1*, 535.

Davidson, P. R., Jones, R. D., Sirisena, H. R., Andreae, J. H., Neilson, P. D., & Donaldson, I. M. (1998). *Nonlinear inverse control applied to the adaptive model theory of human purposive movement.* Proceedings of the Annual Meeting of the Australasian College of Physical Scientists and Engineers in Medicine, Christchurch, *1*, 12-13.

I also wish to gratefully acknowledge the financial support I have received for this project. The University of Canterbury awarded me the *Keith Laugeson Memorial Scholarship* and the *William Georgetti Scholarship* for PhD research in 1998. The New Zealand Vice-Chancellors' Committee awarded me the *Shirtcliffe Fellowship* in 1998 and the *R.H.T. Bates Scholarship* in 1999, part of which was used for conference travel. In 1999 the Canterbury Medical Research Foundation awarded me a *Travel-Grant-In-Aid* for conference travel to the United States.

List of Symbols

Target	$T(t)$
Predicted Target	$\hat{T}(t)$
Response	$R(t)$
Desired Response	$R^*(t)$
Predicted Response	$\hat{R}(t)$
Motor Response	$MR(t)$
Disturbance	$D(t)$
Exafference	$D'(t)$
Predicted Exafference (Disturbance)	$\hat{D}(t)$
Controlled System (Plant)	P
Forward Model (Input-Output)	$\hat{P}$
Forward Model (Observer)	$\overline{P}$
Efferent Delay (s)	α
Afferent Delay (s)	β
Total Transmission Time	$\Delta t \quad (\Delta t = \alpha + \beta)$
Planning Time (s)	tp
Planned Movement Duration (s)	td
Internal Feedback Loop Gain	K
Adaptation Coefficient	μ

1. Introduction

The scientific field of human motor control aims to demystify the processes underlying the remarkable ability of humans and other primates to make accurate, coordinated, goal-directed limb movements with grace and apparent ease. The field of study traverses a variety of disciplines including anatomy, physiology, psychology engineering, neurology and even philosophy. The first systematic efforts in the area took place in the early 19th century and work has continued, with increasing momentum, to the present day.

Contemporary approaches to the study of human movement vary widely across the field. The neurophysiological approach is based on the study of actual electrical signals in the brain and the peripheral nervous system. This work has yielded information about the location and representation of certain signals in the brain and has provided a framework for understanding the general function of various regions of the nervous system. Unfortunately, neurophysiology has revealed little about the computational processes underlying the control of movement. The psychophysical approach operates at a higher level, studying the characteristics of actual body movements. To date the psychophysical approach has proved more useful in understanding the computational operations occurring in the motor control regions of the brain. Tracking tasks have provided a useful psychophysical insight into human movement, though many other techniques have been used (Laszlo, 1992). Much of the modern groundwork in this area was laid during and immediately after World War II, when identifying individuals skilled at sensory-motor tasks took on unprecedented importance (Schmidt, 1982). It was also during the war that the systems engineering approach was first applied to human motor control, particularly in relation to tracking tasks (Neilson et al., 1995).

More recently, serious attempts have been made to integrate the neurophysiological and psychophysical approaches by seeking direct neurophysiological support for psychophysical models (Shadmehr et al., 1997; Smith et al., 2000; Thoroughman et al., 1999). The work presented in this thesis takes a psychophysical approach to the study of human movement, though the underlying theory is also amenable to neurophysiological analysis. We attempt to uncover the underlying computational processes involved in human voluntary movement and make extensive use of tracking tasks for theoretical validation.

In the following pages an information processing model of the human movement control system based on the linear Adaptive Model Theory, or AMT (Neilson et al., 1988a, 1992, 1995, 1997), is developed and evaluated. AMT is a leading motor control

model which unifies psychological observations, neurophysiological data and a systems engineering approach into a single conceptual framework. The applicability of the current version of AMT is limited by the simplifying assumption that the human body and the external systems it controls are linear dynamic systems (see section 1.3.3.3).

A variant of AMT has been constructed which is capable of operating in a realistic nonlinear dynamical environment while maintaining a high degree of neurobiological plausibility. This new variant is referred to as nonlinear adaptive model theory, or nAMT. A computational implementation of nAMT was constructed and assessed against normal human performance by direct comparison with experimental data from nonlinear dynamical tracking tasks.

1.1 The Motor Control Problem

Paradoxically, our familiarity with human movement hides its intrinsic complexity. Whenever a human moves, the nervous system must perform an extremely complex and computationally intensive task. Simply stated, the task is to transform the desired trajectory, or goal, of a multijoint movement into an appropriate set of neural commands to the muscles. This is an extremely complex problem – approximately 5,000,000 fibres descend from the brain to innervate the muscles of the body and all of these need to be activated appropriately (Neilson et al., 1992).

The problem is ill-posed as it has no unique solution due to the hugely excessive number of degrees of freedom under control (i.e., there are an infinite number of ways to perform the same movement, see section 1.1.1). A suitable multi-dimensional movement trajectory therefore needs to be to generated in real time. Enormous numbers of variables need to be considered in generating this movement accurately, as do interactions between these variables. Several multi-dimensional coordinate systems and frames of reference are involved and must be considered. The properties of the controlled system (or plant), the human body, are extremely complex and any external loads and disturbances encountered while moving must be accounted for. Forward and reactive dynamics, including Coriolis forces, must also be considered and the muscles themselves have variable nonlinear properties (see section 1.3.3.3). In addition, sensory signals are known to be noisy and propagate slowly leading to long transport delays. The computational demands of generating appropriate motor commands are, therefore, truly enormous. Despite this, animals of all kinds solve the problem with apparent ease.

1.1.1 Redundancy

It is possible to perform most physical tasks in an infinite number of ways. While this is often useful, as it allows for the selection of the best path from a variety of options (e.g., for obstacle avoidance), it poses difficulties for motor control theorists.

The number of degrees of freedom in a system is defined as the number of dimensions that can be independently varied within that system. There are 100-150 degrees of freedom in the human body (Neilson et al., 1995). Since there are usually many more degrees of freedom involved in a movement than in the target trajectory, the problem of picking a particular path is mathematically underdetermined – that is, there are an infinite number of paths available from which to choose. This path selection dilemma is referred to as the *degrees of freedom (DOF) problem* (Bernstein, 1967).

The issue of redundancy extends beyond the mechanical DOF problem. Redundancy is distributed throughout the motor system. About 5,000,000 descending fibres project from the brain stem to around 150,000 motor neurons which control about 700 muscles which in turn control 100-150 biomechanical degrees of freedom (Neilson, 1993). These 100-150 DOF are often called upon to affect the control of an object in 3-dimensional space. Overall, the redundancy in the system is a daunting problem.

Before looking at specific hypotheses on how the human motor system solves the motor control problem, an overview of the neurophysiology known to be involved in the process is provided.

1.2 Neurophysiology and Neuroanatomy of the Human Motor System

The human central nervous system (CNS) is organized in a hierarchy descending from the motor areas of the cerebral cortex down to the brain stem and finally to the spinal cord. The CNS does not function as a rigid hierarchy, rather there is a complex system of feedback connections between all levels. Here we look at the anatomy and physiology of the regions of the human CNS thought to be primarily involved in motor control.

1.2.1 Sensory Systems

Sensory information from the environment is acquired though receptors at the periphery of the CNS (Kandel et al., 1991). These receptors are the sole sources of information for the system. They are stimulated by limited spectra of a variety of forms of energy (light, sound, chemicals) and encode the stimuli into pulses of electricity for transmission into and processing by the CNS. Ascending sensory signals pass through the thalamus, a structure in the diencephalon above the brain stem (see Fig. 1), before being relayed to the cerebral cortex. All sensory pathways except the olfactory tracts have direct projections to the thalamus which plays an important role in sensory processing. It is thought that sensory information is transformed in the thalamus into a form suitable for processing in the cerebral cortex .

Different sensory modalities are projected from the thalamus to specific regions of the cerebral cortex. The primary visual cortex is located at the posterior of the cerebral cortex in the occipital lobe, the auditory cortex is located in the superior temporal gyrus and the somatic sensory cortex is located in postcentral gyrus in the parietal lobe. In processing the afferent sensory information from its receptors, the sensory system provides the CNS with an internal representation of the environment (of which it is, itself, a part). This internal representation is used to guide motor behaviour. It is important to note that most of the information used in the control of movement is never consciously perceived.

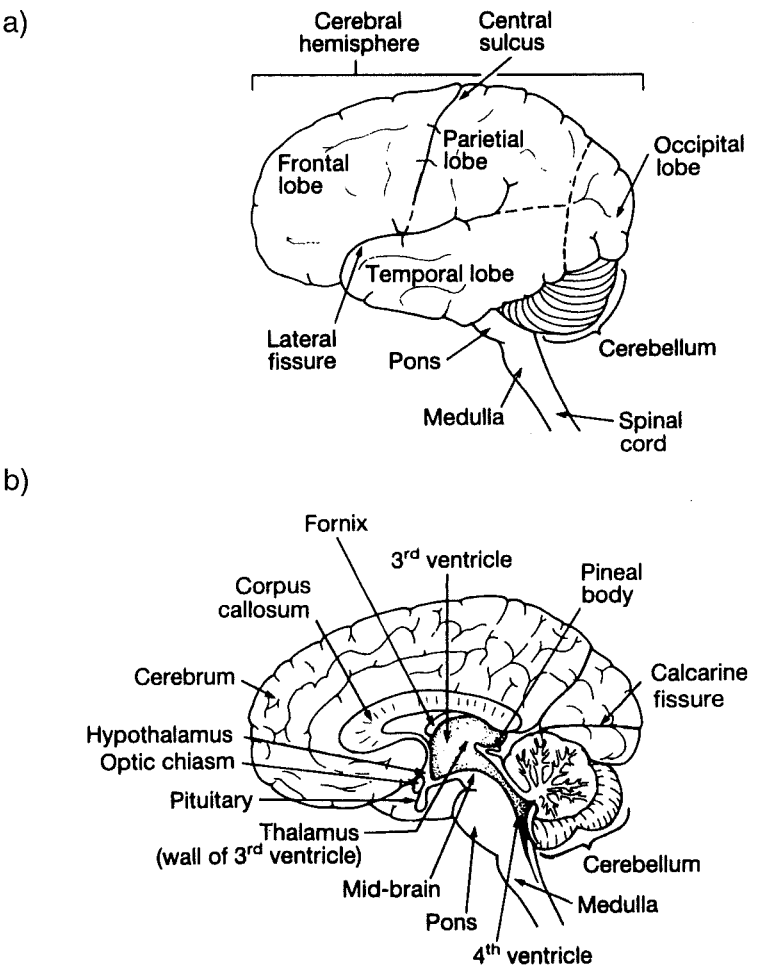

Fig. 1. Anatomical regions of the brain a) lateral view of the left hemisphere, b) medial view of the right hemisphere (Bray et al., 1989).

1.2.2 Motor Regions of the Cerebral Cortex

The regions responsible for high level motor control lie at the top of the cerebral cortex in the vicinity of the central sulcus (see Fig. 2). This region is divided into the motor cortex, the premotor cortex and the supplementary motor area.

1.2.2.1 Motor Cortex

The precentral gyrus is termed the motor cortex. This is thought to be the area most immediately involved in the generation of movement. Electrical stimulation of small areas on the surface of the motor cortex elicits movements in specific parts of the body. This somatotopic representation arises because each region of the motor cortex is connected with motor neurons via the corticofugal tracts (Bray et al., 1989). The motor cortex is thought to encode direction and the amount of force exerted (Cooper et al., 1989).

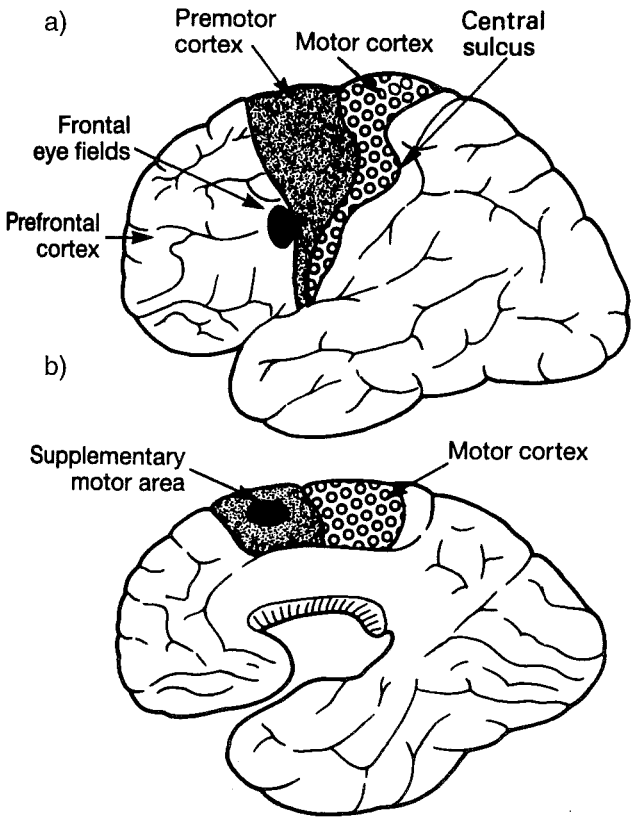

Fig. 2. Motor areas of the brain. a) Lateral view of the left cerebral hemisphere. b) medial view of the surface of the right cerebral hemisphere (Bray et al., 1989).

1.2.2.2 Premotor Cortex

In front of (rostral to) the motor cortex is the premotor cortex. When this region is stimulated in a monkey the animal turns its head and eyes as though it is looking in a particular direction. It is thought that this area organises the sensory guidance of limb movements.

1.2.2.3 Supplementary Motor Area

The supplementary motor area (SMA) is a small region on the medial surface of each hemisphere. Stimulation elicits complex and synergistic movements, often with vocalisation. It is thought that SMA is involved in movement planning and coordination

of bilateral and sequential movements. Hence, the SMA provides relatively high level guidance for the motor system.

1.2.3 The Cerebellum

The cerebellum is a large organ that lies behind the brain stem (see Fig. 1). It contains the most dense concentration of neurons in the nervous system, comprising around 70 billion neurons, or over half the neurons of the brain (Lange, 1975). The cerebellum exhibits a remarkably regular, almost crystalline organisation repeated across the entire cerebellar cortex (Ghez, 1991; Paulin, 1993). Consequently, it is one of the best understood structures in the brain. The organ is thought to play a crucial role in movement and posture by modulating the major descending motor outputs of the brain.

The cerebellum receives input from the motor regions of the cortex. This afferent information is usually interpreted as the plans for movement and is termed corollary discharge. The structure also receives information on motor performance in the form of sensory feedback from the periphery (reafference). The comparison of corollary discharge with reafference enables the cerebellum to correct ongoing movements as they happen.

1.2.3.1 Structure

The cerebellum can be partitioned into three functional divisions (see Fig. 3), each having different connections and phylogenetic origins (Kandel et al., 2000). The vestibulocerebellum governs eye movements and body equilibrium while standing or moving. The spinocerebellum takes most of its input from the spinal column and its outputs return to the descending motor systems. This region is thought to play an important low-level role in the control of limb movement. The cerebrocerebellum (also called the neocerebellum) is phylogenetically the newest region of the cerebellum. Its primary input is from the cerebral cortex through the pontine nuclei and its output is passed to the motor and premotor cortices. The cerebrocerebellum is thus thought to be involved in higher level planning and initiation of movement.

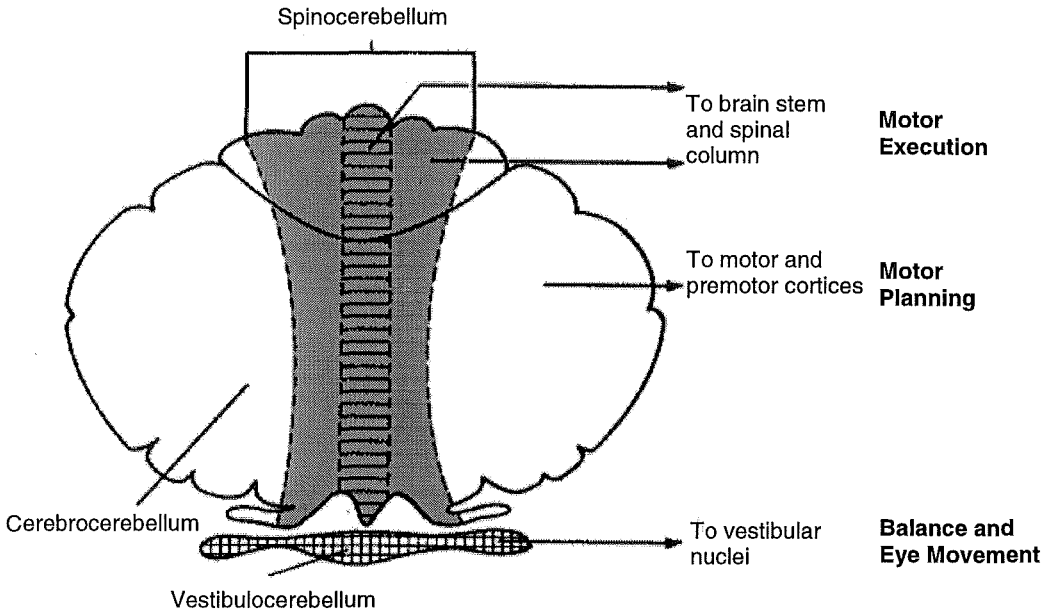

Fig. 3. Functional sections of the cerebellum (Kandel et al., 1991).

The outermost surface of the cerebellum is called the cerebellar cortex. It is simple and uniform in structure and contains five types of neurons: stellate, basket, Purkinje, Golgi and granule cells (which are by far the most numerous). The cerebellar cortex is organized into layers (see Fig. 4).

The outermost layer, called the molecular layer, contains billions of parallel fibres which are the axons of the granule cells. The next layer is the Purkinje cell layer which contains Purkinje cell bodies. These send their dendrites up to synapse with the parallel fibres. The Purkinje cells form the output of the cerebellum, sending their axons down into the underlying white matter. Finally, the granular layer contains enormous numbers of densely packed granule cells.

The input to the cerebellar cortex arises from mossy and climbing fibres. The mossy fibres are the most numerous and these terminate on granule cells, hence indirectly influencing Purkinje cells via parallel fibres arising from the granule cells. The climbing fibre inputs synapse directly on Purkinje cells. Each Purkinje cell receives connections from a single climbing fibre. Stellate and basket cells, located in the molecular layer, tend to synapse perpendicular to the parallel fibres and hence spread the influence of the mossy cells wider across the surface. Golgi cells receive input from the parallel fibres and project to granule cells.

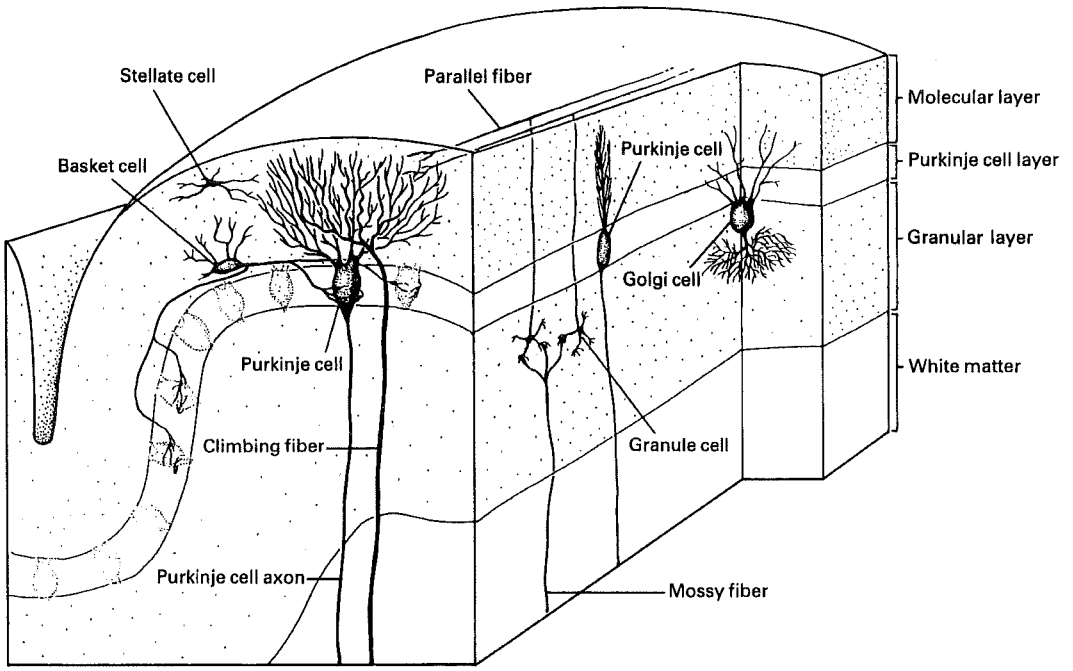

Fig. 4. Structure of the cerebellar cortex (Kandel et al., 1991).

1.2.3.2 Marr-Albus Model

The Marr-Albus model of the cerebellum (Albus, 1979; Marr, 1969) proposed that the climbing fibre input changes the effectiveness of the mossy fibre synapses to Purkinje cells. Hence, the climbing fibres modulate the action of the mossy fibres. This was suggested as the learning mechanism by which the cerebellum achieves motor adaptation The Marr-Albus model was later developed into an adaptive filter model of the cerebellum (Fujita, 1982) which was successfully used to simulate adaptive modification of the vestibulo-ocular reflex. A nonlinear function approximation network model of the cerebellum, the Cerebellar Model Articulation Controller (CMAC) (Albus, 1975), has also been proposed.

1.2.4 Basal Ganglia

The basal ganglia (BG) are a group of nuclei at the base of the brain which are involved in the control of movement. The central nuclei of the BG include the globus pallidus, the putamen, the caudate and subthalamic nuclei and the substantia nigra. The striatum is considered to be the input to the basal ganglia (comprising the putamen and caudate nucleus). The main outputs are the internal segment of the globus pallidus and the substantia nigra (see Fig. 5).

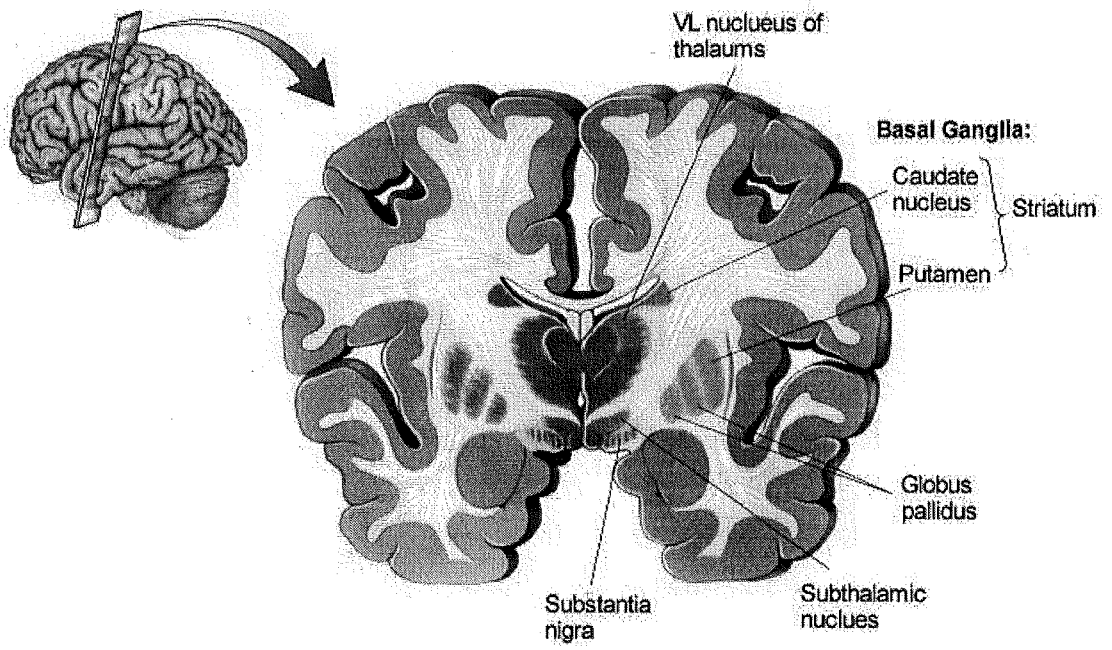

Fig. 5. Section showing the basal ganglia (Bear et al., 1996).

The nuclei of the basal ganglia are richly interconnected and extremely complex. An important internal pathway is the nigrostriatal pathway from the substantia nigra to the striatum. This pathway is dopaminergic and is associated with Parkinson's disease. Complex models of the internal connections of the basal ganglia exist (Parent et al., 1998) but the details are of little concern here. The nature of the afferent and efferent connections of the structure are of more importance.

The striatum receives inputs from the entire neocortex (frontal, parietal, occipital and temporal lobes), the thalamus (intralaminar nuclei) and the substantia nigra. The convergence of information from the entire cortex to the striatum suggests a role for the basal ganglia in the evaluation of contextual information for generating appropriate motor responses.

The globus pallidus and substantia nigra both project to the ventralateral nuclei of the thalamus and from there to the premotor cortex and the prefrontal association cortex. These form by far the most important outflow of the basal ganglia (Ghez, 1991). Projections also exist to the pedunculopontine nucleus (a structure in the midbrain which controls walking) and the superior colliculus (a structure important in the generation of saccadic eye movements).

Importantly, the basal ganglia do not have direct afferent or efferent connections with the spinal cord suggesting a higher, regulatory role for the structure in the control of movement.

1.2.4.1 Function

There is an enormous body of research on the anatomy, physiology and neurochemistry of the BG but little consensus exists as to the exact function of the structure in motor control. The connections of the BG suggest they are involved with high level motor planning, motor sequencing, motor learning and voluntary movements (Graybiel et al., 1994).

Diseases of the BG, such as Parkinson's disease and Huntington's disease, produce involuntary movements (from oscillatory resting tremors and writhing movements through to violent flailing movements), slowness of movement and disorders of muscle tone (rigidity). BG damage also leads to slowness in the initiation and alteration of movement (bradykinesia) (Ghez, 1991).

Recently the BG have been implicated strongly in error correction (Brainard et al., 2000; Lawrence, 2000; Smith et al., 2000). Computational modelling of the BG emphasizes the importance of reinforcement learning and suggests a role in the selection of motor programs (Gillies et al., 2000).

1.2.5 Information Flow in the Motor System

The systems we have looked at are linked together into a vastly complex network of neurons. It is possible to build up a picture of the primary information flows involved in motor control by looking at the direction and type of these major connections between the primary regions. Fig. 6 is a simplified representation of the brain's motor circuits. The diagram illustrates the loops from the cortex through the cerebellum and basal ganglia and the primary flow of motor information from the motor cortex to the spinal column. Note that this diagram does not show the thalamus through which many of the internal signals flow.

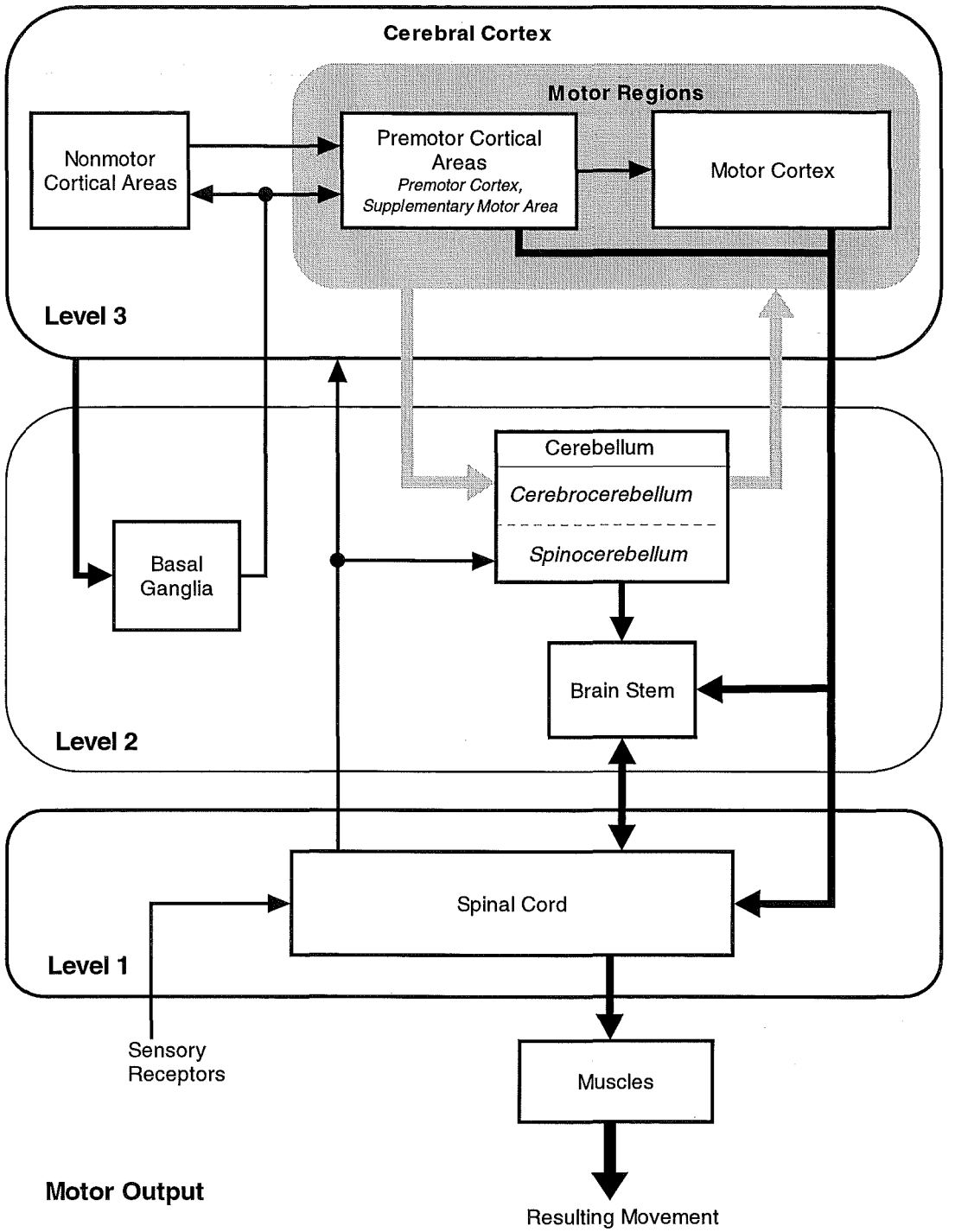

Fig. 6. Information flow diagram for the major motor regions of the brain. The diagram is organized in a hierarchy. The thalamus, through which many signals pass, is not shown in the diagram for clarity.

1.3 Motor Control Hypotheses

In attempting to explain the ability of humans to solve the motor control problem a wide range of approaches have been proposed. The earliest work in the psychological

branch of the field was not aimed specifically at understanding motor behaviour, rather motor behaviour was used as a "window to the mind", assisting research into higher processes such as learning and memory. Later, emphasis shifted toward the understanding of motor behaviour itself. Early work on the neural basis of motor behaviour led to some major discoveries, such as the importance of the cerebellum, but true progress in the field only began when psychologists started to propose motor models.

1.3.1 Foundations of the Field

Coherent scientific hypotheses as to the nature of human movement control did not emerge until an understanding of the fundamental role of the brain and peripheral nervous system were established. Much of this work occurred in the late 18th and early 19th centuries.

Arguably the most important early discovery in neurobiology was that of Luigi Galvani who in 1791 published his work *De Viribus Electricitatis in Motu Musculari Commentarius* (Commentary on the Effect of Electricity on Muscular Motion) on the electrical stimulation of frog nerves (Finger, 2000). This work established that the nervous system employs electricity in its operation and heralded the end of the pre-scientific idea that Cartesian "animal spirits" controlled the human body.

The French physiologist Marie-Jean-Pierre Flourens was the first, in 1823, to recognize that the cerebellum is an essential organ for the generation of movement (Encyclopaedia Britannica inc., 1990). This was based on ablation studies in which he removed the cerebella of pigeons. Cerebellar ablation destroyed the animal's muscular coordination.

When Fritsch and Hitzig (1870) discovered the motor cortex of a dog using electrical stimulation, a wave of interest in the role of the brain in eliciting movement was unleashed. Following this discovery the function of the important motor regions of the brain were revealed. In 1875 Sir David Ferrier described different parts of monkey motor cortex in his hugely influential book *The Functions of the Brain* (1876; cited in Finger, 2000).

The earliest formal theory of motor control was probably that of James (1891), called the *response-chaining hypothesis.* James proposed that an external stimulus sets off the first in a chain of movements. The proprioceptive feedback produced by the initial movement is then used as the stimulus for the selection of the next movement, and so on. This response-chaining theory does not require cognitive attention since once a course of action has been decided the entire chain can be executed without intervention. This mode of motor control is called open-loop, or feedforward, operation (see section 1.3.2.4).

Sir Charles Sherrington was undoubtedly one of the most important early contributors to the field of motor control. Sherrington studied reflexive responses to

stimuli presented at the extremities. He postulated that voluntary movements result from the reflexes he observed, an early motor model. Sherrington originated the concept of the final common path, which refers to the integration of commands from various sources (including the brain and reflexes) at the spinal level (Sherrington, 1906). Sherrington is also notable for describing the synapse and the motor cortex.

1.3.2 History of Information Processing Models

It was Craik (1948) who first proposed that we should look at the brain as a type of computer which processes sensory information as input and executes movements as output. In support of this idea was the observation that humans seem to respond to stimuli in discrete bursts rather than in a smooth continuous way as was previously assumed.

1.3.2.1 Intermittency and the Psychological Refractory Period

This "bursty processing" phenomenon was termed the central intermittency of the nervous system. Evidence for central intermittency derives primarily from classic double stimulation reaction time experiments performed by experimental psychologists (McClelland, 1979; Pashler, 1984; Vince, 1948; Welford, 1952, 1959). These experimentalists observed a delay in the response to the second of two stimuli spaced closely in time which they termed the *psychological refractory period.*

The notion of intermittency led to Welford's (1952) proposition of the *single-channel hypothesis*, which accounts for the psychological refractory period. Welford initially postulated that the brain was an information processing system structured as a single channel, which led to bottlenecks as the processing load increased.

The advent of the information processing approach implied a transition from task orientation to process orientation in movement control (Schmidt, 1982). The process-oriented approach grew rapidly in popularity (Pew, 1970, 1974) and was accelerated more recently by developments in digital computing and adaptive control. Information processing models have been the dominant paradigm in motor control theory since the 1970s (Abernathy et al., 1992). The computer metaphor has allowed information processing concepts from engineering, and particularly control systems, to find a natural place in human movement science. While the approach is popular it is important to note that other quite different approaches have been suggested (see section 1.3.6 on dynamical action theory).

1.3.2.2 Model Structure

Information processing models are usually hierarchical, possessing a number of distinct layers of control, with information generally flowing from the higher (cognitive) layers to the lower (motor output) layers. The lower the level in the hierarchy, the less attention is required by higher brain centres thus freeing these for other tasks (Schmidt,

1982). Response ordering and selection occupy a relatively high level in the hierarchy, while motor execution occupies a lower level. There is a great deal of evidence to suggest that a hierarchy is useful for the understanding of motor control (Rosenbaum, 1991)[1]. This general structure is similar to observations made about the physiological structure of the central nervous system (see section 1.2).

In information processing models the cognitive levels are typically considered to determine a desired motor trajectory R* which is then realized in some fashion by the motor apparatus and converted into an actual motor response trajectory R (see Fig. 7). The task of the motor system is therefore to generate the most appropriate set of nervous signals given a desired movement trajectory and the current sensory feedback (see section 1.1).

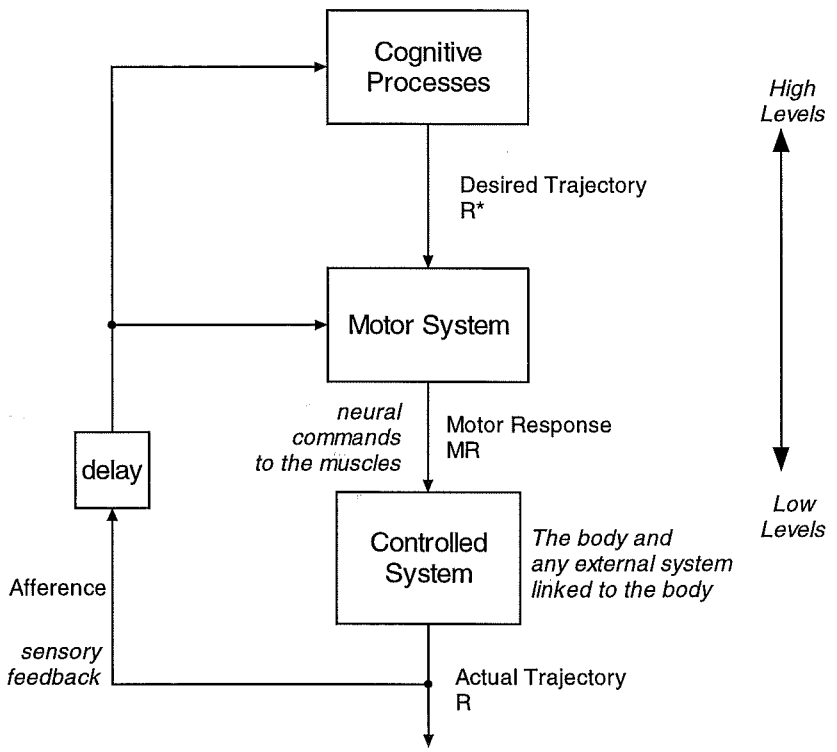

Fig. 7. Simplified hierarchy in a typical information processing model.

1.3.2.3 Closed-loop Control - Adams' Theory

In a closed-loop (or feedback) control system sensory feedback is used directly to guide the control of a task. Adams (1971) suggested that human motor control proceeded through perceptual-motor feedback loops which minimize the error between a desired condition (the *perceptual trace*) and the actual response. Adams' closed-loop theory was very useful for explaining certain aspects of human motor behaviour, particularly

[1] It should be kept in mind that the motor control hierarchy is simply a conceptual model introduced to assist understanding of information flow in the nervous system. The brain itself is unlikely to exhibit this rigidity of structure.

those involving slow movements, and it became the dominant paradigm in motor control in the early seventies.

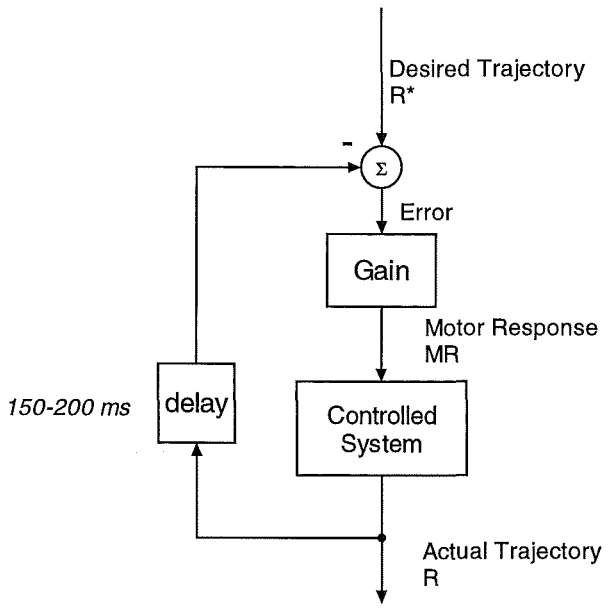

Fig. 8. Closed-loop (feedback) motor model

The theory eventually lost favour as the function of sensory feedback (afference) in the motor system was reassessed. It was realized that visual feedback on arm movements takes 150 – 200 ms to return to the brain (Kawato, 1999) which is a large delay compared with the duration of very fast (or ballistic) movements. Some movements can occur in as little as 150 ms. Deafferentation studies, where sensory feedback is deliberately prevented from reaching the CNS, also impacted the closed-loop model. In 1917 Lashley worked with a patient deprived of sensory afference after a gunshot wound to the spinal cord (Lashley, 1917). The patient was able to produce skilled movement in the absence of any sensory feedback. These observations and more rigorous experiments, like Taub's deafferented monkeys (Taub, 1976), eventually toppled the closed-loop theory as it could not adequately account for skilled movement in the absence of feedback. Adams' closed-loop theory and others like it have more recently been superseded by open-loop and hybrid theories.

1.3.2.4 Open-loop control - Motor Programs

An open-loop, or feedforward, motor control system performs its task without direct reference to sensory feedback (see Fig. 9). The open-loop control hypothesis is one of the most persistent concepts in motor control. James (1891) and Lashley (1917) both thought of ballistic movements as involving pre-planned commands with out any modulation by feedback. In the late 1960s and early 1970s the closed-loop model of Adams gained popularity as the pre-eminent paradigm. The theory was eventually toppled when the open-loop paradigm re-emerged in the form of the motor program (which was first proposed in Keele et al., 1968).

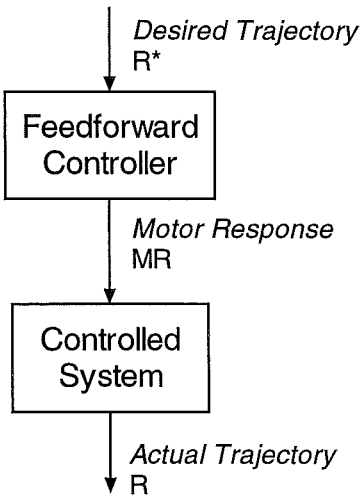

Fig. 9. Open-loop (feedforward) motor model

Keele suggested that movements are stored as a sequence of motor instructions, a "motor program", which is carried out by a central executive in response to appropriate stimuli (Keele et al., 1968). This idea overcomes the difficulties encountered by closed-loop theories in explaining skilled movement in the absence of feedback (see section 1.3.2.3).

Initially it was thought that a motor program needs to be extremely complex, as it seemed that each program must specify a complete "set of muscle commands, structured before the movement begins" (Keele et al., 1968). It has been estimated that at least 100,000 motor programs, specifying a full set of efferent muscle commands would need to be stored in long-term memory to specify speech alone (MacNeilage, 1970). This was identified as the primary difficulty with the motor program concept and is referred to as the *storage problem* (Schmidt, 1982).

This problem was addressed by the concept of the "generalized motor program" wherein one program is stored for each broad kind of motion. The program is then tuned by altering parameters to produce the observable variety of human movements. The generalized motor program concept certainly alleviates the storage problem but some questions remain. Given that 100-150 biomechanical degrees of freedom need to be controlled by the output of approximately 5,000,000 descending motor fibres (Neilson et al., 1992) and the enormous variety of movements that are under control in the human system, even a generalized motor program would require very large amounts of data storage capacity. This is referred to as the *degrees of freedom (DOF) problem* (see section 1.1.1).

1.3.2.5 Reconciliation

In the 1970s a debate raged between adherents of closed- and open-loop models of the human motor system, the centralist vs. peripheralist debate. The debate was eventually settled when it was realized that both modes of control were necessary and

could be combined in a single control scheme (Neilson et al., 1992). Most recent models include both feedback and feedforward control elements.

Motor program theory achieved wide acceptance as the mechanism for feedforward control in the motor system in the 1980s, leading Alexander et al. (1992) to comment: "Over the past two decades the idea that movements are controlled by motor programs has become so popular that the view is now inherent, in one form or another, in the vast majority of contemporary theories of motor control". The concept of the motor program has been refined in the 1990s with more sophisticated combined feedforward and feedback adaptive control schemes based on modern theories of adaptive control and bio-mechanics.

There are currently two major feedforward control schemes in the literature, the equilibrium-point control hypothesis and the inverse dynamics model hypothesis (Wolpert et al., 1998).

1.3.3 Inverse Dynamics Model Hypothesis

The idea that we might store an updateable internal model of the outside world was first suggested in the literature as early as Craik (1943). In the context of motor control, internal models might be used to overcome long transmission delays and implement an accurate feedforward control scheme. Internal models effectively specify an efficient means of building a generalized motor program.

1.3.3.1 Forward Models

Forward models predict sensory consequences from efference copies of outgoing motor commands. As such, a forward model essentially mimics the behaviour of the controlled system. A forward model of the human motor system would take the efferent motor command signals as input and produce an estimate of the sensory consequences of the resulting movement trajectory as output (see Fig. 10). Ito (1970) was the first to propose that the cerebellum contains forward models of the limbs that are used for adaptive feedback control.

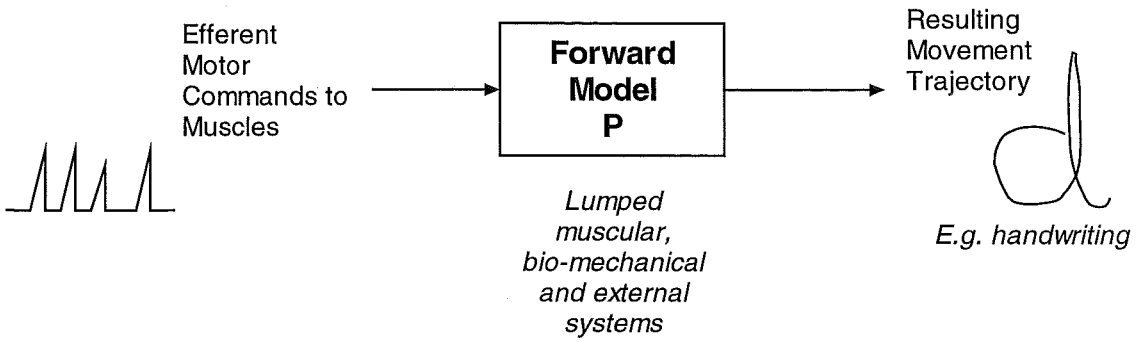

Fig. 10. A forward model of the motor system takes nervous commands, generated as inputs to the muscles and converts these to movements of the overall biomechanical system.

1.3.3.2 Inverse Models

The problem of generating an appropriate set of outgoing motor commands is greatly simplified if the forward model is inverted so that a desired trajectory (coded in terms of sensory consequences) is applied as input, and the required motor commands simply appear as output. This results in an inverse model.

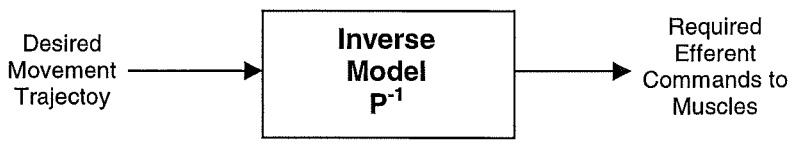

Fig. 11. An inverse model can be used to simplify the generation of motor commands.

The concept that we might store an internal inverse model is linked with advances in control systems engineering. Kawato et al. (1987) used an inverse kinematics model for robot control, with some success. In an inverse kinematics model a desired trajectory is converted into a time varying set of joint angles. An inverse dynamics model goes further; here the trajectory is converted directly into a set of time varying forces (or, equivalently, muscle input signals) to be applied to produce the required joint angles. Neilson et al. (1988b) proposed the storage of an inverse dynamics model for efficient motor control.

The task of finding the inverse model is termed the *inverse dynamics problem.* The nervous system implicitly finds a solution to this complex problem whenever a coordinated movement is produced. The mechanism by which this is achieved in the brain is a major area of research and is investigated in this thesis.

1.3.3.3 Nonlinear and Dynamic Systems

Forward and inverse models of the human motor apparatus are complex multiple input-multiple-output systems. A system may also be classified as static or dynamic depending on how its outputs depend on the temporal history of its inputs. The output of a static system depends only on the present value of the inputs, while the output of a dynamic system depends on both its present and past inputs. Most biological systems, particularly the musculoskeletal system, are highly dynamic.

Systems can also be classified as linear or nonlinear. The outputs of a linear system are directly proportional to its inputs. Linear systems are, therefore, easy to model and manipulate mathematically. Nonlinear systems do not exhibit this property. One of the results of this is that for nonlinear systems the well known mathematical principle of superposition does not apply. This makes nonlinear systems considerably more difficult to deal with mathematically.

It is worth remembering that all real world systems are nonlinear, to some degree. Linearity, when it is applied, is always a convenient approximation. The validity of the approximation varies between systems. Unfortunately, the systems involved in the human motor control system are highly nonlinear (Kawato et al., 1992) so that an assumption of linearity would be invalid.

In summary the forward and, therefore, the inverse models proposed in the internal model hypothesis must be both nonlinear and dynamic multiple-input multiple-output systems.

1.3.3.4 Motion Planning

Storing an internal inverse model allows higher levels of the CNS to plan motion exclusively in terms of movements through space. This concept is appealing and was supported by Bernstein (1967): "The projection of space in the nervous system may prove to be very strange and unexpected; we must not expect to find in the cortex some sort of photograph of space, even an extremely deformed one. Still, the hypothesis that there exists in the higher levels of the CNS projections of space, and not projections of joints and muscles, seems to me at present more probable than any other."

If motion can be generated internally in terms of the movements through space, or equivalently the expected sensory consequences thereof, the storage problem (see section 1.3.2.4) is significantly reduced. Movements need only be specified and stored in terms of the, relatively low dimensioned, output movement trajectory. In this case a motor schema needs only specify the trajectory of a movement through space, as opposed to an entire set of motor commands.

1.3.3.5 Adaptive Control

The human motor control system is adaptive in nature. This is evidenced by numerous studies showing that the human operator can adapt to changing control-

display relationships (Davidson et al., in press; Held et al., 1963) and dynamic environments (Shadmehr et al., 1994).

Forward and inverse models specify complex transformations. The task of determining this transformation is known as system identification (Box et al., 1970; Ljung, 1999). It is often suggested that internal models are formed by adaptive tuning based on observation of past inputs and outputs of the model. When these models are adaptively tuned on-line an adaptive control system results (Astrom et al., 1995; Widrow, 1996; Widrow et al., 1985).

It has been suggested that a primary function of the cerebellum is to form adaptive internal models of the controlled system (the human body) which are then embedded into an optimal control structure (Jordan et al., 1992; Kawato et al., 1988; Miall, Weir, Wolpert et al., 1993; Neilson et al., 1992; Wolpert et al., 1995). The basal ganglia have also been hypothesized to contain internal models, specifically of *external tools* (Neilson et al., 1992).

1.3.4 Equilibrium-Point Control Hypothesis

The equilibrium-point control hypothesis was inspired by the work of Fel'dman (1966) who felt that the spinal reflex loop acts as a spring with a variable rest length specified by neural activation (Abernathy et al., 1992). This was called *the λ-equilibrium-point hypothesis.* Later work showed that the muscles also had equilibrium properties, leading to the mass-spring model and *the α-equilibrium-point hypothesis* (Bizzi et al., 1976).

The equilibrium-point hypothesis allows a control system to be devised which is simple, stable and independent of limb dynamics and initial conditions. Once a final limb position is specified by neural activation the system will naturally move to that position in spite of any perturbations or disturbances that might occur during the movement. The approach implements stable feedforward control and simplifies the complex inverse dynamics problem that must otherwise be solved (see section 1.3.3.2). Equilibrium-point control can operate within an information processing framework since it simply specifies a simple and efficient transformation from desired trajectory to resultant movement.

In recent years, equilibrium-point control has undergone much criticism (Laszlo, 1992; van Ingen Schenau et al., 1995). Evidence has recently emerged against the approach which demands that viscoelastic forces increase for fast movements. Gomi and Kawato (1996) observed low joint stiffness and consequently rejected the equilibrium control hypothesis, though the study was criticized by Latash, Aruin, & Zatsiorsky (1999). Further evidence against the approach was provided by Shadmehr & Mussa-Ivaldi (1994) who performed a study in which subjects adapted to a viscous force field. When the field was removed the subjects showed "mirror image" after-effects which were inconsistent with the equilibrium point hypothesis but consistent with the formation of internal models.

1.3.5 Combined Structures

In reality the spring like properties of the muscles are likely to be used in combination with adaptive feedforward and feedback control techniques base on internal models. Just as it is possible to integrate feedforward and feedback control to avoid the centralist vs peripheralist debate, so it is possible to include equilibrium control ideas in the overall control model.

1.3.6 Dynamical Action Theory

Dynamical action theory (Kelso, 1982) is an alternative approach to the study of motor behaviour which is conceptually based on the work of Bernstein (1967) on coordination and that of Gibson (1979) on perception (Fitch et al., 1982). The approach represents a complete rejection of the information processing approach to the study of motor control and consequently has sparked controversy within the field (Abernathy et al., 1992).

The theory attempts to describe the way humans move without reference to internal representations of the world, such as internal models, motor programs or memory. Human motor behaviour is seen as arising from self-organisation which constructs movement from the dynamic interactions between the body and the environment. Dynamical action theory contends that movements are emergent self-assembling effects which can only be studied in the context of a task and the environment. Unlike in information processing models, movement kinematics are not represented centrally but are an emergent property of the underlying motor system. Some extreme adherents of the approach even reject the concept of memory since it implies internal representation (Abernathy et al., 1992).

The theory arises in part from Bernstein's concerns regarding the degrees of freedom problem (see section 1.1.1) and the failure of existing theories to consider the varying biomechanical state of the body, referred to in the literature as *content-conditioned variability* (Turvey et al., 1982). In dealing with these problems, adherents of dynamical action theory have embraced ecological psychology and refer to themselves as "ecological realists".

Many of the original objections have since been addressed in modern information processing models based on internal model theories and adaptive control (Kawato et al., 1992; Neilson et al., 1992). The differences now appear to be predominantly philosophical in nature, with Gibsonian adherents contending that information processing theories imply the existence of a homunculus, or a "ghost in the machine"[2].

---

[2] For logical consistency Gibsonians must also accuse engineers of designing homunculi into their control systems. Where is the ghost in an air-conditioning unit?

Some attempts at reconciling the Gibsonian dynamical action theory and the information processing approach have been made. As Hurley (1998) notes, "... we should be ecumenical. Many aspects of ecological and motor theories can be combined, and conceptual liberality sharpens empirical issues." Dynamical action theory is probably best viewed as a higher level approach to describing the same system.

1.4 Adaptive Model Theory

The Adaptive Model Theory (AMT) is a comprehensive somatomotor control model based on the inverse dynamics model hypothesis (see section 1.3.3). It is a computational information-processing model which borrows concepts from adaptive control theory and is realisable in digital circuitry. The theory is particularly useful as it accounts for many of the classic observed psychological effects and is neurobiologically plausible. The theory exhibits tight coupling with the physiology of the motor control circuits in the human brain. All the control structures hypothesized by AMT can be implemented by distributed parallel processing in neural circuits.

The central hypothesis of AMT is that the brain computes and stores inverse models of the world around it and uses these models to produce smooth, coordinated purposive movement of the body in three dimensions. These inverse models are able to set and adaptively maintain parameters describing the multiple-input multiple-output non-linear dynamic relationship between outgoing motor commands and the sensory consequences of movement (Neilson et al., 1992). In AMT the inverse models can be rapidly retrieved from motor memory allowing for quick switching between tasks.

AMT has an hierarchical structure based on CNS physiology. At the highest levels in the hierarchy are cognitive processes such as attention and motivation. These levels affect all lower processes but are difficult to account for in a mathematical model. AMT presently describes levels in the hierarchy from trajectory planning down to final motor execution. The higher cognitive levels are usually considered to facilitate the performance of the lower processes at their optimum levels (Sriharan, 1997).

1.4.1 Intermittency in AMT

One of the most important features of AMT is its ability to naturally account for the psychological refractory period (see section 1.3.2.1) by introducing intermittency. The intermittency of the human motor control system has also been detected in manual tracking tasks (Miall, Weir, & Stein, 1993). AMT divides the information processing to be performed into three stages which are executed in a pipelined fashion. Each three-stage sequence is termed a Basic Unit of Motor Production or "BUMP" (Neilson et al., 1992). Other three-stage models of this type have been used to account for the psychological refractory period in information processing models, notably Welford (1980), but never in a control systems style model.

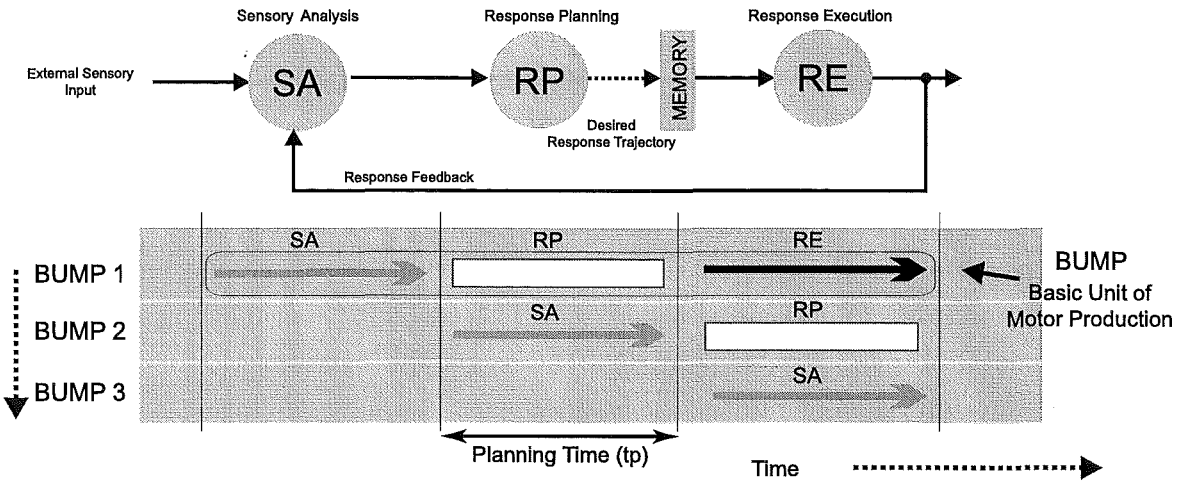

Fig. 12. Illustration of the intermittent flow of information through the AMT system. Each complete sequence in the pipeline is referred to as a BUMP (Adapted from Neilson et al., 1995).

Intermittency is introduced in the response planning (RP) stage (see Fig. 12). Here the nervous system pre-plans trajectories of desired perceptual consequences for the forthcoming movement. This process takes a finite amount of time (the *planning time tp*) and occurs in parallel with response execution (RE) and sensory analysis (SA) stages, which operate continuously on the results of an earlier RP-stage. In this way the model is able to plan a response to a stimulus, with multiple degrees of freedom, while concurrently executing a response to a previous stimulus. Consequently AMT provides a bridge between reaction time experiments and observed performance in continuous tracking tasks (Neilson et al., 1988a).

It is this ability to accommodate intermittency that sets AMT apart from other similar models of human motor control (such as feedback-error learning, see section 1.5). The concept has not be accommodated well in models where the stimulus and the response are continuously related. In these models inter-stimulus time is proportional to inter-response time. The importance of intermittency in tracking was highlighted in a study by O'Dwyer and Neilson (1998) where a step target was used. By changing the tracking system dynamics during a response, intermittent corrective behaviour was elicited. This result was consistent with a bottleneck in processing leading to intermittency.

The intermittency introduced in the response planning stage effectively divides the inherent delays associated with the human motor system into two components, the transmission time and the planning time. The total transmission time Δt is composed of the time taken for signals to flow from the periphery to the brain (the afferent delay, or β) and the time taken for signals to flow from the brain to reach and activate the muscles (the efferent delay, α). The total transmission time Δt contributes only about 100-150 ms of the total delay time. The remaining delay is attributed to the planning time delay ($tp \approx 50$ ms).

1.4.2 Response Planning Stage

AMT hypothesises that the frontal lobes of the brain require a finite interval (100 - 200 ms, depending on the workload) to effect the planning of a response trajectory of desired perceptual consequences (see section 1.3.3.4). The frontal lobes are implicated in response planning as they have tight coupling with the parietal and temporal regions allowing access to the sensory feature signals necessary for movement planning (these are produced in the SA stage of AMT). The region also has access to long-term memory information via loops through the hippocampus. Responses are planned in terms of the same code as feedback from the resulting movement thereby allowing a direct comparison between intended and actual responses (Neilson et al., 1992) and avoiding the sensory versus motor language problem discussed by Schmidt (1982).

In AMT, response planning is modelled as a discrete process intermittently outputting results based on control input and feedback information from other stages. The planning system does not begin planning a second response until the first has been completed. Planned responses are partially executed in the RE stage while new responses are being planned.

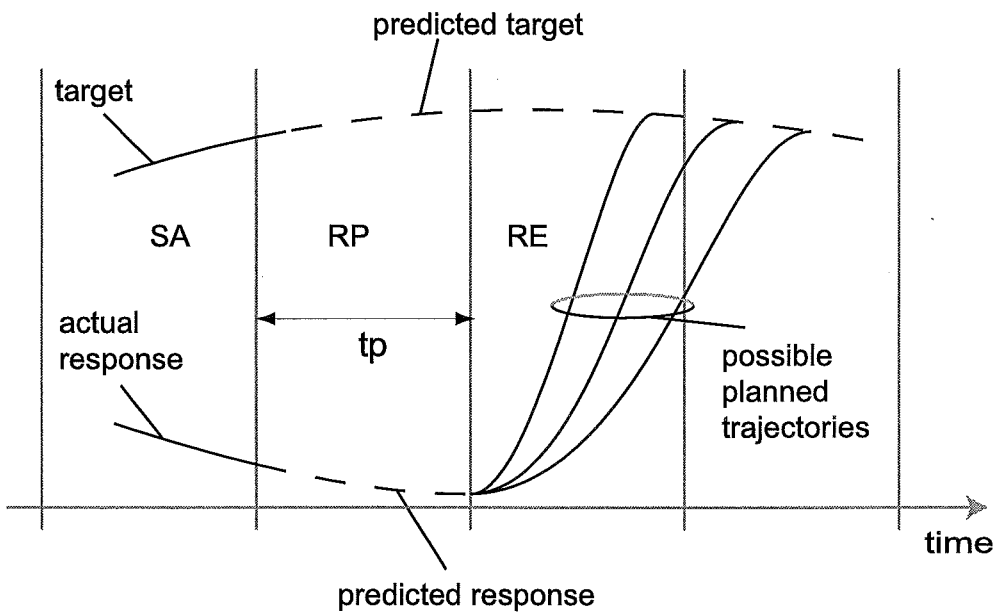

Fig. 13. Response planning in AMT. SA provides feedback on target and response and predicts these signals into the future. During RP trajectories for the following RE stage are planned.

1.4.2.1 Trajectory Generation

AMT employs an optimum trajectory generator (OTG) to plan individual response trajectories during the RP stage. The OTG produces a trajectory with minimum mean square acceleration given an initial state, final state and required movement duration (td) (Neilson et al., 1995).

Instead of planning a single ballistic corrective movement for execution within one planning time interval, the RP system plans multiple sub-movements over several reaction times. This allows the system to implement a speed-accuracy trade off, a well known property of human reaching movements and tracking task behaviour. As movement speed decreases, spatial accuracy increases and vice versa. The famous Fitts' law (Fitts, 1954) sums up this relationship for reaching movements:

$$M = a + b\log_2\left(\frac{2A}{W}\right) \tag{10.1}$$

where M is the movement time, A is the amplitude of the movement, W is the width of the target and a and b are constants. Movement time is therefore proportional to the logarithm of the ratio of movement amplitude and target size.

In AMT it is proposed that in a tracking task the operator strikes a balance between the control signal and the observed error to minimize a cost function. Hence, the problem of response planning is formalized in terms of a mathematical optimisation problem. Neilson proposes that the human operator plans corrective movements to minimize mean square acceleration while moving from the current state to the desired state *td* seconds ahead (Neilson et al., 1995). This is akin to Flash and Hogan (Flash et al., 1985) minimizing jerk (the derivative of acceleration). The duration of the planned curve defines the speed accuracy trade-off.

1.4.2.2 Optimum Trajectory Generator

The mathematics of the AMT optimum trajectory generator (OTG) has been described in detail by Neilson, Neilson, & O'Dwyer (1998) and Sriharan (1997). The OTG generates a minimum mean square acceleration trajectory R* over N samples given an initial state and a desired final state N steps ahead. Interestingly, for an inertial system, minimizing the mean square acceleration is equivalent to minimizing the input energy (Neilson et al., 1995).

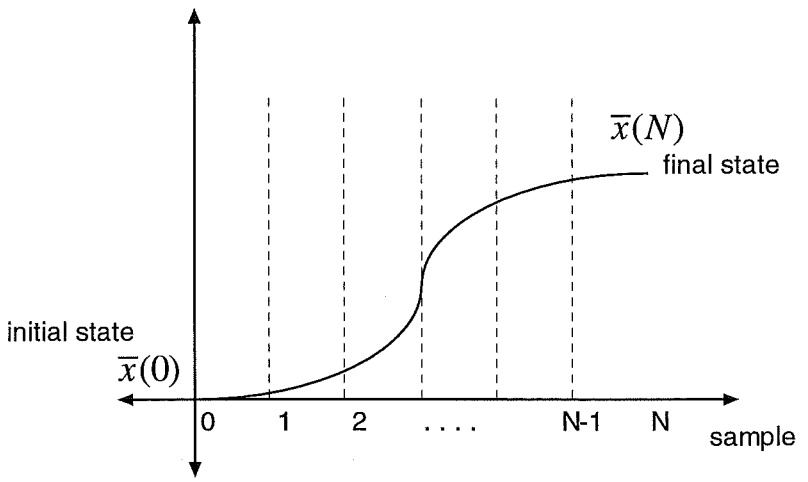

Fig. 14. Trajectory generated when OTG is supplied with initial state x(0) and final state x(N), from (Sriharan, 1997).

The continuous time, state-space description of a double integrator, which integrates an acceleration signal to give velocity and position signals, is defined as follows:

$$\begin{bmatrix}\dot{x}_1\\ \dot{x}_2\end{bmatrix}=\begin{bmatrix}0 & 1\\ 0 & 0\end{bmatrix}\begin{bmatrix}x_1\\ x_2\end{bmatrix}+\begin{bmatrix}0\\ 1\end{bmatrix}u(t) \tag{10.2}$$

where x_1 is position, x_2 is velocity and u(t) is an input acceleration signal. This is equivalent to the discrete time equation:

$$\begin{bmatrix}x_1(k+1)\\ \dot{x}_2(k+1)\end{bmatrix}=\begin{bmatrix}1 & 0.05\\ 0 & 1\end{bmatrix}\begin{bmatrix}x_1(k)\\ x_2(k)\end{bmatrix}+\begin{bmatrix}0.00125\\ 0.05\end{bmatrix}u(k) \tag{10.3}$$

which can be rewritten as:

$$\overline{x}(k+1)=G\overline{x}(k)+Hu(k) \tag{10.4}$$

where $\overline{x}(k)$ is a state vector.

Under these conditions it can be shown (Neilson et al., 1995) that for minimum mean square acceleration

$$\overline{x}(k)=G^k\overline{x}(0)+\Gamma(0,k)\Gamma^{-1}(0,N)\left[\overline{x}(N)-G^N\overline{x}(0)\right] \tag{10.5}$$

where

$$\Gamma(0,k)=\sum_{j=0}^{k-1}G^jHH^TG^{T(N-k+j)}\,. \tag{10.6}$$

This mathematical operation is a simple matrix transformation of the initial and final states. These can easily be implemented in neural circuits of the type used elsewhere in AMT (Neilson et al., 1995).

It has been noted (Neilson et al., 1995) that the intermittency of AMT in combination with optimum trajectory generation produces a system equivalent to a generalized predictive controller (GPC) (Clarke et al., 1987) or receding horizon optimal controller. At each BUMP the OTG produces a trajectory to move the response into alignment a set distance ahead in time (the prediction horizon). The mathematics describing GPC provides a useful reference for understanding AMT.

1.4.3 Sensory Analysis Stage

In contrast to the discrete output of the RP-stage, the sensory analysis (SA) stage operates continuously and in real time. The occipital, temporal and parietal lobes of the brain contain sensory analysis circuits. Signals from the periphery converge on these regions, passing thorough specialized networks which extract sensory feature signals from the raw information. The processed sensory information is then employed by the motor regions of the cortex for motor planning.

1.4.3.1 Redundancy and Orthogonalisation

There is likely to be an extremely high level of redundancy in the information reaching the sensory cortex. Even the information about a movement around a single degree of freedom is communicated to the brain by many thousands of sensory channels. This redundancy increases the reliability of the noisy neural circuits but the workload in analysing all of these channels separately would be prohibitive.

AMT suggests that redundancy is removed from the signals in the sensory cortex with adaptive orthogonalising networks (Neilson, 1993). These networks generate outputs which vary independently so that the encoded output contains the same information as the input but in an optimally efficient coordinate system. The number of non-zero orthogonal output signals equals the number of degrees of freedom in the original sensory input. The method used is the well known Gram-Schmidt orthogonalisation technique.

Orthogonalisation allows AMT to plan movements *independently* in several orthogonal dimensions. The neural circuitry to plan for one degree of freedom can therefore be replicated identically several times for planning movements in multiple degrees of freedom. The complexity of a task consequently depends on the number of degrees of freedom under control.

The orthogonalising networks can act in reverse to generate intercorrelated signals from a set of orthogonal sensory feature signals. This provides an elegant solution to the problem of controlling the highly redundant movement of the human body. AMT

employs an *adaptive synergy generator* to produce functional synergies from orthogonal motor commands.

1.4.3.2 Prediction

The other important function performed by the SA stage is stochastic signal prediction. The pure transmission and central processing time delay in the nervous system needs to be compensated for by the nervous system. In AMT adaptive neural circuits form predictive models of the orthogonal sensory feature signals. The resulting signals are then used by the OTG in the response planning stage for planning optimal movements.

1.4.3.3 Separation of Reafference and Exafference

AMT proposes that the CNS is capable of separating sensory signals (*afference*) into feedback signals produced by the body's own motor actions (*reafference*) and signals generated by external inputs (*exafference*). AMT employs a forward model of the controlled system to estimate the exafference component of the orthogonalized afferent signal. The exafference component is then stochastically predicted to overcome transmission delay and fed back to the response planner to improve the accuracy of the planned response trajectory.

1.4.4 Response Execution Stage

The response execution (RE) stage operates continuously to translate desired sensory consequences into coordinated motor movements by passing them through inverse models implemented as adaptive neural filters. The adaptive filters control the appropriate timing and amplitude of muscle output.

1.4.4.1 Inverse Model Cascade

Neilson et al. (1992) proposed that the overall inverse model is physically realized in the form of three serially cascaded inverse models (Fig. 15). The three inverse models reflect the three levels of the controlled system – the muscle control system (MCS), the biomechanical system (BM) and the external system (E). These three subdivisions are not arbitrary and correspond to the four levels of continuously available sensory feedback in the human motor system. Each model is considered to reside in a distinct region of the CNS.

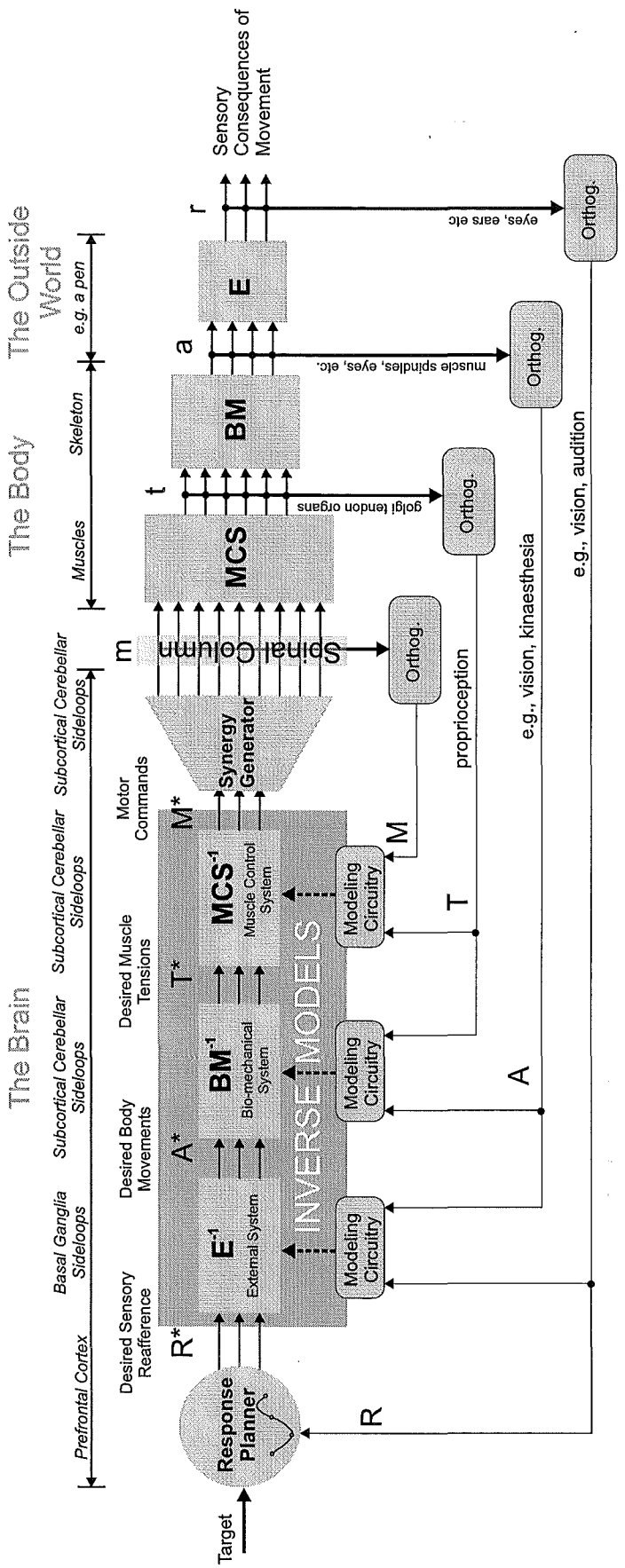

Fig. 15. Summary of information flow for adaptive model theory (based on a diagram in (Neilson et al., 1997)).

Motor command signals from the brain activate the cranial nerves and alpha motor neurons (m) and constitute the input to the controlled system. Feedback on these outgoing motor commands is available to the brain and is called *efference copy*. The motor command signals cause the muscles to contract and produce tension. The resulting tension is sampled and fed back to the brain via the Golgi tendon organs. Thus, the brain has both the input and output signals for forming a model of the muscle control system (MCS).

The tensions in the muscles pull on the bones and result in movement of the body. Kinaesthetic feedback on muscle length and joint angles (from muscle spindles and Ruffian and Pacinian endings in joint capsules respectively (Kandel et al., 1991)) provide feedback on body position. Thus another input-output pair is available; this time for forming a model of the biomechanical (BM) system.

Finally, the movement of the body acts on an external system which reacts to generate a set of sensory consequences. The consequences of the movement are sampled by the sensory system and a model of the external system (E) can therefore be formed. Driving a car provides a good example of an external system. The input to this external system is the movement of the hands (on the steering wheel and gear stick), and feet (on the foot pedals). The output of the external system is the set of sensory signals resulting from the moving image of the road and the interior of the car on the retina, in combination with kinaesthetic and vestibular information on mechanical forces resulting from the movement of the car.

These three systems, MCS, BM and E, in cascade represent the controlled system (or plant) in the human motor system.

Inverse Model of the External System (E)

The OTG produces a trajectory of desired sensory consequences in the SA stage. These must be converted into the body position necessary to produce this desired movement. In AMT this is achieved using sensory information on body position and the actual movement to form an inverse model of the external system E^{-1}. Specifying the complex transformation from desired body trajectory to joint angle, known in robotics as 'inverse kinematics', is therefore part of the function of E^{-1}.

It is thought that E^{-1} is modelled in side loops through the basal ganglia. As noted in section 1.2.4 the basal ganglia take input from the prefrontal cortical areas (thought to be involved in motor planning) and send output to the supplementary motor and premotor cortical areas via the thalamus. Thus, these loops form the correct anatomical connections for converting planned movement trajectories into desired body position.

Inverse Model of the Biomechanical System

The resulting body movement commands then pass through sub-cortical side loops to the second inverse model, conceptually corresponding to the body's biomechanical

system BM^{-1}. This is postulated to be formed in the microzone circuits of the cerebellar cortex and produce the required muscle tensions as output (see section 1.2.3.2).

Inverse Model of the Muscle Control System

The final inverse model, MCS^{-1}, is also hypothesized to reside within cerebellar sub-cortical side-loops and produce the set of motor commands necessary to implement the required movement. While this transformation would seem to be enormously complex, some convincing recent evidence suggests that joint torques are produced through the modulation of pre-defined primitives in the spinal cord (Mussa-Ivaldi et al., 2000). This would simplify the MCS^{-1} transformation enormously.

While the desired trajectory flows through the inverse model cascade serially, the inverse models themselves are adapted independently and in parallel.

1.4.4.2 Spinal Feedback Loops

In AMT the feedback control loop via the gamma motor neurons and the stretch reflex loop modulate the feedforward control provided by the alpha motor neurons in an extension of the servo-assist theory of muscle control (Neilson et al., 1997).

It should be noted that the inverse model of the muscle control system naturally makes use of any mass-spring behaviour of the muscles and in the spinal feedback loops. If the equilibrium point hypothesis (section 1.3.4) were correct then BM^{-1} and MCS^{-1} would reduce to very simple transformations. Conversely, if equilibrium point control is insufficient, as seems likely for ballistic movements at least, then the inverse dynamics model would become active and improve movement accuracy.

1.4.4.3 Modelling Structure

In AMT, a linear adaptive FIR filter has been used to model the formation of the forward and inverse models. The assumption of linearity allows the inverse model to be formed analytically from the forward model. This linear model is based on the idea that the cerebellum acts as an adaptive linear filter, as proposed by Fujita (1982). A linear FIR filter (see Fig. 16) can be defined mathematically as

$$y(k) = \sum_{i=0}^{N-1} w_i(k)u(k-i) \qquad (10.7)$$

where $y(k)$ is the output of the filter, $u(k)$ is the filter input and $w_i(k)$ is the i^{th} filter tap weight.

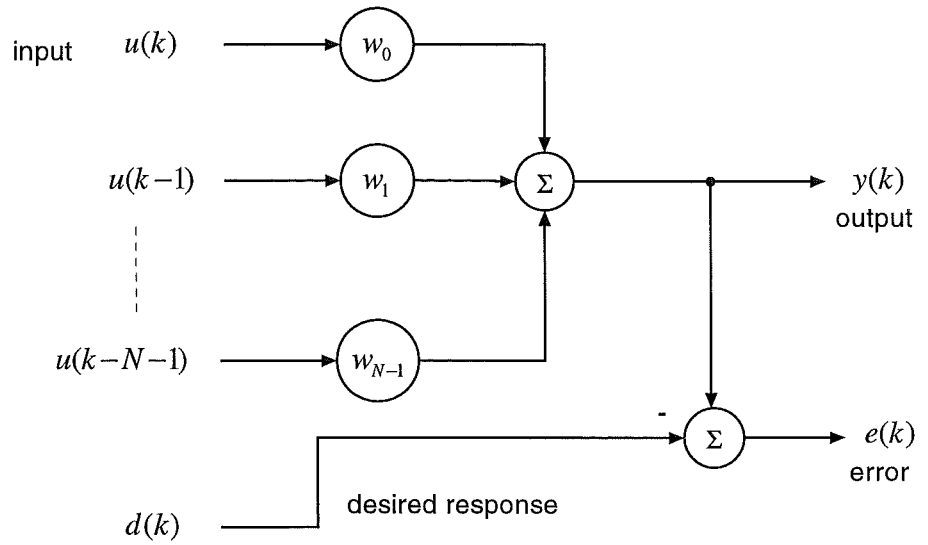

Fig. 16. Linear adaptive filter structure.

The NLMS algorithm (Widrow et al., 1985) is used to tune the adaptive FIR filter in AMT as follows, assuming $d(k)$ is the desired value of the filter output at time k. Using vector notation for simplicity, $\mathbf{w}(k)$ is a vector of N filter tap weights and $\mathbf{u}(k)$ is a vector of N delayed inputs.

$$e(k) = d(k) - y(k) \tag{10.8}$$

$$\mathbf{w}(k) = \mathbf{w}(k-1) + \mu \frac{\mathbf{u}(k)e(k)}{1 + \mathbf{u}^{\mathrm{T}}(k)\mathbf{u}(k)} \tag{10.9}$$

Once a forward model based on a linear adaptive fir filter has been formed the inverse relationship can be established directly from (10.7)

$$u(k) = \frac{y(k) - \sum_{i=1}^{N-1} w_i u(k-i)}{w_0} \tag{10.10}$$

The same simple relationship would be unavailable if we were to use a nonlinear adaptive filter in place of the linear FIR filter. Finding the inverse of a nonlinear system is a difficult problem which has attracted much interest (Jordan et al., 1992; Kawato et al., 1992; Widrow, 1996). The implications of this problem form the initial focus of this work.

1.4.5 Tracking Task Simulation

In computer simulation of tracking tasks using AMT a number of simplifying assumptions are generally made. It is usually assumed that MCS^{-1} and BM^{-1} are sufficiently accurate, when fine tuned by the spinal feedback loops, that the control system including BM and MCS approximates a unity transfer function. This allows us to

focus on the control of the external system, the tracking system itself. For this reason we primarily consider a single controlled system and inverse model and neglect the cascade structure in simulation.

A diagram of the structure used for tracking task simulation with linear AMT is shown in Fig. 17.

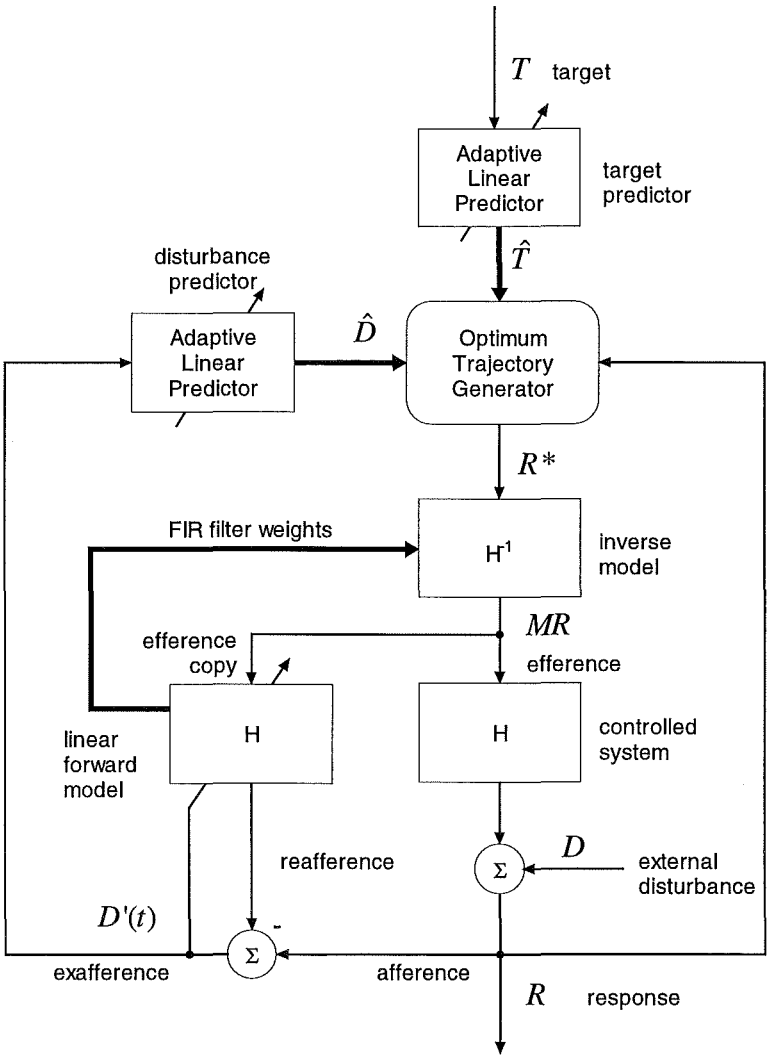

Fig. 17. Computer simulation diagram. Diagonal arrows indicate an adaptive circuit.

1.5 Feedback-Error Learning

Feedback-error learning (FEL) is a computational theory of supervised motor learning. The scheme specifies a method for the efficient formation of nonlinear inverse models in neural networks (Kawato et al., 1987). The approach has been generalized into a comprehensive human motor control model based on the inverse dynamics hypothesis (Kawato et al., 1992). The scheme is philosophically similar to AMT in that that it suggests that libraries of inverse dynamics models are formed and used for control. The

scheme also attempts to map computational functions onto a neurophysiological substrate.

Whereas AMT uses a serial combination of feedback and feedforward control, the feedback error learning structure uses a parallel combination. This has advantages for the direct formation of inverse models. Inverse models in FEL, however, do not yield naturally to independent parallel adaptation as in AMT (though a possible solution to this problem was devised by the author - see Appendix I). The computational detail of FEL is expanded upon in a later section on inverse modelling structures (see section 3.2.4).

FEL proposes that the climbing-fibre inputs to the cerebellum represent motor command errors in motor command coordinates. This contrasts with AMT where cerebellar inputs are in body movements and muscle tension coordinates. The motor command errors are generated in the motor networks of the cortex and spinal cord (Kawato et al., 1992). FEL includes a parallel feedback controller which is summed with feedforward motor commands in the motor cortex. As in AMT, the desired body trajectory is sent to the cerebellum for inversion and the result returns to motor cortex via the thalamus.

1.6 Objectives

The main objectives of this PhD project are summarized by the sub-headings in this section.

1.6.1 Enhancement of the AMT Model

In AMT, adaptive FIR filters were selected as an appropriate model based on the observation that the cerebellum has appropriate circuitry for their implementation. The system is, however, required to control multijoint limb movements which exhibit highly nonlinear dynamics (Kawato et al., 1992). Linear dynamic FIR filters are, therefore, insufficient as a general model of the motor control system. Consequently, a more realistic generalization of the AMT model was necessary. The development and testing of such a generalization was a primary goal of this project.

This involved looking for a neurobiologically plausible system identification structure that would fit within the existing AMT framework. The structure would not only need to possess sufficient nonlinear dynamic representational capacity but also exhibit a learning rate comparable to that observed in the human motor system. Appropriate nonlinear inverse modelling structures, again retaining the intermittent serial control structure of AMT, also required specification for a full nonlinear generalization.

The predictive circuits of AMT assumed a linear stochastic model (see section 4.1.3) which limited the class of signals that could be predicted with accuracy. A nonlinear extension of this circuitry was, therefore, also necessary.

In summary, the primary goal of the project was to propose a nonlinear generalization of AMT (to be called nAMT), maintaining a high degree of neurobiological plausibility and mimicking the behaviour of the human motor system to the greatest extent possible.

1.6.2 Experimental Study of Adaptive Inverse Modelling in Humans using Tracking Tasks

Once a suitable nonlinear generalization of the AMT structure had been constructed it was intended that the new model be tested against human behaviour. An experimental study was therefore designed to provide reference data for comparison with the model. The experiment was designed so that it also revealed more fundamental properties of the human motor control system and attempted to answer some important outstanding questions in the field.

The study was primarily aimed at confirming the presence of an adaptive inverse modelling in the nervous system, thus justifying the fundamental assumption made by AMT - the acceptance of the inverse modelling hypothesis.

The experiment was also intended to look at human behaviour in the absence of feedback and elucidate the extent to which adaptive feedback and feedforward control are involved in the control of external tools.

1.6.3 Comparison of the nAMT Model with Experimental Data

Following the experimental study, the ability of the nAMT model to synthesise the observed human behaviour was tested. It was intended that the model capture both the kinematic and learning characteristics of the motor control system of a typical human subject.

2. Neurobiological System Identification

Engineering control system designs often assume the availability of accurate models of both the controlled system (the plant) and of the stochastic properties of system disturbances. The task of constructing such models is called system identification (Ljung, 1999). A control systems engineer can often derive an appropriate plant model directly by applying physical principles. In the human motor control system, however, knowledge of the plant is restricted to deductions based on sensory information: on efference copy (plant input) and afference (plant output). An engineering control system is usually designed to operate the same plant for its entire lifetime. In the case of the human control system the plant can alter from moment to moment as we change tasks. If we are to suggest that the human motor system operates according to the internal model hypothesis then the neural circuits of the central nervous system must be capable of forming and maintaining accurate models of systems which may alter rapidly and unpredictably. The time-varying nature of the plant demands an adaptive on-line system identification technique. Such problems are tackled in modern engineering control systems using the theory of adaptive control (Ljung, 1999).

A variety of useful adaptive on-line system identification techniques exist in the literature. Here, however, we are bound by the requirement that the computational substrate be neurobiologically plausible. Consequently, we need to find an adaptive structure that mimics the adaptive behaviour of neural circuits in the brain before we can approach the system identification problem.

In AMT, adaptive FIR filters were selected as an appropriate model based on the observation that the cerebellum possesses appropriate circuitry for their implementation. This model had previously proved useful for modelling the involvement of the cerebellum in adaptively compensating for the dynamics of eye movements (Fujita, 1982). The plant, in the case of the horizontal vestibulo-ocular reflex, exhibited approximately linear dynamics. In contrast, our model is required to control multijoint limbs which exhibit highly nonlinear dynamics (Kawato et al., 1992). The existing linear dynamic system identification approach, therefore, is insufficient as a general model. A similar adaptive system capable of representing nonlinear dynamics is necessary.

2.1 Forming a Forward Model

The two basic system identification tasks in AMT are the formation of a forward model (see section 1.3.3.1) and the formation of a stochastic disturbance model. Since the two tasks are very similar, only the forward modelling case will be examined here. The structure required to form a forward model of the controlled system in a neurobiologically realistic model is shown in Fig. 18.

An appropriate transformation $\hat{P}$ must be found such that its output matches the output of the plant as accurately as possible. To achieve this, the difference between the model output and the actual output, the *error signal*, is observed and used to adjust $\hat{P}$ in some way. The manner in which the output of $\hat{P}$ is calculated from present and past inputs determines the structure of the model. The way the model is adjusted, based on the error signal, determines the adaptation algorithm. The present task is to determine an appropriate model structure and adaptation algorithm for nAMT.

The model transformation $\hat{P}$ must be a nonlinear dynamic function and the adaptation algorithm must be as fast as the neural adaptation process and mathematically stable. It is important to understand that a wide variety of structures are capable of forming an appropriate model. The structures examined and developed in this chapter are candidates that match with the observed function and neurobiology of the brain circuits we are attempting to emulate.

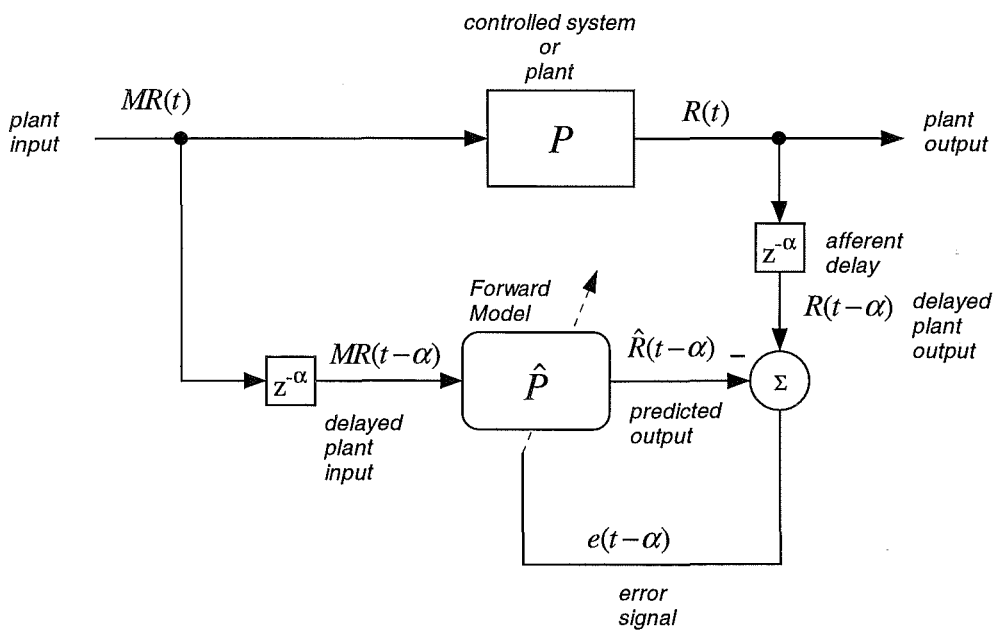

Fig. 18. The basic system identification task in motor control. A forward model of the plant must be formed which is capable of predicting plant outputs R(t) given a sequence of input MR(t).

2.2 Nonlinear Functional Representation

Before looking at specific techniques for modelling nonlinear dynamic systems, it is important to establish a method for describing a nonlinear plant. Functional representation of nonlinear systems is more difficult than of linear systems, though there are well recognized methods for the general description of nonlinearities.

2.2.1 NARMAX Representation

NARMAX models are a nonlinear generalization of the class of ARMAX (Auto-Regressive Moving-Average with eXogenous inputs) models. ARMAX models provide a general description of linear systems, relating an input sequence to an output sequence with a linear, constant-coefficient difference equation (Pearson et al., 1997). An ARMAX model is defined as follows:

$$y(k) = \sum_{j=1}^{p} a_j y(k-j) + \sum_{j=0}^{q} b_j u(k-j) + \sum_{j=0}^{r} c_j e(k-j) \qquad (11.1)$$

Where u(k) is the input sequence, y(k) is the output sequence and e(k) is a Gaussian white noise sequence representing the modelling error. Here the output depends on past outputs (the 'Auto-Regressive' component) and past and present inputs to the system (the 'Moving-Average' component).

This general description of linear systems can be extended to nonlinear systems in the form of the NARMAX (Nonlinear Auto-Regressive Moving-Average with eXogenous inputs) model (Ljung, 1999):

$$y(k) = f\begin{pmatrix} y(k-1), y(k-2), \ldots y(k-p), \\ u(k), u(k-1), u(k-2), \ldots u(k-q), \\ e(k-1), e(k-2), \ldots e(k-r) \end{pmatrix} + e(k) \qquad (11.2)$$

Where f(.) is a nonlinear function of the input {y(k)}, output {u(k)} and error {e(k)} sequences. The NARMAX model encompasses an extremely wide class of nonlinearities and most other models are a subset of the NARMAX class. The accuracy of the NARMAX model depends on the value of the order parameters p, q and r.

Since the function f(.) is not specified, the NARMAX model specifies a regression function but does not specify the basis function of the parametrization.

2.2.2 Volterra Models

Volterra models provide a description of a useful class of nonlinear systems known as *fading memory* systems. They are a special case of the broad NARMAX class of models. Volterra models are particularly useful as they provide a method of describing these

systems analogous to the impulse response description used in linear systems. Volterra models employ *global basis functions* and therefore exhibit excellent generalization abilities.

Fading memory nonlinear systems are loosely defined as systems in which the dependence on past inputs fades "rapidly enough" with time (Boyd et al., 1985). This effectively reduces the class of nonlinearities to be controlled to "well behaved" systems. Such systems do not exhibit multiple steady states or other related phenomena such as chaos (output multiplicities). Consequently, Volterra models are only valid within the basin of attraction of a single steady state (Henson et al., 1997).

A discrete time Volterra model is defined with the following series:

$$\begin{aligned} y(k) &= y_0 + \sum_{j=0}^{\infty} a_j u(k-j) \\ &+ \sum_{i=0}^{\infty}\sum_{j=0}^{\infty} b_{i,j} u(k-i)u(k-j) \\ &+ \sum_{l=0}^{\infty}\sum_{i=0}^{\infty}\sum_{j=0}^{\infty} c_{l,i,j} u(k-l)u(k-i)u(k-j) + \ldots \end{aligned} \tag{11.3}$$

Where the coefficient matrices **a, b, c.** etc., are known as Volterra kernels and are analogous to the impulse response of a linear system. A standard linear system is a special case of the Volterra series (obtained by restricting the description to the 1st order kernel: **b, c,** . . . = 0).

Volterra models are polynomial NARMAX models with p=0 (i.e., they do not depend on past system outputs). A Volterra series is also a temporal equivalent of the Taylor series (Henson et al., 1997). Just as Taylor series are limited to approximating analytic functions, Volterra series are limited to describing fading memory functions.

The orders of Volterra kernels included in a description define the accuracy of the model. Unfortunately, Volterra kernel descriptions quickly grow to include an unreasonable number of parameters. For practical modelling this necessitates applying structural restrictions to the model. These restrictions involve limiting the order of the system, truncating the system memory and pruning the Volterra kernel matrices.

Importantly, it is also possible to construct a Least Mean Squares (LMS) adaptive filter based on the Volterra representation (Widrow, 1996). This is directly analogous to the LMS linear adaptive filter approach used in AMT (Widrow et al., 1985). This approach to nonlinear modelling in AMT was followed by Sriharan (1997). The difficulties encountered by both Sriharan and Widrow (1996) in modelling general nonlinear systems led us to reject the global basis function approach and, hence the Volterra model approach, in favour of a *local basis function* representation. Artificial neural networks, whose model structures are based on a biological neuron analogy, employ local basis functions.

2.3 Neural Network Models and their Biological Plausibility

Here we look at the applicability of modern neural network architectures to neurobiological modelling. Artificial neural networks were originally conceived as very simple models of their biological analogues (McCulloch et al., 1949). They were intended to capture only the essential features of information processing in a biological neuron. This functionalist outlook has attracted criticism from commentators who feel that the models are overly simplistic; they have been referred to as "stick and ball models" of real neurons (Douglas et al., 1991). The very intent of neurobiologically motivated neural network research, however, is to produce minimal models that, as Dawson & Shamanski (1994) put it, "(permit) one to make rigorous claims about what they can do, or about why the brain might have the particular structure that it does". Such models must be as complex as necessary to capture the essence of the neuron, and no more. The relationship between connectionist neural network models and more detailed electrophysiological neuron models is similar to that between psychophysical and neurophysiological motor control research – simple higher-level descriptions of complex systems often offer greater insight than complex low level descriptions.

Existing neural network architectures provide a good foundation on which to build functional models of brain regions. They provide a distributed structure capable of learning and memory. Do these existing structures fairly represent the data processing action of biological networks? Here we hope to assess the various approaches available for supervised learning in the nervous system, and suggest the most appropriate approach for a model of human motor control.

2.3.1 Neuron Models

The emphasis in this section is placed firmly on the generic connectionist neuron, which is derived from the McCulloch-Pitts neuron. While other more complex models do exist, none have shown superior performance in function modelling applications.

2.3.1.1 The McCulloch-Pitts Neuron Model

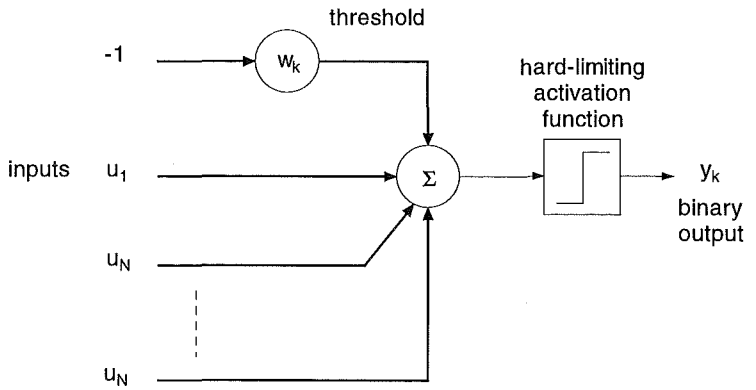

Fig. 19. The McCulloch-Pitts neuron.

The isolated McCulloch-Pitts neuron, the prototype for most neural models in use today, captures the basic data processing action of a single neuron (McCulloch et al., 1949). Its "all-or-none" action is similar to the on-off characteristics of the action potential in biological neurons. This digital model of neuron action helped to popularise the computer-brain analogy, the idea that neurons in the brain act like binary switches in digital computers. No mechanism for learning is included in this model, allowing McCulloch-Pitts networks to account for performance but not learning.

2.3.1.2 The Perceptron

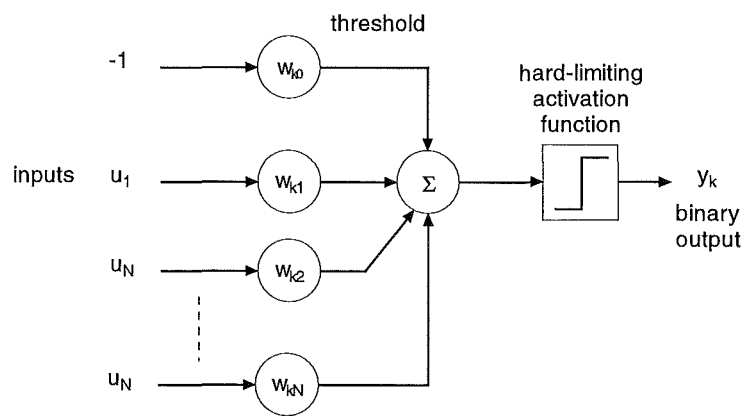

Fig. 20. The Rosenblatt perceptron.

The "perceptron" of Rosenblatt (1958) improved upon the McCulloch-Pitts neuron by including modifiable *synaptic input weightings*, which were then summed and compared to an activation threshold (or *bias*, see Fig. 20). This forms a reasonable model of the summing of dendritic currents at the soma of a biological neuron. The structure also provides, in the modification of synaptic weights, a mechanism for implementing learning in a neural network. The synaptic weightings are interpreted to represent the efficacy of

the synaptic connection. The output of the simple perceptron of Rosenblatt is hard limiting, maintaining the digital switch analogy set by the McCulloch-Pitts neuron model.

2.3.1.3 Multilayer Perceptron (MLP) Networks

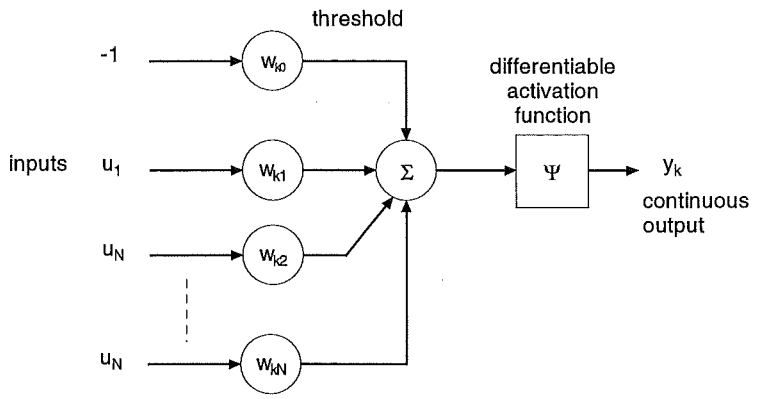

Fig. 21. The MLP perceptron.

The use of hard-limiting activation functions in the early work on neural networks made sense as it produced a digital output, thought to represent the on-off characteristics of the axonal action potential. Such networks suffer from one major limitation: training cannot be applied to multiple layered structures.

When Rumelhart and McClelland (1986) suggested the use of the back-propagation algorithm for training multiple layered perceptron networks, the hard limiting activation function was replaced by a differentiable function, typically a sigmoid (see Fig. 22).

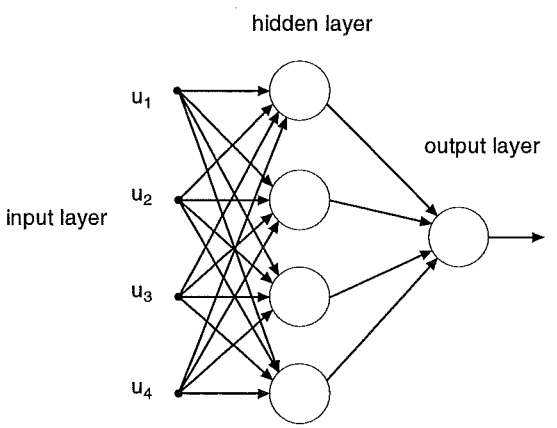

Fig. 22. A three-layer MLP network (neurons represented as circles). The arrows between layers represent adjustable weights.

Back-propagation (see section 2.3.2.4) provides a means of training networks containing multiple layers of neurons (see Fig. 21). Typically all the synaptic weights and bias thresholds are modified by this algorithm. Unfortunately there is no evidence to suggest that neuron activation thresholds are plastic (Dawson et al., 1994), which is a serious drawback for the use of MLP networks in biological modelling. The modelling efficiency of MLP networks drops significantly when activation thresholds are not

adapted (Dawson et al., 1994). However, during the process of cell pruning the neurons with optimum thresholds can be selected resulting in an effect similar to threshold adaptation.

2.3.1.4 Monotonic Activation Functions

When the hard-limiting activation function was replaced with a differentiable nonlinearity the neurophysiological interpretation of the output of the neuron model was altered. Instead of representing an on/off state the axonal output now represented the average firing frequency of the neuron. This is a reasonable interpretation and there is even some evidence of sigmoidal activation occurring in biological neurons (Kernell, 1965).

The activation function in a back-propagation network must be differentiable and monotonic. The latter condition has attracted criticism on biological grounds, as some neurons exhibit non-monotonic activation functions (Dawson et al., 1994).

2.3.1.5 Modelling Functional Units

Rashevsky (1960) was the first to suggest the modelling of groups of neurons, or functional units, to average out the randomness inherent in the behaviour of individual neurons. This led to the interpretation of the perceptron as a continuous model of these neural functional units. An interesting consequence of this point of view is that the sigmoid function, which is useful in many network architectures, emerges naturally. If the activation threshold within the functional group is assumed to have a Gaussian distribution, then the expected value of the firing frequency is a sigmoidal function of activity.

It is possible to conceptualise the McCulloch-Pitts neuron as representing the ensemble-averaged activity across a group of neurons. The approach also takes into account the refractory phase of real neurons (Haykin, 1994).

2.3.2 Learning Algorithms

While networks of simple neurons may reasonably be included in a serious biological model, it is more difficult to find learning procedures sufficiently realistic for this purpose. Since their inception, a rich variety of learning algorithms have been suggested for the training of artificial neural networks. Some were inspired directly by neurobiology; others were the result of a purely engineering-oriented effort. Unfortunately, the development of learning algorithms has largely been directed at mathematical efficiency, with biological plausibility taking a back seat. However, the perspective of the originator is of no relevance to the biological plausibility of the resulting algorithm and, consequently, a survey of the available learning algorithms was conducted with the intention of establishing the most suitable approach for modelling the motor circuits of the brain.

2.3.2.1 Hebbian Learning

To date there is only one learning mechanism that has been experimentally verified to occur in the nervous system (Harston, 1990). This mechanism is known as Hebb's rule (Hebb, 1949). Hebb hypothesized that the conductance of a synapse between two neurons is increased as that synapse is repeatedly activated. The rule was first utilized for training a neural network by Rosenblatt in his perceptron, where the simple McCulloch-Pitts neuron was combined with Hebbian learning (Rosenblatt, 1958). Since then, Hebbian learning has been used widely as a neural network training method.

Biological feasibility

Hebbian learning is a feasible mechanism for information storage in the brain. In fact, direct evidence for the occurrence of Hebbian learning in the brain is provided by studies of long-term potentiation in the hippocampus (Bliss et al., 1993; Bliss et al., 1973). Another appealing characteristic of Hebb's rule is that its simple local mechanism would require little genetic code for its description.

Unfortunately, the ability of Hebbian learning to train neural networks for complex tasks is very limited. While the approach has been shown to be sufficient to account for topographical mappings and plasticity in cortical representation (along with some other special cases), its associative memory mode of operation offers an incomplete explanation of brain function. Hebbian learning requires synchronous stimuli, which is particularly problematic in inherently sequential motor control problems. Additionally, Hebbian learning is unable to teach an MLP network arbitrary, nonlinear decision boundaries (Anderson, 1998). It might be envisaged that pure Hebbian learning could be used in an assisting role in motor control, for example to filter input signals into more efficient representations.

2.3.2.2 Biased Random-Walk Algorithms

In biased random walk algorithms the synaptic weights of a network are perturbed in a spontaneous random fashion. This approach is similar to Hebbian learning, except that a supervisory signal is used to indicate the success or failure of the perturbation. A recent example of a random-walk algorithm is the chemotaxis algorithm, named for its analogy to the strategy employed by bacteria to find chemoattractants in a spatial concentration gradient (Anderson, 1998).

The chemotaxis algorithm proceeds as follows. Perturb the weight vector by adding a Gaussian distributed random vector. If the error increases revert to the original weight vector, if the error decreases add the weight vector again and continue to do so until the improvement stops.

The simplicity of the algorithm is extremely appealing. The principle disadvantages of the approach are a low rate of learning and high susceptibility to local minima.

Importantly, the approach is significantly slower than back-propagation, which is itself often criticized for being too slow to converge.

Biological Feasibility

In support of his chemotaxis algorithm, Anderson says: "... the mechanism for synaptic change is local and independent of any higher teaching signals." This is not strictly correct, as each synapse needs access to one indispensable piece of global information - the network error. This is a necessary fault of all supervised learning architectures, and occurs repeatedly in the other learning schemes.

The chemotaxis algorithm has the advantage that the same scalar error signal is required across the entire network. Some extra-neural reverse flowing agent, possibly chemical in nature, might well supply this information. Critically, when multiple outputs are required from the network, chemotaxis is forced to rely upon a single scalar error measure, while the gradient descent schemes to be discussed use a vector of errors with respect to each unit. This leads to a major loss of the performance relative to other algorithms.

2.3.2.3 Widrow-Hoff Gradient Descent (LMS) Learning

In an effort to overcome the limitations of Hebbian learning, much of the recent work on neural network training algorithms has concentrated on gradient descent methods. Here an error function is minimized by altering the system's parameters in a direction opposite to the gradient.

One of the earliest supervised neural network learning schemes was the Widrow-Hoff gradient descent method, which minimized the mean square error by adjusting the network's synaptic weights in a direction opposite to an *instantaneous estimate* of the gradient. The method is also called Least Mean Squares (LMS) learning or occasionally the delta method. Windrow-Hoff learning was first introduced with the Adaline neural network (Widrow et al., 1985) and is still commonly used in a variety of single layered neural network structures, including the CMAC structure (Albus, 1975). The rule is also used in Fujita's adaptive linear filter model of the cerebellum (Fujita, 1982) and consequently in AMT itself (Neilson et al., 1992).

The primary limitation of the method is that it is only capable of training a single-layer network and, consequently, cannot represent certain classes of functions (Widrow-Hoff learning was later generalized to multiple-layered networks in the form of back-propagation, see section 2.3.2.4).

Interestingly, it has recently been noted that the Widrow-Hoff algorithm can be recast as a form of Hebbian learning when a teaching input is provided to the neuron (Kalveram, 1999). This improves the argument for the biological feasibility of the Widrow-Hoff algorithm considerably.

Biological Feasibility

The Widrow-Hoff method is a strictly local algorithm, meaning it only requires information already present at a particular node for its operation: the input, the actual output and the desired output. Consequently the method adheres to the fundamental connectionist principle of local computation: since each node needs no knowledge of other nodes in the network, the structure can be replicated widely with little genetic overhead.

Psychological evidence suggests that Widrow-Hoff style learning does indeed occur in the nervous system; for example, the Rescorla-Wagner model of rat learning has been shown to be equivalent to the Widrow-Hoff method (Sutton et al., 1981). The Widrow-Hoff method can also explain data from human and animal experiments (Gluck et al., 1988; Gluck et al., 1987). It seems reasonable then to use the Widrow-Hoff approach to model the functional characteristics of the brain, even though it is unclear whether it actually occurs at the neural level as suggested in the original Widrow-Hoff literature.

2.3.2.4 Back-propagation

The back-propagation algorithm is a generalization of the Widrow-Hoff algorithm for training multi-layer neural networks. The algorithm works by propagating the available overall network error back progressively through each layer to form a new vector of valid error signals for all neurons. The network's synaptic weights are then adjusted by applying the Widrow-Hoff method to the back-propagated vector.

Biological Feasibility

Back-propagation is currently the most powerful method available for training multi layer neural networks. If this process could be shown to occur in the brain it would represent a major breakthrough in our understanding of biological neural systems. Unfortunately there is very little evidence to support back-propagation at the neural level. A lot of literature has been generated debating the neurobiological feasibility of the algorithm.

The principle objections to the approach are as follows:

Back-propagation requires non-local processing (Hecht-Nielsen, 1989). Each neuron depends upon data from many other neurons for its synaptic weight adaptation, violating the connectionist principle of local computation. This objection has been addressed, resulting in several strictly local implementations of back-propagation which do not require access to global information (Fausett, 1990; Hecht-Nielsen, 1989). These algorithms are mathematically identical to standard back-propagation but require certain restrictions on the network architecture.

Back-propagation requires weight transport. Grossberg (1987) argued that back-propagation requires feedback of synaptic weight values, which is clearly biologically unrealistic. Stork (1989) disproved the necessity for weight transport soon after, but this

objection is still often raised in arguments hostile to biological modelling with back-propagation.

Back-propagation requires finely structured neural connectivity (Anderson, 1995; Stork, 1989). The complex feedback projections that back-propagation requires within the network must synapse in precisely the correct location for the algorithm to work. The required structure has not been observed and would probably require excessive genetic overhead for its description and reproduction. This is perhaps the strongest argument against back-propagation. Several minimal structures necessary for the implementation of back-propagation have been suggested (Hecht-Nielsen, 1989; Stork, 1989), indicating that the brain may at least possess the basic units necessary to implement a form of back-propagation. These structures have not been observed but more complex arrangements in the actual brain may prove to be functionally equivalent.

In a strictly local implementation of back-propagation this deficiency could be overcome if reverse signalling within the neuron were possible. Such 'antidromic' signalling was traditionally thought impossible; however backward feedback across synapses has been demonstrated to occur and cytoskeletal signalling through microtubules has been suggested as a mechanism by which information might propagate back along an axon (Dayhoff et al., 1992).

Back-propagation has not been detected. There has been no direct evidence of back-propagation occurring in the nervous system although, in some experiments with squid nerve cells, an output consistent with back-propagation learning has been demonstrated.

In summary, back-propagation occurring directly in the brain is feasible but unlikely. However, given the complex feedback exhibited within a neural mass, it is certainly conceivable that a process with characteristics similar to back-propagation of error may be occurring (Hinton, 1993). It has been shown that back-propagation can be used to arrive at a set of synaptic weights with a character similar to those predicted by electrophysiological recordings (Crick, 1989) but back-propagation may not be the way the brain arrives at these weightings.

2.3.2.5 Gradient Descent in Neural Populations

When entire populations of neurons are considered at once (see section 2.3.1.5), gradient descent becomes a more attractive learning approach (Gupta, Rao et al., 1993). It is possible that feedback axonal connections from the output of a population might modulate the input of that population in such a way as to reduce the error at the output. A gradient descent algorithm may provide a reasonable model for such an arrangement, even if the details of the structural substrate are not well established. Modelling of this sort represents a higher level of abstraction than the established neural network modelling approach. Such a model may be capable of mimicking the learning and representational capabilities of the actual network. Given the lack of knowledge of the

operation of neurons at lower levels this may prove to be a more appropriate level of abstraction for modelling and verification purposes.

2.3.2.6 Suitability for nAMT

Of all the proposed mechanisms for supervised learning in the nervous system, the random walk approach is probably the most directly biologically feasible. Unfortunately, pilot studies showed that the adaptation rate of random walk algorithms was vastly slower than both gradient descent algorithms and observed neural learning rates. This leaves the single-layer Widrow-Hoff algorithm as the best choice for a biologically feasible structure. It is proposed, therefore, that multi-layer gradient descent algorithms be used in this work as a model for the as yet incompletely understood learning mechanisms known to occur in the brain.

2.4 Neural Networks for Nonlinear Dynamic System Identification

As previously discussed (section 1.3.3.3), the plant in the human motor control system is a *nonlinear dynamic* system. Most well known artificial neural networks (like the MLP), however, are nonlinear static structures. This renders them unsuitable for modelling the human motor system.

Static neural network structures can be modified to model dynamics by buffering the input signal with a tapped delay line. The difficulty with this technique is primarily in setting the temporal depth of the buffer. A finite memory horizon must be decided *a priori*. Where the required buffer depth is very, long the required complexity of the network grows, limiting the utility of the technique.

Recurrent neural networks, where feedback is employed within the network, are capable of modelling dynamic systems without explicitly setting the buffer depth. Long temporal dependencies can be modelled using these structures due to an internal adaptive trade-off between temporal depth and accuracy. The training algorithms required by recurrent networks, however, are much more complex and are strongly architecturally dependent (Campolucci, 1998).

Examples of network types were studied for their feasibility as the dynamic system identification technique employed by the human motor control system.

2.4.1 Cerebellar Model Articulation Controller (CMAC)

The CMAC is particularly appealing in the AMT context as it was inspired directly by the structure of the cerebellum (Albus, 1975). The network offers a possible functional analogue of the cerebellar microzone circuits and was therefore considered potentially

suitable for nAMT. The CMAC is simple, very computationally efficient and ideally suited to on-line training. The simple Albus CMAC uses binary local basis functions.

The CMAC falls into the Associative Memory Network (AMN) class of neural networks which includes Radial Basis Function (RBF) networks, Kanerva's Sparse Distributed Memory Model (KSDMM) and B-spline networks. The differences between these AMNs are minor, with each being a small structural variation of a basic pattern.

The CMAC model employs a lattice network which divides the input space a priori into a rectangular lattice. This has its advantages and disadvantages. The structure is simple to construct and the mapping is cheap to compute. Unfortunately as the input dimensions increase the memory requirements of the method increase exponentially, which has been referred to as the 'curse of dimensionality' (Haykin, 1994). This can be eased using a hash coding scheme, at the expense of introducing noise into the network. It is also possible to use a coarser lattice in higher dimensions to reduce the problem (Albus, 1979). In any case the astronomical number of connections in the cerebellum means that each microzone circuit may harbour as many as 40 million weights (Albus, 1979) which seems adequate for reasonably high-dimensional functions.

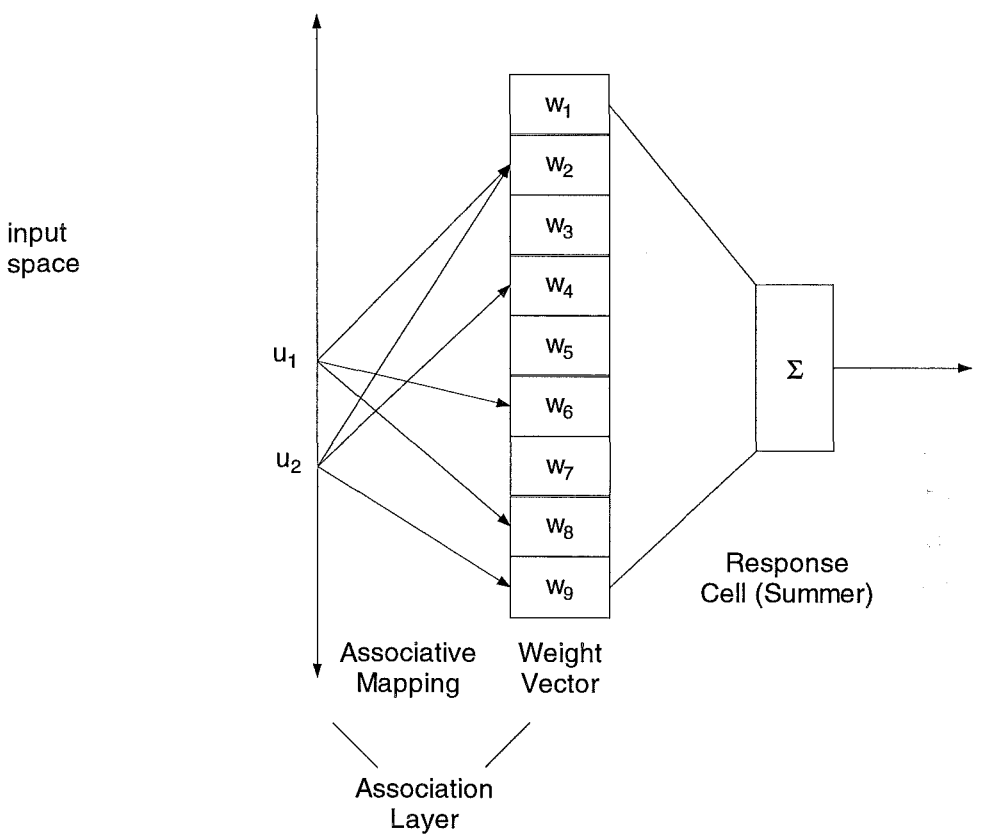

Fig. 23. CMAC maps inputs u1 and u2 to a set of weights. The weights selected by each mapping are termed association cells. Where these cells overlap, as in this example, generalization occurs. The weights are summed to generate an output.

2.4.1.1 CMAC Modelling Capacity

To assess the performance of the Albus CMAC as a nonlinear dynamic system identification element for nAMT, a number of simulations were performed. The CMAC proved capable of converging quickly to the forward model of an arbitrary static nonlinear system, which is in agreement with the literature (Albus, 1979; Brown et al., 1994). Multi-dimensional CMAC structures with tapped delay inputs were used for dynamic systems. For modelling general dynamic systems a high-dimensional (at least 30) tapped delay-line input is required. If each dimension can take on, say , 100 distinguishable values, this requires $100^{30} = 10^{60}$ weights! To simulate this calculation in digital circuitry memory hashing is essential so that memory requirements can be reduced to a more realistic level (say 10^6 weights). Hashing of this sort introduces a lot of noise into the system. Simulations showed that, given sufficient input dimensions and a large enough association vector size, the CMAC would converge tolerably to nonlinear systems (2nd and 3rd order Volterra nonlinearities were tested).

2.4.1.2 CMAC in AMT

Despite the representational capacity of the system, little success was achieved using CMAC as the system identification element in AMT simulations. The binary CMAC model showed a tendency to introduce instability into the system when unexpected inputs or disturbances were encountered. Since the model employs local binary basis functions, the model output often produces discontinuous step changes in its output. When embedded in an AMT control loop this characteristic tends to lead to instability. The corrective action of the optimal trajectory generator often generates input values outside the previously trained input space of the inverse model, producing a sudden step change in the output thereby leading to oscillation and instability. The extreme local nature of the binary basis functions, therefore, seems inappropriate and suggests a move to Gaussian-type basis functions.

The network operates well in feedforward control simulations where the input range is well defined in advance and most of the training can occur offline and preferably very slowly.

Modelling of dynamic systems with the CMAC also introduced difficulties. Since the CMAC requires a buffered input with approximately 30 inputs in this application (giving a buffer depth of 1.5 s at 20 Hz) the hashing needs to be extreme, even on the most modern computers. This introduces a large amount of noise into the system and tends to produce unacceptable performance. It was also noted that the learning rate for the Albus algorithm was low, though this has been addressed in recent revisions of the CMAC (Brown et al., 1994).

2.4.1.3 Modified CMAC algorithms

The difficulties encountered with the simple CMAC structure triggered a search for alternative nonlinear modelling structures. Modifications of the CMAC structure were investigated, revealing some promising possibilities. For example the Fuzzified CMAC , or FCMAC (Nie et al., 1994), attempts to apply a fuzzy control approach. This results in an efficient way to deal with arbitrarily dimensioned inputs without quantisation of the input space. The algorithm uses a Kohonen self-organizing map to assign reference vectors and a fuzzy rule set for addressing. This is effectively a move from algorithm based addressing (as in Albus's scheme) to similarity measure based addressing. In essence, the FCMAC moves the CMAC a step towards radial basis function network generality and releases the algorithm from its set lattice structure. This would ease the storage problem associated with the traditional CMAC. Generalized CMAC structures using non-binary basis functions have also been suggested.

These schemes, though possibly appropriate, introduced considerable additional complexity to the system. The CMAC structure was, therefore, set aside so that other promising structures could be investigated.

2.4.1.4 Possible role for CMAC

The characteristics of the CMAC system - slow learning and difficulty in adapting to new systems but a large representational capacity - allow it to fit very nicely as a model of the relatively stable MCS inverse model. Since the inverse MCS needs to be adapted only slowly over the lifetime of an individual and undergoes no rapid switching or modification most of the difficulties associated with CMAC inverse control are avoided.

The MCS is extremely complex and requires a network with excellent representational capabilities. A CMAC style network with sufficient memory and time to learn should be capable of learning a complex inverse of this type to sufficient accuracy. Given that the cerebellum contains over half the brain's neurons it would certainly appear to meet the memory requirement. The slow development of motor skills during development is also consistent with a slow tuning process as we learn to control our bodies during childhood. Consequently, it is suggested that in AMT the cerebellum be considered to harbour an inverse model of the muscle control system (MCS^{-1}) in a CMAC style network. This inverse would be connected in cascade with less accurate but substantially faster adapting inverses of the external and biomechanical systems. Further characterization of adaptation to changes in the muscle control system are required to test this suggestion.

2.4.2 Locally Recurrent Neural Networks

It was considered highly desirable to find a network free of the necessity to decide on a buffer depth a priori. This led to the investigation of the class of *recurrent neural networks.* Recurrent neural networks include internal feedback within the network. Where delays are also included this allows recurrent networks to represent dynamic functions. Locally

Recurrent Neural Networks (LRNNs) are a sub-class of the more general recurrent neural network. In these structures adaptive Infinite Impulse Response (IIR) linear filters are employed within the network structure. This allows a variety of architectures to be devised depending on how the IIR filter is included in the network structure. The earliest architecture to be investigated was the IIR-MLP, where static synapses of a standard multi-layer perceptron network (Rumelhart et al., 1986) are replaced with IIR adaptive filters (Back et al., 1991). Campolucci provided a succinct review of proposed LRNN structures (Campolucci et al., 1999).

By constraining the structure of a fully recurrent neural network the LRNN approach allows simplified training algorithms to be devised. On the other hand, the powerful modelling capacity of each neuron allows the overall size of the network to be minimized. It has also been pointed out that LRNN networks have pre-wired forgetting behaviour (Frasconi et al., 1992) which is useful for system identification and the control of time-varying systems.

The most powerful feature of locally recurrent neural networks is their ability to dynamically trade off the temporal depth and memory resolution. This means the temporal features of the problem at hand do not need to be known a priori, as they do for a CMAC with buffered input. LRNN networks do not show the "finite memory horizon" introduced by the buffered input in the CMAC. The question of how long to set the buffer and how much memory to assign to each input dimension are circumvented in a LRNN.

2.4.2.1 Dynamic Neural Units

Gupta, Rao & Nikiforuk (1993) suggested a form of locally recurrent neural network specifically intended to model the dynamics of groups of biological neurons. The *dynamic neural unit* (DNU) was developed to provide an alternative to ANN models which are merely a "parody of biological neural structures". A fully connected network of DNUs is effectively a special case of the activation feedback LRNN (Frasconi et al., 1992). Instead of each synapse possessing dynamics, as in the case of the classic IIR-MLP, in a DNU network the soma itself exhibits the dynamics. The fully connected DNU network employed in this work has an identical structure to an MLP network (see Fig. 22), except that each neuron is a DNU possessing somatic dynamics. These dynamics are implemented as IIR filters constructed using the *direct canonic realization* for computational efficiency (Baher, 1992) (see Fig. 24). Simple single layer DNU networks have been shown to work well in control applications (Rao, Gupta et al., 1993; Seong-Wook et al., 1995).

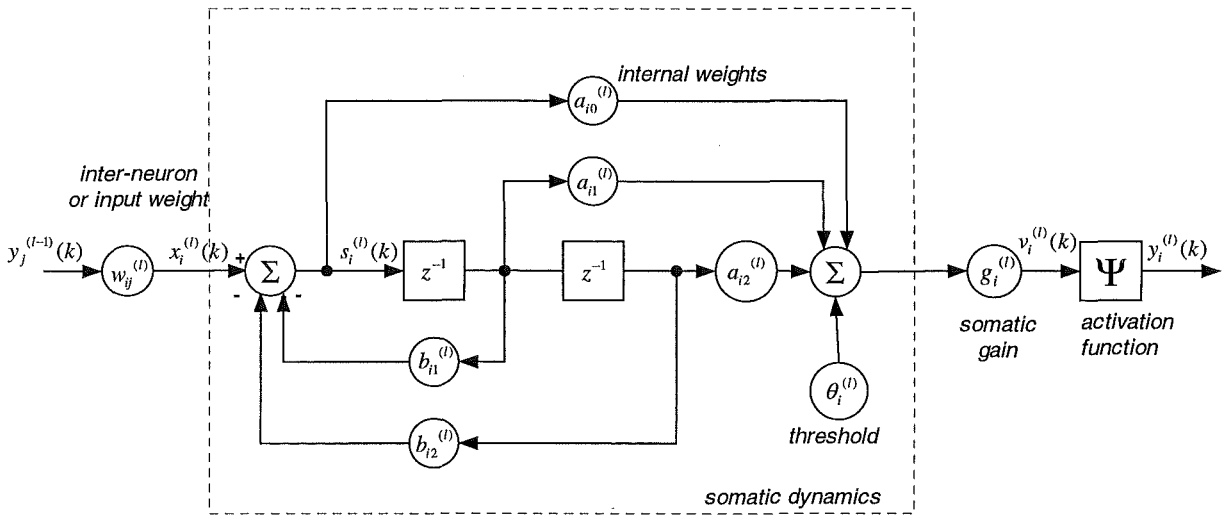

Fig. 24. Dynamic neural unit (DNU) structural diagram. This represents the i^{th} DNU on layer l of a fully connected network. This is a 2nd order DNU (L = 2).

The neurobiological analogy employed in a DNU network is effectively a dynamic equivalent of the MLP biological analogy (section 2.3.1.3). A network of DNUs can be thought of as representing a network of interconnected clusters of neurons. Complexly interconnected groups of neurons can be found in the motor circuits of the brain, particularly in the basal ganglia (see section 1.2.4). The basal ganglia are considered, in AMT, to possess internal models of external systems (E, see section 1.4.4.1). DNU networks may, therefore, be particularly suitable for computational simulation of the formation of internal models of E.

It has also been shown that a DNU network satisfies the Stone-Weierstrass theorem and is thus capable of approximating any continuous function to arbitrary accuracy (Rao & Gupta, 1993). For consistency with established practice, each DNU element will henceforth be referred to as a neuron.

2.4.2.2 DNU Multi-layer Network Adaptation Algorithm

The original DNU training algorithm employs a simple gradient descent approach (Rao, Gupta et al., 1993). Extension of the training algorithm to multiple layers requires a form of back-propagation training. An adequate multi-layer generalization of the training algorithm for multi-layer on-line dynamic back-propagation has never been specified in the literature. Consequently, a suitable training algorithm for a multi-layer DNU network was derived.

The resulting algorithm was found to be a Back-Tsoi type dynamic learning algorithm (Back et al., 1991) and the recent enhancements for the improvement of learning rate at the expense of complexity for such algorithms are therefore applicable (Campolucci et al., 1997).

2.4.2.3 Algorithm Details

The description of this algorithm makes use of the notation shown in Fig. 24.

The input to the somatic dynamics $x_i^{(l)}(k)$ for neuron i on layer l can be expressed as

$$x_i^{(l)}(k) = \sum_{j=1}^{N_{l-1}} y_j^{(l-1)}(k) w_{ij}^{(l)}, \tag{11.4}$$

where $w_{ij}^{(l)}$ is the weight between neuron i in layer l and neuron j in layer $l-1$, $y_j^{(l-1)}$ is the output of neuron j in layer $l-1$ and N_u is the number of neurons in layer u.

The activation value $v_i^{(l)}(k)$ for this neuron can then be calculated as

$$s_i^{(l)}(k) = x_i^{(l)}(k) - \sum_{p=1}^{L-1} \left[b_{ip}^{(l)} s_i^{(l)}(k-p) \right], \tag{11.5}$$

$$v_i^{(l)}(k) = g_i^{(l)} \left[\sum_{p=0}^{L-1} \left[a_{ip}^{(l)} s_i^{(l)}(k-p) \right] + \theta_i^{(l)} \right]. \tag{11.6}$$

where L = order of the IIR somatic dynamics (usually set to 2). $a_{ip}^{(l)}$ are the feedforward IIR weights and $b_{ip}^{(l)}$ are the feedback IIR weights for this neuron (layer l, neuron i). The output is generated by passing the results through the nonlinear activation function Ψ, so that the neuron output $y_i^{(l)}(k)$ is

$$y_i^{(l)}(k) = \Psi\left(v_i^{(l)}(k)\right). \tag{11.7}$$

Learning Rule

The standard performance index employed in neural networks, the squared error, is used in this algorithm allowing us to define the performance index to be minimized E

$$E = \sum_{n=1}^{N_T} \left(d_n(k) - y_n^{(T)}(k) \right)^2 \tag{11.8}$$

where $d_n(k)$ is the n^{th} desired output at time t and T is the total number of layers.

Let $\rho_i^{(l)}$ represent any adaptable parameter in the i^{th} neuron on layer l, then with the gradient descent method and the chain rule

$$\Delta\rho_i^{(l)} = -\frac{\mu}{2}\frac{\partial E}{\partial \rho_i^{(l)}} = -\frac{\mu}{2}\frac{\partial E}{\partial v_i^{(l)}(k)}\frac{\partial v_i^{(l)}(k)}{\partial \rho_i^{(l)}} = \delta_i^{(l)}\frac{\partial v_i^{(l)}(k)}{\partial \rho_i^{(l)}} \tag{11.9}$$

where μ is the adaptation coefficient

$$\delta_i^{(l)}(k) = -\frac{\mu}{2}\frac{\partial E}{\partial v_i^{(l)}(k)}. \tag{11.10}$$

Sensitivity Signals

$\frac{\partial v_i^{(l)}(k)}{\partial \rho_i^{(l)}}$ is often called the sensitivity with respect to parameter $\rho_i^{(l)}$. Unique sensitivity expressions must be derived for each parameter in the network.

Feedforward Weights

By direct inspection of (11.6)

$$\frac{\partial v_i^{(l)}(k)}{\partial a_{ip}^{(l)}} = g_i^{(l)} . s_i^{(l)}(k-p), \tag{11.11}$$

so this signal can be calculated directly from $s_i^{(l)}(k-p)$ within the filter (see Fig. 24).

Feedback Weights

Using the z-transform

$$\frac{\partial v_i^{(l)}(k)}{\partial b_{ip}^{(l)}} = \frac{\partial V_i^{(l)}(z)}{\partial b_{ip}^{(l)}}, \tag{11.12}$$

$$\text{where} \quad V_i^{(l)}(z) = g_i^{(l)} \left[X_i^{(l)}(z) \frac{\sum_{p=0}^{L-1} \left[a_{ip}^{(l)} z^{-p} \right]}{1 + \sum_{p=1}^{L-1} \left[b_{ip}^{(l)} z^{-p} \right]} + \theta_i^{(l)} \right]. \tag{11.13}$$

Using the chain rule

$$\frac{\partial V_i^{(l)}(z)}{\partial b_{ip}^{(l)}} = \frac{\partial V_i^{(l)}(z)}{\partial u} \frac{\partial u}{\partial b_{ip}^{(l)}}, \tag{11.14}$$

$$\text{let } u = 1 + \sum_{p=1}^{L-1} \left[b_{ip}^{(l)} z^{-p} \right] \tag{11.15}$$

$$\Rightarrow \frac{\partial u}{\partial b_{ip}^{(l)}} = z^{-p} \tag{11.16}$$

$$\frac{\partial V_i^{(l)}(z)}{\partial u} = -X_i^{(l)}(z) \frac{\sum_{p=0}^{L-1} \left[a_{ip}^{(l)} z^{-p} \right]}{u^2} \tag{11.17}$$

$$\frac{\partial V_i^{(l)}(z)}{\partial b_{ip}^{(l)}} = -X_i^{(l)}(z) \frac{\sum_{p=0}^{L-1} \left[a_{ip}^{(l)} z^{-p} \right]}{\left(1 + \sum_{p=1}^{L-1} \left[b_{ip}^{(l)} z^{-p} \right] \right)^2}. \tag{11.18}$$

Input Weights

Also using the z-transform

$$\frac{\partial v_i^{(l)}(k)}{\partial w_{ij}^{(l)}} = \frac{\partial V_i^{(l)}(z)}{\partial w_{ij}^{(l)}} \tag{11.19}$$

and from (11.4)

$$X_i^{(l)}(z) = \sum_{j=1}^{N_{l-1}} Y_j^{(l-1)}(z) w_{ij}^{(l)} \tag{11.20}$$

and, referring to (11.13)

$$\frac{\partial V_i^{(l)}(z)}{\partial w_{ij}^{(l)}} = g_i^{(l)} Y_j^{(l-1)} \frac{\sum_{p=0}^{L-1} \left[a_{ip}^{(l)} z^{-p} \right]}{1 + \sum_{p=1}^{L-1} \left[b_{ip}^{(l)} z^{-p} \right]}. \tag{11.21}$$

Somatic Gain

By inspection of (11.6)

$$\frac{\partial v_i^{(l)}(k)}{\partial g_i^{(l)}} = \sum_{p=0}^{L-1} \left[a_{ip}^{(l)} s_i^{(l)}(k-p) \right] + \theta_i^{(l)}. \tag{11.22}$$

Threshold

Also by inspection of (11.6)

$$\frac{\partial v_i^{(l)}(k)}{\partial \theta_i^{(l)}} = 1. \tag{11.23}$$

This brings us to the backpropagation stage of the derivation. We need to find an expression for delta error relative to each layer. Using (11.10) and the chain rule, note that

$$\begin{aligned} \delta_i^{(l)}(k) &= -\frac{\mu}{2} \frac{\partial E}{\partial v_i^{(l)}(k)} \\ &= -\frac{\mu}{2} \frac{\partial E}{\partial y_i^{(l)}(k)} \frac{\partial y_i^{(l)}(k)}{\partial v_i^{(l)}(k)} \\ &= -\frac{\mu}{2} \Psi' \left[v_i^{(l)}(k) \right] \frac{\partial E}{\partial y_i^{(l)}(k)} \end{aligned} \tag{11.24}$$

So we simply need to find $\dfrac{\partial E}{\partial y_i^{(l)}(k)}$.

$$\frac{\partial E}{\partial y_i^{(l)}(k)} = \begin{cases} -\left(d_i(k) - y_i^{(T)}(k)\right) = -e_i & for\ l = T \\ \sum_{j=1}^{N_{l+1}} \frac{\partial E}{\partial y_j^{(l+1)}(k)} \psi'(v_i^{(l)}) \frac{\partial v_j^{(l+1)}(k)}{\partial y_i^{(l)}(k)} & for\ 1 \le l \le (T-1) \end{cases} \quad (11.25)$$

The difficulty here is in calculating $\frac{\partial v_j^{(l+1)}(k)}{\partial y_i^{(l)}(k)}$. Applying strict static back-propagation:

$$\frac{\partial v_j^{(l+1)}(k)}{\partial y_i^{(l)}(k)} = g_i^{(l)} . a_{i0}^{(l)} w_{ji}^{(l)}, \quad (11.26)$$

so that the error is back-propagated through the dynamic IIR filter without regard to the dynamics. This completes a full derivation of a gradient descent type adaptation algorithm for the case of a multi-layer network of DNUs.

The result is strictly correct according to the instantaneous performance index E as defined in (11.8). It has recently been shown (Campolucci et al., 1999) that performance can be improved by minimizing E over the entire input sequence (as in back-propagation through time (Werbos, 1990)) at the expense of additional computational complexity. The extended method results in equation (11.25) being a non-causal function, necessitating an approximation so that the algorithm can implement on-line adaptation. The resulting causal algorithm exhibits approximately a 5 dB reduction in the asymptotic mean square error, but does not justify the increased algorithmic complexity for our purposes. Refinements to this learning algorithm are a possibility for further investigation.

2.4.2.4 Stability Control Technique

The stability of the DNN structure can be assured by restricting the poles for each IIR filter within the network so that they fall within the unit circle. This can be achieved using a nonlinear squashing function (Campolucci et al., 1998). The resulting structure allows a higher adaptation rate to be used. In practice, however, it was found that performance was not improved significantly since the adaptation algorithm itself was still able to go unstable. The modified algorithm was, therefore, rejected in favour of the standard algorithm. It was found that provided the adaptation rate was kept low the structure was suitably stable.

2.4.2.5 Linear Bypass

The LRNN and adaptation algorithm derived above is capable of representing arbitrary nonlinear dynamic functions. The performance of the system was , however, found to be relatively poor for simple linear systems. Learning was slow relative to a simple adaptive FIR filter and, importantly, relative to human performance. To bring online performance up to a reasonable level it proved necessary to add parallel linear

bypass circuitry (as described in Widrow et al., 1985). This reduced the load on the nonlinear LRNN, allowing it to model only the nonlinear aspects of the task. The resulting performance improvement was considerable. The linear adaptive FIR filter employed in AMT (see section 1.4.4.3), which was based on a neurobiologically plausible cerebellar model , was used to construct this linear bypass.

2.4.2.6 LRNN Performance Evaluation

To demonstrate the performance of the resulting LRNN system identification architecture a representative system identification task was performed. A nonlinear dynamic plant was constructed by concatenating a linear dynamic system and a nonlinear system to form Wiener type dynamic nonlinearity. The adaptation rate of the network was set to 10^{-5}. A pseudo-random input signal was generated which was scaled into the range [-1,1] with 0.6-Hz bandwidth and linear statistical characteristics. The signal had a 3-Hz sample rate and was 180 samples long. 32 learning runs through the same input signal were performed (epochs). The RMS error of each epoch was compared to judge performance.

A variety of LRNN structures were used. All employed a linear FIR bypass with 64 taps and employed a single hidden layer of dynamic neurons. A linear output layer was employed for dynamic range. The number of dynamic neurons in the hidden layer was varied from 4 to 64. The results are shown in Fig. 25. Results for a network without linear bypass are not shown in the diagram the RMS error for this simulation remained very high (> 60) over the entire 30 runs.

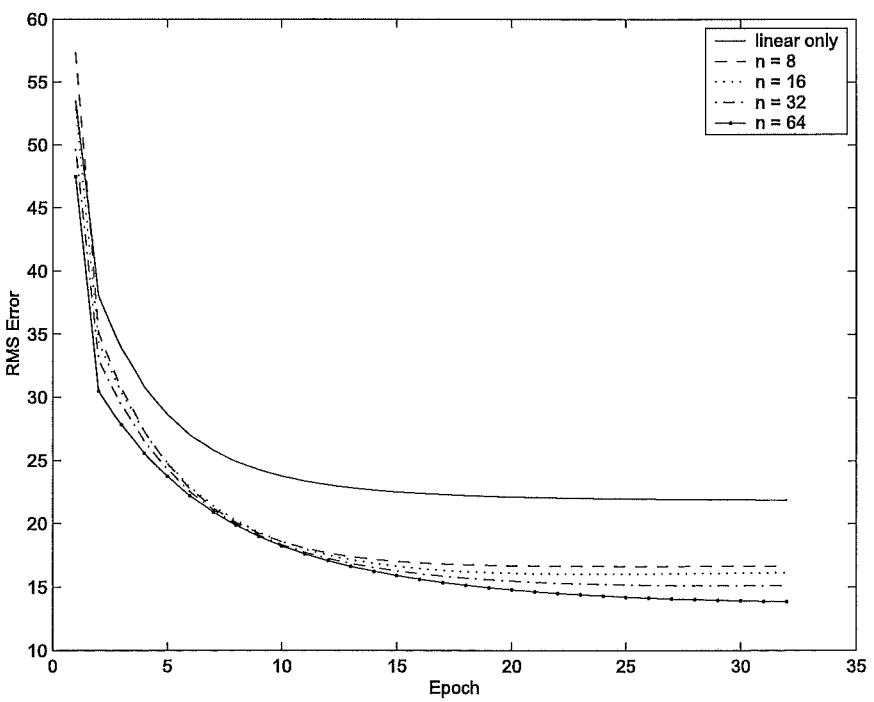

Fig. 25. Performance of input-output nonlinear system identification. n = number of hidden layer units in the LRNN.

The results show a clear advantage over a simple linear system and increasing performance as neurons are added to the network.

2.4.3 Summary

The DNU network specified above proved capable of modelling a variety of nonlinear systems. The structure's neurobiological plausibility, efficiency and performance make it ideal for performing the role of nonlinear dynamic system identification network in nAMT. This is particularly true in the case of modelling the external system, E, which is thought to occur within networks of neurons in the basal ganglia. In particular the DNU type LRNN structure allows nonlinear dynamics of arbitrary temporal depth to be modelled without the a priori specification of a buffer depth. This feature provides a major advantage, in terms of neurobiological plausibility, over buffered neural network models (like simple networks MLP or CMAC) where the temporal depth of the dynamics must somehow be decided before modelling can begin.

The CMAC structure also has the potential to perform well if the structure is generalized to use Gaussian type basis functions. The fundamental limitation imposed by the necessity to buffer the input, however, led to the selection of the LRNN as the modelling element for nAMT.

3. Nonlinear Adaptive Control Structures

Having selected a suitable system identification structure it is necessary to embed this structure in a control architecture capable of achieving acceptable performance. Internal models formed via adaptive system identification form the foundation of AMT. They provide the only source of adaptive performance improvement in the system. Their contribution is, however, worthless if their supporting control structures are inappropriate.

As an inverse control scheme, AMT requires that the adaptive models be utilized to identify an inverse model of the plant. In existing implementations this has been achieved using an adaptive FIR forward model which was analytically inverted, as described in section 1.4.4.3. The formation of a nonlinear dynamic inverse model is mathematically a much more difficult problem. A reliable method for solving this problem needed to be devised.

In addition to finding a method for the formation of a nonlinear dynamic inverse model, it was necessary to decide upon the control structure in which the inverse would operate. The control structure determines how the adaptive feedforward control provided by the inverse model and the adaptive feedback control elements are integrated. In some cases the inverse modelling method itself determines the necessary control structure implicitly, while in other cases more freedom is afforded.

Constraints on possible control structures are imposed by the serial intermittent processing nature of AMT. Looking at all possible structures, however, facilitates a more complete understanding of AMT and its relationship with motor control models. An understanding of these control structures is also of critical importance for understanding the section on the experimental validation of the AMT model which follows (see Chapter 5).

3.1 Control Structures

As discussed in section 1.3.2.5, it is now generally accepted that the human nervous system combines central and peripheral influences to implement some combination of feedforward and feedback adaptive control. There are four basic ways in which these two elements can be combined and each of these will be examined. The structural diagrams in this section are shown with reference to the control of an external system

using visual feedback (i.e., the diagrams representing a manual tracking system). Similar structures could be constructed, by serial or parallel extension, to control the other two divisions of the human plant: the MCS and BM systems.

The necessity for both forward and inverse models is emphasized by the explicit inclusion of a forward model, acting as an observer (see section 4.2.2 for a definition), in the feedback path. Since the forward model is acting as an observer two inputs are shown on the diagrams. The forward model represents an adaptive feedback capacity to complement the adaptive feedforward control of the inverse model.

3.1.1 Parallel combinations

Fig. 26 shows the two possible *parallel* combinations of feedforward and feedback adaptive control. The structures differ only in the location of the summation point where the two control methods are combined. The efferent (α) and afferent (β) processing and transmission delays (totalling approximately 200 ms) in the visual feedback loop are compensated for using a forward model observer to predict the response $\hat{R}(t+\alpha)$ given the motor response $MR(t+\alpha)$ and feedback $R(t-\beta)$. The forward model observer represents adaptive feedback control in these diagrams, though other adaptive structures could also have been used.

Of the two systems shown, Fig. 26b is the more likely to exist in the human control system because the output of the feedback controller MR_{fb} also provides a valid training signal for the inverse. This technique is referred to as feedback-error learning (Kawato et al., 1987) (see section 3.2.4). Since the inverse model may be inaccurate, or even unstable, early in the adaptation process, Fig. 26a would be relatively unstable since the feedback controller acts through the inverse.

In Fig. 26b the error passing into the feedback gain block is represented in sensory coordinates. The output of the controller is added to the output of the inverse model in body position coordinates. This apparent conflict rarely causes a problem assuming K is selected appropriately.

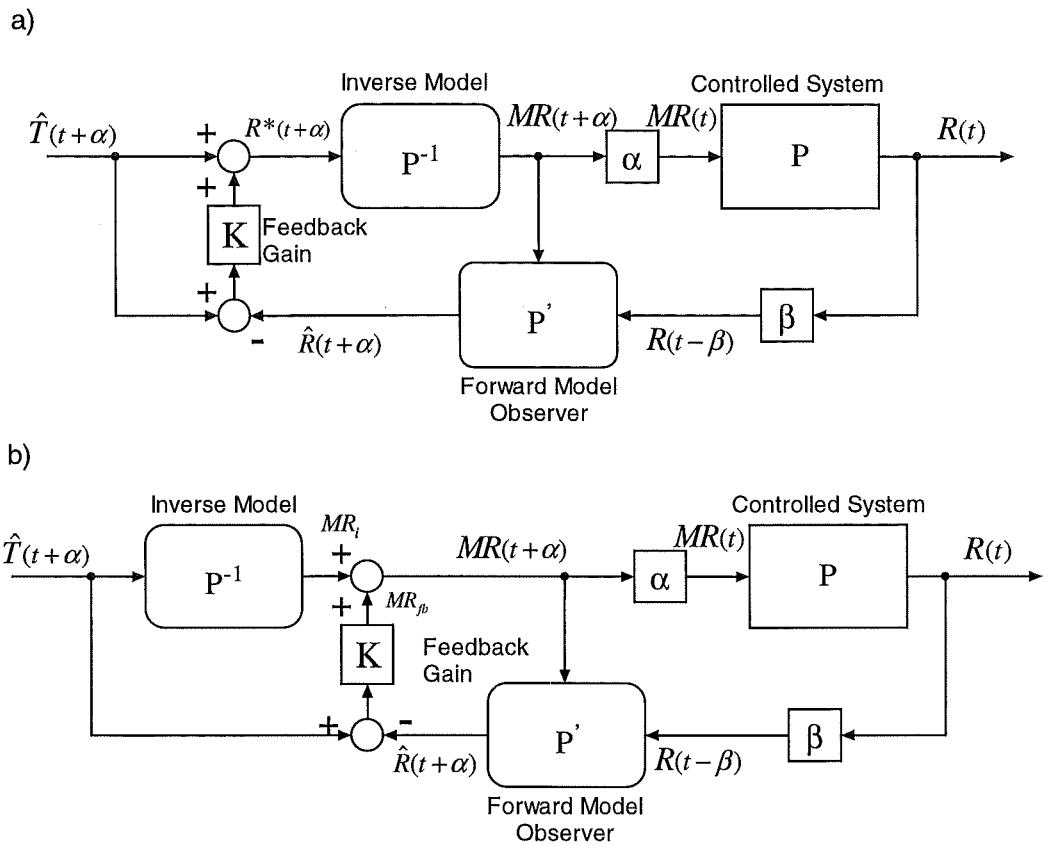

Fig. 26. Parallel combinations of feedforward and feedback control. α is the delay from the brain to the generation of measurable force in the muscles. β represents the delay before visual feedback via the transcortical loop becomes available to the motor circuits. a) Summation before the inverse. b) Summation after the inverse (as in feedback-error learning).

3.1.2 Series Combinations

The other possibility is a series combination of the two control techniques. In principle there are again two choices concerning the point where the pathways are combined. In this case the choice is more straightforward.

An inner feedback loop (Fig. 27a) would require that visual feedback be passed through a second copy of the inverse model and converted to body position coordinates so that a valid error could be calculated by comparison with the output of the primary inverse. The resulting structure would have some appealing features. The error at the output of the feedback controller could be used to train the inverse in a similar way to the FEL structure in Fig. 26b, though the training process would be slower and less stable since the error estimate depends on the accuracy of the inverse model (which will inevitably be low initially).

A more feasible option is an outer closed-loop controller which encircles the inverse (Fig. 27b). One well known structure which uses this mode of feedback integration is the *internal model controller* (Economou et al., 1986). Internal model control is a well established control structure which lends itself to nonlinear systems. Here a forward

model is placed in parallel with the actual system. The difference between the system and model output (the plant disturbance) is then fed back into the forward path. In the forward path are a feedback gain and an inverse model, as shown in Fig. 27b.

A version of the structure in Fig. 27b is also used in adaptive model theory. In AMT the closed-loop controller consists of an intermittent trajectory planner which implements receding horizon optimal control (the OTG, see section 1.4.2.2). AMT is, therefore, related to the internal model control approach. The difficulty with this structure is that the corrective action of the feedback controller must pass through the inverse. When the inverse is inaccurate, as it will be early in learning, the resulting corrective movements may be inaccurate. This makes the structure in Fig. 27b less stable early in learning than Fig. 26b.

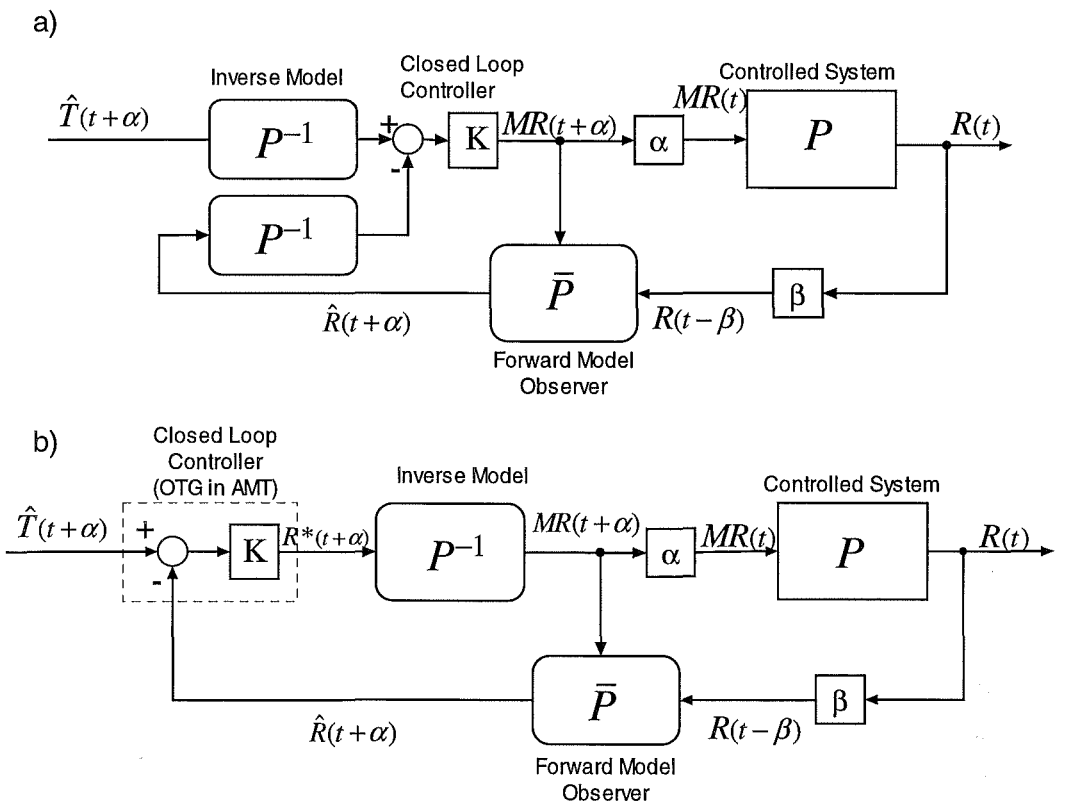

Fig. 27. Series combinations of feedforward and feedback control. a) Feedforward control system with inner feedback loop. Requires feedback through inverse. b) Feedforward control system with outer feedback loop.

3.1.3 Comparison

The preceding investigation revealed that only two of the four possible feedback/feedforward control combinations are really feasible options for the human motor control system. These were the networks shown in Fig. 26b and Fig. 27b. These possibilities correspond to the structures used FEL and AMT respectively. Hence, the

way in which the two models combine feedback and feedforward control is their most fundamental point of difference.

The parallel structure in Fig. 26b has the advantage that a suitable error signal MR_{fb} is available for training the inverse model. Since MR_{fb} is required, the FEL nonlinear inversion technique, as described in section 3.2.4, can be used with this structure alone. The feedback loop acts in parallel, bypassing a possibly inaccurate inverse, so the system is also relatively stable. To accommodate intermittency (see section 1.4.1) in this structure, both the target and response predictions would need to be updated intermittently as opposed to AMT where intermittency arises from a single source – the OTG.

AMT, which uses the serial structure shown in Fig. 27b, proposes that all responses, including corrective movements, are planned intermittently by the closed-loop controller (or OTG, see section 1.4.2.2) in sensory coordinates. Hence, all sensory information is integrated at a single location. A sensory processing bottleneck forms at this location which leads to intermittent response planning (see section 1.4.1).

It is important to note that AMT and FEL are fundamentally tied to their respective serial and parallel combined control structures. They are, therefore, mutually exclusive. While the issue is not looked at here, this observation may provides a way to tell the two models apart experimentally (see section 7.2.5.2).

3.2 Nonlinear Inverse Modelling Methods

In this section we outline five possible architectures for forming nonlinear dynamic inverse models and investigate their suitability for extending AMT to nonlinear inverse control.

Any of the system identification (modelling) approaches described previously could be used in these architectures. The choice of modelling circuitry merely determines the accuracy and biological plausibility of the resulting internal model. The following diagrams contain learning algorithm blocks which take an error signal as input. The learning algorithm attempts to minimize this error signal (usually in a *mean square* sense) by adjusting internal parameters. All of the modelling blocks operate in the same way as for the simple forward model shown in Fig. 18.

In this section, y_d indicates the desired response trajectory, y represents the actual response trajectory, and x is the plant activation signal.

3.2.1 System Error Inversion

System error inversion (see Fig. 28) is the simplest way to generate an on-line inverse model. Here, the inverse is simply placed before the plant and the observed error between the plant output and the target is used as the error signal to train the inverse

model. This inverse modelling approach can serve as a control structure with no modification, and represents a control-while-learning approach. An important advantage of this approach as a control structure is its 'goal-directed' nature. Since the desired output forms the input to the model the inverse is inherently learned over the desired range.

The primary flaw in the structure is that the error at the plant output is used in training rather than the error at the output of the inverse. If this 'system error' is used with LMS adaptive algorithms the inverse is "almost guaranteed to go unstable or find an irrelevant solution" (Widrow et al., 1985). The work of Gupta and associates on both linear and nonlinear inverse controllers, however, makes use of the system error inverse and claims success (Gupta et al., 1992; Gupta & Rao, 1993; Gupta, Rao et al., 1993; Rao, Gupta et al., 1993). It seems likely that the results are tolerable for a class of simple plants.

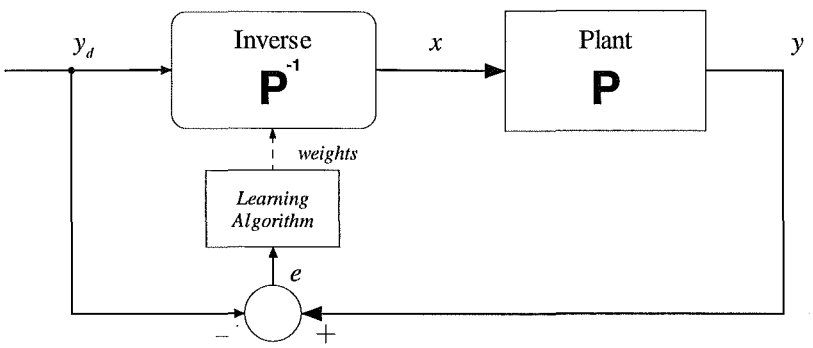

Fig. 28. Inverse modelling based on system error

3.2.2 Direct Inverse Modelling

The direct inverse modelling structure is shown Fig. 29. The structure is an extension of the classical linear adaptive inverse control structure (Widrow et al., 1985). In this approach the inverse model is cascaded after the plant. This arrangement is necessary so that that an appropriate error signal is available (*modelling error* as opposed to *system error*, as mentioned in section 3.2.1). A copy of the inverse model is then placed in front of the plant to complete the control structure.

In general non-linear blocks do not commute, which would seem to prevent an inverse learned in cascade at the output of the plant being used before the plant. Widrow & Plett (1996) claim that nonlinear inverses do commute but Sriharan (1997) notes that commutation is not valid when the inverse is inexact, as it will always be in practical situations.

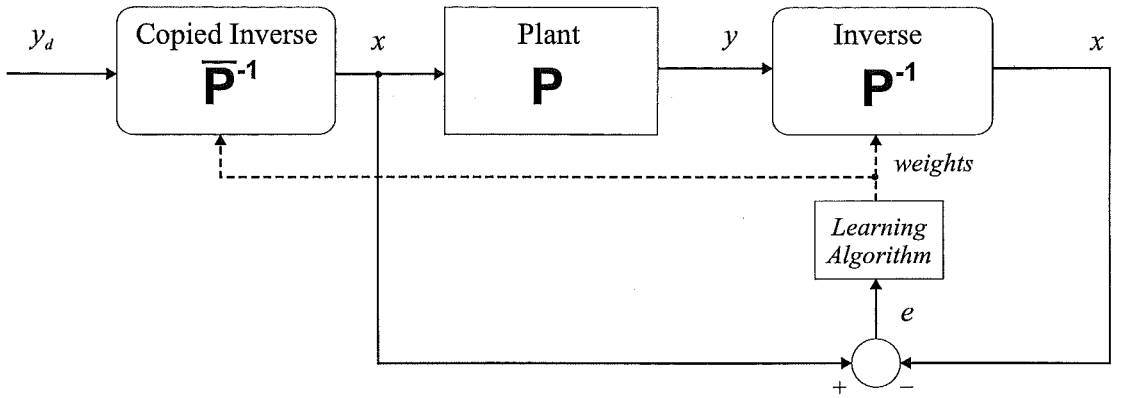

Fig. 29. Direct inverse modelling control structure

The method has the advantage of simplicity but also some fundamental disadvantages:

- This structure cannot be relied upon to produce valid results where only the target signal is applied to the input. This would result in the inverse being learned over an incorrect range. In general, a separate training signal (at x in Fig. 29) must be selected a priori and an appropriate signal is not always easy to define. The structure is not 'goal-directed' (Jordan et al., 1992), in that it requires knowledge of appropriate system inputs as well as of outputs.
- If the correspondence between input and output is not one-to-one then an accurate inverse cannot be obtained (Jordan et al., 1992). A many-to-one mapping will produce an averaged output, which in general is incorrect. Thus, if the goal is to model a broad class of non-linear systems, as it is in AMT, the direct inverse method is problematic.

3.2.3 Adaptive Model Control (Indirect Inverse Modelling)

In Adaptive Model Control (AMC, see Fig. 30), a forward model of the plant is formed and an inverse model is then deduced in some way from the parameters of the forward model (Widrow et al., 1985). A linear version of this scheme is used in AMT, where the inverse is calculated analytically from the forward model parameters. When the forward model is nonlinear a simple analytic mapping from forward to inverse model is unavailable and the transformation is more complex.

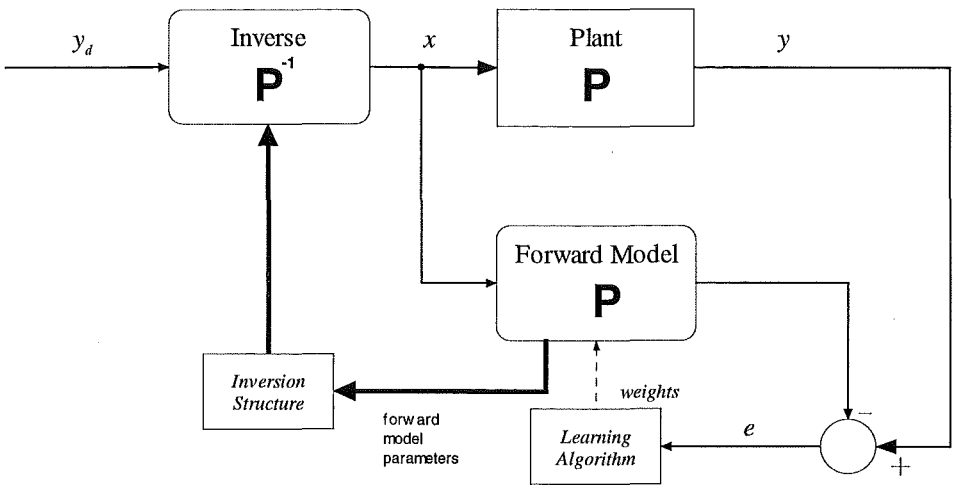

Fig. 30. Adaptive Model Control

3.2.3.1 Quasi-linearisation

When this linear adaptive model control method is used to control a nonlinear plant, the linear model is forced to approximate the nonlinear system about the current operating point. The adaptive algorithm continuously updates the estimate as the operating point moves. More complex schemes can be derived where the models are partitioned to model different input spaces of the plant. Hence, the adaptive algorithm allows a linear structure to approximate the control of a nonlinear plant. This approach is very attractive since linear analysis is well established and easier to understand than nonlinear analysis. The approach is particularly appealing if additional feedback loops, such as those present in AMT, are used to correct any errors introduced by unmodelled nonlinearities. AMT can be considered to employ a simple form of quasi-linearisation whenever a nonlinear plant is used.

The quasi-linearisation approach has been assessed for the case of 2nd order Volterra nonlinearities by Sriharan (1997). Unfortunately the approach proved to be heavily restricted to those nonlinear systems which do not deviate "significantly" from linear systems. While humans were able to learn to control this system, a quasi-linear AMT implementation was unable to control the plant acceptably.

3.2.3.2 Mental Rehearsal

The mental rehearsal algorithm (Fig. 31), a nonlinear adaptive model control method, was suggested by Sriharan (1997) for use in AMT. The scheme is, in fact, very similar to the *filtered ε nonlinear inverse controller* proposed by Widrow (1996). In the mental rehearsal algorithm the inverse model is generated by using direct inversion of a forward model. The forward model is learned online during control of the actual plant. To train the inverse model the forward model is excited either online, using efference copy of the motor response x, or offline using an internally generated signal. When an internal stimulus is employed the inverse model, and hence actual motor performance, improves

without performing an actual task so the approach is analogous to mental rehearsal - hence the name.

Sriharan achieved little success with the structure despite several refinements aimed at avoiding nonlinear commutation. Sriharan concluded that, though it works well for linear systems, the mental rehearsal algorithm is too limited in its ability to invert nonlinear systems in an on-line environment for use in AMT. Consequently the approach was not pursued in this work.

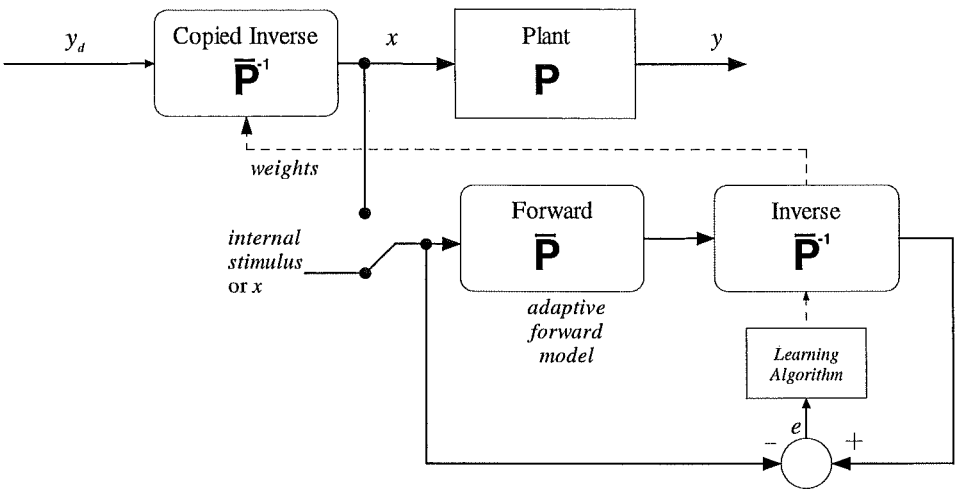

Fig. 31. The mental rehearsal algorithm. Adaptive circuitry not shown (see section 2.1 for details). This scheme uses direct inversion of a forward model to generate an inverse model. To train the inverse model the forward model is excited either online, using efference copy of the motor response *x*, or offline using an internally generated signal. Training with the internal stimulus might be employed for offline refinement of the inverse model, hence "mental rehearsal".

3.2.3.3 Forward-and-inverse Modelling (or Specialized Inversion)

This nonlinear adaptive model control structure, suggested by Jordan and Rumelhart (1992), again places the inverse before the plant and includes a parallel forward model (see Fig. 32). The inverse is trained by observing the error between the forward model (or sometimes the plant) output and the training signal. The error is then back-propagated through the forward model to obtain an appropriate modelling error. This back-propagation process is effectively equivalent to multiplying the system error e_y by the derivative of the output of the forward model with respect to the input dy_f / dx. This results in an approximate modelling error e_x.

The system error can be derived from the output of the plant or of the forward model. Like the simple system error approach, this structure is goal directed and can be used online. Additionally, the structure is theoretically capable of producing an exact inverse even in the absence of an exact forward model, assuming the output of the plant is used to derive the system error (Jordan et al., 1992). Specialized inversion also avoids

the need to commute the nonlinear inverse, thus avoiding the difficulty mentioned in section 3.2.2.

In practical implementation, the forward and inverse modelling scheme is very slow and unreliable where the forward model is not known a priori. The use of the back-propagation algorithm to find the modelling error is also unlikely to occur biologically (see section 2.3.2.4). This is particularly true if backpropagation is used to train the forward model, as in this case the backpropagation of two different error signals through the same structure is required.

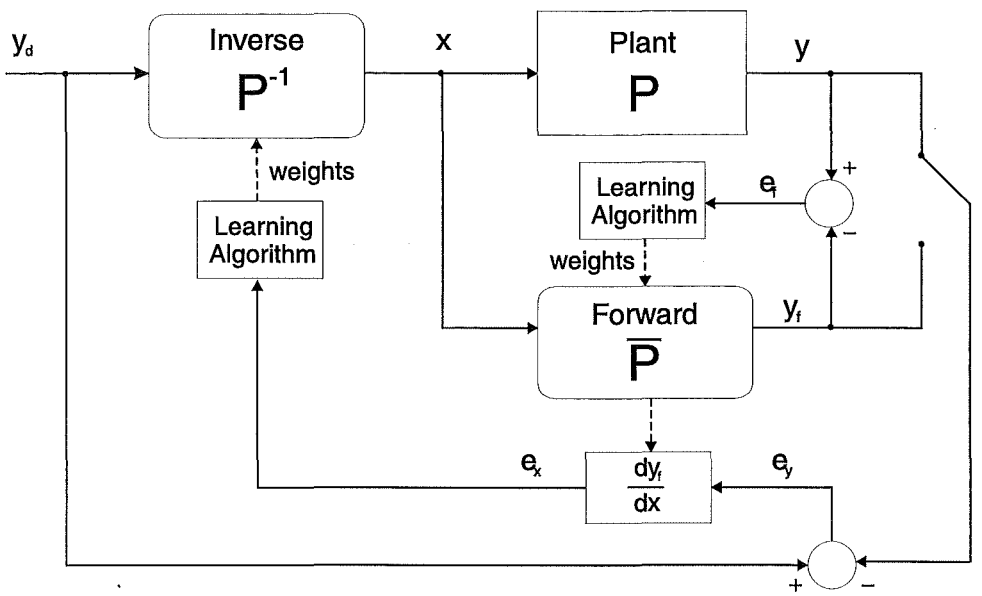

Fig. 32. Forward-inverse modelling structure (as suggested by Jordan). The difference between the input signal y_d and the output of either the plant or the forward model is back-propagated through the forward model. The resulting error signal e_x is a valid error signal for training the inverse model.

3.2.3.4 High-gain Internal Feedback Loop

Both the mental rehearsal and the forward-and-inverse modelling approaches attempt to form an inverse model by making use of an existing internal forward model. In theory an inverse model can always be determined from an accurate forward model since the forward model contains all necessary information. In the two cases looked at previously a unique inverse model was formed with the forward model acting as a sort of teacher.

It is, however, possible to generate an inverse model directly from the forward model by making use of a continuous feedback loop. The idea is based on the simple observation that a forward model placed in a high gain feedback loop approximates the inverse of that model (see Fig. 33).

$$\frac{z}{x} = \frac{1}{\frac{1}{K} + \hat{P}} \tag{12.1}$$

$$\lim_{K\to\infty}\frac{z}{x} = \hat{P}^{-1} \tag{12.2}$$

From (12.1) it can be seen that as K increases, the overall transfer function of the loop approaches the inverse of the forward model $\hat{P}^{-1}$.

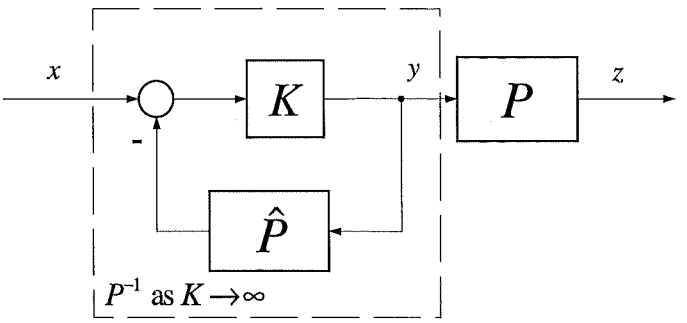

Fig. 33. Feedback loop with forward model in feedback path. Structure approximates an inverse model as $\hat{P}$

This simple and elegant approach has been suggested several times as the physiological mechanism for inverse control in the motor system (Foulkes et al., 2000; Miall, 1999; Miall, Weir, Wolpert et al., 1993; Miall et al., 1996; Wolpert et al., 1998). Unlike FEL, this inversion technique is not tied to any particular control structure and can therefore easily be applied to AMT.

An essential advantage of this approach is its parsimony. Since most motor control models (notably including FEL) contend that forward models are formed and stored *in addition* to inverse models, the storage requirements are essentially halved by removing the need to store a separate inverse model.

Applied to the AMT framework, the forward models would maintain their role in the identification of exafference while simultaneously performing the function of an inverse model by being embedded in an internal feedback loop. Physically, the comparator would need to be located near both the input and output of each model to avoid introducing excessive propagation delays into the internal loop. The inevitable fixed short propagation delays could be compensated for by using predictive forward models. If necessary, stability could be maintained by replacing K with a filter.

In conclusion, then, the high-gain internal feedback loop is the most promising nonlinear adaptive model control technique for application to AMT. For this reason the method was selected for further research and use in nAMT.

3.2.4 Feedback-Error Learning

The feedback-error learning scheme was originally suggested as a full model of human motor control (Kawato et al., 1987). The scheme uses a conventional feedback controller to stabilize the system in the early stages of learning and, simultaneously, to provide the error signal for training an inverse model. As the inverse model improves it

gradually and automatically takes over the control of the system by virtue of the parallel combination of feedback and feedforward control used in the system. Interestingly, similar automatic transfer of control between parallel feedback and feedforward loops was suggested by Jordan (1992) for the forward and inverse modelling structure.

In this structure the necessity to back-propagate the error through the plant, as in forward and inverse modelling, is ingeniously avoided. The inverse model is formed directly with no need for the prior or contemporaneous formation of a forward model. Instability problems in the initial training stages are also cleverly avoided, as the system is under parallel feedback control until the inverse is functioning accurately (an inaccurate inverse will have no effect on the accuracy of the feedback controller). It should be noted, however, that all other methods mentioned here can also be embedded into a parallel feedback loop to improve stability (see section 3.1.1). In FEL this embedding within a feedback loop is essential. The architecture of an FEL controller is shown in Fig. 34.

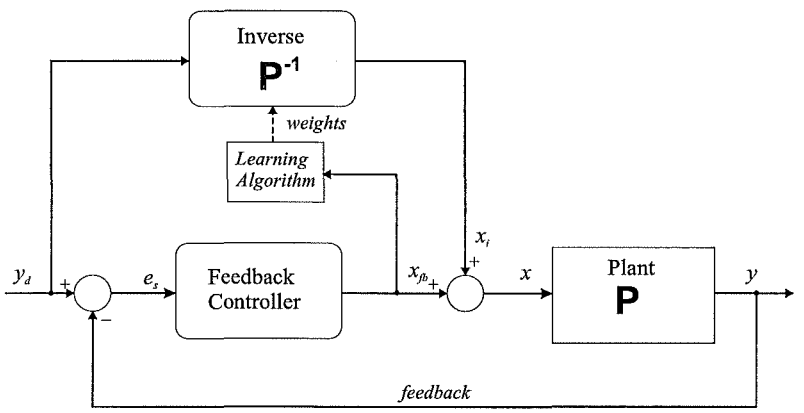

Fig. 34. The feedback error learning (FEL) architecture

Looking at the structure in Fig. 34, the inverse model output x_i and feedback controller output x_{fb} are added to produce x, the control signal for the plant.

$$x = x_i + x_{fb} \tag{12.3}$$

We want the inverse to take over control from the feedback controller as learning proceeds, which implies minimizing the contribution of x_{fb} to the overall control. This is equivalent to minimizing the difference between x (the control effort) and x_i (and inverse model output). An error signal for the inverse model e_i can therefore be defined as follows

$$e_i = x - x_i \tag{12.4}$$

$$\Rightarrow e_i = x_{fb} \tag{12.5}$$

so that the output of the feedback controller is simply used as the error input for the inverse model.

The exact nature of the feedback controller is not critical provided the loop is stable for the given plant. An adaptive feedback controller is often used to overcome the delay inherent in the feedback path (Bhushan et al., 1999a). Since the performance requirements for this feedback controller are low, and the inverse model should quickly take over control, the tuning of the feedback controller is usually not considered to be an important problem (Kawato et al., 1992).

For application to AMT the feedback error learning structure would need to form three inverse models which operate in a serial cascade. The simplest way to form a serial cascade with an FEL structure is shown in Fig. 35.

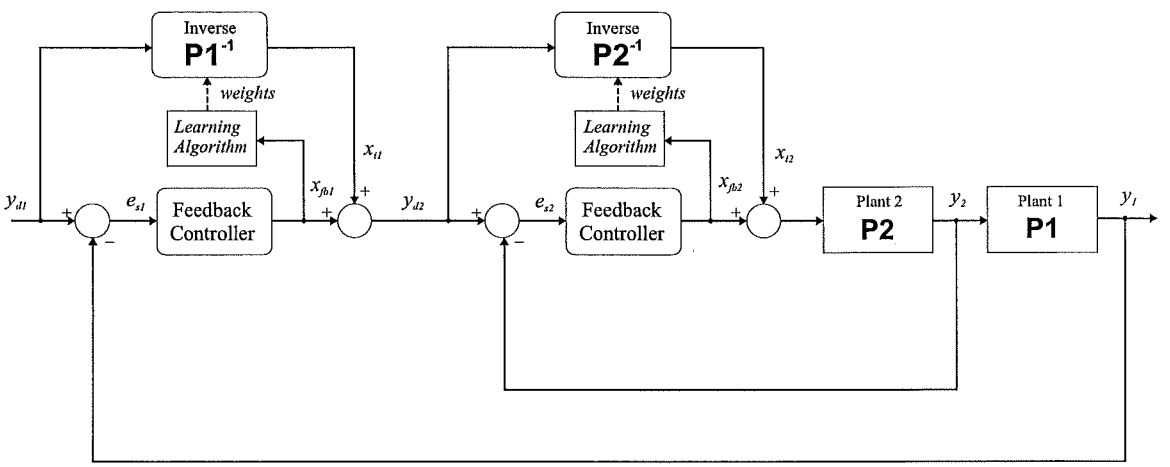

Fig. 35. FEL arranged in a serial cascade (only two serial plants shown).

The problem with this structure is that the inverse models run and adapt serially, destroying the attractive parallel independence of models which are a feature of the AMT model. Additionally, feedback is integrated continuously at the output of each inverse model through the feedback controller. A parallel version of the serial FEL structure was devised which overcomes the serial adaptation problem but maintains the continuous integration of feedback at all levels (see Appendix I for a full development).

Unlike the other inverse modelling approaches covered here, FEL is inextricably tied to its control structure. This makes it virtually impossible adapt to the ingenious learning technique used in FEL to the serial processing structure of AMT. For these reasons, after extensive investigation, the FEL structure was rejected as a candidate for nAMT although it is recognized as a leading alternative motor control hypothesis.

The FEL structure has gained great popularity in the recent literature as it appears to solve the neurophysiological inverse nonlinear modelling problem. This learning scheme cannot, however, be applied to AMT due to fundamental structural differences (see section 3.1.3). Further experimental work is required to settle which motor control model best matches the human control system 7.2.5.2.

3.2.5 Summary

Of all the options listed in this section the most appealing are the feedback-error learning structure and the high gain internal feedback structure.

An FEL control scheme is relatively stable and provides an efficient means for learning the inverse model directly. The structure is also highly neurobiologically plausible unlike the particularly unlikely forward-and-inverse modelling method. The scheme cannot, however, be applied to AMT.

The high-gain internal feedback loop option offers similar advantages to the FEL system. The approach is also more parsimonious than most nonlinear inversion technique since only the forward needs to be learned and stored in memory model (instead of both the forward and inverse models). The question of stability early in learning proved to be of little concern in simulation since the gain can be kept low while the inverse model is trained (see Chapter 6). Importantly, the approach can be applied to any control structure and consequently is applicable to AMT. The structure is also as neurobiologically plausible as FEL. For these reasons this nonlinear inversion technique was pursued in the development of nAMT.

4. Nonlinear Adaptive Model Theory (nAMT) Structural Details

This chapter details a set of proposed alterations to Neilson's linear AMT structure designed to generalize the model to more realistic nonlinear operation. Together, the changes constitute a new variant of AMT which will henceforth be referred to as nonlinear adaptive model theory, or nAMT.

4.1 Stochastic Prediction

The characteristic reaction time delay inherent in the human motor system is caused by a combination of neural transmission delays and processing delays in the brain. It is well established that human subjects are capable of compensating for this reaction time delay when performing pursuit tracking tasks (McDonald et al., 1983; Neilson et al., 1988b; Poulton, 1952, 1957). The delay is represented as a backward time shift and must be compensated for with a forward shift to avoid a delay in the tracking response. The forward shift operation, however, is non-causal and is therefore physically unrealisable. A causal approximation is required and this is achieved through stochastic prediction. There is evidence that the statistical properties of a target signal can be learned by human subjects and used to predict the most likely future location (Jones et al., 1989; Neilson et al., 1988b; Poulton, 1957). Since the reaction time delay is often large relative to the total movement time, 250 to 300 ms for the visuomotor system (Schmidt, 1982; Welford, 1980), the ability to perform stochastic prediction has a major effect on performance.

AMT hypothesises that the stochastic properties of the target and disturbance signals are modelled adaptively in neural circuitry so that an optimum prediction of the future values might be generated (Neilson et al., 1988a, 1988b, 1993, 1995). The existing AMT approach to stochastic prediction is explained in the following sections and a generalization of the existing approach is then suggested and explained.

4.1.1 Linear One-step Predictor

Highly autocorrelated time series, such as those encountered in tracking tasks, can be regarded as arising from a series of statistically independent "shocks" (white noise). In

this framework, a time series, or *stochastic process*, is generated by passing white noise through a filter which defines the stochastic properties of the process (Box et al., 1970). In system identification a general linear stochastic process is often modelled with the following relationship (Box et al., 1970; Ljung, 1999):

$$y(t) = H(q)e(t) \tag{13.1}$$

where $y(t)$ is the value of the process at time t and e(t) is a white noise process with zero mean and variance λ. $H(q)$ is a linear filter capturing the stochastic properties of $y(t)$. q is the foreward shift operator, so that $y(t).q = y(t+1)$. A linear stochastic process y(t) can thus be generated as shown in Fig. 36.

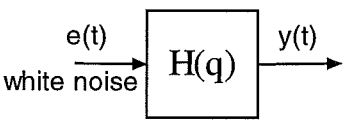

Fig. 36. General linear stochastic signal model.

Note that in a discrete system y(t) can equivalently be described as an infinite weighted sum of previous observations of e(t)

$$\begin{aligned} y(t) &= \sum_{k=0}^{\infty} h(k)e(t-k) \\ &= e(t)h(0) + \sum_{k=1}^{\infty} h(k)e(t-k) \end{aligned} \tag{13.2}$$

where h(k) is the impulse response of H(q).

In practice, the summation of (13.2) must be truncated, giving a finite weighted sum of n observations of e. This results in a moving-average (MA) model as was used by Neilson in the AMT predictor (Neilson et al., 1992):

$$y(t) = e(t)h(0) + \sum_{k=1}^{n-1} h(k)e(t-k). \tag{13.3}$$

Note that other parametrizations of (13.1) are possible and these will be elaborated upon later.

At time t-1 only the term e(t)h(0) is unknown. Since $e(t)$ has zero mean, $E[e(t)h(0)] = 0$ and consequently the optimum prediction of $y(t)$ at time t-1 is simply

$$\hat{y}(t \mid t-1) = \sum_{k=1}^{n-1} h(k)e(t-k). \tag{13.4}$$

It is important to note that this can be implemented with a standard FIR filter if e(t) is delayed by one sample and the following transformation is made

$$\hat{y}(t \mid t-1) = \sum_{k=0}^{n-2} h'(k)e(t-k-1) = H'(q)e(t-1) \tag{13.5}$$

where $h'(k) = h(k+1)$ for $k \geq 0$.

It also follows from (13.2) and (13.4), scaling so that h(0)=1, that

$$\hat{y}(t \mid t-1) - y(t) = e(t) \tag{13.6}$$

which reveals that the one-step prediction error is a white noise signal and hence exhibits zero autocorrelation.

4.1.1.1 Parameter Estimation Method

In AMT the prediction-error approach to parameter estimation is employed to form the stochastic model $H'(q)$. The LMS method is used to form an online adaptive predictor, though other online techniques are mathematically valid (Ljung, 1999). LMS was selected for use in AMT on the same neurobiological grounds that the algorithm is used for forward modelling (see section 1.4.4.3). This technique is acceptably robust and widely used in practical signal-processing problems (Ljung, 1999; Widrow et al., 1985). The goal of the parameter estimation circuitry is to generate the linear MA model H'(q) and this is achieved using a standard adaptive LMS FIR filter.

An appropriate adaptive circuit for forming $H'(q)$ is illustrated in Fig. 37. The adaptive filter tunes so that the one-step prediction error is itself entirely unpredictable (i.e., is white noise). In AMT models $H'(q)$ is a an adaptive NLMS FIR filter (Neilson et al., 1992) (see section 1.4.4.3). Note that Fig. 37 is functionally identical to the circuitry specified in the original AMT structure (Neilson et al., 1992; Sriharan, 1997).

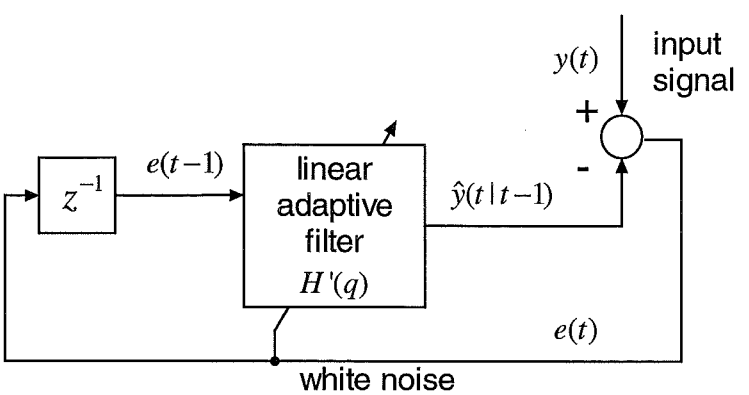

Fig. 37. Circuitry for forming moving average (MA) stochastic model H'(q) of the input signal.

4.1.2 Linear 'n'-step Predictor

Once the MA model H'(q) has been formed it can be used to generate an 'n'-step prediction as defined by

$$\hat{y}(t+n \mid t) = \sum_{k=n-1}^{\infty} h'(k)e(t-k-1+n), \quad n = 1,2,... \tag{13.7}$$

Equation (13.7) can be implemented by progressively stepping $E[e(t+n)] = 0$ into the filter H'(q). This can be achieved recursively by running the filter in accelerated time or by spreading the filter out in a cascade structure. Standard AMT employs a cascade structure since this is more neurobiologically plausible (Neilson et al., 1992).

4.1.3 Predictor Model Structure

The use of an MA model structure of (13.3) in the original AMT model was an arbitrary choice. Though the structure performs well at predicting most signals other model structures could equally have been used to form the one-step predictor. There is no specific justification for the use of this structure in the existing literature.

The effect of employing other model structures for the predictor was investigated as a prelude to the nonlinear generalization to follow. In linear system identification there are three basic model structures: the Moving-Average (MA) model, the Auto-Regressive (AR) model and the more general Auto-Regressive Moving-Average (ARMA) model. Mathematically the three structures are equivalent for infinite time depth, since they all approximate the general linear model of (13.2), but the choice of model structure becomes important when dealing with real systems where the parametrization is necessarily finite. The choice of structure determines how many parameters are required to achieve a particular degree of accuracy in the model. Hence, a sensible model leads to a parsimonious (efficient) description of the system. Parsimony is an essential property when a model is implemented in a physical system, like the human brain, since information storage capacity is finite.

4.1.3.1 Auto-Regressive (AR) Model

The moving-average MA model of (13.3) expresses the stochastic process y(t) as a function of a finite number of previous observations of the random shock signal e(t). In contrast, the auto-regressive model (AR) model expresses y(t) as a function of a finite number of previous observations of itself. The AR equivalent of (13.3) is

$$y(t) = \sum_{k=0}^{n-1} a(k)y(t-k) + e(t)\,. \qquad (13.8)$$

where n is the order of the linear model.

The resulting LMS predictor circuitry is shown in Fig. 38.

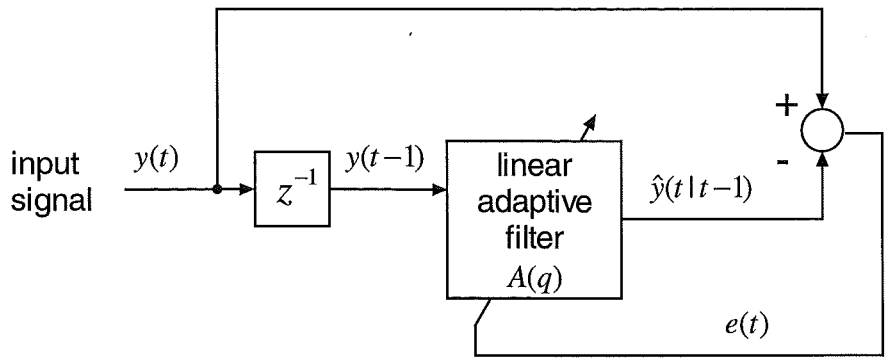

Fig. 38. Circuitry for forming an auto-regressive (AR) stochastic model A(q) of the input signal.

4.1.3.2 Auto-Regressive Moving Average (ARMA) Model

The ARMA model combines the AR and MA type models to produce a more flexible and general model.

$$y(t) = \sum_{k=0}^{n-1} a(k)y(t-k) + e(0)h(0) + \sum_{k=1}^{n-1} h(k)e(t-k) \qquad (13.9)$$

The predictor circuitry (Fig. 39) in this case requires two inputs. Each input enters its own adaptive filter the outputs of which are them summed to form y'(t|t-1)

ARMA models are typically more parsimonious than individual AR or MA models (Box et al., 1970). Mathematically, an AR process has an autocorrelation function that is infinite in extent (trailing off asymptotically) while its partial autocorrelation function is finite (cutting off instantaneously). Conversely, a MA model has a finite autocorrelation function and its partial-autocorrelation function is infinite in extent. The ARMA model combines both properties and is able, in principle, to represent systems both with infinite autocorrelation and partial-autocorrelation functions. This endows the ARMA model with the ability to model a wider range of systems.

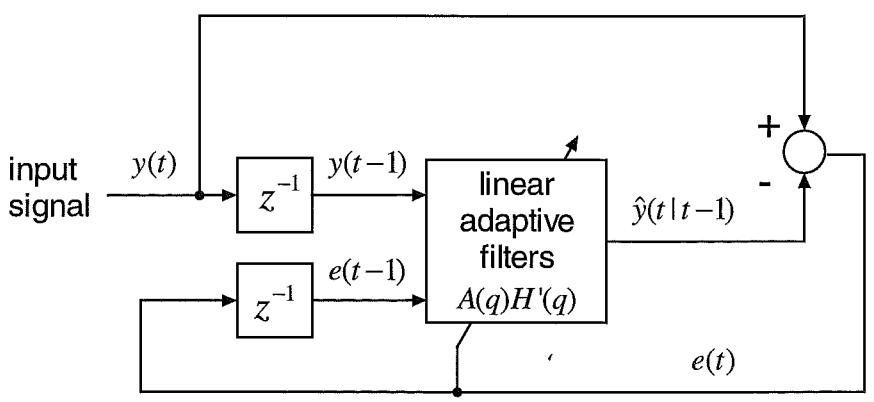

Fig. 39. Circuitry for forming an auto-regressive moving-average (ARMA) stochastic model $A(q)H'(q)$ of the input signal.

4.1.3.3 Linear Model Performance Comparison

A simulation study was carried out to compare the performance of the existing MA model with an AR type model and the more general ARMA model. A 180 sample input signal with a 3 Hz sample rate was generated by passing white noise through a 0.6 Hz low pass filter followed by a static nonlinearity. The signal exhibited nonlinear dynamic stochastic properties for realism, since nonlinear signals are often encountered in reality, and so that performance could be directly compared with the nonlinear prediction schemes mentioned later. The signal was then applied 200 times (200 training epochs) to each of the three one-step predictor structures previously described. The RMS error in the prediction across each epoch was then calculated and plotted. The same number of adaptive parameters (32) was used for all models (the two FIR filters in the ARMA model each had 16 parameters). The adaptive filters were trained as detailed in section 1.4.4.3, except that the standard LMS algorithm, as opposed to NLMS, was employed (see (Widrow et al., 1985)). The adaptation coefficient $\mu = 1 \times 10^{-5}$.

The results (see Fig. 40) show that the ARMA model produced superior results for the nonlinear dynamic input signal. The experiment was repeated with several other inputs to test the generality of this result. Similar results were obtained for an input signal with linear dynamic statistical characteristics and a 20 Hz sample rate (not shown). The incumbent MA model structure again exhibited the worst performance.

The poor MA test results are likely be specific to the input signals under study which were produced by passing white noise through an FIR low-pass filter and static nonlinearity. This imposes an autoregressive structure on the signals. The optimum parametrization for a signal depends on the stochastic structure of the signal, hence just as these signals yielded to parametrization with an AR model, other signals are better suited to parametrization with a MA model. In all cases, however, the mixed ARMA model produced better results. This is consistent with Box & Jenkins (1970) where they note that a mixed autoregressive-moving average (ARMA) model is often necessary to achieve the best parametric parsimony. That is, more often than not the ARMA model achieves the most efficient representation. Since we have no a priori knowledge of the signal characteristics in this application the most general model is probably the most appropriate.

Consequently, it is suggested that the MA model used in AMT be replaced with an ARMA model to achieve superior performance in AMT under a wider range of conditions. Simulation results suggest that the ARMA model often provides a performance advantage using the same number of parameters.

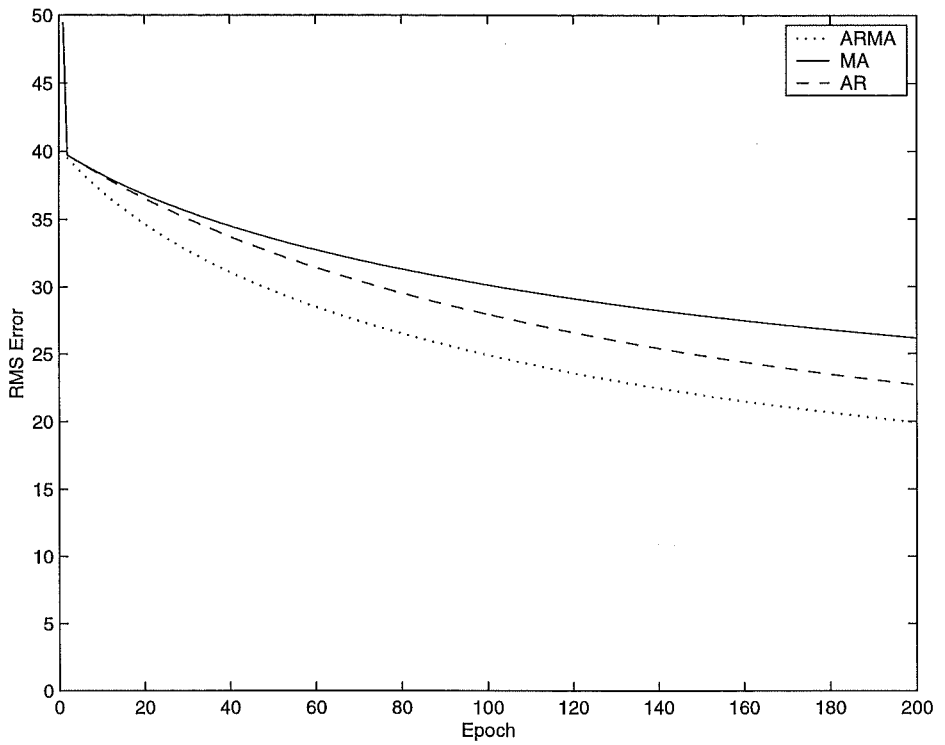

Fig. 40. Relative performance in one-step prediction for 3 linear models. ARMA is the most efficient model.

4.1.4 Nonlinear One-step Predictor

While the linear models examined so far produce acceptable results, the generality of the approach is limited by the basic assumption of linearity. In reality few time series have linear stochastic properties and the model can therefore only approximate the true statistical characteristics of the signal[3]. It is therefore necessary to generalize the prediction methods so far examined to the nonlinear case. This can be achieved using the LRNN modelling circuitry developed previously (see section 2.4.2).

The general linear model of (13.1) can be generalized to nonlinear systems. A general nonlinear black-box model can be formed by concatenating two mappings (Ljung, 1999). The first mapping forms a regression vector $\varphi(t)$; the second maps this vector to the output. Regressors are typically chosen in the same way as for linear models, and this is the logical choice for this application. We can generalize (13.1) as follows

$$y(t) = f(\varphi(t)) \qquad (13.10)$$

[3] As a simple example, a signal exhibiting increased variance on one side of its mean has nonlinear stochastic properties, e.g  .

where the regressor $\varphi(t)$ is, in this case, formed from past observations of the e(t) and $f(x)$ is some nonlinear dynamic mapping.

In practice the nonlinear mapping will be provided by a neural network, specifically the LRNN network. The choice of regressor is of primary importance in determining model performance. By analogy with the linear case it is possible to use AR, MA and ARMA type regressors to form NAR, NMA and NARMA models (Bonnet et al., 1997; Connor et al., 1994).

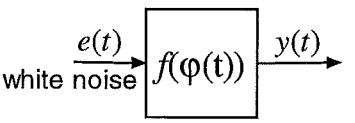

Fig. 41. Proposed general nonlinear stochastic signal model.

Thus the functional descriptions of each model are as follows:

Nonlinear Moving Average (NMA) model

$$y(t) = f\left[e(t)h(0) + \sum_{k=1}^{n-1} h(k)e(t-k)\right] \tag{13.11}$$

Nonlinear Auto-Regressive (NAR) model

$$y(t) = f\left[\sum_{k=0}^{n-1} a(k)y(t-k)\right] + e(t) \tag{13.12}$$

Nonlinear Auto-Regressive Moving Average (NARMA) model

$$y(t) = f\left[\sum_{k=0}^{n-1} a(k)y(t-k) + e(0)h(0) + \sum_{k=1}^{n-1} h(k)e(t-k)\right]. \tag{13.13}$$

Since there is a strong analogy with the linear models of section 4.1.3 the same predictor structures can be employed. The only alteration necessary is that the linear FIR filter modelling elements must be replaced with nonlinear neural network filter modelling elements.

4.1.4.1 Absolute versus Differential Models

AMT specifies that the input to the predictor is a differenced version of the actual signal, $\nabla y(t) = y(t) - y(t-1)$. This causes the circuitry to form a model of the change in signal as opposed to modelling absolute level. In practice this provides a strongly beneficial effect on performance for on-line prediction of linear stochastic processes.

Modelling the change in input position, rather than the absolute position, also provides a better match with observed human behaviour. When a human is unable to predict the change in target position, the response lags the target by a reaction time delay (Neilson et al., 1993). When the differenced model cannot predict the target the one-step prediction $\nabla\hat{y}(t \mid t-1)$ becomes zero, so that the output is $\hat{y}(t \mid t-1) = y(t-1)$. Hence, the model matches human behaviour since the predicted signal lags the actual signal by one reaction time.

Unfortunately, in moving to a nonlinear prediction strategy this simple differential approach becomes impossible because a nonlinear model requires absolute position information. Conversely, moving to a model based entirely on absolute position produces unacceptable performance (see section 4.1.4.2).

This difficulty has been solved in this thesis by dividing the model into parallel linear and nonlinear sub-systems and providing these with differential and absolute inputs respectively. The outputs of the parallel sub-systems are added together and the error signals adjusted accordingly. It has already been suggested that nonlinear modelling circuitry in the brain operates in parallel with a linear circuit, since this produces large benefits in on-line learning performance (see section 2.4.2.5). This is, therefore, a natural modification to the model.

The resulting network exhibits improved performance in predicting nonlinear signals without any degradation in performance for predicting linear signals. The complete network for a NARMA one-step predictor is shown in Fig. 42. All the other models studied here are special cases of this network.

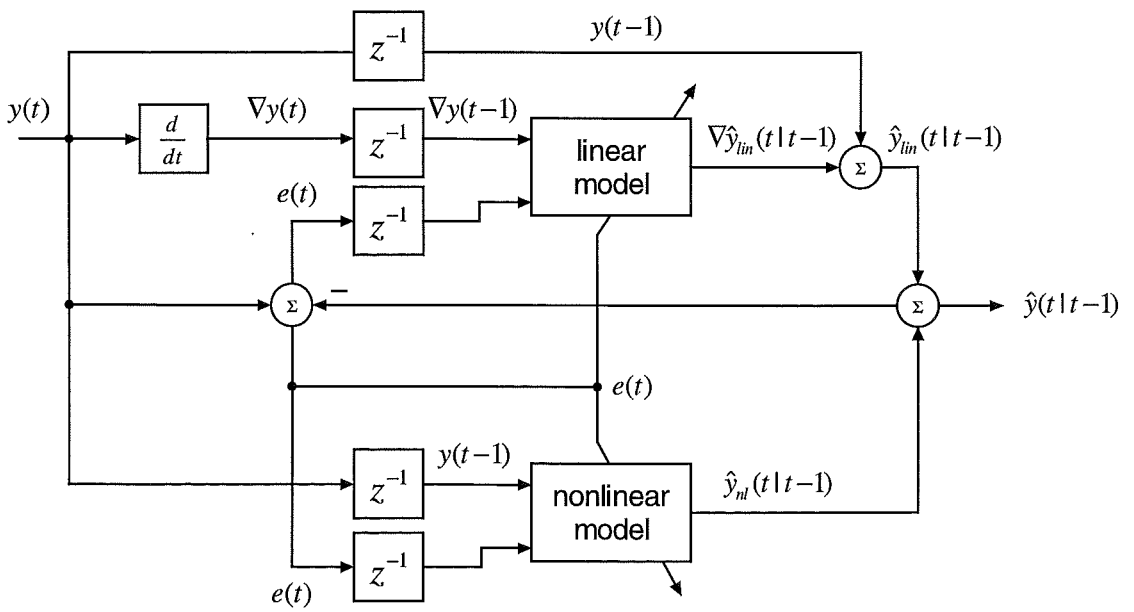

Fig. 42. Circuitry for forming a nonlinear auto-regressive moving-average (NARMA) stochastic one-step predictor. The circuitry uses a novel combined parallel differential-linear and absolute-nonlinear structure.

4.1.4.2 Nonlinear Model Performance Comparison

The performance of the NAR, NMA and NARMA models at predicting a stochastic signal generated with a nonlinear filter was tested. The test was set identically to that described in section 4.1.3.3. All nonlinear models consisted of 2 layer LRNNs with 16 hidden units. The three nonlinear models were compared directly with the unmodified AMT MA model. The results are shown in Fig. 43.

A purely absolute NARMA model (in which the differentiator at the input to the linear model was removed) was also tested. The results were very poor and are consequently not shown in Fig. 43; the model generated an RMS error of 198.9 in the first epoch and took 185 epochs to reach the same level of performance that the mixed absolute-differential approach achieved in epoch 1. This poor performance, in addition to Neilson's human behaviour argument from section 4.1.4.1, support the necessity for a mixed differential and absolute predictor.

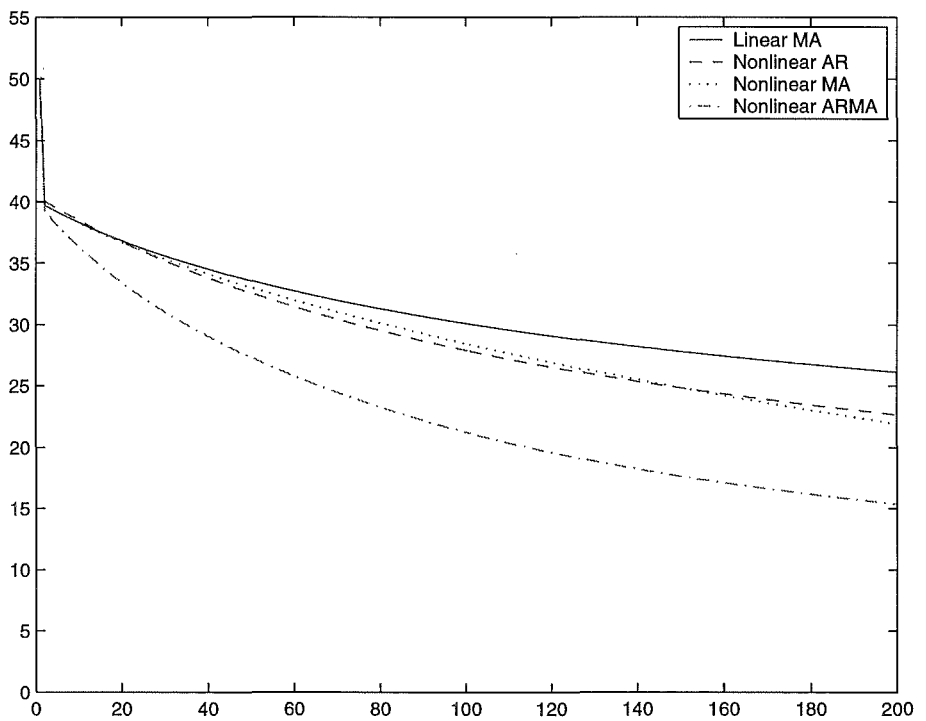

Fig. 43. Relative performance in one-step prediction for 3 nonlinear models. NARMA is the most efficient model.

In these results the NMA and NAR models showed similar performance, with a lower RMS error than the linear MA model. The NAR model is only slightly better than the linear AR model (see to Fig. 40). The NARMA model performed better than all other models examined, including the linear ARMA model.

These experiments confirm the superior parsimony of the NARMA / LRNN parametrization over the linear MA parametrization used in AMT, at least for the signals under study. The result is not surprising since the ARMA model structure combines the mathematical properties of the individual AR and MA models (see discussion in section 4.1.3.3).

Thus, on the basis of the theoretical and experimental superiority of the combined parallel differential-linear and absolute-nonlinear NARMA stochastic prediction method, it is proposed that this technique replace the linear MA model of AMT. Further experimental investigation is required to determine whether the superior performance of this model matches human behaviour more closely than other models. On the basis of parsimony and performance this model is the best candidate.

4.2 Forward Modelling

4.2.1 Existing Structure – Linear Input-Output Forward Model

AMT uses a linear adaptive FIR filter to form a forward model of the controlled system. This model is used for two distinct purposes. Its primary function is to act as an intermediate step in forming an inverse dynamic model. This is possible because a linear forward model can be inverted analytically. Its secondary purpose is for the identification of the disturbance component in the sensory feedback signal. This is achieved by subtracting the output of the forward model, the expected output or *reafference estimate*, from the actual sensory feedback. The remainder is that part of the afference generated by external influences and is called the *exafference*.

An input-output (IO) forward modelling technique is employed in AMT (see Fig. 44). This means that the controlled system output is expressed as a function of its input signal, the motor response $MR(t)$.

$$\hat{R}(t) = \hat{P}(MR(t)). \tag{13.14}$$

AMT employs a Smith Predictor type approach because the loop-delay is cancelled by introducing corresponding internal delays (Smith, 1959). This is accomplished by delaying the motor response to achieve synchronicity with the available response signal $R(t-\beta)$. An error signal, here labelled $\hat{D}(t-\beta)$, can then be generated for training the forward model.

$$\hat{D}(t-\beta) = \hat{R}(t-\beta) - R(t-\beta). \tag{13.15}$$

The internal delay must be accurate and therefore requires the slow adaptive formation of a delay model. This process is aided by the fact that the loop-delay is normally invariant (Foulkes et al., 2000). The delay models, while not explicitly specified,

are implied in the AMT literature, as delays are lumped into a single transmission delay element Δt.

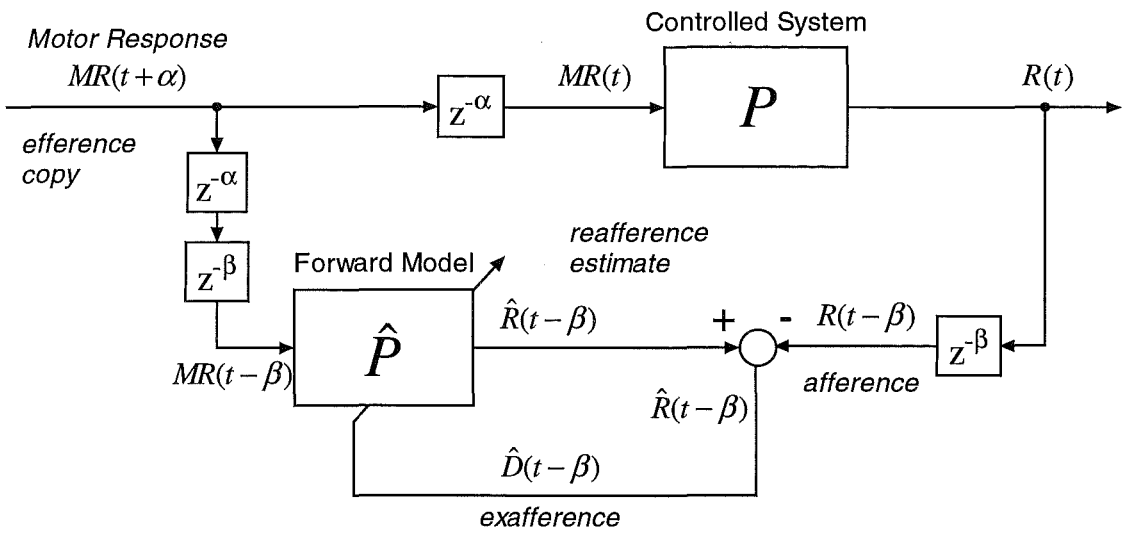

Fig. 44. Existing AMT forward modelling structure. AMT uses an input - output approach.

It is a trivial exercise to generalize the linear forward modelling approach to the nonlinear case provided that a suitable nonlinear modelling structure is available. The LRNN structure introduced in section 2.4.2 is suitable for forming a nonlinear IO forward model. This allows $\hat{P}$ in (13.14) to become a nonlinear dynamic function of $MR(t)$.

4.2.2 Modified Structure – Nonlinear Forward Model Observer

The nonlinear forward model observer (FMO) approach offers a useful alternative to the incumbent IO modelling approach. To form an observer model the plant is represented as a function not only of its current input signal, as in IO modelling, but also as a function of its previous output signals. Thus, observer models include an additional input which can be seen as providing an estimate of the current state of the plant. The method can also be used to improve response prediction (see section 4.3).

A forward model observer expresses the controlled system as a function of its input signal, the motor response $MR(t)$, and the previous sample of the response signal $R(t-\Delta)$:

$$\hat{R}(t) = \overline{P}(MR(t), R(t-\Delta)). \qquad (13.16)$$

The required changes to the AMT structure for the implementation of a forward model observer are shown in Fig. 45. In practice, all that is required is the addition of a

second input to the forward model for the delayed response signal. This can be seen as a state estimation input.

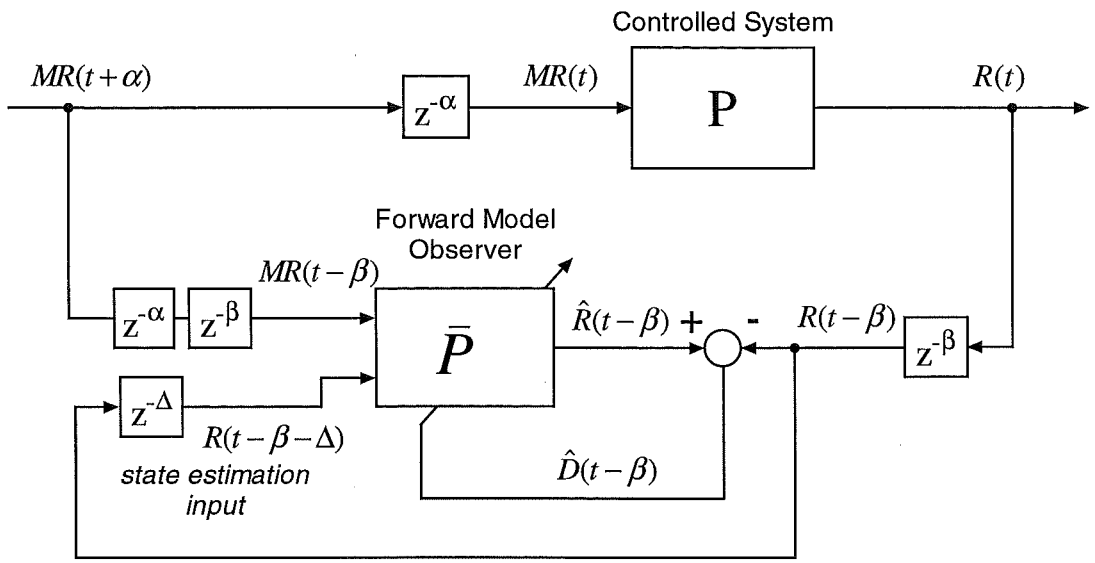

Fig. 45. Suggested forward model observer forward model. The response input can be used for state estimation allowing more accurate response prediction.

The FMO is valid where $\overline{P}$ is linear or nonlinear. For nAMT the LRNN previously described can be provided with an additional input for the delayed sensory response signal. Hence $\overline{P}$ becomes a nonlinear dynamic multiple-input single-output function.

4.2.3 Forward Model Observer compared with Input-Output Modelling

A representative system identification task was performed to confirm the ability of the state-space model to efficiently represent a controlled system in AMT.

A nonlinear dynamic system was formed by cascading a linear dynamic and a nonlinear static system to form a Wiener nonlinearity (these systems were as used in the experimental study of section 5.2.2.1). An autocorrelated signal with 0.6-Hz bandwidth and a 3-Hz sample rate, 180 samples long, was generated and used as input. The adaptation rate was set to $\mu = 1 \times 10^{-5}$. 32 training runs (epochs) were performed and the RMS error of each epoch was calculated for performance comparison. n = 64 units were placed in the hidden layer of the LRNN. The performance of the IO and FMO modelling approaches were thus assessed under identical conditions. Performance with no nonlinear capacity was also tested by setting n = 0, leaving only the linear bypass circuitry in the model. The original AMT implementation corresponds to the n=0, IO model, curve.

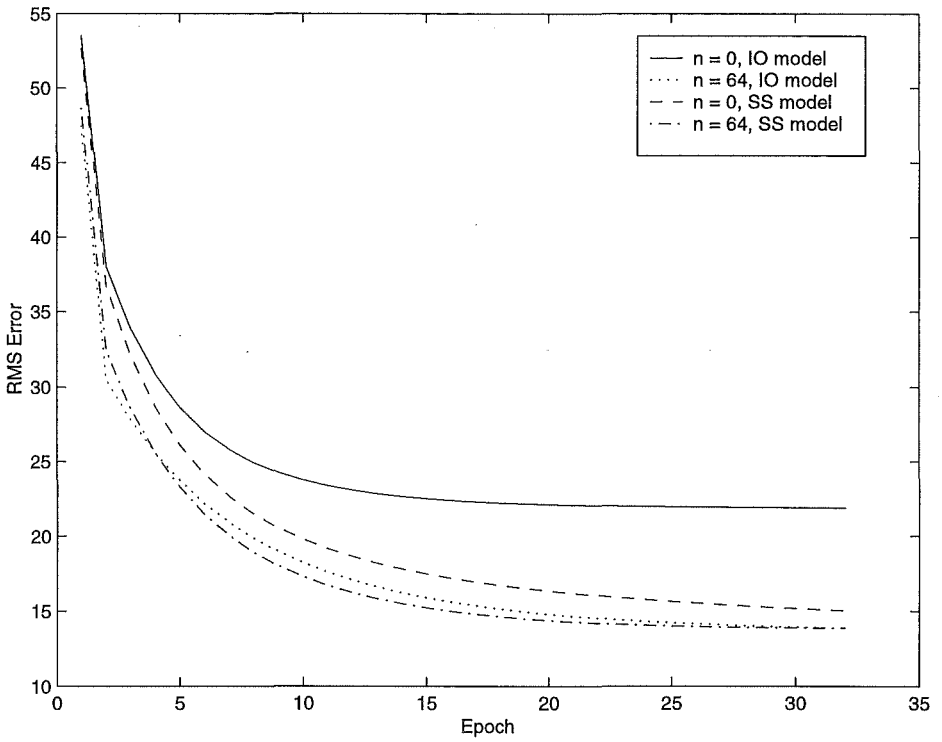

Fig. 46. Comparison of state-space and input-output based modelling approaches. n is the number of hidden units in the LRNN, n = 0 indicates a linear model only.

The results confirm that the FMO produces superior performance to the IO model. The nonlinear forward model observer exhibited the best performance. The linear (n = 0) models showed a strong improvement in moving from the IO to the FMO approach.

The performance of the linear model is almost equivalent to that of the nonlinear model in the FMO case. This is due to the use of an autocorrelated input signal. Since the FMO approach involves estimating change in state as opposed to the absolute state, as in the IO method, a high linear correlation between input samples will make the task of estimating the next sample a relatively simple linear operation – even for a highly nonlinear external system. This reduces the advantage of the nonlinear modelling capacity.

Longer tests runs (200 epochs) showed that the nonlinear model retains a small advantage over the linear model for this input signal. The advantage of the nonlinear model also increases as the degree of autocorrelation in the input signal is reduced. These results are not shown.

4.3 Disturbance Compensation

4.3.1 Existing Structure

In AMT the disturbance signal is modelled as a stochastic process added to the output of a deterministic plant. This allows the disturbance component of motor afference to be identified by subtracting the reafference estimate, generated by the forward model, from the actual afference. The resulting disturbance signal is called the exafference, that part of the sensory feedback "generated by external inputs". The future exafference is then predicted using the stochastic methods mentioned earlier. The scheme is illustrated in Fig. 47.

The stochastic disturbance predictor is important as it bestows on AMT an adaptive feedback control capacity in addition to the adaptive feedforward capacity imparted by the target predictor and inverse model. An adaptive deterministic model in the feedback loop, however, is notably absent. This is addressed in section 4.4.

The AMT disturbance predictor is reminiscent of the motor control model of Miall et al. (1993) suggesting that the cerebellum acts as a Smith Predictor. Additional sophistication is bestowed on the AMT system by the stochastic disturbance predictor and its function for planning future trajectories.

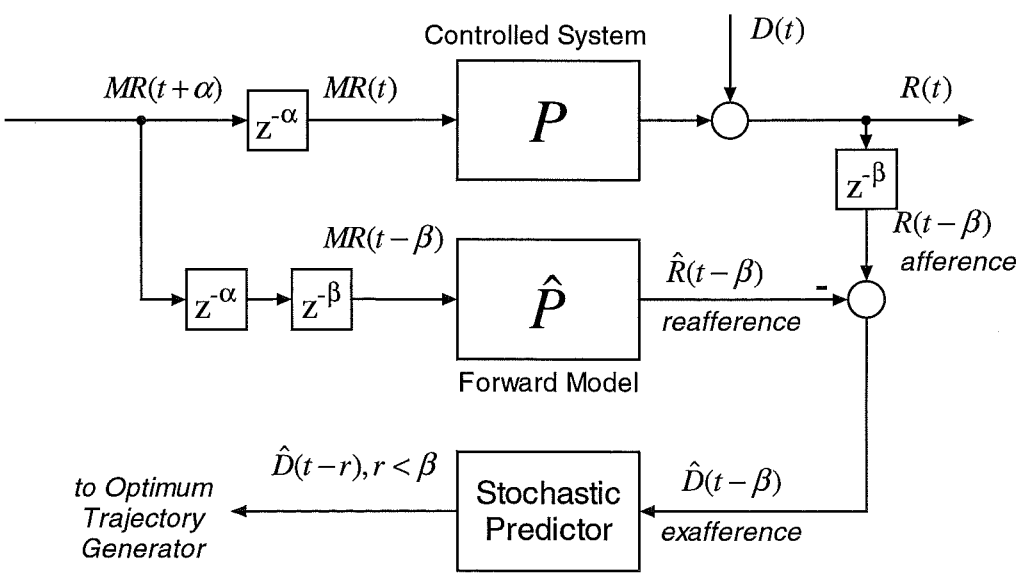

Fig. 47. Existing disturbance prediction scheme

4.3.2 Modified Structure

The existing scheme suffers from some inefficiency related to the fundamental assumption that disturbances are added at the output of the plant. In reality, disturbances are often best considered to affect the internal state of the plant. The effect of a state

disturbance on the output signal is highly dependent on the characteristics of the plant itself. In the existing AMT model the effect of state disturbances must be captured in the stochastic model, leading to a partial replication of the function since both the IO forward model and the stochastic model must represent characteristics of the plant. An observer type forward model, as introduced in section 4.2.3 can, however, be used to prevent state disturbance effects reaching the stochastic predictor (as shown in Fig. 48).

When using a forward model observer, the deterministic effects of disturbances are no longer compensated for by the stochastic disturbance predictor. This implies that they must be accounted by the model in some other way. The solution is to introduce a *deterministic* adaptive model in the feedback path to complement the *stochastic* adaptive model already in place. An *adaptive response predictor,* based on the forward model observer, can be constructed to achieve this (see section 4.4).

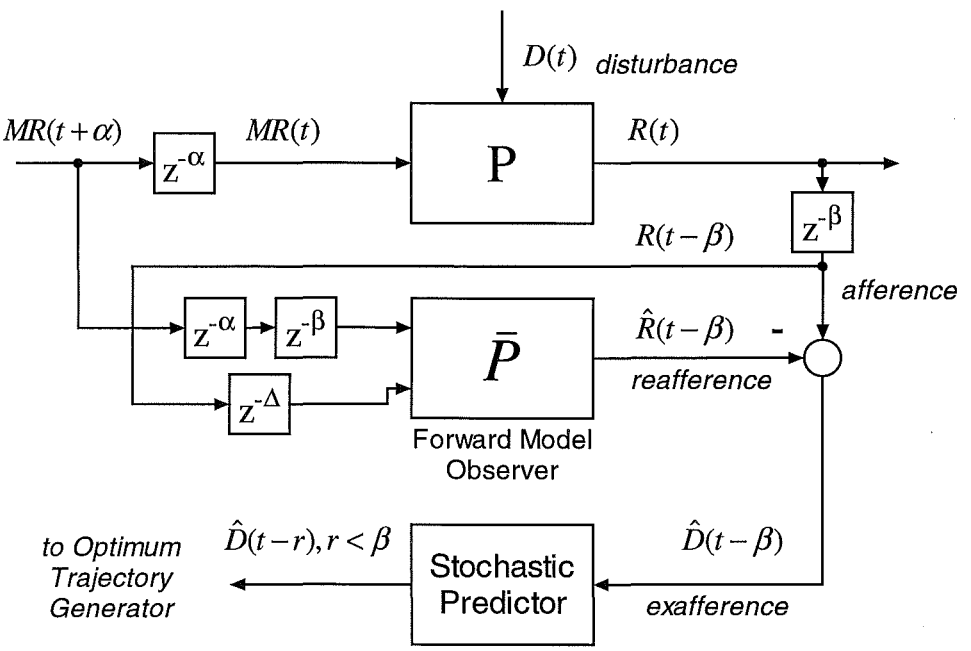

Fig. 48. Modified structure employing state-space model. This change is accompanied by introduction of adaptive response prediction.

The modified disturbance compensation structure (Fig. 48) is essentially unchanged. The forward model now uses the delayed response signal $R(t-\beta)$ to update its internal state estimate, leading to a forward model observer structure. The resulting predicted output $\hat{R}(t-\beta)$ represents the deterministic component of the current response signal (the reafference estimate). This new estimate is based on all available information and not only on the motor response as was previously the case. The result is that the effects of state disturbances are largely removed from the exafference signal.

4.4 Adaptive Response Prediction

4.4.1 Existing Structure

In the existing AMT structure the adaptive element of the response prediction circuitry is entirely contained in the stochastic disturbance predictor (Neilson et al., 1995). Deterministic response prediction is performed entirely inside the optimum trajectory generator (OTG) based on previously planned responses. The predicted response trajectory $\hat{R}(t-r), -\alpha \leq r < \beta$ is generated by applying the differenced responses previously planned for the present time interval and the predicted disturbances to the fed back response signal $R(t-\beta)$.

The scheme does not make reference to the actual motor response in the interval from MR(t-β) to MR(t). While this arrangement is optimal for the linear inverse model employed by AMT, for a nonlinear generalization this can lead to substantial inaccuracy in the prediction.

4.4.2 Modified Structure

The existing AMT structure (see Fig. 47) does not make use of all information available to the system at time t in planning a future trajectory. To generate an exafference signal it is necessary to ensure that the predicted and actual response signals are synchronous. This necessitates delaying the motor response signal by the total loop-delay $\alpha + \beta$ before passing it through the forward model. Consequently, in the existing AMT structure the motor response signal from $MR(t-\beta)$ to $MR(t)$ is not taken into account when predicting the response. When the forward model is more accurate than the inverse this additional information becomes essential for predicting the most likely response trajectory. In linear AMT, the forward and inverse models are equally accurate. In nAMT, however, the forward model will be more accurate than the inverse since, in general, a nonlinear forward model cannot be inverted analytically.

The optimal remedy for this problem is to use the forward model to predict a response trajectory based on $MR(t-r), -\alpha \leq r < \beta$. This could easily be achieved by passing $MR(t+\alpha)$ through the existing forward model to form a prediction $\hat{R}(t+\alpha)$ and then using this predicted response in the OTG. It is important to note that this innovation would be of no benefit in linear AMT because the linear inversion process is precisely accurate. Consequently, the response predicted using this method is identical to the desired response and, hence, the substitution would be redundant. In a nonlinear generalization, however, it is highly desirable.

Further benefit can be gained if the forward model employed has an observer structure. In this case, state predictions, based on the available response signal $R(t-\beta)$,

can be used to improve the accuracy of the response prediction. Hence, the predicted response will remain accurate despite a disturbance to the controlled system. This arrangement can only be employed when the disturbance prediction method is also based on an observer estimate to ensure that state disturbances are only compensated for in one place.

4.4.3 Response Predictor Implementation

Assuming a forward model observer is available, a *predictive cascade* of these models can be formed to generate the response predictions from $\hat{R}(t-\beta+\Delta)$ to $\hat{R}(t+\alpha)$ in steps of size Δ in time. These accurate predictions can then be used by the OTG (see section 1.4.2.2) in planning future sub-movements. The predictive cascade is suitable for predictions up to $t+\alpha$, up to which time motor response information is available. For predictions beyond this, up to one planning time period tp ahead of $t+\alpha$, the existing method based on the pre-planned desired response can be used for prediction. The predictive cascade of forward models is shown in Fig. 49.

The method takes the most recently available response information $R(t-\beta)$ and passes this into the state-estimation input of the forward model observer. Delayed motor response information $MR(t-\beta+\Delta)$ is passed into the other input and the model produces a response estimate for $\hat{R}(t-\beta+\Delta)$. This new response estimate is used as the state-estimation input to the next forward model in the cascade and so on until $\hat{R}(t+\alpha)$ has been generated.

The modified response predictor thus formed captures the deterministic effects of state disturbances and the effects of recently issued motor commands in an optimum prediction of the response signal at time $t+\alpha$. This allows the disturbance predictor (section 4.3) to focus on predicting stochastic disturbances which are independent of the properties of the plant.

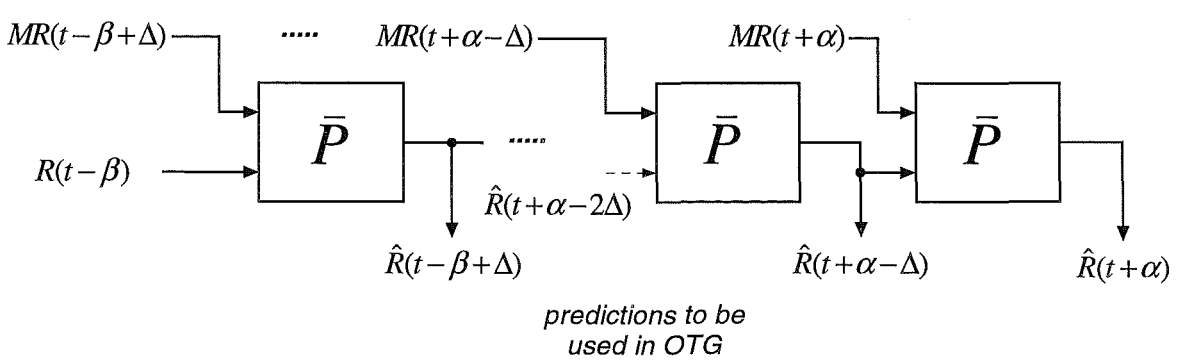

Fig. 49. Response prediction cascade using state-space forward model $\overline{P}$.

4.5 High-Gain Internal Feedback Loop Inverse

It has already been noted (see section 3.2.3.4) that the high-gain internal feedback loop approach to inversion is the most appropriate for nAMT. Certain modifications are necessary for the structure to fit into the AMT context.

In practice it was found that the loop-gain K can take the form of a PID controller to trade accuracy in inversion for feedback loop stability. That is, in s function notation the following look gain K was used:

$$K = P + Is + D/s. \qquad (13.17)$$

Hence the three adjustable parameters P, I and D were used to tune to feedback loop so that it maintained stability. As the accuracy of the forward model increases, and hence the modelling error decreases, the value of the parameters are allowed to increase. No other use of a PID controller to improve the stability of an internal feedback loop was found in the literature.

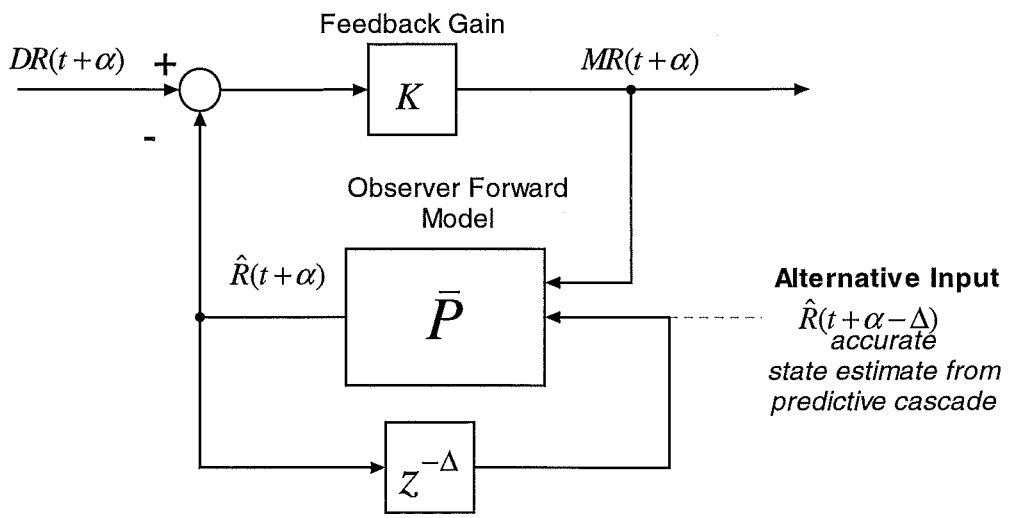

Fig. 50. Proposed nonlinear inversion scheme. A state estimate based on the present sensory feedback signal could be used to improve the accuracy of the inverse. This would, however, be inconsistent with the intermittency principles of AMT so delayed output feedback is employed to form an IO forward model.

When using an observer type forward model in the inversion loop there are additional options. Sensory feedback can be allowed to pass into the forward model to update its internal state estimate. This would lead to a more accurate inverse and improved performance. Unfortunately, the method would also lead to the immediate compensation for plant disturbances with no intermittent processing. Since intermittency is one of the fundamental tenets of AMT (see section 1.4.1) this option was rejected. This interesting option was noted in Fig. 50 but is not formally included in the model.

To maintain intermittency, an IO type forward model can be formed from an observer forward model by feeding back the model output delayed by one sample, so that the model provides its own state estimate.

4.6 Summary of Innovations

The suggested modifications to the existing linear AMT structure for operation in a more realistic environment with nonlinear signals and systems are as follows. In combinations, these modifications make up a variant of AMT called nonlinear adaptive model theory, or nAMT.

1. *Nonlinear stochastic prediction* of target and disturbance signals. This is implemented using a nonlinear auto-regressive moving-average (NARMA) predictor formed with a single-layer locally-recurrent neural network (LRNN). Linear-differential and nonlinear-absolute models were combined in parallel to form a novel, and efficient, one-step predictor structure. This new structure facilitated the efficient online learning of the NARMA stochastic model.

2. *Nonlinear observer forward modelling* replaces linear input-output forward modelling for the calculation of exafference and the formation of inverse models. This forward modelling is achieved with a LRNN.

3. *Nonlinear adaptive response prediction* replaces static response prediction. This is necessary since the nonlinear forward and inverse models do not form a precise inverse pair with a unity transfer function as in the linear case. This is effectively a deterministic extension of the stochastic disturbance predictor in AMT.

4. *Nonlinear inverse modelling* is achieved by placing the nonlinear forward model in a high-gain feedback loop. The loop gain is adjusted to maintain stability. In simulation this was achieved by using a PID internal feedback loop-gain. Since this technique only requires the storage of a forward model for each system, instead of both a forward model and an inverse model, the approach is more parsimonious than other similar models.

5. Human Open-loop Tracking Study

5.1 Introduction

A control system employing an internal model may be categorized as implementing some combination of feedforward and feedback control, depending on the way it utilizes sensory feedback. Feedforward systems typically employ inverse models to effect a desired response, whereas feedback systems often employ forward models to overcome sensorimotor delays (Gomi et al., 1990; Miall et al., 1996; Wolpert et al., 1995). The combination might be serial or parallel depending on the structure of the system (see section 3.1). The contribution of each in the human motor control system remains unclear. In this chapter an experimental study is describe which aims to clarify the extent of the feedforward and feedback control contributions .

Removal of feedback, or deafferentation, has long been a favourite technique of motor control experimentalists. For example, Lashley (1917) studied a subject whose legs were deafferented by a gunshot wound to the spine. The subject was able to extend his knee to 45° while blindfolded as accurately as a normal subject. Surgical deafferentation (dorsal rhizotomy) of monkeys was used by Taub to demonstrate near normal movement in the absence of feedback (Taub, 1976): deficiencies in fine motor control were observed but the animals were otherwise unimpaired. These deafferentation studies show that feedforward control plays a major role in the human motor control system, particularly when controlling a well understood system like the body. They do not demonstrate that a feedforward strategy is employed early in the learning process or to control all systems. In a more recent deafferentation experiment Sainburg, Ghilardi, Poizner & Ghez (1993) showed that proprioceptive feedback is necessary for the accurate control of reaching movements and suggested that feedforward control mechanisms are used early in a movement when sensory feedback is unavailable.

Adaptive inverse control is often suggested as the mechanism for implementation of feedforward motor control in the nervous system (Kawato et al., 1987; Neilson et al., 1988b, 1993; Shadmehr et al., 1994). In this the brain forms and adaptively maintains inverse models of the physical systems it controls. This allows motion to be planned in terms of sensory consequences; the inverse takes care of the generation of appropriate

motor command signals. As inverse control does not require feedback, accurate ballistic movements, which may occur faster than feedback returns from the periphery, are also possible (Kawato, 1999).

It is now rarely suggested that an adaptive inverse element is the sole contributor to voluntary control in the human motor system. Adaptive feedback and feedforward control structures often work in combination in motor control hypotheses (Smith et al., 2000). The feedback control component often guarantees stability, particularly early in the learning process, with the inverse controller automatically taking over control as its accuracy improves (Jordan et al., 1992; Kawato et al., 1987). Others have argued a modulatory role for spinal feedback (Neilson et al., 1997), again with an automatic transfer to feedforward control.

Experimental research has emphasized the importance of an adaptive feedback control component in the nervous system. Bhushan and Shadmehr (1999b) looked at adaptation of reaching movements of the hand in a novel dynamic force field and showed strong similarities between actual trajectories and those predicted assuming a combination of feedforward and feedback control (employing a forward model). Preliminary results also indicated that the forward model may adapt faster than the inverse model when performing reaching movements (Bhushan et al., 1999a). Sainburg, Ghez and Kalakanis (1999) suggested that the control of arm movements progresses through three sequential stages. Movements begin under anticipatory feedforward control, are then corrected as sensory feedback becomes available and are fine-tuned through postural mechanisms as the movement terminates.

There remains little direct experimental evidence for the adaptive formation of inverse models in the nervous system. Consequently, the primary aim of this study was to look for evidence of inverse model formation by examining the characteristics of feedforward adaptation in the human brain. Beyond this, the study aimed to elucidate the relative extent of the feedforward and feedback control contributions. To achieve this, the 'deafferentation' approach, through the removal of visual feedback, was adopted and applied to motor learning. The pursuit tracking task is an ideal tool since feedback about the characteristics of the external system (i.e., the relationship between hand motion and response cursor motion) is purely visual. By blanking the response cursor it is possible to eliminate feedback of the external system entirely and in circumstances free from discomfort or surgery for the subject.

5.1.1 Distinguishing Control Structures

The human motor control system is effectively 'black box', since it is difficult to acquire direct information about the internal state of the controller. Consequently, knowledge about the controller's structure is restricted to deductions based on observations about the relationship between input and output signals.

Response blanking in a pursuit tracking task offers the opportunity to observe the effect of systematically removing an input signal that is otherwise continuously available. This technique can be used to demonstrate adaptive feedforward control in action in the motor system.

When feedback is available, feedforward and feedback adaptive controllers are difficult to distinguish. Both classes of controller use feedback as input for their adaptive processes and consequently exhibit improved performance over time.

In an adaptive feedforward controller, feedback is used to tune an adaptive element such as an inverse model (see Fig. 51a). This model is still available for use when feedback is removed. The action of the controller does not depend on feedback, so withholding it simply suspends the adaptation process – performance otherwise remains unaffected. During normal operation, the model is tuned and controller performance gradually improves. A similar gradual improvement should therefore be evident in the feedback-free performance of the controller when deprived of feedback periodically during learning.

Assuming adaptation is temporarily halted when feedback is removed, a plot of temporal variation in performance with feedback (unblanked performance), and corresponding performance without feedback (blanked performance), can then be constructed. If all the unblanked learning is indeed captured in an inverse model (as predicted for ideal adaptive inverse control) then a direct proportional improvement in blanked performance will be evident (Fig. 52a).

An adaptive feedback controller (Fig. 51b) will also gradually improve its performance when feedback is available. When feedback is removed, however, an inappropriate control effort is produced because a feedback controller depends on a continuously available feedback signal. In a plot comparing ideal unblanked and blanked performance a feedback controller shows no performance improvement when blanked (Fig. 52b).

Note that the use of a feedback control mechanism does not preclude the formation of an inverse model in the brain. For example, Gomi and Kawato (1990) suggested a feedback control structure that employs an adaptive inverse model to improve the controllability of the plant.

If both feedforward and feedback adaptive elements are present in the controller (Fig. 51c), the results would show some (unequal) improvement in blanked performance (Fig. 52c). Fig. 51c shows a parallel combination of adaptive elements but a series combination is also possible and does not alter the interpretation of results. Assuming all blanked improvement is due to the action of an adaptive feedforward component, the relative contribution of each control component can be estimated. Note that it is also possible for a combination controller to exhibit no improvement in unblanked performance while showing strong improvement in blanked performance, since the feedforward component can learn from superior feedback behaviour (Jordan et al., 1992).

Feedback blanking, therefore, gives us a method both for detecting adaptive feedforward control in the motor control system and for judging the extent of the contribution of each mode of control.

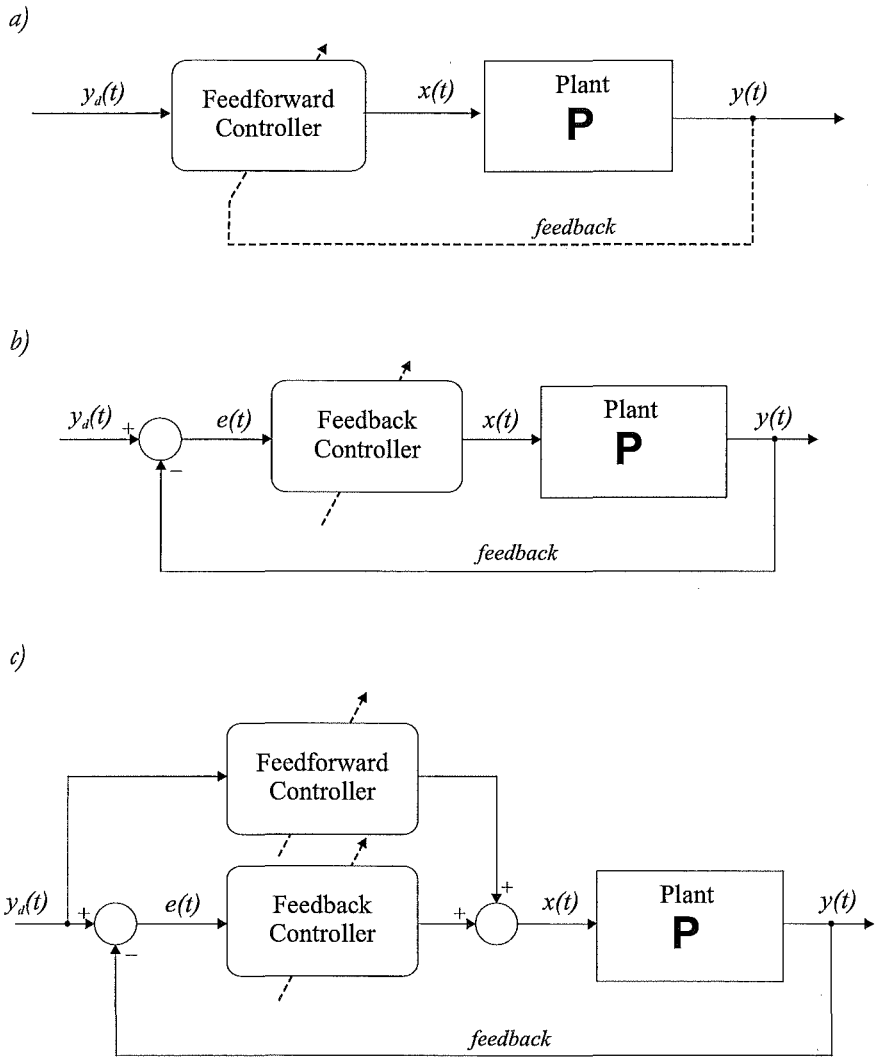

Fig. 51. (a) A simple adaptive feedforward controller. In this case feedback is only used to adapt the controller so that it approximates the inverse P^{-1} of the plant. $y_d(t)$ is the desired trajectory, $y(t)$ is the actual trajectory, and $x(t)$ is the control effort. (b) A simple adaptive feedback controller (representative structure). Feedback is required to produce the control effort $x(t)$. (c) A possible parallel combination of adaptive feedback and feedforward control. Dotted arrows indicate adaptation.

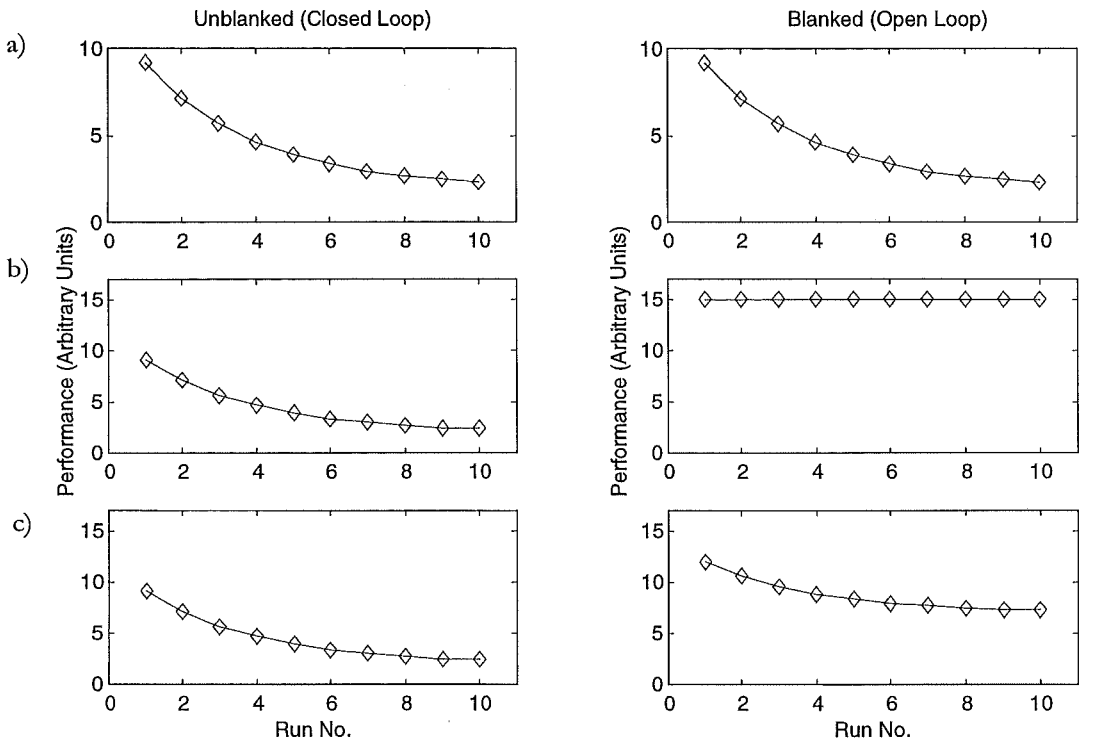

Fig. 52. (a) Tracking performance for an ideal adaptive feedforward controller. The blanked runs are performed immediately after the unblanked runs. All learning exhibited in the unblanked runs is available and exhibited in performance on the blanked runs. (b) Representative tracking performance for an adaptive feedback controller. Removing feedback results in an invalid control signal. Blanked performance shows no improvement. (c) Representative tracking performance for a combined adaptive feedforward/feedback controller. Blanked performance does not improve in proportion to unblanked performance.

5.1.2 Experimental Approach

Each subject is trained on a pursuit tracking task with visual feedback for a short interval, during which they partially learn to control the system. Feedback is then removed by blanking the response cursor. This training and blanking cycle is then repeated several times.

The performance of the subject in each interval is then assessed. Improvement in blanked performance is interpreted as adaptive feedforward learning and, therefore, as evidence for the formation of an adaptive inverse model.

This experiment offered the opportunity to test for inverse modelling of the visuomotor relationship, to study the formation of the model during learning and to investigate how adaptation varies with different external systems. It is important to note that this experimental paradigm can only investigate inverse modelling for external systems (i.e., those whose input is the motion of the human body) but it is reasonable to suggest that similar mechanisms might also be in effect throughout the motor system.

5.2 Methods

5.2.1 Subjects

Twenty subjects (13 male and 7 female) with no history of significant neurological or musculoskeletal disorder participated in the study. All subjects passed a standard visual acuity test prior to beginning the experiment, which confirmed their ability to resolve 1 pixel (0.31 mm at 130 cm) on the screen. The ages of the subjects ranged between 20 and 56 years (median 29.5 years) and the group included 3 left-handed individuals. The subjects were randomly divided into two equal sub-groups labelled 'A' and 'B', each of which learned to control a different system.

5.2.2 Apparatus

The apparatus included a PC with two colour monitors: one displaying test stimuli for the subject and the other used by the assessor for task generation and analysis. All tests were run and analysed with the tracking program SMTests (Jones, 2000; Jones et al., 1986; Jones et al., 1993). Subjects were seated in front of their monitor (312 x 234 mm) with an eye-to-screen distance of approximately 130 cm. All of the visuomotor tests were one-dimensional and employed a steering wheel (395 mm diameter) as the subjects' output sensor. Rotation of the wheel moved an arrow horizontally on the screen.

Both the screen response and the motor output response were recorded for analysis. Data was sampled at 60 Hz - the screen update rate - which is well above the Nyquist sampling frequency.

5.2.2.1 External Systems

Arbitrary external systems were implemented by passing the motor output signal from a linear transducer through a nonlinear dynamic filter, the output of which was represented on the screen.

System input θ (i.e., steering wheel angle) was measured such that at $\theta = 90°$ the steering wheel was centred with the subject's hand at top centre. Output $f(\theta)$ (i.e., response cursor position) corresponded to horizontal displacement (mm) from the left edge of the display.

Group A controlled a linear dynamic system. The dynamics were produced by passing the motor response through an IIR filter: a 3rd order Chebyshev Type I low-pass filter with cutoff frequency of 3 Hz. This was selected in accordance with a preliminary study that showed that the bandwidth of the human/steering wheel system is approximately 4 Hz. Thus, it should be possible for the human operator to excite the system sufficiently to gain a good model of the dynamics of the system within the pass-

band. The Chebyshev response within the pass-band is not flat, providing a challenging response for the operator to model (see Fig. 53).

Group B was required to learn a static nonlinear system (see Fig. 54). The system was a cubic function of input angle, scaled to provide a challenging variation in gain while remaining controllable. The function was displaced from centre to increase the difficulty of the task by avoiding symmetry:

$$f(\theta) = 312\left(6\left(\frac{\theta}{180}-0.4\right)^3 + 0.2\left(\frac{\theta}{180}-0.4\right) + 0.474\right)$$

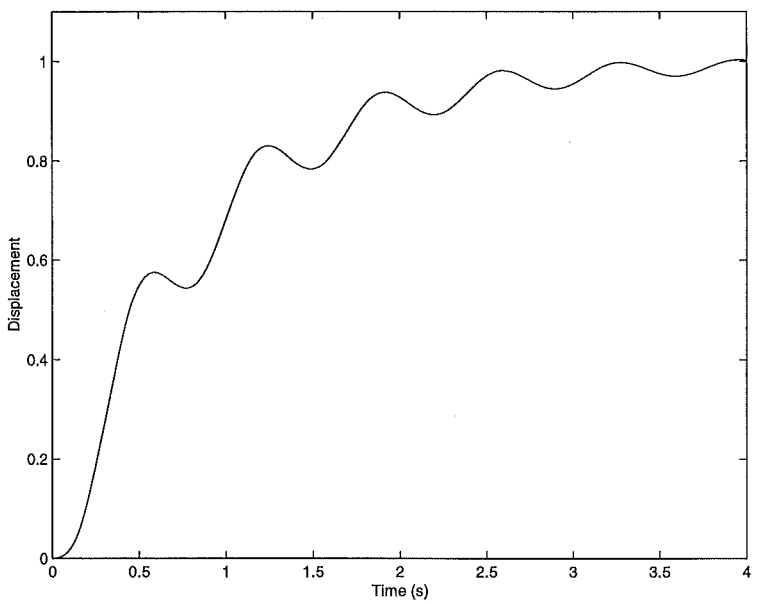

Fig. 53. Step response of dynamic linear system controlled by Group A.

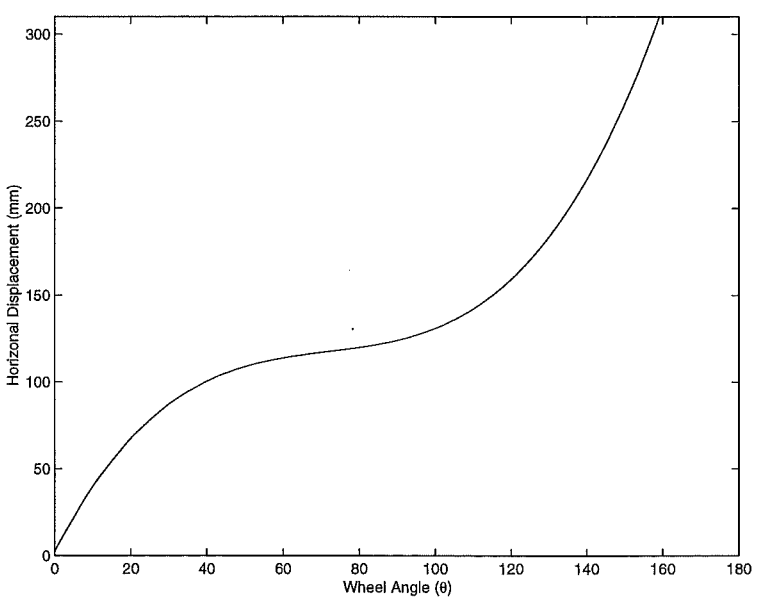

Fig. 54. Static nonlinear system controlled by Group B. θ is steering wheel angle (centred at 90°), displacement measured from left edge of screen.

5.2.2.2 Target

The target signal comprised two consecutive sections as follows:

Unblanked Training Signal – 68 s of a pseudo-random waveform generated from superposition of 50 sinusoids of equal amplitude and equally spaced in frequency with random phase from 0.007 Hz up to 0.6 Hz, 75% full scale deflection. The random nature of the signal ensured that the dynamic controlled systems were excited sufficiently to allow the subject to maximally learn their characteristics.

Blanked Assessment Signal – Identical to the first 28 s of the training signal except for removal of feedback to the subject by turning off the response arrow.

The two sections were combined and separated by a 7-s interval where the target returned to the centre of the screen. All three sections combined to form a single continuous 103-s target signal, which was used for all runs in the experiment. The subject was also presented with an 8-s preview of the target to eliminate the need to predict the target signal and, hence, minimize a possible confounding source of learning.

A horizontal line was provided on screen to constrain the subject's error estimate to one dimension. Without the line, the subject would have been forced to estimate the vertical position of the pointer when blanked, which increases the difficulty of the task.

A small box was placed at the intersection of the horizontal line and the target signal. This emphasized the position of the target, as experience showed that subjects often 'lose' the target when looking ahead slightly. The screen setup is shown in Fig. 55.

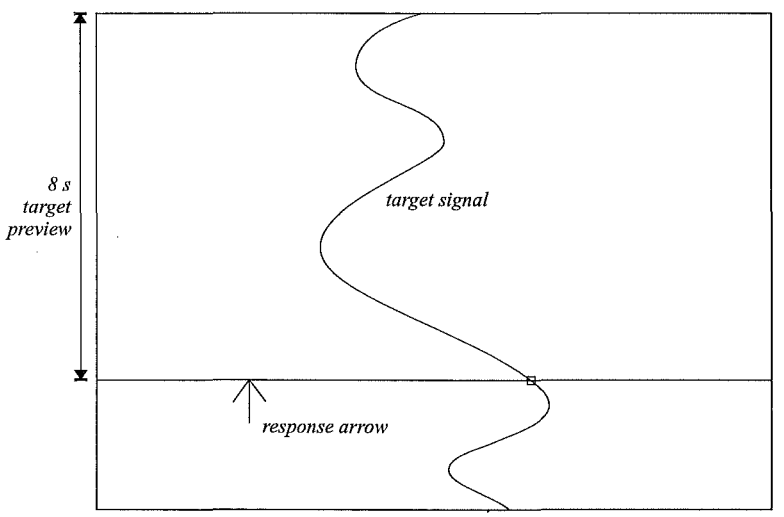

Fig. 55. Preview random tracking task. Subject alters horizontal position of arrow to keep point on descending target waveform. Arrow moves along horizontal line. Note small box at intersection of line and target intended to emphasize current target position.

5.2.3 Experimental Procedure

The experiment[4] comprised 25 consecutive tracking runs, each of 103-s duration (i.e., the length of the target signal). For each run the following procedure was followed:

1. The investigator positioned the screen pointer exactly on top of the target thereby preventing the subject from gaining knowledge of the system prior to the run.
2. The subject was asked to hold the wheel at the marked position (top-centre) with their dominant hand.
3. The subject was asked to 'keep the point of the arrow on the line as accurately as possible'.
4. The subject was told that the arrow would disappear late in the run and that they were required to continue the task by estimating the position of the arrow.
5. When the subject was ready, the investigator started the run.
6. On completing the run, the subject was told their mean absolute error (MAE) score for the unblanked section of the run (as an incentive to improve their performance).
7. The subject was then given a minimum 20-s rest (to prevent fatigue) before commencing the next run. A 5-minute rest was given following the 10th run.

The total time for a complete session averaged 70 minutes.

5.2.3.1 Practice – 10 tracking runs

All subjects were initially asked to control a simple zero-order external system (i.e., wheel angle proportional to response pointer position). These practice sessions were intended to allow the subjects to learn as much about the target and tracking system as possible. This facilitates the assumption made later in analysis that only the external system is learned in the following runs.

Ten runs of the zero-order task were performed, after which learning was deemed to have essentially plateaued. At this point the stochastic characteristics of the target signal, the kinematic and dynamic properties of the steering wheel and the wheel to display relationship are considered to have been maximally learned. Additional runs were considered undesirable as they were judged likely to introduce unacceptable fatigue later in the experiment.

---

[4] Ethical approval for this experiment was gained from the *Canterbury Ethics Committee.*

5.2.3.2 External Systems – 15 tracking runs

The subjects were then asked to control a new visuomotor relationship, implemented by altering the characteristics of the external system. The specific external system they were to control depended on which group they belonged to.

Both groups were required to train on their new external system for 15 runs. This duration was selected to be long enough to characterize any learning trend but not so long as to introduce noticeable fatigue. A summary of the runs performed by members of each group is shown in Table 1.

Table 1. Experimental Procedure for Each Group

	Run No. 1-10	Run No. 11-25
Group A	Zero Order	Dynamic Linear
Group B	Zero Order	Static Nonlinear

5.2.4 Performance analysis

5.2.4.1 Root Mean Square Error

The primary performance metric used in the analysis of results was the root mean square (RMS) error between the target and the response. The RMS error score was suitable for the comparison performance between runs as the same target signal was used for each run. RMS error scores were calculated for the blanked and unblanked sections of each run.

5.2.4.2 Error Spectrum

To provide a more detailed analysis of tracking behaviour, the power spectrum of the error signal (the error spectrum) was calculated. This is a function indicating error power and, hence, performance as a function of frequency. The integral of the error spectrum across all frequencies (the total area under the curve) equals the total power in the error signal and, equivalently, the mean square error.

The error spectrum was calculated for both the blanked and unblanked sections of all runs. The correlation method (Ljung, 1999) was employed to generate error spectral estimates at 5 frequencies within the target bandwidth, providing a frequency resolution of 0.15 Hz. Additional spectral estimates were made where error power was present beyond the target bandwidth.

5.2.4.3 Quasi-linear Analysis

A full quasi-linear analysis using the correlation method was performed, in which the transfer function and coherence functions were calculated (see review in Appendix I, Neilson, 1980). The remnant power function was represented by calculating the

coherence function[5] (which specifies essentially the same information). This analysis was performed to ensure that important effects were not masked in the error spectral analysis. Spectral estimates were again calculated at 5 frequencies within the target bandwidth, providing a frequency resolution of 0.15 Hz.

5.2.4.4 Statistical Analysis

Analysis of variance (ANOVA) was employed to look for learning trends. RMS error scores were analysed using a single-factor between-groups ANOVA with repeated measures, where the repeated measures were upon each individual's RMS error scores across runs. The error spectrum results were analysed with a two-factor between-groups ANOVA with repeated measures. The design compared spectral results for each run (factor 1) at each frequency within the target bandwidth (factor 2). Appropriate transformations were first applied to the data to satisfy the ANOVA assumption of homogeneity of within-cell variance and, critically, to eliminate correlation between means and variances in the data. Investigation revealed that a logarithmic transformation was appropriate for unblanked data, while blanked error spectral data required a square-root transformation.

Linear trend analysis was performed to establish the significance of trends in the data. This was achieved through the specification of linearly weighted contrasts across all runs (Winer, 1971).

5.3 Results

5.3.1 RMS Error

The mean and standard deviation RMS error results for each external system are shown in Fig. 56. These graphs appear to show clear learning for all three external systems in the unblanked results. No learning trend was visible in the blanked results for Group A. In contrast, a slight learning trend can be seen in the blanked results for Group B. The variance of the blanked RMS error was much greater than for the corresponding unblanked data. This large difference in variance violated the ANOVA assumption of homogeneity of variance, preventing a direct comparison between blanked and unblanked data in the ANOVA design. However, by separating the blanked and

---

[5] The *coherence*, or *coherence-square* function essentially provides a correlation coefficient for each frequency. The coherence between signals $x(t)$ and $y(t)$ is defined by $C^2(\omega) = |P_{XY}(\omega)|^2 / P_{XX}(\omega).P_{YY}(\omega)$ where P_{XX} and P_{XX} are the power spectra of $x(t)$ and $y(t)$ respectively, and P_{XY} is the cross-power spectrum.

unblanked ANOVAs, different data transformations could be applied to the blanked and unblanked results which improved the power of the tests.

a) Practice Runs

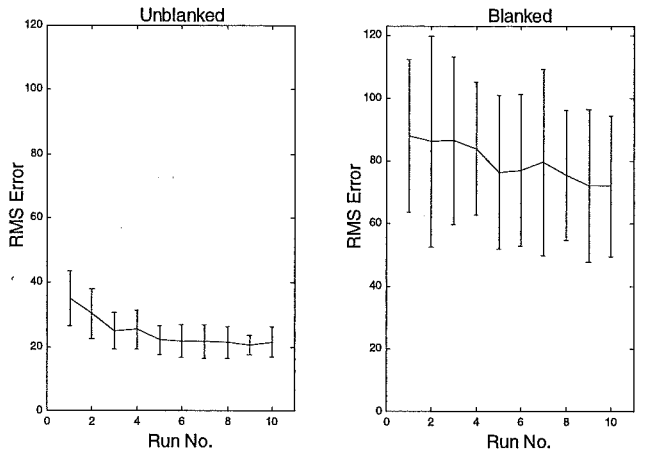

b) Group A

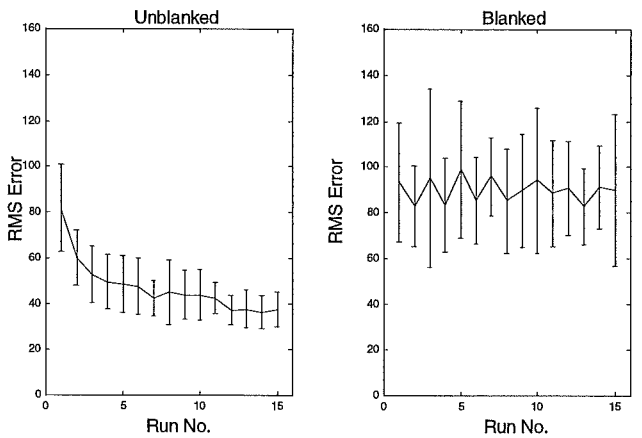

c) Group B

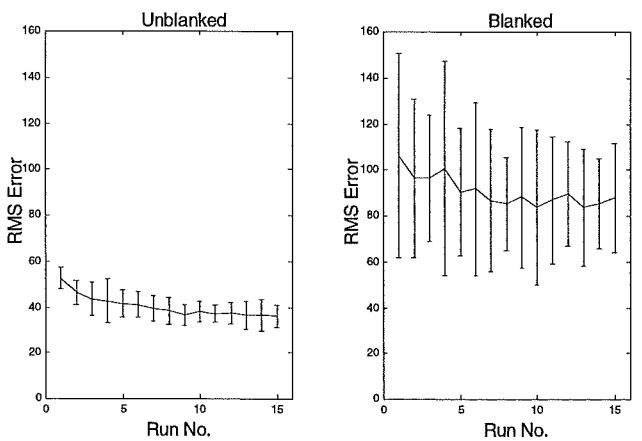

Fig. 56. Mean RMS error with standard deviation for the unblanked and blanked runs of (a) practice (zero-order system), (b) Group A (dynamic linear system) and (c) Group B (static nonlinear system).

5.3.1.1 Overall ANOVA analysis

A summary of the overall ANOVA results for RMS error is provided in Table 2. Results from the practice runs showed an effect for run number in both the unblanked and the blanked sections ($p < .001$), confirming that the mean RMS error scores differ between runs (linear trend analysis was performed to confirm the nature of this variation, see section 5.3.1.2)

In the experimental runs the unblanked section showed a significant effect for run (indicating that performance differs between runs). The blanked data failed to show any significant effects, although this could well have been a reflection of the high variance of the data.

Table 2. Analysis of Variance for RMS Error

Effect	Unblanked Runs *(log transform)*							Blanked Runs						
	Effect		*Error*					*Effect*		*Error*				
	df	*MS*	*df*	*MS*	*F*	*p*		*df*	*MS*	*df*	*MS*	*F*	*p*	
Practice														
R	9	0.11	171	0.003	34.9	0.000	***	9	1.77	171	0.53	3.34	0.000	***
Experimental														
G	1	0.21	18	0.074	2.8	0.113		1	51.39	18	8057	0.01	0.937	
R	14	0.09	252	0.003	37.5	0.000	***	14	343.89	252	276.6	1.24	0.244	
G×R	14	0.01	252	0.003	4.5	0.000	***	14	361.29	252	276.6	1.31	0.204	

*Note: G = Group, R = Run; $p < .05$ = *, $p < 0.01$ = **, $p < 0.001$ = ****

5.3.1.2 Linear Trend Analysis

The linear trend analysis of RMS error results are summarized in Table 3. A linear trend of reduction in RMS error was observed in both the unblanked and blanked practice runs ($p < .001$). The unblanked and blanked runs showed unequal reduction in mean RMS error from the first run to last run (33% improvement unblanked vs. 18% improvement blanked).

The unblanked practice runs showed no linear trend over runs 6 to 10 ($F(1, 19) = 1.40$, $p = .25$), suggesting that the learning effect was confined to the first half of the practice runs and supporting the assumption that learning had essentially plateaued by the end of practice. Similarly, no linear trend was observed over runs 6 to 10 for the blanked runs ($F(1,19) = 3.26$, $p = .087$).

Group A showed the strongest learning in the unblanked section (54% reduction in mean RMS error) but, surprisingly, exhibited no discernible learning trend in the blanked section.

Group B showed substantial improvement in the unblanked section, although to a lesser degree than that observed for Group A (Fig. 56). However, in contrast to Group A, performance was seen to improve with a significant linear trend during the blanked sessions ($p = .037$, see Table 3). Group B did not show a proportional reduction in mean RMS error from the first run to last run in the blanked and unblanked responses (35% improvement unblanked vs 17% improvement blanked). This difference suggests a feedback control component for Group B.

Table 3. Linear Trend Analysis for RMS Error

Group	Unblanked Runs *(log transform)*							Blanked Runs						
	Effect		*Error*					*Effect*		*Error*				
	df	*MS*	*df*	*MS*	*F*	*p*		*df*	*MS*	*df*	*MS*	*F*	*p*	
Practice	1	0.762	19	0.006	137.3	0.000	***	1	14.16	19	0.679	20.8	0.000	***
A	1	0.923	18	0.004	239.6	0.000	***	1	23.6	18	767.8	0.0	0.862	
B	1	0.246	18	0.004	64.0	0.000	***	1	3879	18	767.9	5.1	0.037	*

$p < .05 = *, p < 0.01 = **, p < 0.001 = ***$

5.3.2 Error Spectra

5.3.2.1 Mean Error Spectra

Fig. 57 shows the mean error spectra for the first and last runs across all subjects. As in the RMS error results (see section 5.3.1) variance was much greater for the blanked data than the unblanked data. This necessitated a similar separation of blanked and unblanked ANOVA analyses.

Practice Runs

The mean error spectrum for the practice runs shows that error power was largely restricted to the target bandwidth (0 - 0.6 Hz) for both blanked and unblanked runs (Fig. 57a). The mean blanked error spectrum exhibited a peak at very low frequencies (0 - 0.3 Hz) accounting for a large proportion of the total error power. Blanked and unblanked spectra show a similar behaviour at frequencies above 0.3 Hz, with both exhibiting a small peak at approximately 0.5 Hz and a smooth decline to negligible power around 0.7 Hz (the level of error power for the unblanked runs was much higher).

Group A

The power spectra for Group A were remarkably similar to those from the practice runs. Almost all error power was again restricted to the target bandwidth (0 - 0.6 Hz) for both blanked and unblanked runs; the blanked spectrum exhibited a peak at very low frequencies (0 – 0.3 Hz) and all spectra appear to show similar behaviour at frequencies above 0.3 Hz. Fig. 57b shows that mean spectra for the first and last blanked runs of Group A are very similar. Hence, little no improvement was observed in the blanked runs despite a large reduction in error power during the unblanked runs.

Group B

Error power for Group B was spread across a wider bandwidth than for Group A (see Fig. 57c). Power tapered off slowly from 0.7 to 1.5 Hz, with levels reducing quickly to negligible levels beyond 1.5 Hz. The long tails of the spectra reflect the nonlinearity introduced by the controlled system. The high frequency tails could not be included in the between groups ANOVA analysis since Group A showed negligible power at high frequency, thereby introducing a strong correlation between mean and variance. Consequently the high frequency tails of Group B were analysed in a separate ANOVA design.

The blanked spectra show greater error power than the unblanked spectra at all frequencies. In common with the previous spectra, the Group A results exhibited a peak in the blanked spectra at low frequencies (0 - 0.3 Hz) which is unrelated to the unblanked behaviour and all spectra appeared to show similar behaviour at frequencies above 0.3 Hz (both blanked and unblanked spectra exhibit a peak between 0.5 – 0.6 Hz).

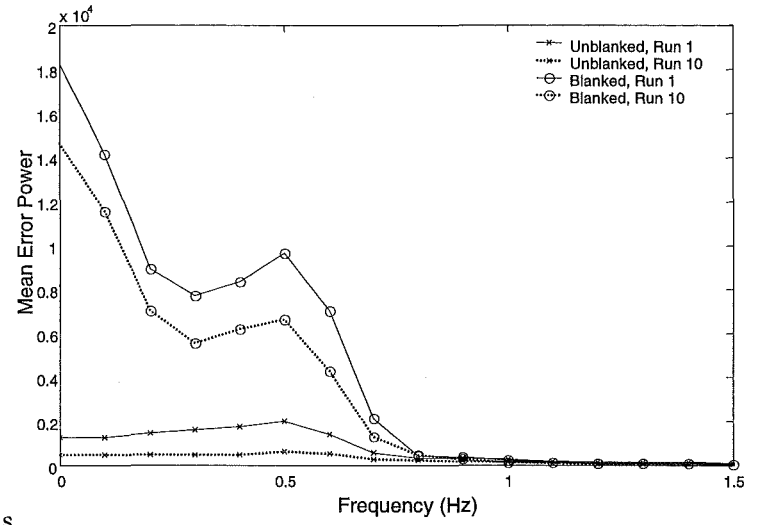

a) Practice Runs

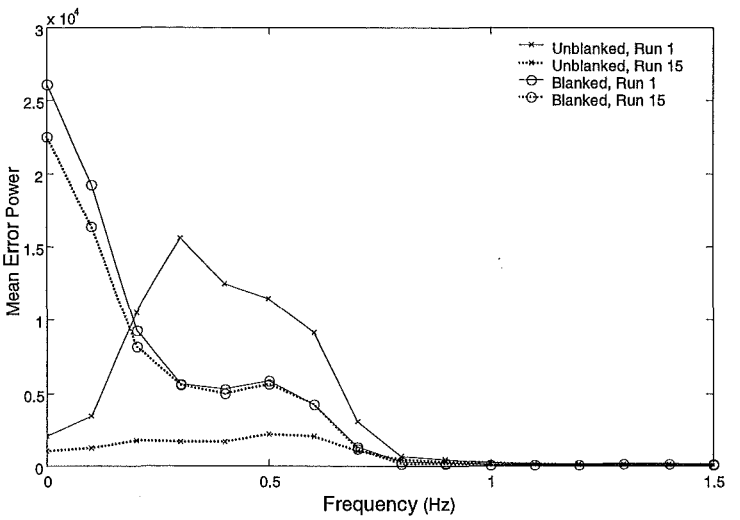

b) Group A

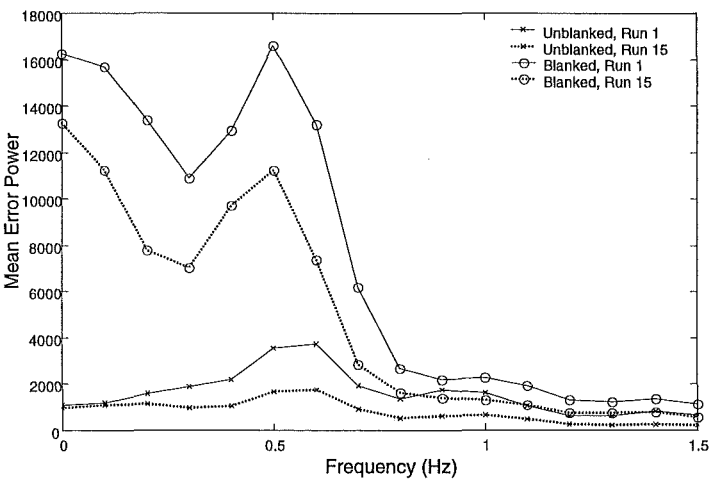

c) Group B

Fig. 57. Mean error power spectra for the unblanked and blanked sections of the first and last runs of (a) practice (zero-order system), (b) Group A (dynamic linear system) and (c) Group B (static nonlinear system).

5.3.2.2 Overall ANOVA Analysis

The overall effects are summarized in Table 4. In the practice runs, both the unblanked and blanked sections showed significant effects for run and frequency but no interaction. This lack of interaction indicates that the variation in error power with run is independent of frequency for both the unblanked and blanked runs.

Table 4. Analysis of Variance for Error Spectra

Effect	Unblanked Runs *(log transform)*							Blanked Runs *(square root transform)*						
	Effect		*Error*					*Effect*		*Error*				
	df	*MS*	*df*	*MS*	*F*	*p*		*df*	*MS*	*df*	*MS*	*F*	*p*	
Practice Runs														
R	9	2.55	171	0.09	29.0	0.000	***	9	2507	171	1182	2.1	0.030	*
F	4	0.45	76	0.05	8.7	0.000	***	4	87707	76	2206	39.8	0.000	***
R×F	36	0.01	684	0.01	0.6	0.982		36	103	684	195	0.5	0.990	
Experimental Runs ***(at frequencies within the target bandwidth)***														
G	1	4.60	18	4.15	1.1	0.306		1	126	18	33361	0.0	0.952	
R	14	1.49	252	0.35	4.2	0.000	***	14	1548	252	1051	1.5	0.122	
F	4	23.03	72	1.23	18.7	0.000	***	4	168480	72	3795	44.4	0.000	***
G×R	14	0.82	252	0.35	2.3	0.005	**	14	1298	252	1051	1.2	0.250	
G×F	4	1.82	72	1.23	1.5	0.218		4	7402	72	3795	2.0	0.111	
R×F	56	0.48	1008	0.20	2.4	0.000	***	56	255	1008	200	1.3	0.088	
G×R×F	56	0.15	1008	0.20	0.7	0.937		56	209	1008	200	1.0	0.392	

*Note: G = Group, R = Run, F = Frequency (in effect column only); $p < .05$ = *, $p < 0.01$ = **, $p < 0.001$ = ****

For the experimental runs the unblanked data showed effects for run and frequency and an interaction between the two. This interaction can be accounted for by the relatively small amount of learning shown at very low frequencies in the unblanked experimental runs (see Fig. 59). The only significant effect in the blanked runs was for frequency. The lack of an overall effect for run was, perhaps, not surprising given the lack of improvement in RMS error for Group A. There was no effect for group in either the blanked or the unblanked runs, indicating that both external systems elicited similar error spectra within the target bandwidth.

5.3.2.3 Linear Trend Analysis

Linear trend analysis results from the error spectral data are summarized in Table 5. The unblanked practice runs exhibited strong improvement at all frequencies (see Fig. 58). There was an overall linear trend in the blanked practice runs ($p = .001$), and at all other frequencies within the target bandwidth ($p < .02$), except at 0 Hz.

In another linear trend analysis, no learning trend was found over runs 6 to 10 when all frequencies were considered ($F(1, 19) = 0.23, p = .64$), nor at any individual frequency, the most significant result appearing at 0.45 Hz ($F(1, 19) = 0.50, p = .49$). This further confirms that no learning occurred over the final half of the practice runs.

Group A showed significant improvement at frequencies above 0.3 Hz and an overall trend in the unblanked runs, but this was not reflected in the blanked runs (see Fig. 59). No improvement was detected at any frequency – in agreement with the RMS results from Group A.

The analysis for Group B was divided into 2 sections. First an overall analysis was performed (in combination with Group A) at frequencies within the target bandwidth (Fig. 59). Beyond this range the Group B data was analysed in an isolated 2 factor repeated measures design (see Fig. 60).

The unblanked results for Group B showed improvement at high frequencies (0.45 Hz, $p < 0.05$; 0.75 Hz and above, $p < .001$). In contrast, the only learning trends in the blanked runs occurred at low frequencies (from 0 Hz to 0.3 Hz, $p < .05$).

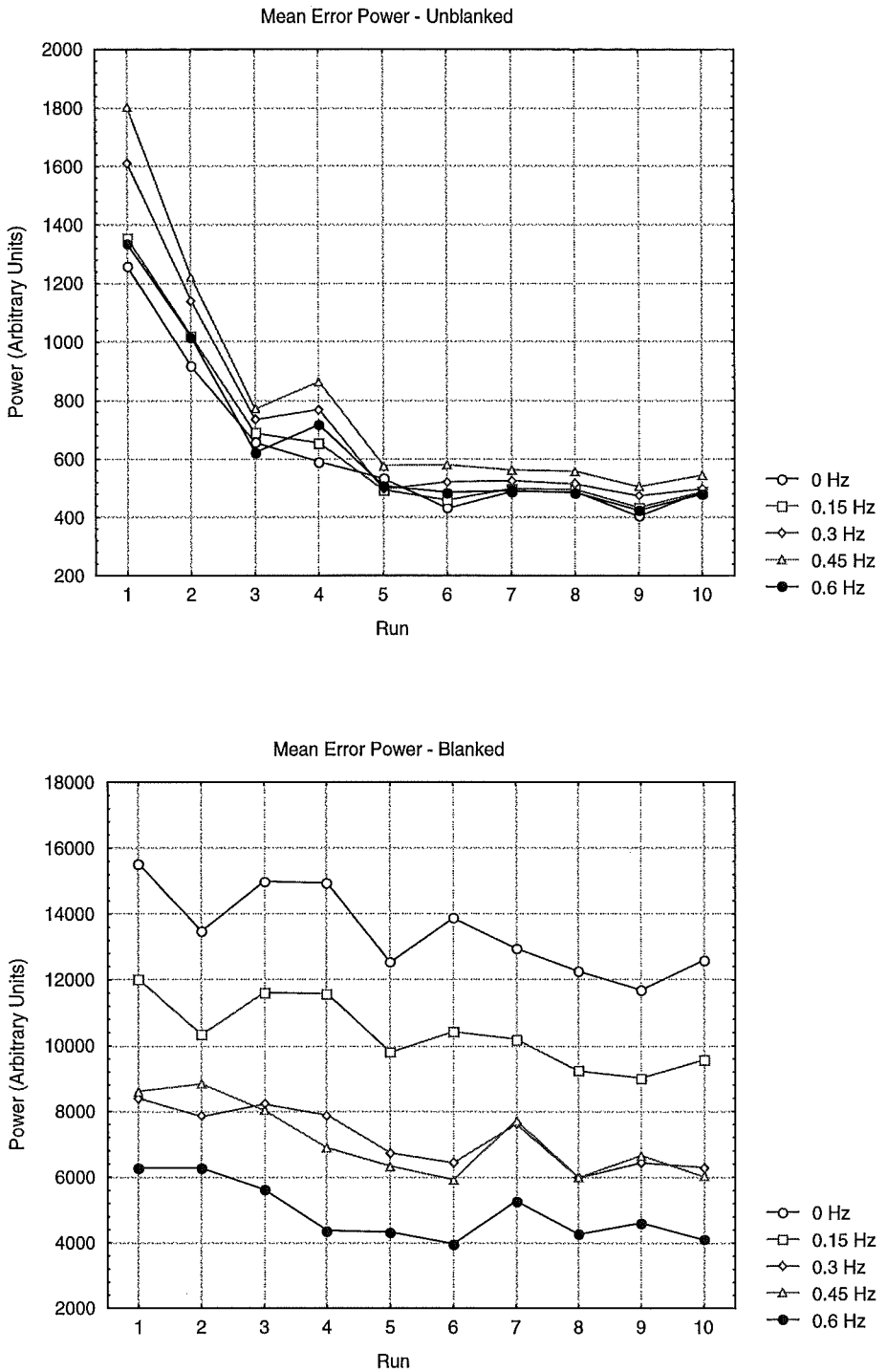

Fig. 58. Mean error power for each frequency in ANOVA analysis for the unblanked and blanked sections of the practice runs (zero-order).

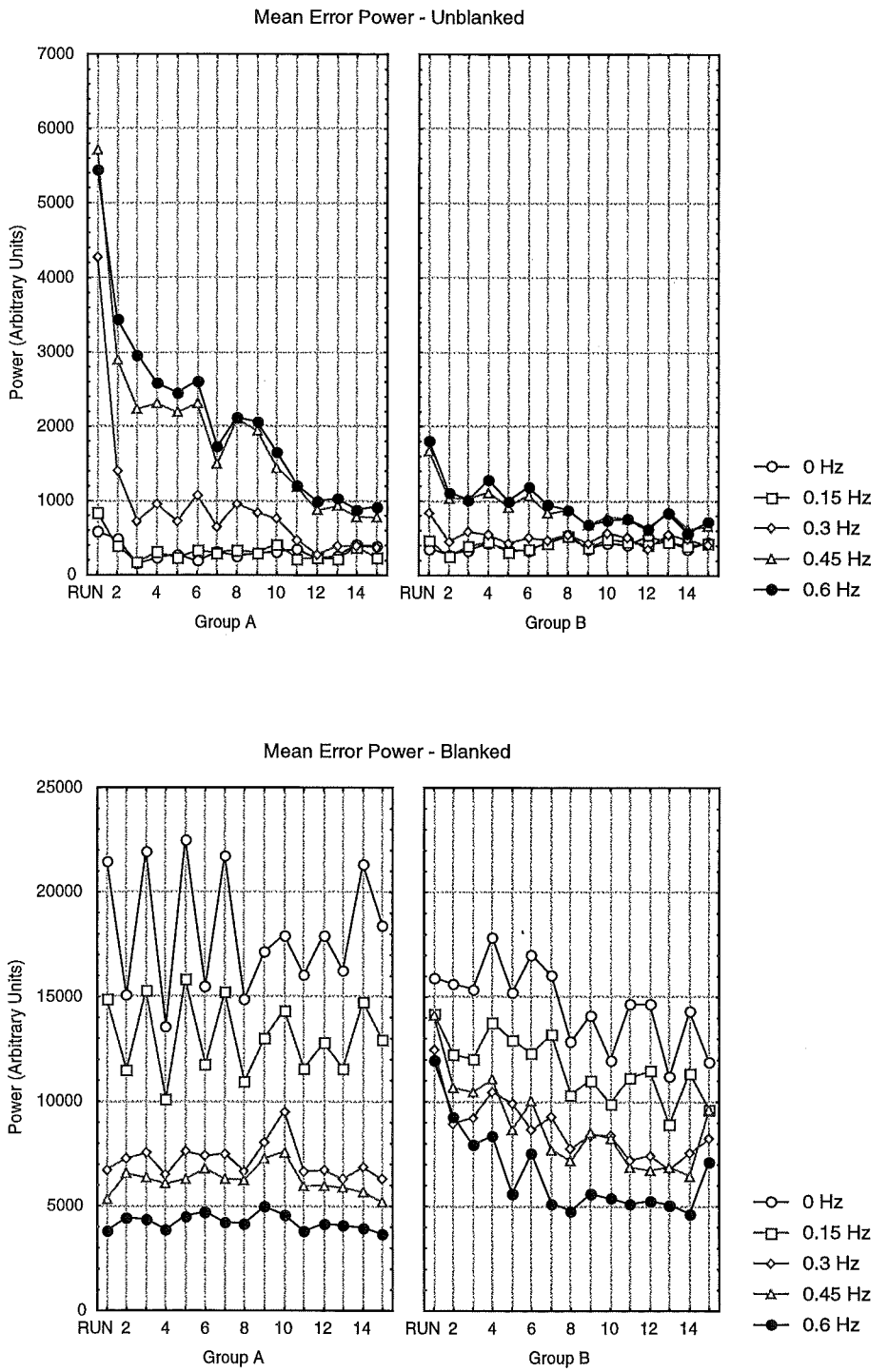

Fig. 59. Mean error power for each frequency in the combined ANOVA analysis for the unblanked and blanked experimental runs.

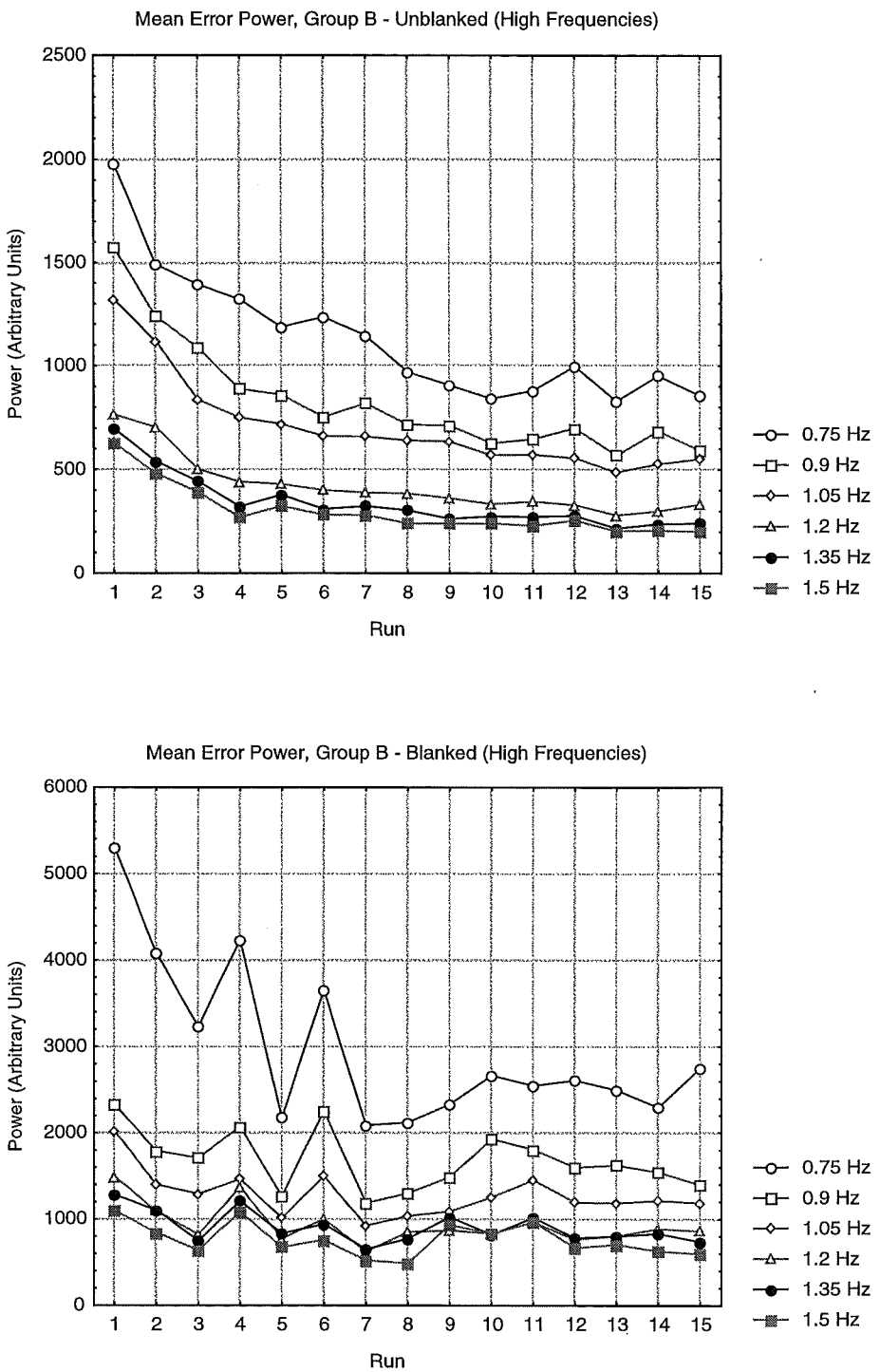

Fig. 60. Mean error power for frequencies outside the target bandwidth in the ANOVA analysis for the unblanked and blanked runs of Group B.

Table 5. Linear Trend Analysis for Error Spectra

	Unblanked Runs *(log transform)*							**Blanked Runs** *(square root transform)*						
	Effect		*Error*					*Effect*		*Error*				
	df	*MS*	*df*	*MS*	*F*	*p*		*df*	*MS*	*df*	*MS*	*F*	*p*	
Practice Runs														
All f (0-0.6 Hz)	1	16.97	19	0.16	106.9	0.000	***	1	17596	19	1223	14.4	0.001	***
f = 0 Hz	1	2.70	19	0.05	54.1	0.000	***	1	3109	19	1015	3.1	0.096	
f = 0.15 Hz	1	3.45	19	0.03	99.8	0.000	***	1	3128	19	448	7.0	0.016	*
f = 0.3 Hz	1	4.06	19	0.04	102.3	0.000	***	1	3307	19	190	17.4	0.001	***
f = 0.45 Hz	1	3.82	19	0.05	77.6	0.000	***	1	4558	19	390	11.7	0.003	***
f = 0.6 Hz	1	3.03	19	0.04	71.3	0.000	***	1	3588	19	339	10.6	0.004	***
Group A (combined between-groups analysis)														
All f (0-0.6 Hz)	1	15.61	18	0.56	27.9	0.000	***	1	517	18	3093	0.2	0.687	
f = 0 Hz	1	0.99	18	0.72	1.4	0.257		1	29	18	800	0.0	0.852	
f = 0.15 Hz	1	0.21	18	0.23	0.9	0.359		1	76	18	416	0.2	0.674	
f = 0.3 Hz	1	10.92	18	0.23	46.6	0.000	***	1	97	18	685	0.1	0.711	
f = 0.45 Hz	1	8.36	18	0.26	32.4	0.000	***	1	154	18	1650	0.1	0.763	
f = 0.6 Hz	1	10.09	18	0.53	19.0	0.000	***	1	210	18	1605	0.1	0.722	
Group B (combined between-groups analysis)														
All f (0-0.6 Hz)	1	0.04	18	0.56	0.1	0.793		1	18061	18	3093	5.8	0.027	*
f = 0 Hz	1	2.39	18	0.72	3.3	0.085		1	4472	18	800	5.6	0.029	*
f = 0.15 Hz	1	0.85	18	0.23	3.6	0.073		1	4114	18	416	9.9	0.006	**
f = 0.3 Hz	1	0.10	18	0.23	0.4	0.514		1	3101	18	685	4.5	0.048	*
f = 0.45 Hz	1	1.39	18	0.26	5.4	0.032	*	1	3120	18	1650	1.9	0.186	
f = 0.6 Hz	1	1.99	18	0.53	3.7	0.069		1	3358	18	1605	2.1	0.165	
Group B (isolated analysis for high frequencies)														
All f (0 - 1.5 Hz)	1	10.73	9	0.08	134.2	0.000	***	1	16042	9	5760	2.8	0.129	
f = 0.75 Hz	1	1.49	9	0.04	37.4	0.000	***	1	1614	9	1207	1.3	0.277	
f = 0.9 Hz	1	1.81	9	0.02	106.2	0.000	***	1	290	9	340	0.9	0.380	
f = 1.05 Hz	1	1.65	9	0.01	149.5	0.000	***	1	299	9	283	1.1	0.331	
f = 1.2 Hz	1	1.70	9	0.01	127.6	0.000	***	1	340	9	238	1.4	0.263	
f = 1.35 Hz	1	2.14	9	0.02	86.7	0.000	***	1	217	9	208	1.0	0.333	
f = 1.5 Hz	1	2.20	9	0.05	43.1	0.000	***	1	142	9	212	0.7	0.434	

$p < .05$ = *, $p < 0.01$ = **, $p < 0.001$ = ***

5.3.3 Response Trajectories

Mean error signal power was much higher in the blanked runs than the unblanked runs. The cause of this discrepancy was initially explored by taking the mean response across all subjects for each run. This analysis revealed a mean trajectory that, for all external systems, is quite distinct from the target.

This unusual mean trajectory is evident during the practice runs and, as the range curves in Fig. 61 show, is surprisingly invariant. This might indicate conversion to a signal distinct from the target or a very slow learning rate.

Similar analysis for Group A again shows a stable mean across all runs (Fig. 62), though less so than for the practice or Group B runs. Despite the dramatic change in visuomotor characteristics, the mean is similar to that observed in the control runs.

The mean blanked responses for Group B was again distinct from the target (Fig. 63) and was similar to the mean responses for both the practice runs and those performed by Group A. That is, the similarity in mean response trajectories between groups was present despite considerably different visuomotor relationships. The mean response for Group B shows a greater tendency to overshoot in the 60 mm to 100 mm response range. This is the high gain region of the nonlinear function shown in Fig. 54, which indicates that this region is incompletely modelled.

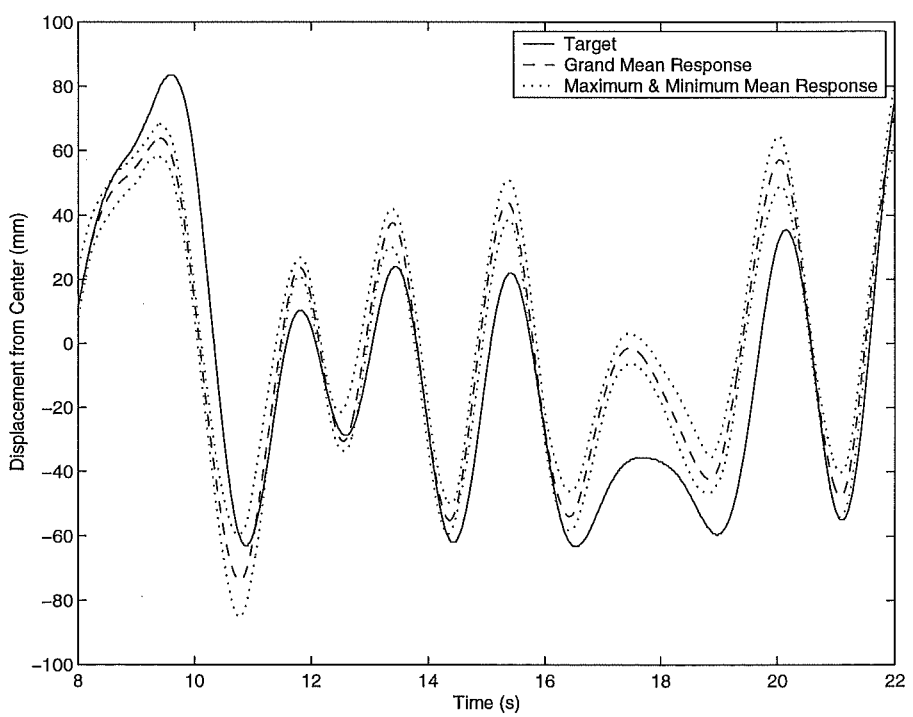

Fig. 61. Mean blanked responses for practice runs (zero-order system). Dotted lines indicate the upper and lower limits of the mean (across subjects) for each run. Hence, the mean for any particular run falls between the dotted lines.

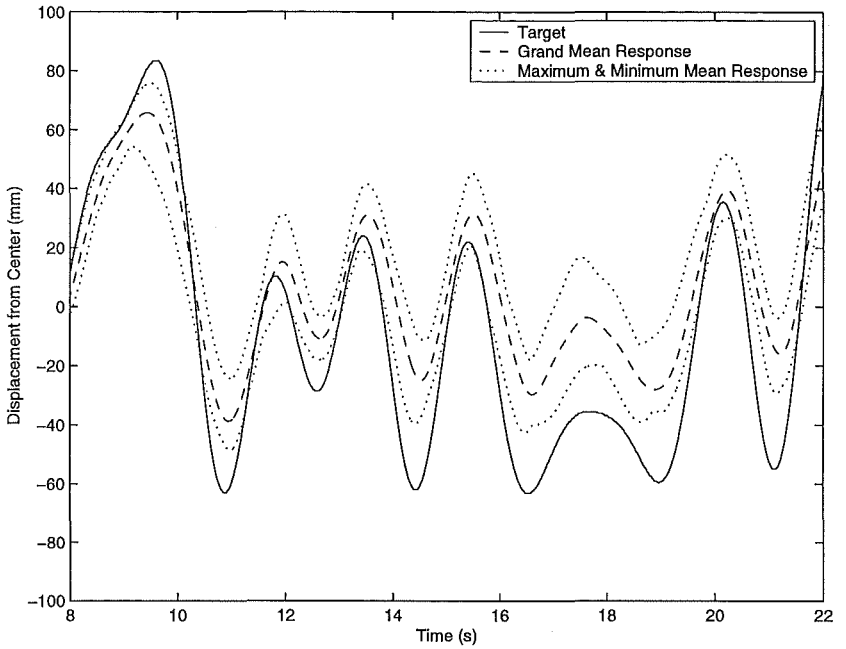

Fig. 62. Mean blanked responses for Group A (dynamic linear system). Dotted lines indicate the upper and lower limits of the mean (across subjects) for each run. Hence, the mean for any particular run falls between the dotted lines.

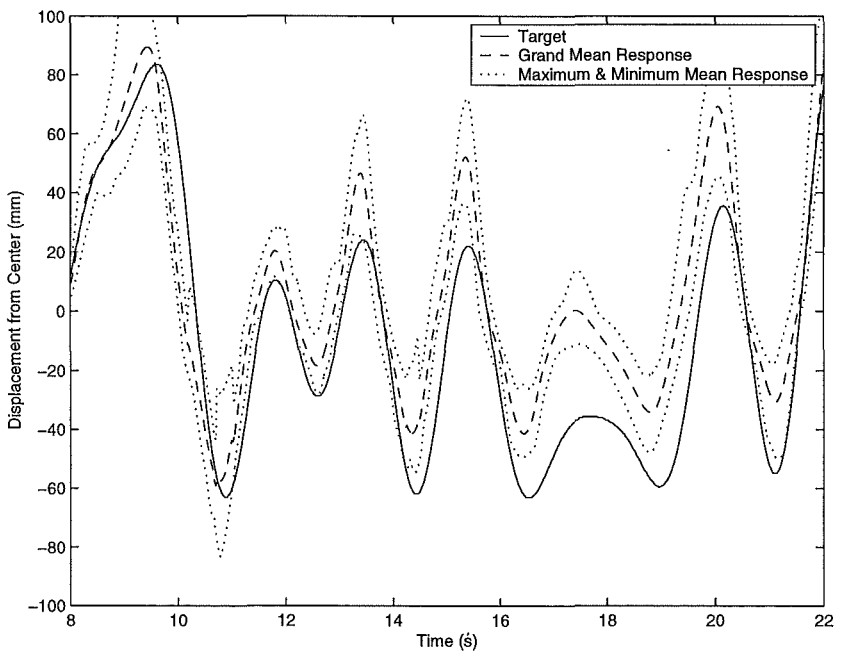

Fig. 63. Mean blanked responses for Group B (static nonlinear system). Dotted lines indicate the upper and lower limits of the mean (across subjects) for each run. Hence, the mean for any particular run falls between the dotted lines.

5.3.4 Quasi-linear Transfer Function Analysis

A full quasi-linear transfer function analysis was performed on the experimental data to further reveal the nature of the unusual blanked trajectories. The analysis also served to ensure that important learning effects were not masked in the error spectral analysis.

5.3.4.1 Mean Results

The mean results across all runs for the transfer function analyses of the blanked and unblanked (closed- and open-loop) results are shown in Fig. 64 and Fig. 65 respectively. When interpreting these mean results it is important to note that learning trends existed within the data, particularly in closed-loop, so that the mean does not reflect the transfer function after convergence. More detail on variance in the data is given in the full ANOVA analyses shown in Table 7, Table 8 and Table 9 in Appendix III.

Unblanked Transfer Function

As expected, the mean closed-loop transfer function closely approximated unity within the target bandwidth for all three external systems (see Fig. 64). This assertion is also supported by the clear trends toward unity shown in Fig. 91 (Appendix III). There were, however, clear differences between external systems.

For Group B and the practice runs the mean gain appears to drop slightly at higher frequencies. Conversely, group A shows a gain boost at 0.45 Hz.

All phase responses exhibited a lag. Results for the two static external systems (practice and Group B) exhibited similar phase responses characterized by a small lag with phase returning zero at 0.6 Hz. Group B, the dynamic external system, showed a phase lag monotonically increasing to 10° at 0.6 Hz. Individual phase responses exhibited a small lead or lag which was typically approximately linear within the target bandwidth (this effect is masked in Fig. 67).

Mean coherence was high across the target bandwidth for all external systems, particularly for the practice runs, though a small trend to reduced mean coherence with increasing frequency was observed for all three external systems.

These results were consistent with the subjects learning to control the external system so that the output tracks the target signal as accurately as possible.

Blanked Transfer Function

In contrast with the closed-loop responses, the mean open-loop transfer function did not exhibit accurate tracking of the target signal. The mean open-loop gain response showed a distinctive high-pass characteristic with a cut-off frequency of approximately 0.3 Hz (Fig. 61). Hence, low frequency performance appears to have been impaired substantially in open-loop.

The mean phase responses for the practice runs and Group B were again similar, exhibiting a maximum lead of 20° at 0.3 Hz and then reducing to around 15° at 0.6 Hz. Group B again showed increasing phase lag above 0.2 Hz. It is worth noting that the inter-subject variability was very large in both gain and phase, with one subject exhibiting a 50° phase lag at 0.6 Hz.

Mean coherence, like gain, was reduced below approximately 0.3 Hz.

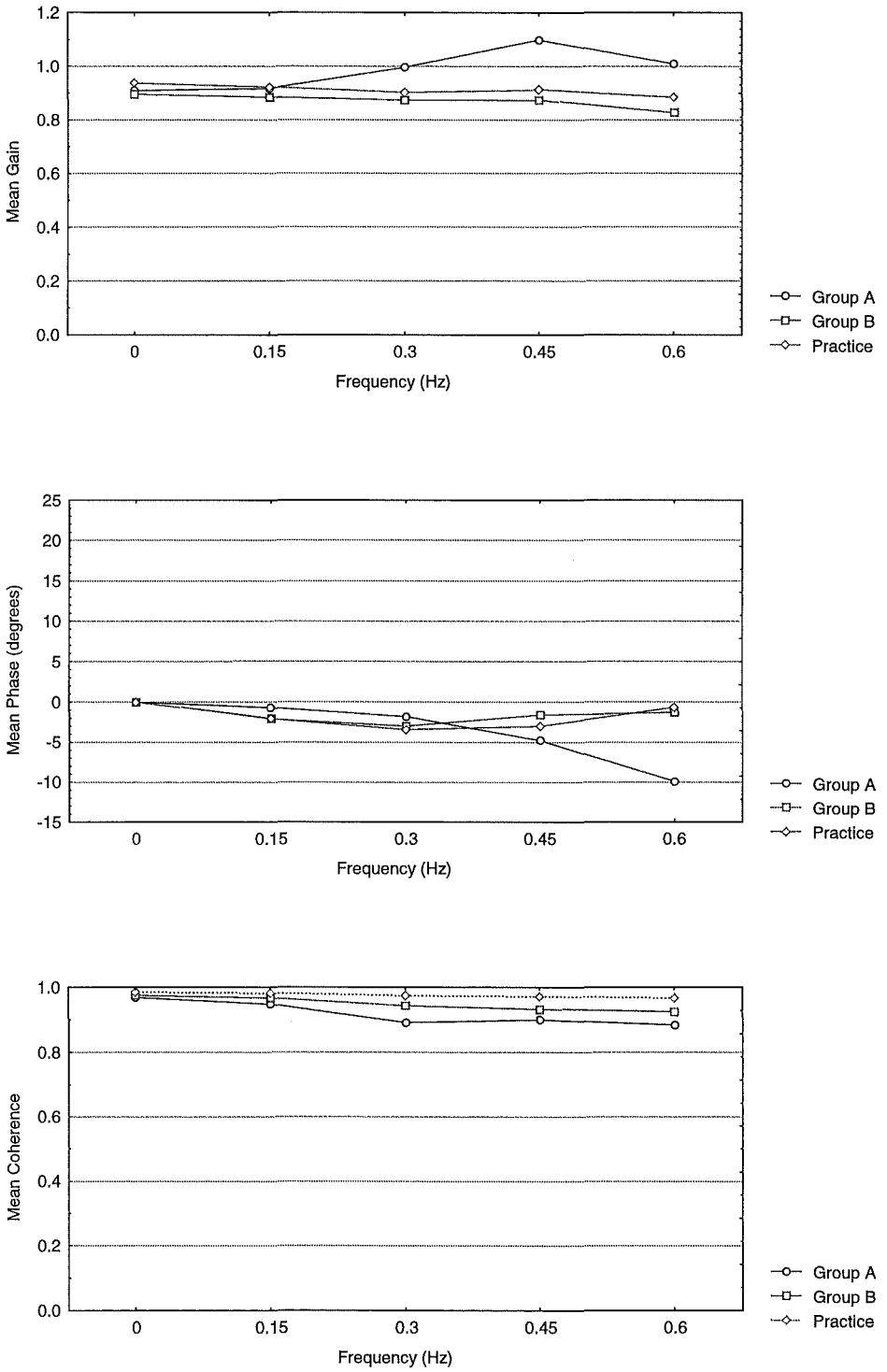

Fig. 64. Mean transfer function analyses across *all* unblanked (closed-loop) runs.

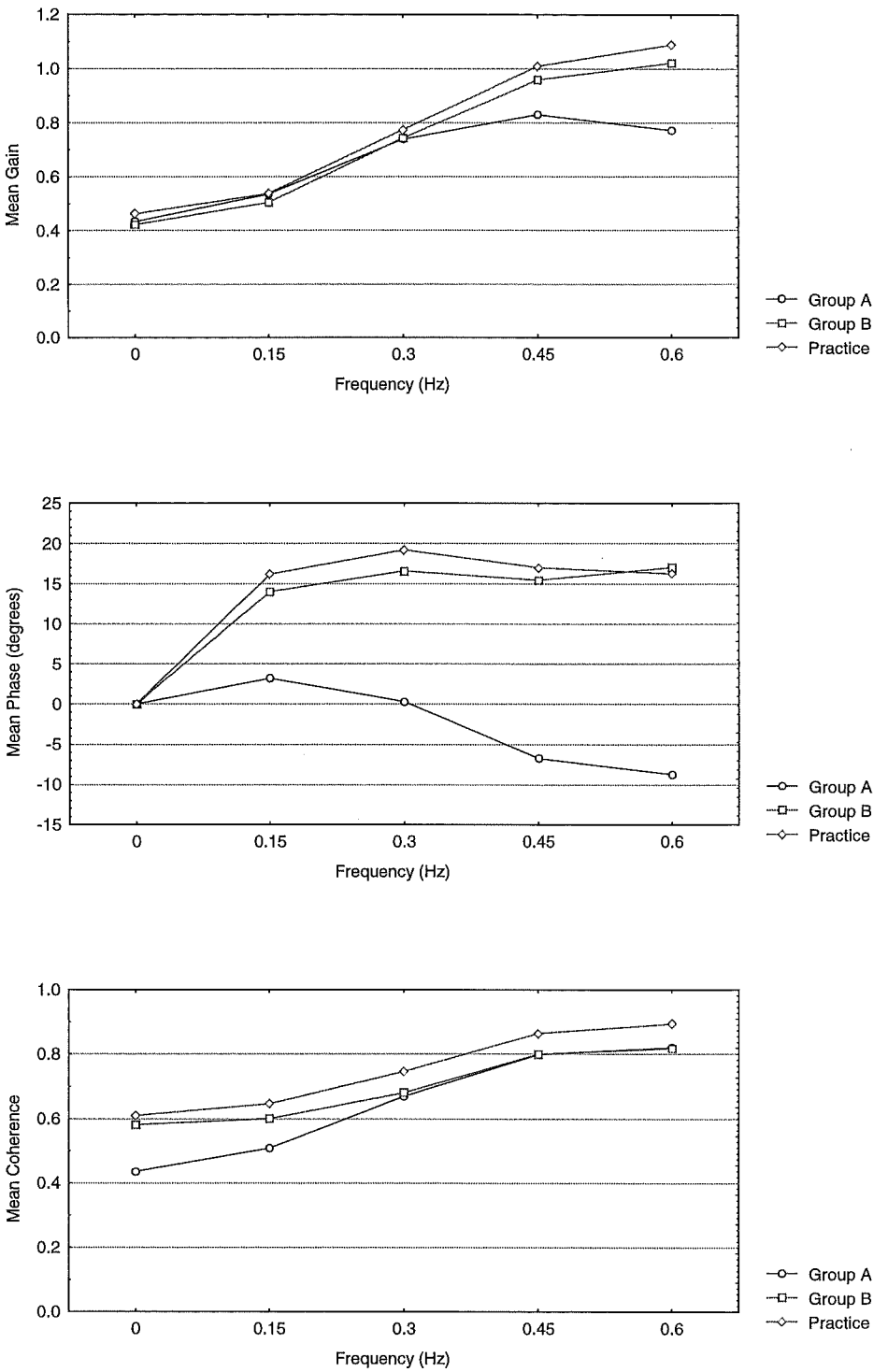

Fig. 65. Mean transfer function analyses across *all* blanked (open-loop) runs.

5.3.4.2 Graphical Indication of Variance (Zero-Order System)

Full analyses of variance for this data are provided in Table 7, Table 8 and Table 9 in Appendix III. A graphical representation of the between subjects variance for the closed- and open-loop results is provided in Fig. 66 and Fig. 67 respectively. These plots show results for the practice runs 6-10, representing behaviour after learning has essentially plateaued.

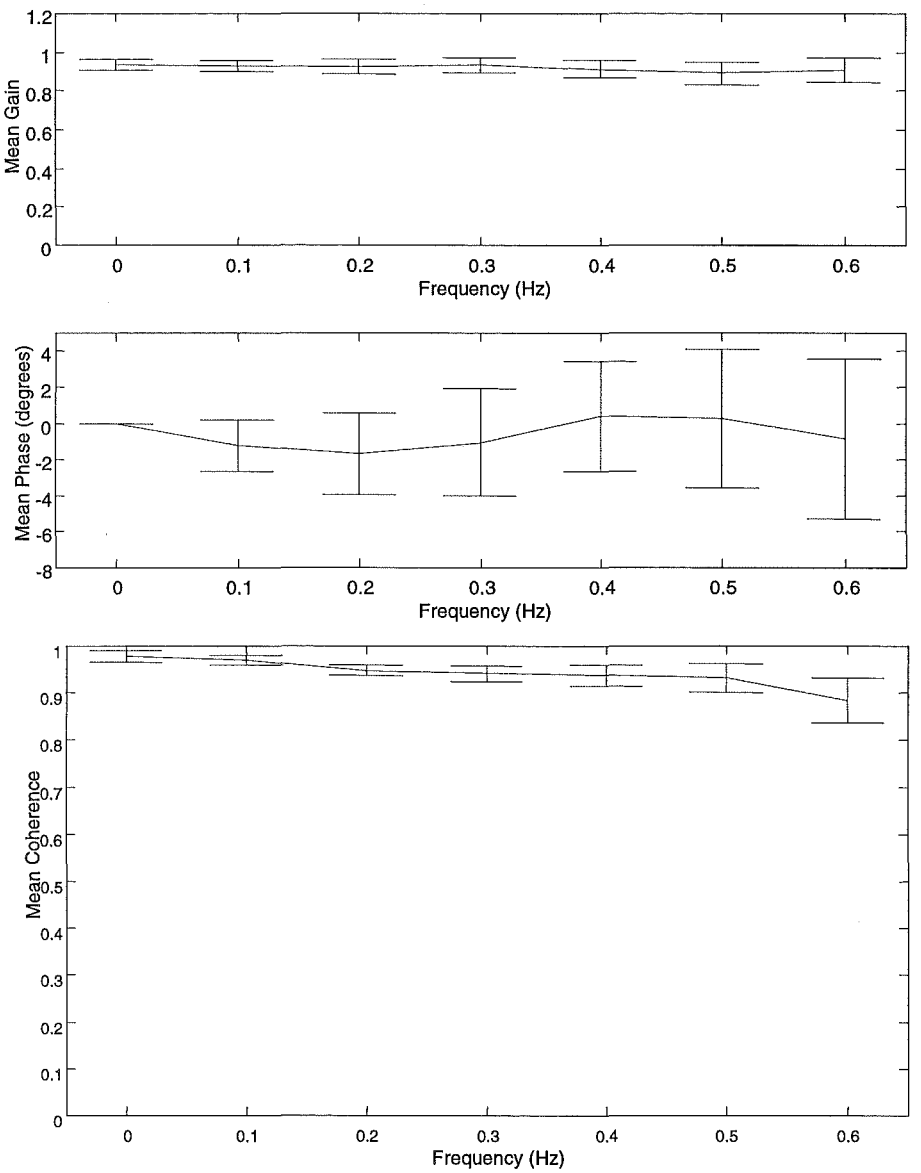

Fig. 66. Mean closed-loop transfer function, bars indicate standard deviation. Zero Order System, runs 6 –10 (following plateau).

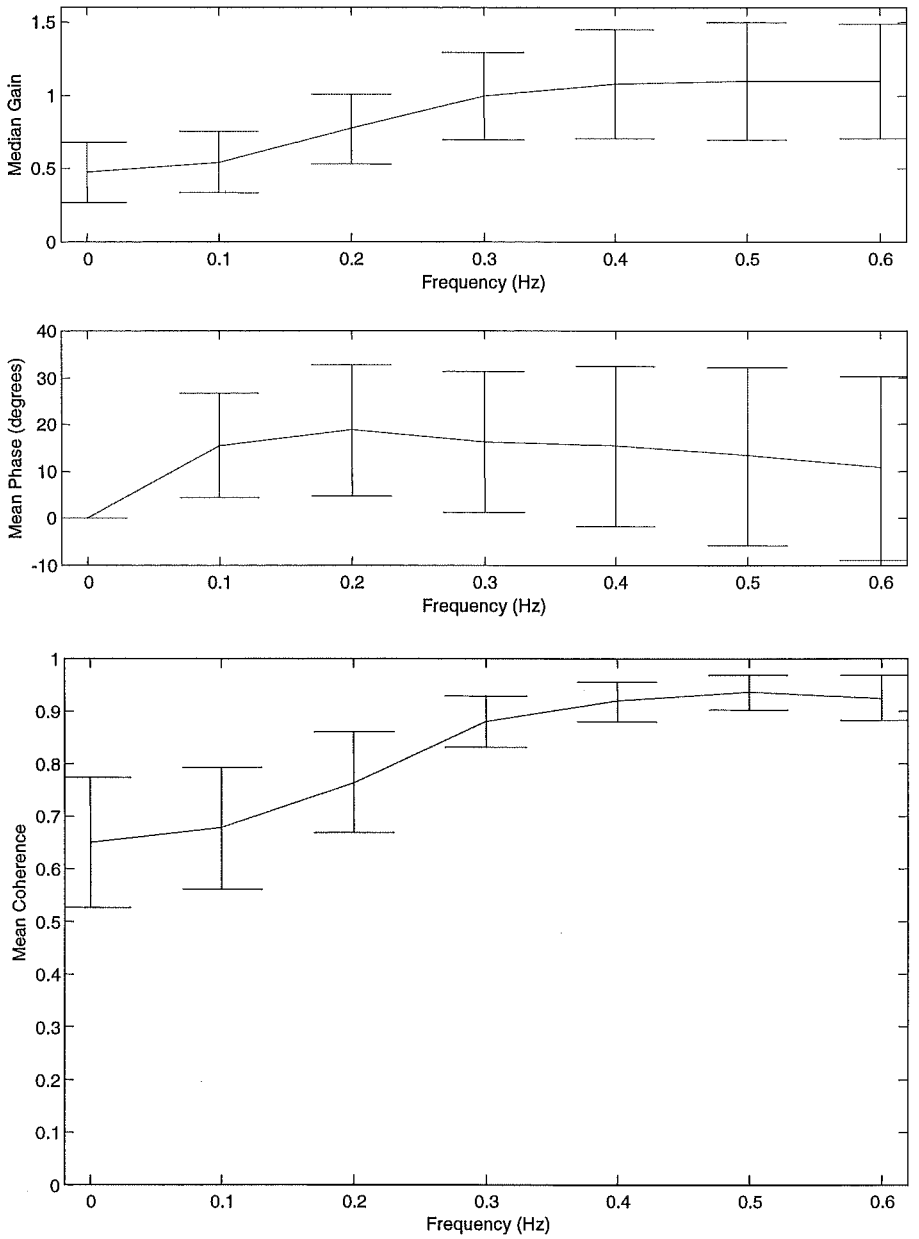

Fig. 67. Mean open-loop transfer function, bars indicate standard deviation. Zero Order System, runs 6 –10 (following plateau). Note the higher frequency resolution (0.1 Hz).

Open-loop variance is much greater than closed-loop variance. Open-loop gain and phase variance was greatest at higher frequencies while coherence variance was greatest at low frequencies.

5.3.4.3 Learning Trend Analysis

The statistical power of the trend analysis of the quasi-linear analysis results was low given the high degree of variance in the data. Subdivision of the data into gain, phase and coherence made it difficult to distinguish learning trends with statistical significance (see section 5.3.2.3 for a more meaningful analysis). The lengthy results of the full analysis are presented in Table 10 in Appendix III.

The practice runs showed learning trends in coherence (p = .002) but not in gain or phase. The experimental results yielded learning trends for Group B at 0.3 Hz in phase (p = .021) and coherence (p = .035). No learning trends were evident for Group A.

The mean results are plotted with respect to run in Appendix III (Fig. 91, Fig. 92, Fig. 93 and Fig. 94). These plots show that open-loop learning was not dominated by trends in gain, phase or coherence for the blanked or unblanked runs except for the blanked practice runs where coherence trends dominated.

5.4 Discussion

The finding of a reduction in RMS error over the blanked runs for Group B is consistent with adaptive feedforward control of a static nonlinear external system. Analysis of the error spectra confirmed this result, with learning trends in the lower half of the target bandwidth. This result supports the hypothesis that the brain forms inverse models of external controlled systems. Conversely, the data did not reveal the simple learning transfer from unblanked to blanked runs that would be expected for a pure adaptive inverse controller, hence suggesting the presence of an adaptive feedback control contribution.

No blanked performance improvement was observed for the dynamic linear external system, in RMS error or in the error spectral analysis, despite strong improvement in both during the unblanked runs. This indicates the importance of adaptive feedback in the control of difficult dynamic external systems.

The results imply adaptive feedforward control in the nervous system and are consistent with inverse model formation, though we recognize that other interpretations are possible. For example, the feedback-enabled section might be used to directly learn the necessary sequence of motor commands for use in the blanked section. This form of adaptation would constitute a form of feedforward adaptive control but would not require an inverse model. However, while this possibility cannot be ruled out, we consider it to be an unlikely explanation, particularly given the strong negative results for learning of the dynamic linear system (Group A).

5.4.1 Practice

Our conclusions rely on the assertion that, by the end of the practice sessions, learning of target signal statistics and the characteristics of the biomechanical system have essentially plateaued. Learning was confirmed to have ceased by run 6. This allows us to discount improved control of the biomechanical system (which has full proprioceptive and visual feedback) as a source of subsequent learning. The relative simplicity of the target (augmented with an 8-s preview) and the biomechanical system suggests that learning of their characteristics should plateau rapidly. Also, since the characteristics of the target and biomechanical system continue to be learned during the blanked phase

(when no learning of the external system can take place), our assertion of the rapid learning of these characteristics is strengthened.

5.4.2 Magnitude of the Error Signal

The mean RMS error scores for the blanked runs were much larger than for the unblanked runs, with the possible exception of run 1 for Group A (Fig. 56). The spectral results also show that the blanked runs have much larger mean error power at all frequencies in the target bandwidth, and beyond in the case of Group B (Fig. 57).

A combined feedforward and feedback control structure (as shown in Fig. 51c) would produce similar results if the feedback component adapted at a faster rate than the feedforward component. If the feedback component was still contributing to the control effort at the end of the experiment, then the removal of feedback would be accompanied by an increase in error because all remaining inaccuracies in the feedforward control, previously masked by feedback, would become visible. These inaccuracies may eventually disappear with further practice. Consequently, the results are consistent with a combination of feedforward and feedback adaptive control with each component apparently learning at a different rate. This idea is in agreement with experiments by Bhushan and Shadmehr (1999a) suggesting a learning rate differential between the forward and inverse models of subjects performing reaching movements in a dynamic force field. Their results appeared to show the forward model adapting at a rate five times faster than the inverse. The employment of adaptive feedback control in combination with inverse modelling is also consistent with several other theories including Neilson et al.'s (1992; 1997) adaptive model theory, Kawato et al.'s (1987) feedback-error learning and the offline inverse model learning hypothesis proposed by Jordan and Rumelhart (1992).

5.4.3 Learning Trends

The only significant blanked learning trends occurred for frequencies at and below 0.3 Hz for a static nonlinear external system (Group B, see Table 5). Since much of the error power was also clustered into this band (see Fig. 57), it is possible that higher frequencies did not reach significance due to their lower signal-to-noise ratio.

All three external systems used in the experiment show clearly differing error spectral characteristics between the unblanked and blanked responses in this low frequency range (with only the unblanked responses exhibiting a peak at low frequency). These low frequency peaks in the error spectra could be caused by the deactivation of an adaptive feedback control component. Accurate feedback control of low frequencies is relatively easy to achieve because the transmission delay (approximately 180 ms) is easier to compensate for when tracking a slowly moving target. An adaptive feedback controller might produce excellent low frequency performance when feedback is available, perhaps

with little or no observable adaptation. In this case, an adaptive feedforward component could learn from the behaviour of a feedback component while contributing little to the control effort due its relatively poor performance, as described by Jordan (1992). This may explain the performance improvement observed in the blanked results at low frequencies for Group B when no improvement is exhibited in the corresponding unblanked results (see Table 5). Continuously available and accurate feedback control for low frequencies implies that accurate feedforward control is less important, and might also explain the peak in blanked error power exhibited in this band (Fig. 57).

The apparent lack of feedforward adaptive control of the dynamic system controlled by Group A was particularly striking given the strong learning observed in the unblanked runs. This suggests that adaptive feedback control, probably involving forward modelling, is particularly important where the temporal characteristics of the controlled system are complex and may be related to the computational difficulty of forming inverse models for dynamic systems. Since linearity cannot generally be assumed, a nonlinear dynamic inverse is required which increases the complexity of the inversion problem and is likely to lead to slow adaptation (Hunt et al., 1992). A dominant feedback control component is in agreement with evidence of adaptive feedback control for learning arm movements in a dynamic environment (Bhushan et al., 1999b). Bhushan and Shadmehr were unable to separate the contribution of spinal reflex loops to the control effort. The study presented here suggests adaptive feedback control of an external system, where spinal reflex loops cannot operate.

The dynamic system used in the experiment was difficult to control (as evidenced by the relatively poor unblanked performance) and a less challenging dynamic system might allow faster feedforward adaptation. It is certainly possible that feedforward adaptation would become evident after many additional training runs, thereby providing more time for inverse adaptation. This notwithstanding, there was no evidence whatsoever of adaptive feedforward control of an external dynamic system in our study.

A similar experiment with a longer learning time might produce stronger feedforward learning trends, although this would be difficult to achieve with the current design since fatigue begins to take effect in many subjects by the end of the experimental runs. Extending the experiment over several sessions on different days might produce stronger results for both external systems and allow one to better determine the learning rate differential between the feedforward and feedback control components. There is also a possibility that a rest period between sessions might allow for off-line training of an inverse model (Jordan et al., 1992) and a comparison with the current results has the potential to test this hypothesis.

5.4.4 Blanked Response Trajectories

Despite a high degree of variation in blanked responses between subjects and runs, the mean of all blanked responses per run revealed a remarkably consistent trajectory

which differed strikingly from the target signal. The average response trajectory also varied surprisingly little between external systems and between runs. Further analysis revealed that the unusual trajectories are characterized by a high-pass gain and a phase lead (see Fig. 61). Low coherence in the lower half of the target bandwidth also characterized the response trajectories. These results confirmed that the blanked responses do not converge toward the target signal as predicted by existing control-systems type motor controls.

5.4.4.1 Open-loop Behaviour of Motor Models

If learning was due, even in part, to adaptive inverse control then both the unblanked and blanked response trajectories should become increasingly similar to the target as learning progresses. This is because in all combinations of feedback and feedforward adaptive control (as laid out in section 3.1) the feedforward controller gradually takes over control from the feedback controller. Hence, once a task is fully learned the loss of feedback would not affect the system because the inverse model would be accurate. During learning, therefore, the blanked response trajectory would be expected to become increasingly similar to the target.

We have observed some evidence of this effect, at least for Group B and the practice runs, but the open-loop learning rate is much lower than the closed-loop learning rate. Additionally, the blanked trajectories imply that the inverse model possesses a high-pass gain response which changes only gradually. The bulk of learning must, therefore, be undertaken by an adaptive feedback controller. While this is possible within the AMT framework, the inverse model appears to be surprisingly unimportant in the motor learning process (at least for this target signal bandwidth).

The motor control models represented in section 3.1 also have difficulty explaining how a high-pass characteristic and phase lead might emerge in an adaptive inverse model during learning. Even if the feedback controller is capable of correcting low frequency inaccuracy the inverse would quickly improve its own low frequency performance. Simulation confirms that this is the case. None of the possible combined control structures shown in section 3.1, which include both AMT and FEL, naturally generate a high-pass characteristic during learning.

5.4.4.2 Possible Explanations

The response trajectories might have been perturbed by a natural drift toward the dominant side. It was noted, however, that the mean response for left-handed subjects showed the same characteristics and did not exhibit any greater tendency to drift to the left.

It is possible that the use of the target preview varies between unblanked and blanked runs, which could result in a disturbed desired trajectory and lead to the observed results. The effect of the target preview on blanked performance was tested in a pilot study with

a well-trained subject. The results of this study, which suggest that target preview is not the cause of the unusual response trajectories, are provided in Appendix IV.

The most likely explanation for the observed blanked response trajectories is that the sudden loss of the feedback control caused the remaining inaccuracies in the feedforward control component to become visible. Relating the mean responses to the error spectra and quasi-linear transfer functions suggests that the apparent similarity between blanked responses for all external systems might be accounted for primarily at low frequency (0 – 0.3 Hz) where it has already been observed that error power and transfer function exhibits similar characteristics between systems. How these low frequency open-loop effects might emerge is not immediately obvious. Computer simulation of this experiment is therefore necessary to confirm the source of the unusual blanked responses.

Despite the importance of open-loop control in every day tasks, feedback is rarely absent for more than a few seconds at a time. Consequently, there may have been little selection pressure to maintain an inverse model in a stable state in the absence of feedback over longer intervals. This could provide an explanation for the high level of variance in the open-loop responses.

6. Computational Simulation

6.1 Introduction

Aside from providing direct insight into the extent and role of feedback in the human motor system, the response blanking study presented in Chapter 5 offers a benchmark against which to evaluate the nAMT model. The experimental data set provides information on human behaviour across a wide range of conditions: looking at the control of dynamic, static, linear and nonlinear external systems both with and without visual feedback. A complete human motor control model needs to be capable of reproducing the important effects captured in this human response data across the same range of conditions. In this chapter the nAMT model, as detailed in Chapter 4, is directly assessed against the experimental closed- and open-loop tracking results.

6.1.1 Primary Features of Experimental Results

The human tracking experiment in Chapter 5 produced response trajectories exhibiting unusual characteristics, particularly when the subjects were deprived of response feedback. Both the transfer function characteristics of the responses themselves and the way the characteristics evolve with time have the potential to reveal much about the adaptive processes underlying human motor performance. The primary features of the response trajectories are summarized here, providing the reader with a reference with which to judge the simulated results.

6.1.1.1 Open-loop Transfer Functions

- As shown in Fig. 65, the open-loop responses for all three external systems showed a mean high-pass gain with a cutoff frequency of approximately 0.3 Hz. The mean gains from 0 – 0.3 Hz were remarkably similar across all three external systems. This attenuation effect in the lower half of the target bandwidth, therefore, needs to be explained and reproduced for all three external systems in simulation.
- Fig. 65 also shows that the mean open-loop phase responses all exhibited a phase lead relative to the mean closed-loop phase. The phase lead effect was much stronger for the two static systems (zero-order and nonlinear), which exhibited an open-loop phase lead peaking from 15 - 20°. The dynamic linear system also showed a mean phase lead from 0 – 3 Hz which was absent in closed-loop.

- The open-loop results also exhibited a characteristic low-frequency drop in mean coherence.

The open-loop results do not indicate that the human subjects are attempting to reach a transfer function of unity, representing accurate tracking (as has been observed for closed-loop tracking). In fact, a quite different relationship between target and response appears to have emerged.

6.1.1.2 Closed-loop Transfer Functions

- The mean closed-loop gain functions (Fig. 64) contrast with the equivalent open-loop results. The closed-loop gain is close to unity (as expected for the human operator after extensive training) across the target bandwidth. No attenuation of low frequencies, as observed for the open-loop data, is evident. The gain for the dynamic linear system was higher than the other systems (possibly in compensation for the phase lag introduced by this external system).
- The mean phase responses were close to zero, except for the dynamic linear system which exhibited uncompensated phase lag.
- The mean closed-loop coherence is very close to unity for all three systems, indicating relatively little noise or nonlinearity.

In general, closed-loop performance at lower frequencies is superior to that at higher frequencies. The closed-loop results indicate that, to varying degrees for all three systems, the human subjects ares attempting to reach a transfer function of unity (which represents perfect tracking).

6.1.1.3 Learning Trends

Clear learning trends were evident in the closed-loop results but the learning observed in open-loop was relatively weak (see section 5.3.2.3). This supported the idea that there is a learning rate differential between the feedforward and feedback control components of the human motor control system. No learning was detected for the dynamic linear external system in open-loop. Learning trends were, however, detected in the open-loop results for both the static nonlinear external system and the practice runs.

In nAMT the same parameters, those of the forward model, are used for both feedforward control, through indirect inversion, and feedback control, through response prediction (which operates in combination with an independent stochastic disturbance predictor). This structure was selected in preference to two independent models (as used in FEL, for example) for parametric parsimony – it avoids the storage of multiple representations of the same information. This innovation, intended for efficiency, ties feedforward and feedback learning together to some degree. It is thought that the inaccuracy introduced by using a PID controller in the internal feedback loop (primarily for stability, see section 4.5) may mask some learning in open-loop mode, giving the

impression of a feedforward / feedback learning rate differential. This idea needed to be tested in simulation.

6.1.1.4 Note: Experimental Data on Diagrams

A summary of the experimental results, intended to assist the reader in judging the quality of the simulation, is included in all result diagrams in this chapter. The mean and standard deviation of the *final run* are shown on each diagram. By using only the final run, instead of the mean across all runs, learning effects do not interfere with the interpretation of results. The results represent the optimum transfer function learned by the subjects.

The frequency resolution of the quasi-linear analysis in this simulation was increased from 0.15 Hz to 0.1 Hz. A lower resolution was used in Chapter 5 to minimize the computation involved in the ANOVA statistical analysis.

The means shown in this section do not, therefore, correspond exactly with those presented Chapter 5.

6.1.2 Simulation Goals

The nAMT simulations performed in this chapter were intended to reproduce the key features of the experimental data, as summarized above. It was considered important, however, that the model function acceptably under all experimental conditions and, hopefully, explain the cause of the open-loop response trajectories from Chapter 5.

6.2 Simulation Structure

6.2.1 Overall Structure

The model structure shown in Fig. 68 was used in the closed-loop training phase of all simulations. Full detail on the internal structure of this model was provided in Chapter 4. The inverse model is formed by placing the forward model into a high-gain internal-feedback loop (see section 4.5). In this model, the musculoskeletal system is considered to be perfectly compensated for and is therefore absent from the diagram (as explained in section 1.4.5). The target signal T(t) and the external system P were taken directly from the experimental study. The remaining model parameters were initialized with typical parameters for a normal individual (see section 6.2.3).

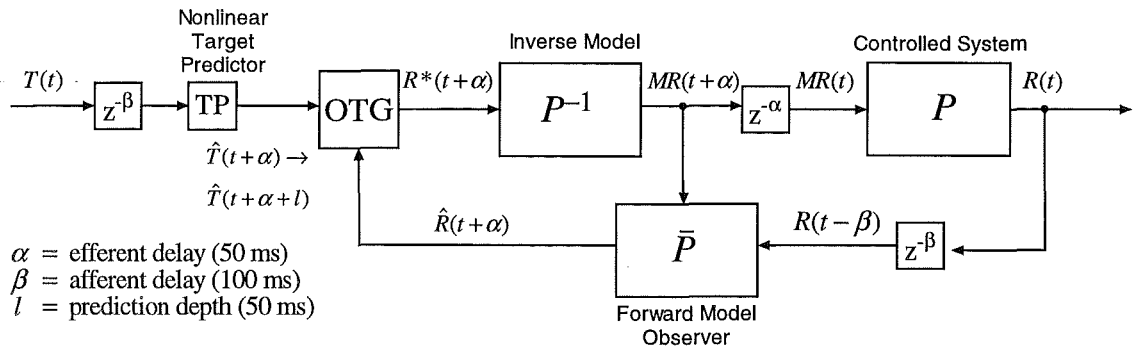

Fig. 68. nAMT model structure used in simulations.

6.2.2 Response Blanking

Response cursor blanking was simulated by removing response feedback $R(t)$ from the model shown in Fig. 68. It is unclear exactly how the nervous system compensates for the loss of this feedback signal and how best to represent this compensation in the model.

The most efficient course of action would probably involve replacing $R(t)$ with the most accurate internal estimate of that signal. $R(t)$ can be replaced at two places in Fig. 68: immediately after sensory feedback reaches brain at $R(t-\beta)$, or immediately prior to reaching the OTG at $\hat{R}(t+\alpha)$. In the absence of $R(t)$ itself, the desired response $R^*(t)$ provides the most accurate internal estimate, hence $R(t-\beta)$ may be replaced with $R^*(t-\beta)$ or $\hat{R}(t+\alpha)$ may be replaced with $R^*(t+\alpha)$.

6.2.2.1 Open-loop Structure 1 - Suspension of Corrective Movements

Losing response feedback could reasonably be expected to cause the controller to stop making corrective movements. This implies the complete disengagement of the feedback control pathways. In the model this can be achieved by replacing the predicted response $\hat{R}(t+\alpha)$ with the desired response $R^*(t+\alpha)$ (see Fig. 69). Because the error between desired and actual response observed by the OTG becomes zero no corrective movements are executed. Note that the OTG continues planning optimum trajectories but based only on target signal predictions.

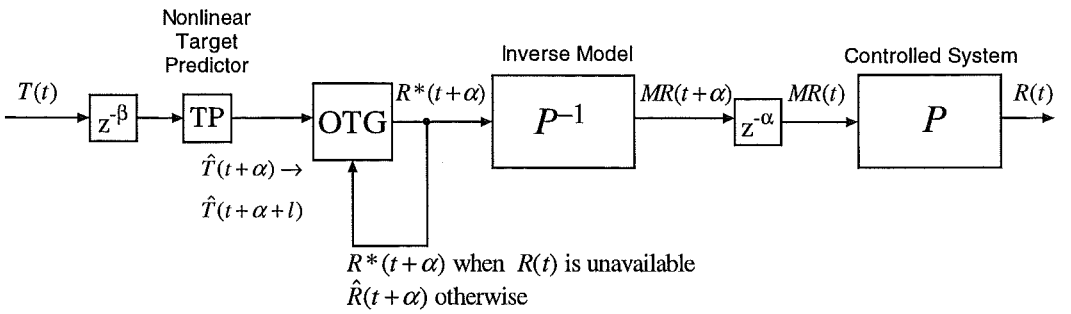

Fig. 69. Open-loop Structure 1. Approach based on suspending corrective action.

When response feedback is unavailable the error signal, the difference between R(t) and $R^*(t)$, becomes invalid. To avoid catastrophic detuning of the internal models, the adaptation process, which is driven by the error signal, must also halt. This simply requires the error to drop to zero whenever the response signal pathways become inactive. This could feasibly be implemented by a biological neural network.

This structure is probably the more neurobiologically plausible option of the two presented here. The changes required to move into open-loop mode are minimal and can be contained entirely within the response planning circuitry (i.e. within the OTG). Hence, when an invalid or nonexistent $\hat{R}(t+\alpha)$ input is detected the OTG simply ceases planning corrective movements. The disengagement of the corrective movement planning mechanism could be achieved by internally re-routing $R^*(t+\alpha)$, as shown in Fig. 69 and as is done in simulation, or by some other method depending on the specific internal structure of the OTG neural circuitry.

6.2.2.2 Open-loop Structure 2 - Ongoing Adaptation

The second suggested approach is to replace the response feedback input to the forward model observer $R(t-\beta)$ with the best internal estimate, a delayed version of the desired response $R^*(t-\beta)$. This differs from the previous arrangement in that an approximate error signal is now available so that adaptation can remain in action during open-loop operation. The new error signal is in fact an estimate, the accuracy of which depends on the accuracy of the inverse. Since the inverse is never entirely accurate, this error will cause perturbation of the model weights during response blanking. An effect like this has the potential to mask closed-loop learning in the inverse model when the system enters open-loop mode and is therefore potentially in agreement with the experimental results.

The predicted response input to the OTG used in this structure $\hat{R}(t+\alpha)$ is likely to be more accurate than that used in structure 1 $R^*(t+\alpha)$, since the former takes the actual motor response $MR(t+\alpha)$ into account, thereby partially compensating for

inaccuracy in the forward model. Whether this results in open-loop responses closer to those observed experimentally remained to be determined experimentally.

The principle disadvantage of structure 2 is that $R*(t+\alpha)$, which is considered to originate in the response planning circuitry in the frontal lobes of the brain, would need to be available at the $R(t-\beta)$ input to the forward model, which normally projects from the sensory cortices. While this is possible, the special purpose collateral connections required to implement the structure seem less likely to be used by the brain than the simple, and spatially local, reorganisation suggested in structure 1. Hence, while the approach may implement more accurate control it is probably less likely to be employed in the brain based on the AMT neuroanatomical model.

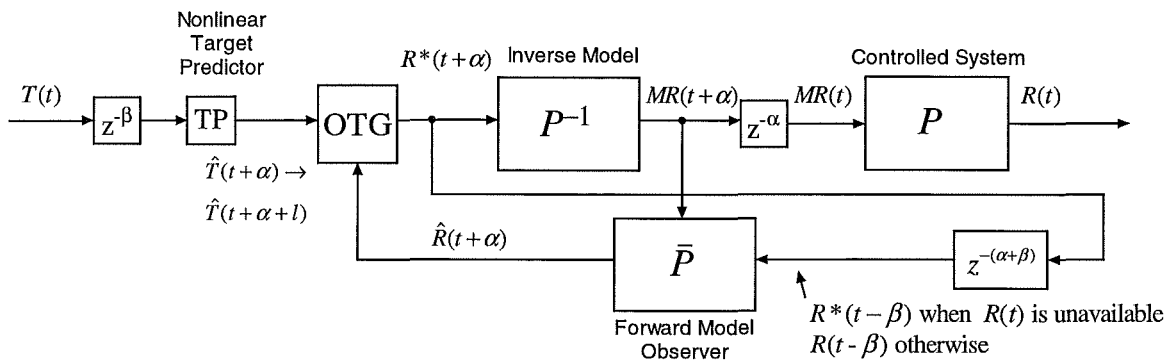

Fig. 70. Open-loop Structure 2. Structure allows adaptation to remain on during open-loop operation.

6.2.3 Noise Simulation

Internal noise was modelled by adding band-limited Gaussian white noise to the motor response $MR(t+\alpha)$. The noise was correlated with movement size by multiplying the noise signal by the change in MR over the previous sampling interval. This is based on the principle that faster movements are less accurate (Fitts, 1954). Correlating the noise magnitude with movement size allowed the noisy simulation to settle into a relatively noise-free steady state as observed during the experiment. The bandwidth of the noise was restricted to the target bandwidth. The variance of the Gaussian white noise generator ϕ was set to zero for noise-free simulations.

6.2.4 Initial Parameters

6.2.4.1 Delay Values

The efferent delay α represents the time between the generation of a motor command in the brain and the first measurable force in the muscles. This was set to $\alpha = 50$ ms in the simulation. The afferent delay, representing the remaining loop delay

(including visual processing time), was set to $\beta = 100$ ms. The delay values were quantized in accordance with the 50-ms sampling period of the simulation and are within the normal range quoted in the literature (Bhushan et al., 1999b; Schmidt, 1982).

6.2.4.2 Optimum Trajectory Generator

The parameters of the optimum trajectory generator were set to the typical values as determined experimentally by Sriharan (1997). The response planning time tp was set to 100 ms and the planned movement duration (or *prediction horizon*, th) was set to 150 ms.

6.2.4.3 Target Predictor

In the experimental design, care was taken to eliminate target-trajectory prediction as a confounding source of learning. Consequently the target predictor (see Fig. 68) was assumed to have been accurately tuned from the beginning of the simulation of the experimental runs. The predicted values $\hat{T}(t+\alpha)$ to $\hat{T}(t+\alpha+l)$ were set to their exact values.

6.2.4.4 Modelling Structure Details

All system identification units were constructed from 3 layer DNU networks. These networks possessed 16 neurons in the hidden layer and one output neuron. There were 1 or 2 inputs depending on location (there were 2 inputs in the case of the forward model observer). A linear bypass circuit was also included with buffer depth of 3 s. The simulation was run at a sampling rate of 20 Hz, in accordance with the existing AMT structure (Neilson et al., 1992), except for the high-gain internal feedback loop circuit which was simulated as a continuous feedback loop using Simulink®.

6.2.4.5 Initial Forward Model Parameters

The practice runs (see section 5.2.3.1) were simulated with the target predictor and internal model parameters initialized to small random values. The parameters reached after 10 simulated runs in control of the zero-order practice system were then used in the ensuing simulations. This ensured that the simulator was in approximately the same state as the experimental subjects at the beginning of the experimental runs.

6.2.4.6 Internal Feedback Loop Gain

The choice of gain of the feedback loop used for inversion of the forward model (see section 4.5) had a strong impact on model behaviour. The gain function was defined as follows:

$$K(e) = Pe + I\int e.dt + D\frac{de}{dt} \qquad (15.1)$$

where P, I and D are adjustable gain parameters and e is the feedback loop error.

For the purposes of this work it was assumed that the loop gain was constant throughout the simulation. A small integral component was necessary to eliminate steady-state error in the inverse model. Consequently, $I = 0.05$ was used for all runs and is not explicitly quoted in the following results where loop gain parameters are mentioned.

It is possible that the internal feedback-loop parameters vary as the internal model adapts and simulation of this behaviour is suggested as an area for further investigation.

6.3 Methods

6.3.1 Simulation of Practice Runs - Determining Model Parameters

The simulation began with ten practice runs as performed in the experimental study. In these a simple zero-order gain was assigned as the external system. The adaptation coefficient of the forward model μ was set to 0.001 which was found, by trial error , to approximate the learning rate observed during the experimental practice runs (see section 5.3.1). It was important that μ be set so that learning had essentially plateaued after the final (10^{th}) run, and $\mu = 0.001$ satisfied this requirement. The internal feedback loop-gain was set to $P = 10$ to provide acceptable inverse model performance during the initial learning process. This arbitrary value was acceptable since the loop-gain has relatively little effect on the learning of the forward model (an assertion that was confirmed by adjusting K and comparing forward model characteristics). The model weights at the end of the ten practice runs were stored for use in the subsequent experimental runs.

The simulated practice results could not be compared directly with the experimental results until after the internal model had approximately converged, which should have happened by the end of practice. This is because the human subjects are likely to begin the practice runs using an approximate internal model based on past experience, whereas the model was simply initialized with random weights (see section 6.2.4.5).

It was desirable to determine appropriate values for the loop-gain and adaptation rate parameters prior to the full experimental run simulations. These full simulations were relatively time consuming, requiring 15 full runs each, rendering iterative tuning of the parameters impractical.

Once the practice run learning was complete, the forward model itself was affected only minimally by variation in loop-gain and adaptation rate (provided stability was maintained). This allowed a strategy to be devised whereby appropriate parameters for the experimental runs could be determined a-priori. The previously learned zero-order forward model was loaded into the nAMT model, with adaptation turned off, and

iterative alterations to the parameters were made so that their effect on closed- and open-loop trajectories could be judged efficiently.

It was hoped that a single set of parameters could be found that would perform acceptably across *all* conditions in the experiment.

6.3.1.1 Internal Feedback Loop Gain

The function of the internal feedback loop is to approximately invert the internal forward model (see section 4.5). In theory the loop-gain should be set as high as possible but, in practice, the gain is limited by the necessity to avoid instability as the weights of the forward model vary. Fortunately, the AMT feedback loop through the OTG acts to partially compensate for inaccuracy caused by a lower than ideal feedback loop-gain. The overall behaviour of the system, particularly in open-loop mode in which no corrective movement is possible, remains strongly affected by the internal feedback loop-gain.

Open-loop structure 1, shown in Fig. 69, was employed in a set of simulations intended to investigate the effect of internal feedback loop-gain on response trajectories. Several complete runs were performed in which the forward model was initialized with parameters established at the end of the practice runs. A different loop-gain K was used for each run. The parameters used for the four representative runs presented in the results are listed in Table 6 (integral gain $I = 0.05$ not shown). The parameters were adjusted at the end of each run based on the results of the previous results so that, eventually, the simulation output matched the experimental results as closely as possible.

Table 6. Simulated feedback loop-gains.

Run No.	P	D
1	1	0
2	10	0
3	1	4
4	0.5	1

These same simulations were repeated using open-loop structure 2 so that the behaviour of the scheme could be compared directly.

6.3.1.2 Additive Noise

The effect of adding noise, using the noise generator described in section 6.2.3, was investigated, based on the optimal loop-gain parameters determined in the previous investigation. The mean results of ten runs at each of four distinct noise levels are presented. The overall effects of varying the noise level for open-loop structure 1 on the overall transfer function of the system was determined.

Running full experimental simulations including noise analysis would be prohibitively time consuming since each simulation set would need to be repeated many times to

achieve statistically significant results. This was avoided by noting the effect of additive noise on this zero-order system and extrapolating this result to the experimental results.

6.3.1.3 Adaptation Coefficient (Open-loop Structure 2 Only)

Open-loop structure 2 from section 6.2.2.2 was used in a series of simulations where the adaptation coefficient μ was adjusted. This allowed the effect of this parameter on open-loop behaviour to be assessed. The adaptation rate of the internal forward model was expected to have a strong effect on the open-loop response characteristics. Since this simulation was performed with a fully trained forward model, any effect could be interpreted as a perturbation or detuning of that model caused by withholding visual feedback. The adaptation parameter μ was varied between 0 (representing no adaptation) and 0.01, which was marginally stable. The feedback loop-gain was set to $P = 0.5,\ D = 1$ which was found to produce good results for structure 1.

6.3.2 Simulation of Experimental Runs

6.3.2.1 Dynamic Linear External System

Simulation of the experimental runs began with the dynamic linear external system defined in section 5.2.2.1. Fifteen runs were simulated in accordance with the 15 experimental runs performed by the human subjects. The model was initialized with several different adaptation coefficients so that an appropriate learning rate could be determined. $\mu = 0.001$ produced a response with an appropriate closed-loop learning time constant (compared with experimental results from human subjects) and these results are therefore reported.

The internal loop-gain settings found to produce good results for a zero-order system (see section 6.3.1.1) were was also used for these runs ($P = 0.5,\ D = 1$). Trial runs with various other feedback-loop gains produced no clear improvements, and it was very desirable to maintain similar settings between external systems.

6.3.2.2 Static Nonlinear External System

In contrast with the previous external systems, the static nonlinear system was expected to make strong use of the locally-recurrent dynamic neural network (LRNN) component of the modelling circuitry. For consistency, exactly the same experimental procedure and model parameters used for the dynamic linear system were used in this simulation.

Contribution of LRNN Nonlinear Modelling

To determine the importance of the nonlinear modelling circuitry in achieving the quality of the simulated result, the experimental run simulation was repeated with the adaptation coefficient of the LRNN set to zero. This prevents the LRNN from learning

and contributing to improved performance while learning to control the new external system. The linear bypass circuitry was still in operation at the normal adaptation rate so any improvement may be attributed to this adaptive linear model. Note that the existing nonlinear transformation, as formed to model the zero-order system used in the practice runs, remains in place during this simulation. Removing the LRNN circuitry entirely would invalidate the zero-order model learned by the linear circuitry in the practice runs, rendering a fair comparison impossible.

6.4 Simulation Results

6.4.1 Practice Runs - Determining Model Parameters for Experimental Runs Simulations

6.4.1.1 Internal Feedback Loop Gain

Open-loop Structure 1

The results of four runs with differing loop-gains using open-loop structure 1 are shown in Fig. 71. Experimental mean and standard deviations are also shown for comparison.

Selecting a low proportional gain for the internal feedback loop (P = 1) resulted in a low-pass transfer function for both closed- and open-loop. Closed-loop gain was close to unity below 0.2 Hz but reduced markedly at high frequencies. A strong closed-loop phase lag (reaching 36° at 0.6 Hz) was also apparent. The open-loop phase response also shows phase lag though to much reduced extent (10° at 0.6 Hz). The open-loop gain was very low producing poor overall performance.

Increasing the proportional gain ($P = 10$) resulted in an increased gain and reduced phase lag in both feedback modes. Increasing P beyond 10 produced a minor additional improvement in the gain and phase responses (not shown in diagram).

The high frequency gain drop-off, visible for all simulated loop-gains, remains even for very high loop-gains ($P = 100$). At these high loop-gain levels, achievable due to the simplicity of the external system, the inversion of the forward model is very accurate (which does not necessarily imply that the inverse itself is accurate - this depends on the quality of the forward model). This result indicates that the forward model, which was trained prior to performing these simulations, was not completely accurate at the end of the practice runs. Simulating the training of the forward model for longer than the 10 runs performed in the actual experiment does indeed improve high-frequency performance marginally (resulting in a gain at 0.6 Hz = 0.85). It is worth noting that a similar, though much weaker, reduction in high frequency gain was evident in the

experimental results. This effect, however, remains a point of difference between the simulated and experimental results at high frequencies. The effect should be kept in mind when interpreting the simulated results and comparing with actual results. The closed-loop result for P = 10, which is shown in Fig. 71, approximately represents the most accurate inverse that can be achieved for this particular forward model (i.e. increasing P beyond this has little impact). Other behaviour should therefore be judged relative to this result.

Adding a derivative component to the low proportional feedback gain ($P = 1,\ D = 4$) increased the closed- and open-loop gain, and introduced phase lead in open-loop. An attenuation of low frequencies (below 0.2 Hz) is evident in open-loop mode but not in closed-loop. This is important as a high-pass gain and phase lead were characteristic of the experimental open-loop response. In closed-loop the derivative gain produced results similar to those for the high proportional gain, P = 10. This suggested that it is possible to reduce the proportional gain component for improved stability if a derivative gain is employed.

Reducing both the proportional and derivative components produced performance remarkably similar to the experimental observations. $P = 0.5,\ D = 1$ produced little reduction in gain and no change in the phase response in closed-loop relative to $P = 1,\ D = 4$. In open-loop the reduction in low-frequency gain mirrored the experimental results as did the strong phase lead with a peak (of around 20°) at lower frequencies. Interestingly, the phase lead is greater than for the previous $P = 1,\ D = 4$ setting with a much stronger derivative component. With the exception of the high-frequency behaviour, as explained previously, these parameters produce results remarkably similar to the observed experimental results.

The closed-loop coherence remained high irrespective of the feedback gain but adding a derivative component notably reduced the open-loop coherence at frequencies below 0.3 Hz. Low coherence in open-loop mode at frequencies below 0.3 Hz was also characteristic of the experimental results, so this effect may be useful in reproducing the experimental trajectories. $P = 0.5,\ D = 1$ again produced results which were similar to the experimental results. The simulated coherence appears high compared with the experimental results but these simulations were noise free and adding noise was expected to reduce coherence.

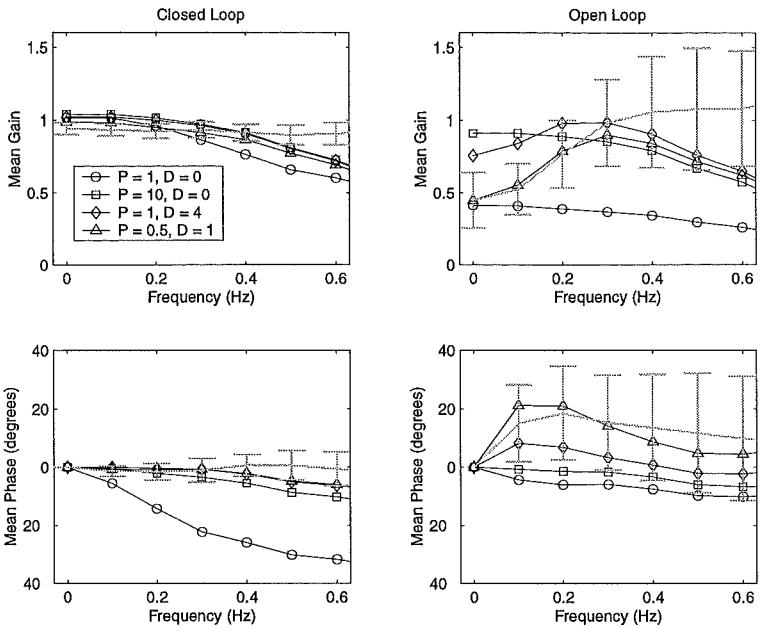

a)

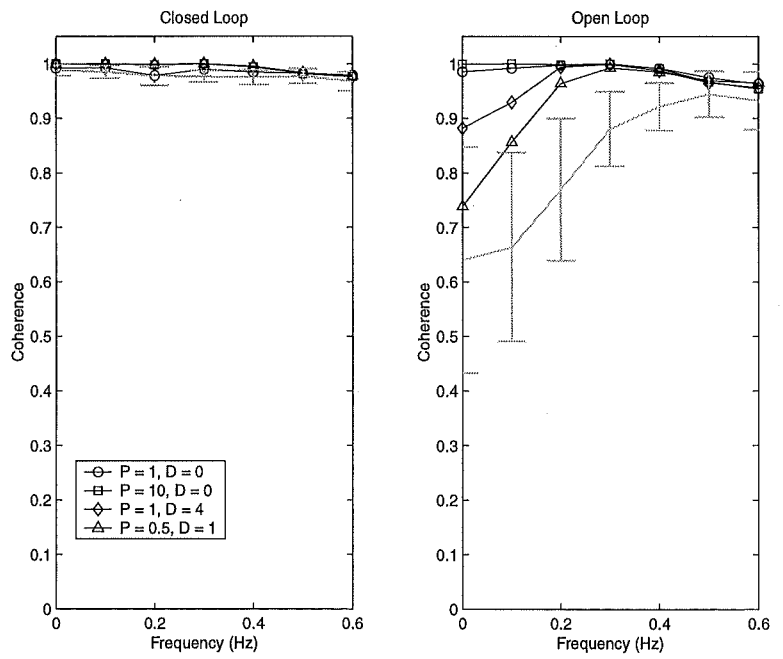

b)

Fig. 71. Effect of internal feedback loop gain on a) the transfer function and b) coherence of simulated response (zero-order external system) with open-loop structure 1. Experimental mean and standard deviation for the final run shown in grey.

Open-loop Structure 2

Using open-loop structure 2 caused large differences in open-loop behaviour. The results for four simulations with different internal feedback loop-gains and using this structure are shown in Fig. 72. This plot can be compared directly with the equivalent result for structure 1 in Fig. 71. Whereas in structure 1 a drop in low frequency gain was

observed when derivative action was included in the internal feedback loop-gain, no such reduction was observed for structure 2. Additionally, no strong drop in coherence at low frequency was observed for any loop-gain as for structure 1. These two features were characteristic of the experimental results (mean and standard deviation shown in Fig. 71) .

Open-loop performance is superior for structure 2 since, as was discussed in section 6.2.2.2, the open-loop behaviour of structure 2 more closely reflects closed-loop behaviour when the inverse is less accurate than the forward model. This strong relationship between closed- and open-loop behaviour contrasts with both the experimental results and those for Structure 1.

6.4.1.2 Additive Noise

Fig. 73 shows the effect of adding noise to the simulation for a loop-gain of P = 0.5, D = 1. A general reduction in the gain of the closed- and open-loop responses with increasing noise level was observed. The exception was for noise variance $\phi = 0.8$ in open-loop where the gain increased. An increase in open-loop phase lead was observed as the noise level was increased.

The results show that adding noise causes a systematic reduction in open-loop coherence across the bandwidth (see Fig. 73). In closed-loop the coherence drops primarily at high frequencies, demonstrating that the feedback-controller has a stronger effect at lower frequencies. At 0.6 Hz the coherence in closed-and open-loop are similar.

Noise variance $\phi = 0.05$ produces the results most similar to the experimental results for the zero-order system.

6.4.1.3 Effect of adaptation coefficient

Raising the adaptation coefficient progressively attenuates the low-frequency gain and introduces the phase advance characteristics observed in the open-loop experimental results. In this structure, however, the effect is accompanied by a degradation of closed-loop performance. This is caused by detuning of the forward model in open-loop mode leading to reduced closed-loop performance. The effect is apparent in the transfer function analysis shown in Fig. 74 (result for $\mu = 0$ shows no detuning).

Overall, the results for structure 2 are inferior to structure 1 in terms of reproducing the key features of the experimental response trajectories. Consequently structure 1 was used for the coming full experimental run simulations.

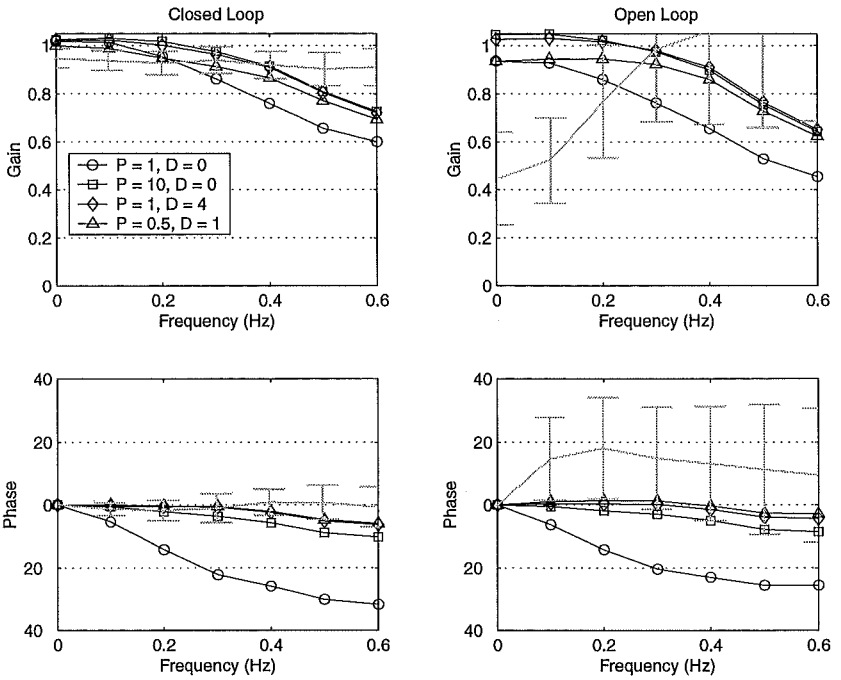

a)

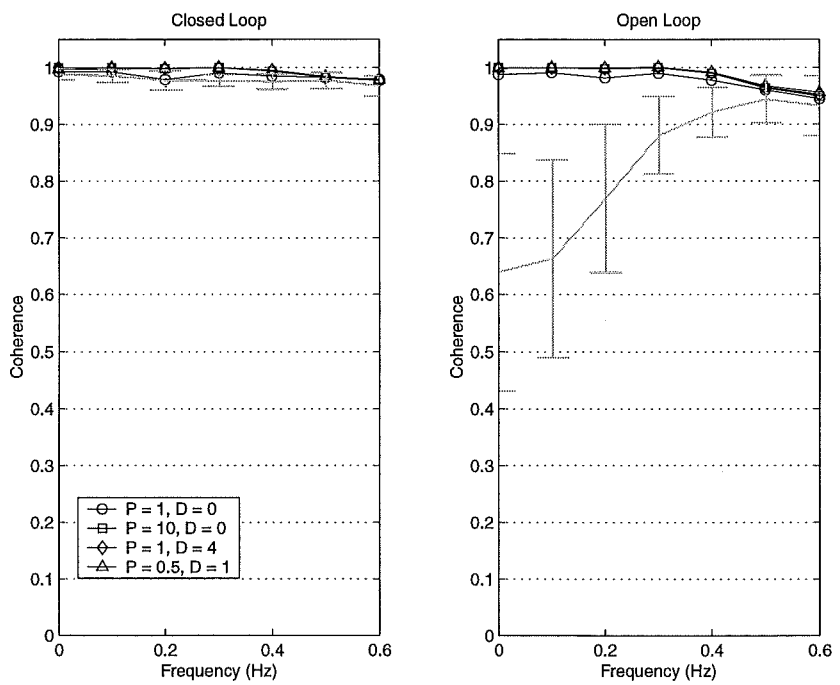

b)

Fig. 72. Effect of internal feedback gain on a) transfer function and b) coherence of simulated response (zero-order external system) with open-loop structure 2. Experimental mean and standard deviation for the final run is shown in grey.

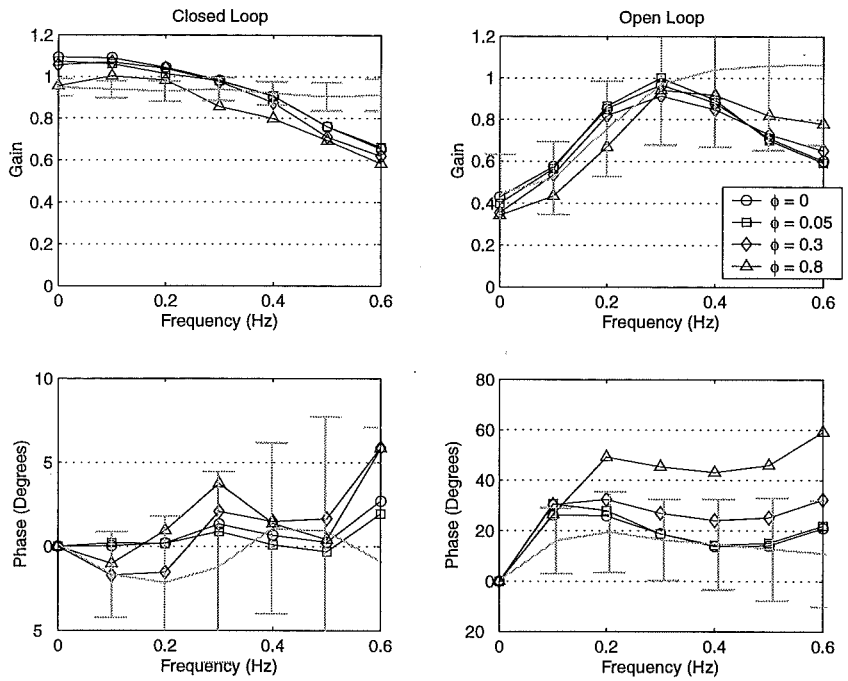

a)

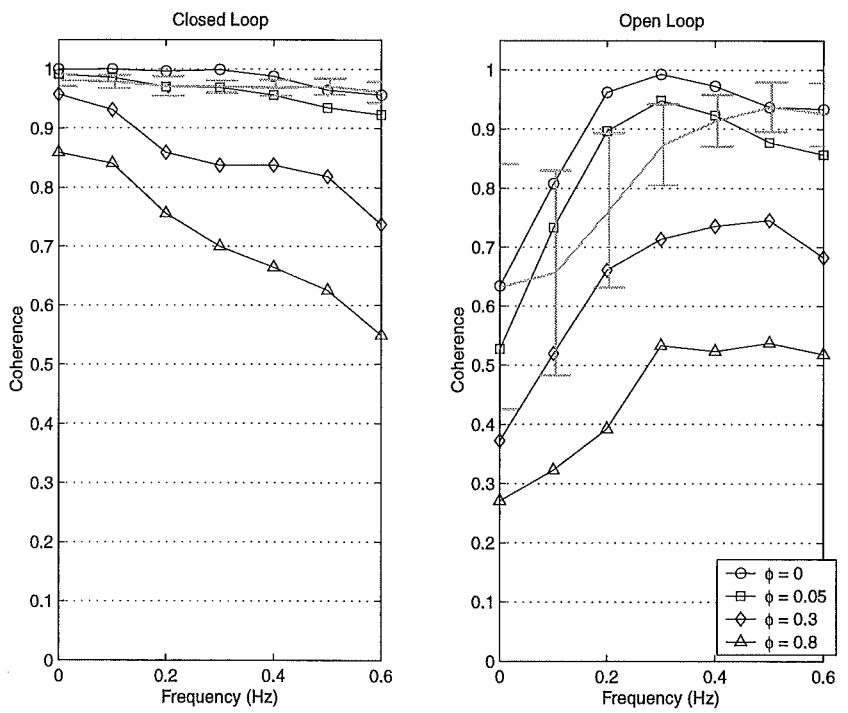

b)

Fig. 73. Effect of noise power on a) transfer function and b) coherence of simulated response (zero-order external system). Results are for the mean of 10 runs, ϕ = noise variance. P = 0.5, D = 1. Experimental mean and standard deviation for the final run is shown in grey.

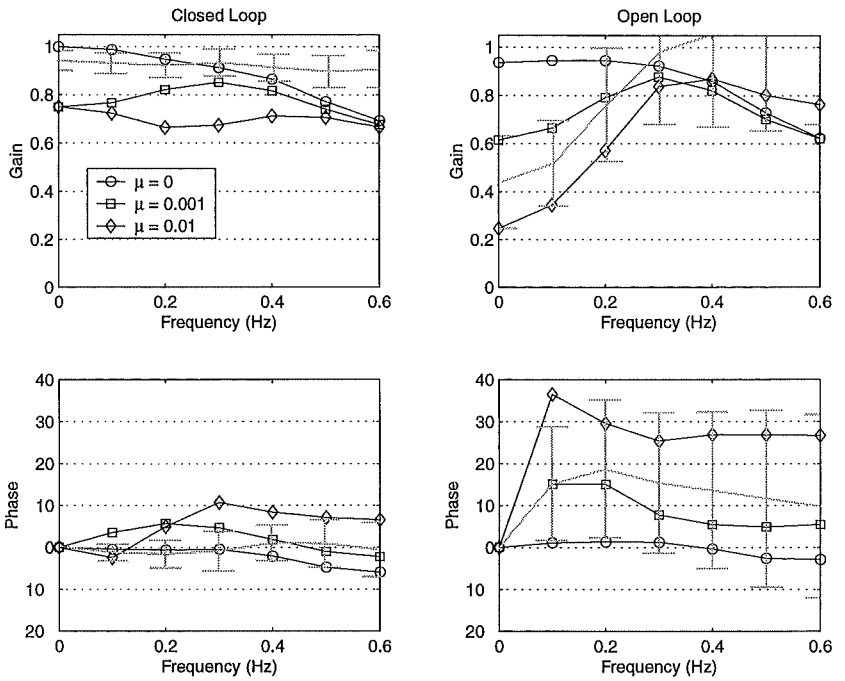

a)

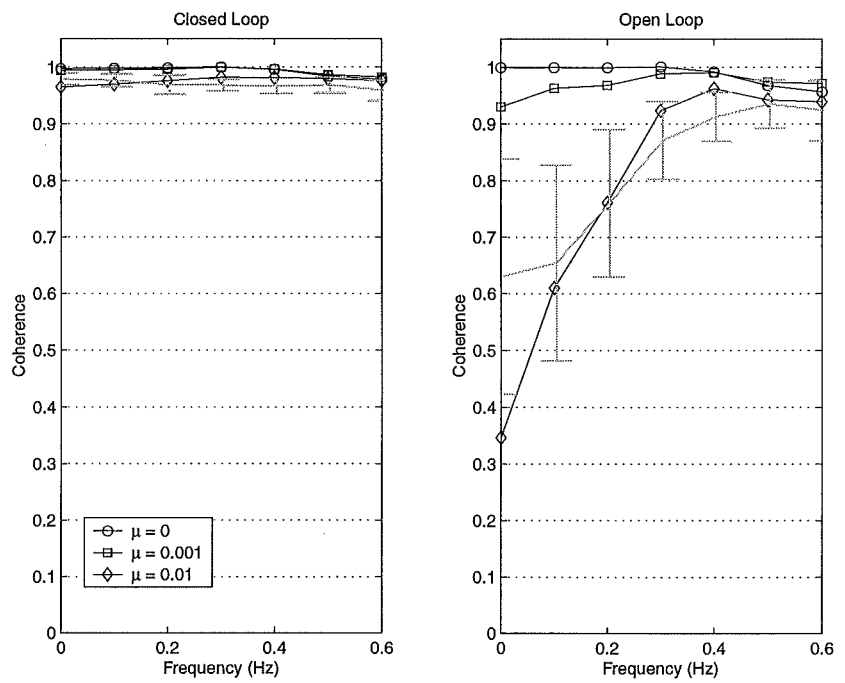

b)

Fig. 74. Effect of adaptation coefficient on the a) transfer function and b) coherence of simulated responses (zero-order external system). P = 0.5, D = 1. Experimental mean and standard deviation for the final run is shown in grey.

6.4.2 Experimental Runs

6.4.2.1 Dynamic Linear External System

Learning - RMS error

The RMS error results for the dynamic linear system are shown in Fig. 75. Removing response feedback caused the RMS error to increase and resulted in a perturbed response trajectory which was consistent with the experimental results. Also in common with the experimental results, the open-loop RMS error did not improve in proportion with the closed-loop RMS error remaining at a much higher level (around 23). Interestingly, while some learning is evident in open-loop, the learning appears to plateau faster than for the closed-loop results which supports the idea that the presence of a relatively low internal feedback loop-gain can obscure closed-loop learning (see section 6.1.1.3). This is necessary if the apparent feedforward /feedback learning rate differential observed in the experimental results is to be achieved in nAMT.

In the human motor control system noise is likely to obscure a minimal open-loop improvement like that observed in Fig. 75. This may explaining why no improvement in open-loop performance was detected experimentally. Both the closed- and open-loop results show lower RMS error levels than the experimental results, which can be attributed to a lack of noise in the simulation since this reduces performance across the target bandwidth (see section 6.4.1.2).

Learning - Error Spectra

Error spectral analyses across all 15 simulated runs, including experimental results, are shown in Fig. 76. The open-loop error spectra (Fig. 76a) show slight learning trends, contrasting with the strong trends in closed-loop. Overall trends are remarkably similar to the mean experimental results (Fig. 76b), with lower frequency power dominating the open-loop error. The addition of noise to the simulation would account for the increased mean values and variance seen in the experimental results.

These results demonstrate that it is possible for the nAMT model to exhibit marked difference in closed-and open-loop results, despite the feedback and feedforward controllers sharing model parameters.

Quasi-linear Transfer Function Analysis

The transfer function and coherence plots for the final run (number 15) are shown in Fig. 77. The closed-loop results show a phase lag and a gain above 0.9 at all frequencies. The coherence is also very high in closed-loop. These superior closed-loop results are due to the action of the feedback controller. The only notable difference between the experimental and simulated transfer functions is the absence in the simulated results of a peak at 0.3 Hz. The cause of this peak in the experimental results is unknown. The

experimental results exhibit less coherence and more variance than the simulation, which was expected because noise was not included in the simulation.

The open-loop results show the same characteristic drop in gain and coherence below 0.3 Hz that was observed in the experimental results. The open-loop results also show a phase lead which is consistent with the results of several individual subjects, though this effect is obscured in the mean .

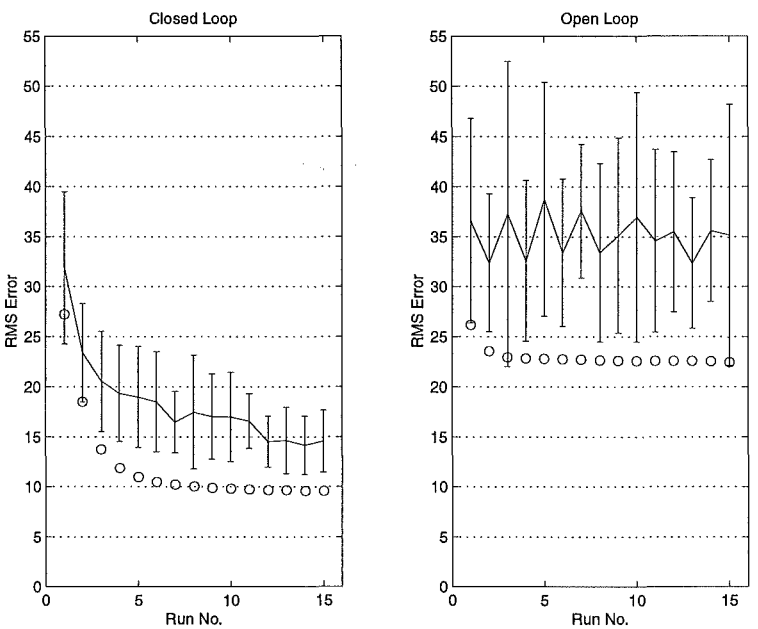

Fig. 75. Simulated RMS error in relation to experimental results (final run, dynamic linear system). Experimental results shown with solid lines. Bars indicate standard deviation. Simulated results indicated with circles.

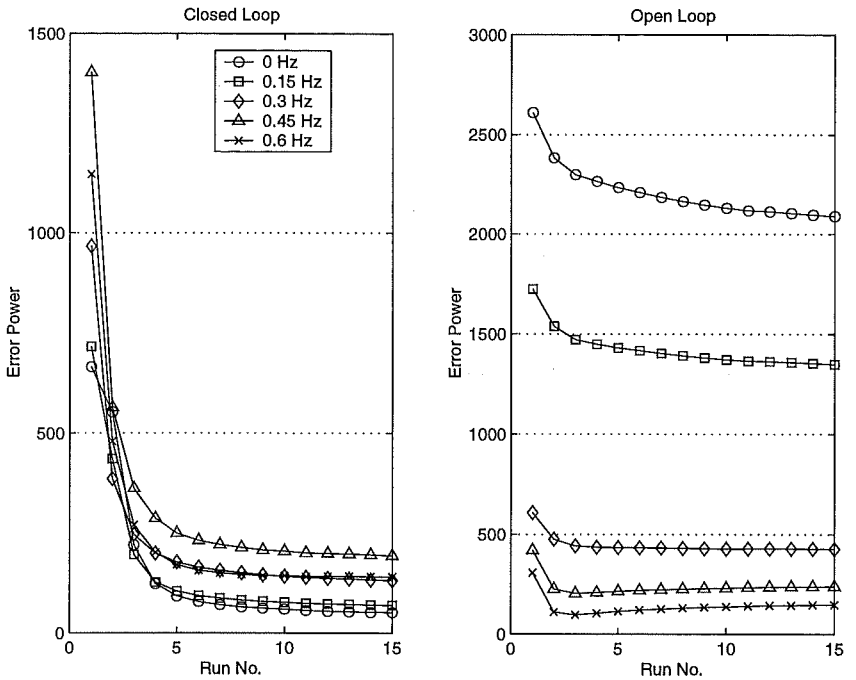

a)

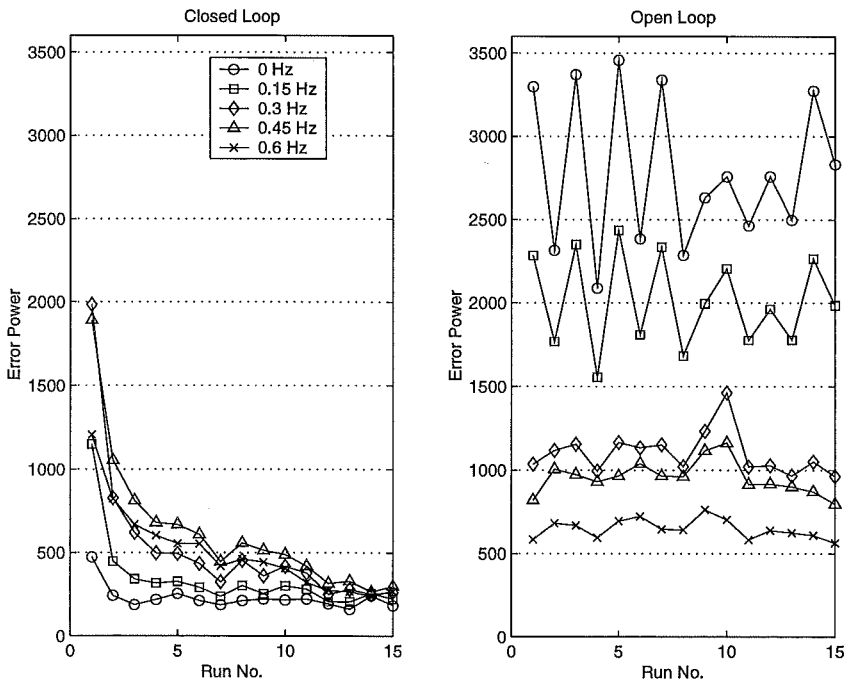

b)

Fig. 76. Simulated error spectra in relation to experimental results (final run, dynamic linear system). a) Simulated results. b) Experimental results.

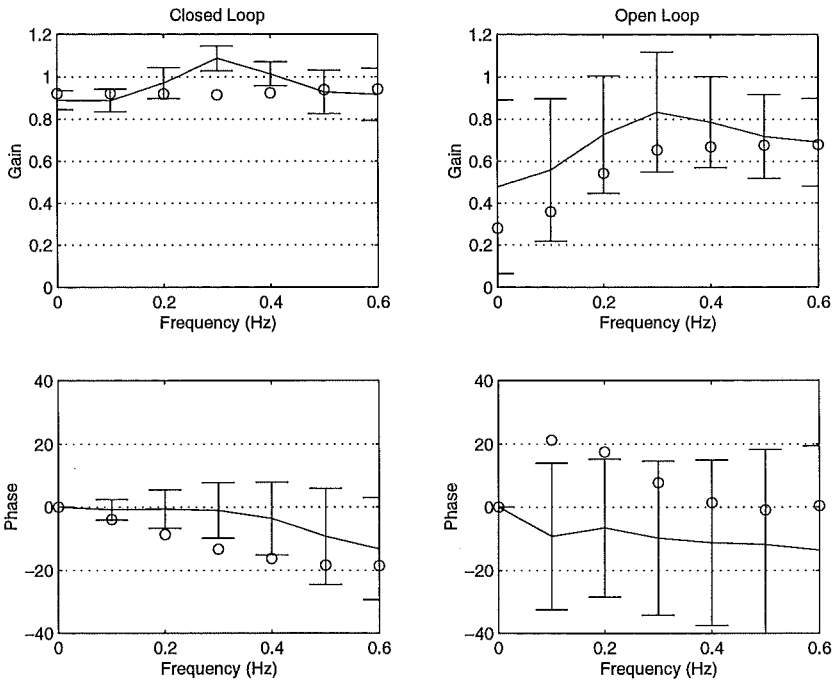

a)

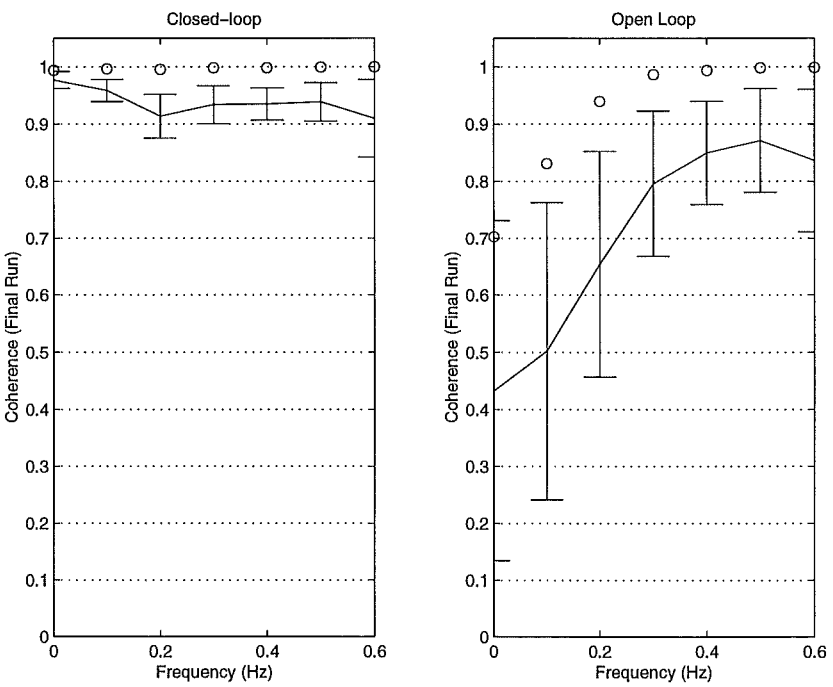

b)

Fig. 77. Simulated a) transfer function and b) coherence in relation to experimental results (final run, dynamic linear system). Experimental results for final run shown with solid lines. Bars indicate standard deviation. Simulated results indicated with circles.

Open-loop trajectory

By the final run the simulated open-loop trajectory exhibits characteristics which are visually similar to the mean response trajectories of the experimental subjects (see Fig. 78). The simulated trajectory remains within one standard deviation of the mean experimental response, so the trajectory shown here could represent a typical human response.

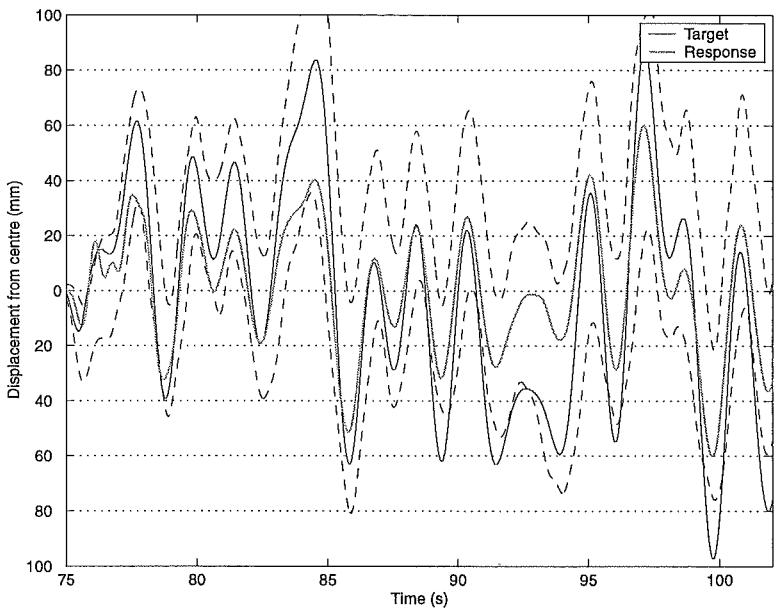

Fig. 78. Simulated open-loop response after 15 runs (dynamic linear system). Dashed lines indicate experimental standard deviation.

6.4.2.2 Static Nonlinear External System

Learning - RMS Error

The closed-loop RMS error results in Fig. 79 show a similar learning trend to the experimental results. This is a noise-free simulation, so the RMS values are slightly higher than ideal but within the acceptable range. Open-loop RMS error results show less learning than observed experimentally, however the increased RMS error and disproportionate learning rate seen in the experimental results are reproduced. It is important to note that the open-loop results are highly dependant on the value of K, so the open-loop learning curve, which is reminiscent of that seen in Fig. 75, could be improved by adjusting K.

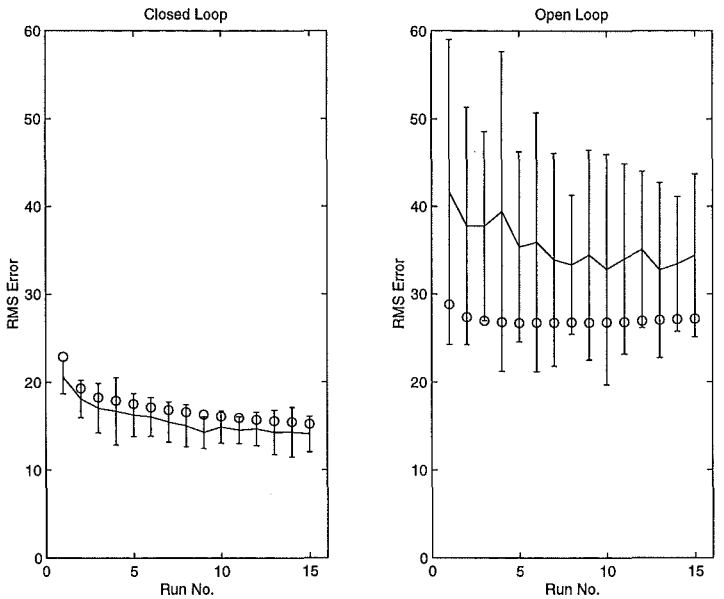

Fig. 79. Variation in RMS error with run. Bars indicate standard deviation. Simulated results indicated with circles.

Learning - Error Spectra

The simulated closed- and open-loop error spectra, both simulated and experimental, are shown in Fig. 80. The closed-loop error spectra are similar to the experimental result. The curves exhibit more low frequency error power than seen experimentally.

In open-loop there is a slight trend to increasing error at low frequency, explaining the 'u' shaped RMS error curve. The open-loop error spectrum is dominated by low frequencies throughout learning and there is a general increasing trend with frequency. Investigation indicates that the adjusting K has the effect of modifying the form of the open-loop learning curves, hence the particular arrangement seen in the experimental results could, in fact, be essentially an artefact produced by the selection of a lucky value of K.

Given that no change has been made in the internal loop-gain between this simulation run and the dynamic linear system, the results are acceptably consistent with the mean experimental results.

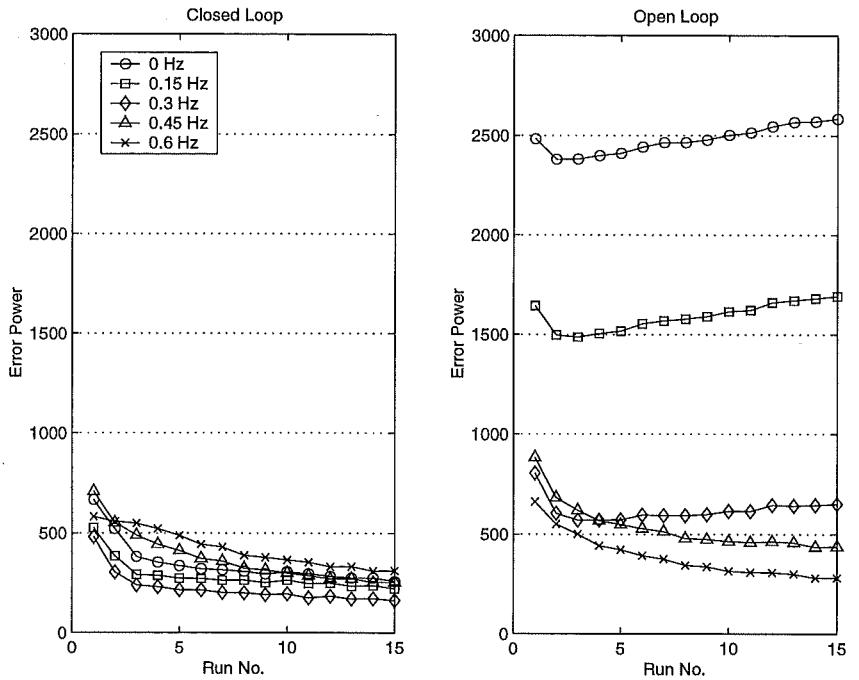

a)

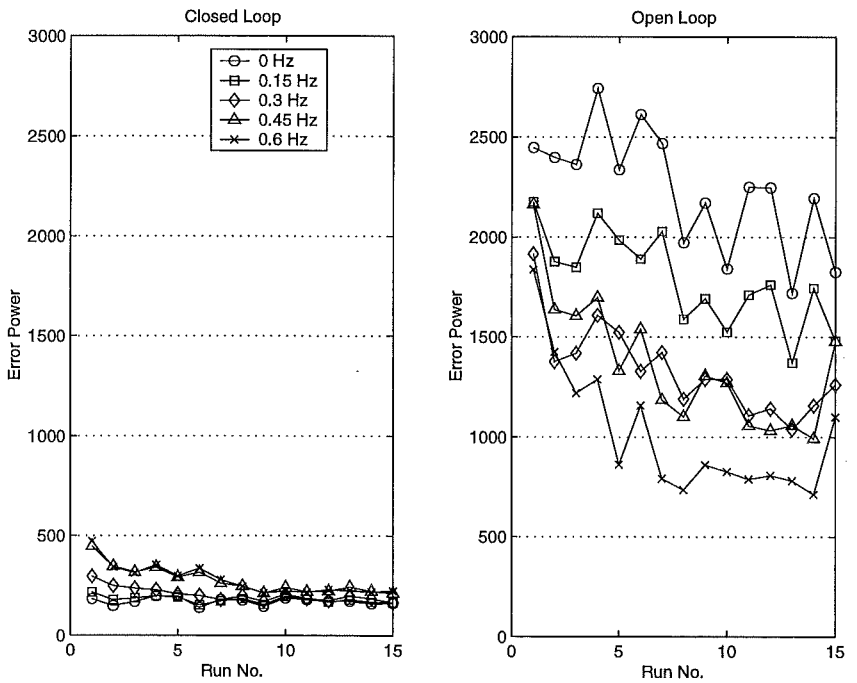

b)

Fig. 80. Simulated error spectrum in relation to experimental results (final run, static nonlinear system). a) Simulated results. b) Mean experimental results.

Quasi-linear Transfer Function

The transfer function and coherence plots for the final run (number 15) are shown in Fig. 81. In closed-loop the simulated gain below 0.5 Hz was higher than observed experimentally. The phase response was very close to the experimental mean, and the

simulated coherence (Fig. 81) exhibited a characteristic drop above 0.4 Hz as seen experimentally.

The open-loop results show the same drop in gain and coherence below 0.3 Hz that was characteristic of the mean experimental results. The gain is lower than the experimental mean across the target bandwidth but remains within one standard deviation of the mean except at very low frequencies.. The simulated drop in coherence is stronger than that observed in the mean human data, with a particularly clear disparity at very low frequency (represented by 0 Hz in Fig. 81). The simulated open-loop results show a strong phase lead for frequencies in the lower half of the target bandwidth. The experimental mean exhibits an approximately linear phase lead to reach 20° at 0.6 Hz. In contrast, in the simulated phase response, a phase lead at low frequencies reverses at higher frequencies, resulting in a slight phase lag from 0.5 - 0.6 Hz. Although this simulated phase response does not appear to match the experimental results it was, in fact, consistent with the phase responses of several individual experimental subjects. Individual subjects' phase responses showed widely varying idiosyncratic characteristics so that the mean does not capture the essence of a typical response. Hence, while the phase appears to be a point of dissimilarity between experimental and simulated results, the simulated response might easily represent a typical subject.

Open-loop Trajectory

Fig. 82 shows the simulated open-loop response trajectory for run 15. The response shows very similar characteristics to the unusual response trajectories observed in the experiment. The simulated trajectory again remains within one standard deviation of the mean experimental response, so the trajectory shown here could feasibly represent a typical human response.

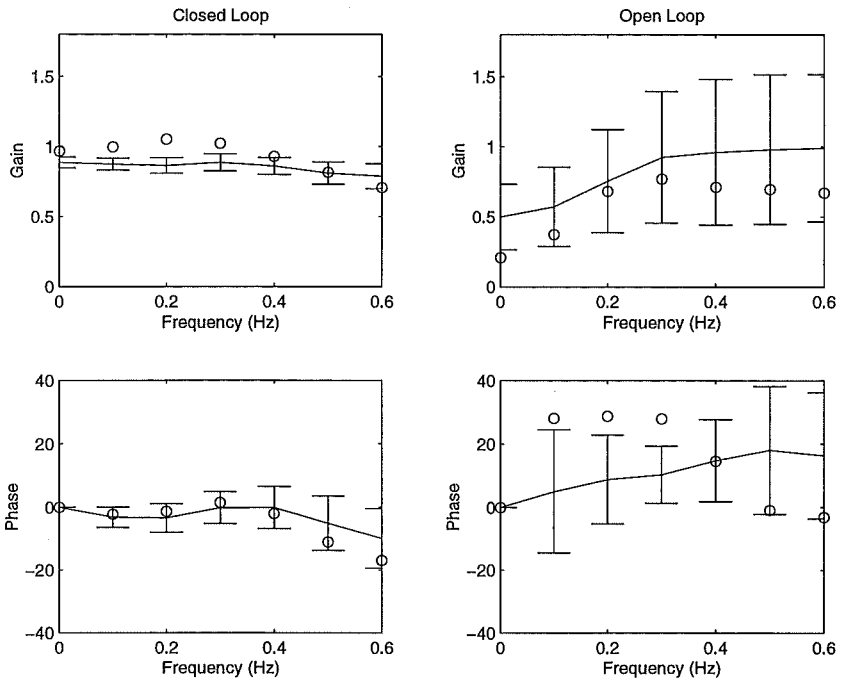

a)

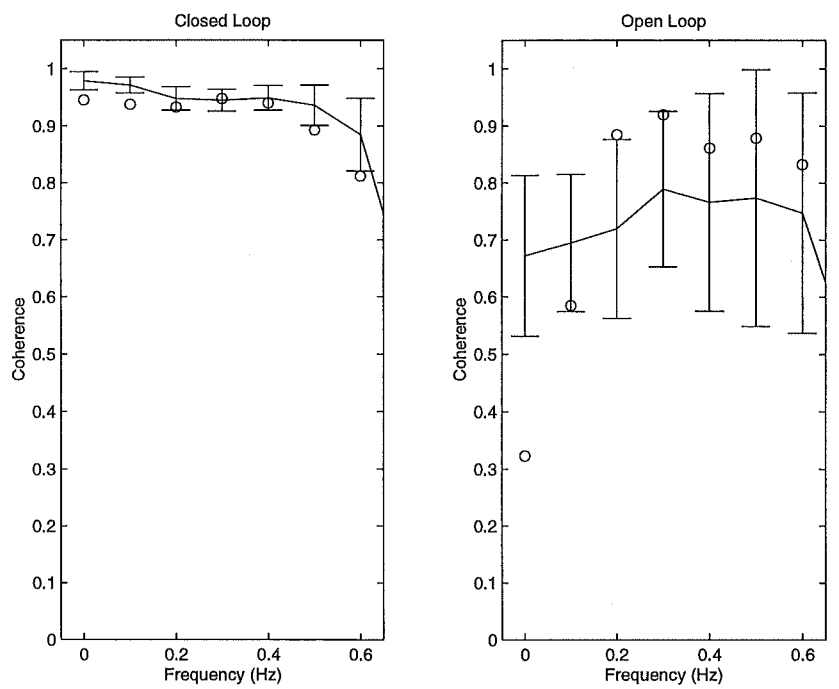

b)

Fig. 81. Simulated a) transfer function and b) coherence for static nonlinear external system after 15 runs. Bars indicate standard deviation. Mean experimental results (final run) shown with solid lines. Bars indicate standard deviation. Simulated results indicated with circles.

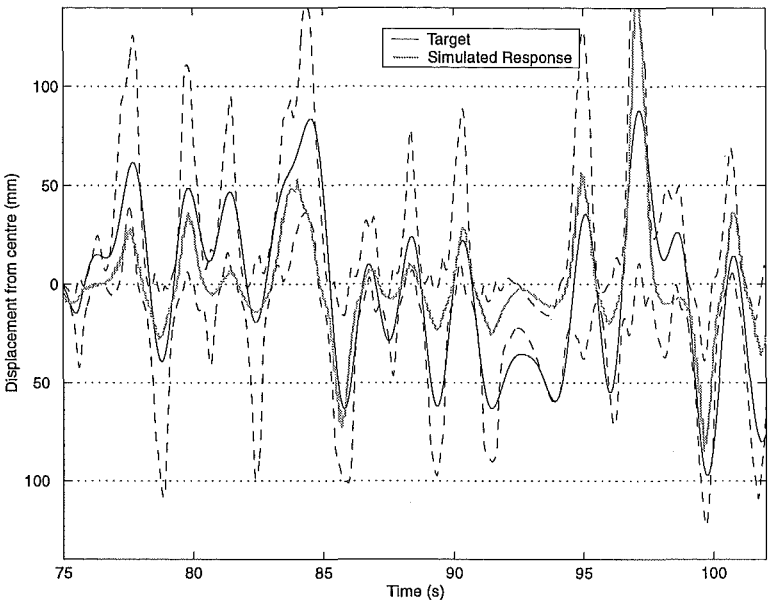

Fig. 82. Simulated open-loop response in relation to the target after 15 runs (static nonlinear system). Dashed lines indicate experimental standard deviation.

Contribution of LRNN Nonlinear Modelling

The RMS error results for nAMT learning to control a static nonlinear external system with and without LRNN adaptation are shown in Fig. 83. These indicate that adaptation within the LRNN, which implements nonlinear modelling capacity, reduced the RMS error relative to an identical system employing only linear adaptation. RMS error reduced in both closed- and open-loop modes when adaptation was turned on.

An error spectral analysis confirmed that the advantage of allowing LRNN nonlinear adaptation is primarily evident at higher frequencies, as expected since the feedback controller is capable of compensating adequately for low-frequency behaviour. Low-frequency behaviour also dominates the RMS error leading to the unusual RMS error learning curve in Fig. 83.

Overall, the contribution of LRNN adaptation to motor learning for this system is surprisingly small. The results confirm that adaptation does take place, but it appears that, at these relatively low frequencies at least, the errors introduced by using a linear approximation can be adequately compensated for by the closed-loop controller.

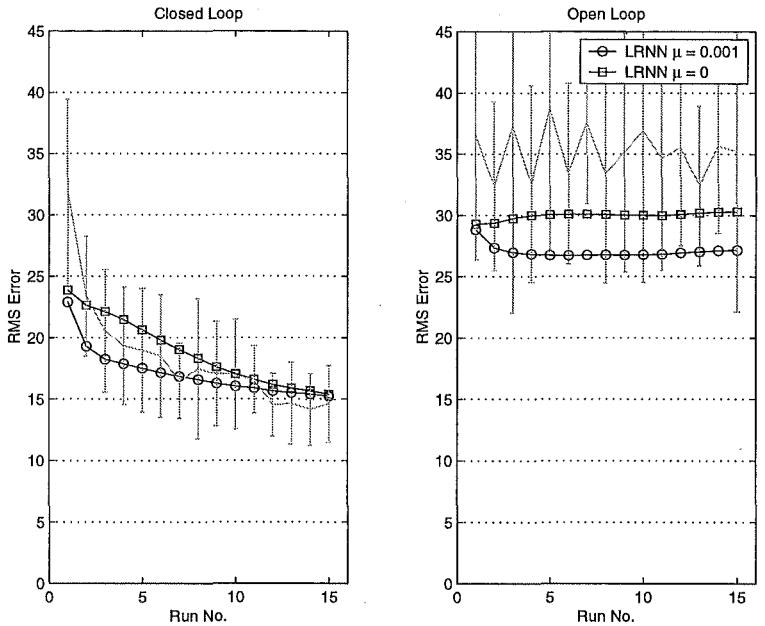

Fig. 83. Effect of turning off LRNN. This figure shows that a nonlinear modelling capacity enhances the control of a nonlinear external system.

6.5 Discussion

6.5.1 Summary

The nAMT computational model succeeded in generating responses which reproduced many of the principle characteristics of the response trajectories obtained during the experimental study (see overview in section 6.1.1). Importantly, these results were obtained using a single set of parameters across the wide range of conditions studied in the experiment (i.e., both closed- and open-loop control and several different external systems). As was hoped, the nAMT model was able to suggest a possible cause for the unusual open-loop trajectories noted in Chapter 5.

It proved possible to generate a high-pass gain with a phase lead in the absence of response feedback while retaining acceptably accurate performance in closed-loop (see Fig. 77 and Fig. 81). The ability of the model to achieve these results arose from the inversion method employed in nAMT, the internal feedback loop, which argues in favour of the existence of similar circuitry in the brain. The internal loop-gain found to optimally reproduce the experimental results was found to be surprisingly low (P = 0.5, D = 1, I = 0.05) which was consistent with the poor open-loop results. It is notable that both FEL and AMT are incapable of reproducing this disparity between closed- and open-loop results without modification to their structures (discussed further in 6.5.2).

It also proved possible to reproduce the disparity between closed- and open-loop learning rates, despite using a single forward model for both adaptive response prediction and inverse model formation (see section 4.5). This supports the decision to include a combined multi-purpose forward modelling structure in nAMT (as is also the case in AMT) instead of separating forward and inverse model adaptation (as used, for example, in FEL).

In both the nAMT simulation and the experimental study presented in Chapter 5 adaptive feedback control appears to dominate adaptive feedforward control. This suggests that the 0.6-Hz target bandwidth used in the experiment may be lower than ideal for observation of strong feedforward adaptation (since feedback control is capable of achieving adequate results). Since feedforward adaptation is not critical here, it is, perhaps, not surprising that a low and therefore stable loop-gain was used for inversion. FEL and AMT, however, predict that rapid feedback control adaptation should be accompanied by rapid feedforward adaptation. This is a major point of difference with the nAMT model, in which the necessity for inverse stability imposes an additional constraint, and may, therefore, explain the relative lack of learning observed in open-loop.

6.5.2 Inverse Model Accuracy

As discussed in section 5.4.4, the combined adaptive feedback and feedforward motor control models shown in section 3.1 all have, at least superficially, similar expected open-loop behaviour. This class of models includes AMT, FEL and the nAMT model developed in this thesis.

It is usually suggested that during learning the inverse model becomes increasingly accurate until final convergence is achieved. In a combined adaptive control structure the open-loop response trajectory would consequently become increasingly similar to the target. There is no obvious reason why only the high frequencies should be learned accurately, as appears to be the case in the experimental results. This is particularly true for a target signal with an approximately flat frequency response like that used in this study.

In simulation, both AMT and FEL behave as predicted: the inverse model becomes increasingly accurate, *particularly* at low frequencies. Indeed, to prevent an accurate inverse model forming at low frequencies an artificial filter needs to be added to deliberately disrupt the model. While such low frequency disruption can be compensated for by the closed-loop controller, and hence would not affect normal performance, it is difficult to suggest why the brain would disrupt the inverse in this manner.

It would appear, therefore, that none of the possible combined control structures shown in section 3.1, which are employed in AMT, FEL and nAMT, naturally generate the observed open-loop trajectories. Since nAMT is closely linked with AMT it was initially thought that the same would apply in this case. Simulation demonstrated that

this was not the case, however, since in nAMT the accuracy of the inverse depends on the loop-gain function.

In nAMT the internal feedback loop-gain essentially filters the inverse model to maximize the stability of the feedback loop. This prevents the inverse from becoming accurate at all frequencies. As mentioned in section 4.5, this inversion method trades inverse model accuracy for stability. Even when the forward model is entirely accurate it may be necessary to keep the loop-gain low to maintain inverse loop stability. Hence, unlike other combined motor models, the nAMT structure could potentially finish learning with a completely accurate forward model but, due to a low loop-gain, retain an inaccurate inverse indefinitely.

The simulations in this chapter employed a low proportional and differential gain, so the inverse accuracy was degraded particularly at low frequencies. This produced acceptable open-loop trajectories without a serious loss of closed-loop performance because the feedback control loop compensates for low frequency errors.

Thus, the experimentally observed behaviour arose from the nAMT structure with no major additions or alterations. This is supportive of the claim that an internal feedback loop is used for the inversion of external systems in the human brain (Miall et al., 1996). Paradoxically, the standard AMT model (Neilson et al., 1992), feedback-error learning (Kawato et al., 1992) and, to our knowledge, all other control-systems-type motor control models are incapable of reproducing these results due to the accuracy of the inversion techniques they employ.

It should also be noted that the performance of the nAMT system was compared with that of a simple tuneable PID controller. It was found that, for satisfactory behaviour in open-loop mode, the closed-loop behaviour was entirely inappropriate, with performance for all runs remaining worse than the mean experimental results for the first run.

6.5.3 Learning Trends

The experimental results showed strong differences between the learning rates and error characteristics in closed- and open-loop (see section 5.4.3). Closed-loop error was dominated by high frequencies while open-loop errors were dominated by low frequencies. These effects posed some possible difficulties for the model. The experimental results imply that most learning occurs in the adaptive feedback controller (hence the strong closed-loop learning). In nAMT the feedback controller must act through the inverse model. Hence, if the inverse is inaccurate, as indicated by the experimental results, the feedback controller is unlikely to be capable of improving performance at any but the lowest frequencies. FEL does not suffer from this possible difficulty since in this model the closed-loop controller acts in parallel with the open-loop controller and does not depend on accuracy and stability of the inverse.

Additionally, nAMT employs a single forward model for both deterministic feedback control and for inverse modelling. This structure was selected in preference to explicitly storing independent forward and inverse models to avoid unnecessary duplication and storage of two versions of essentially the same information. Adaptive feedback control and feedforward control are, therefore, linked together in nAMT. On this basis, it seemed likely that strong learning trends in closed-loop would also appear in open-loop. The inaccuracy, at least at certain frequencies, which is introduced by using a PID controller in the internal feedback loop (primarily for stability, see sections 4.5 and 6.5.2), has the potential to break this linkage and allow nAMT to produce results consistent with the experimental study.

The results presented in this chapter confirm that a differential between closed- and open-loop learning trends can be simulated by nAMT which uses a single forward model with a high-gain internal feedback loop. The RMS error results (see Fig. 75 and Fig. 79) can be interpreted as representing a dominant adaptive feedback control component in the system as observed experimentally.

The error spectral analyses (Fig. 76 and Fig. 80) show that the open-loop error is dominated by low frequencies which, as mentioned in section 6.5.2, is caused by the PD loop-gain used to generate the inverse model. While the order of the simulated open-loop spectral components are similar to those of the experimental results the temporal trends differ. The simulated results for the dynamic linear system (Fig. 76) show trends where none are evident experimentally. Low frequency trends to reduction in error are compensated by trends to increasing error at higher frequencies which result in a weak overall trend in the RMS error results. Similarly, the static nonlinear system (Fig. 80) shows trends to increasing error from 0 – 0.15 Hz which are not evident experimentally. In the simulated results these low frequency trends tend to cancel the improvement observed at high frequency, leading to the weak learning curve seen in the open-loop RMS error (Fig. 79). Hence, while trends are evident at individual frequencies (indicating the presence of underlying adaptive process) these trends cancel out when combined into the open-loop RMS error.

During the simulation work it was noted that adjusting the characteristics of the loop-gain K changed the learning trends exhibited in open-loop without dramatically affecting closed-loop results. Hence, by introducing fine adjustments to K for individual systems it may be possible to find an optimum match for the open-loop trends. No parameters were found, however, that produce superior results for both systems. This indicates that while the parameters selected for K ($P = 0.5,\ D = 1,\ I = 0.05,\ \mu = 0.001$) produce reasonable results, some fine tuning between external systems may be necessary. Adaptive adjustment of K has also been suggested (see 4.5), so adaptive fine tuning may explain some of these disparities.

Notably, increasing K (to say P = 1, D = 1) caused strong learning trends to appear in open-loop. This behaviour is characteristic of linear AMT where a linear inverse model calculated accurately from the forward model.

It should be noted that these simulations were carried out in the absence of noise. Weak trends like those seen at high frequencies in Fig. 80 might well be obscured by noise.

The important result of these simulations is that it is possible to achieve strong learning in closed-loop mode while achieving little improvement in open-loop while using only a single set of (forward model) parameters for feedforward *and* feedback control.

6.5.4 Model Parameters

A single set of parameters was established that worked acceptably across all external systems in the experiment ($P = 0.5$, $D = 1$, $\mu = 0.001$, $I = 0.05$, ϕ=0.05). While some fine tuning may be desirable to achieve a perfect match (see section 6.5.3), the characteristics of the closed- and open-loop responses were similar enough to suggest that only fine adjustment of K would be needed for the simulations in this chapter. It is worth noting, however, that the importance of the feedback control component in this experiment appears to be quite small so there may be little need for the system to dramatically alter open-loop behaviour in this particular case.

Though not explicitly followed up in this experiment, the results indicate that additive noise of $\phi = 0.05$ provides a reasonable match with the experimental results and does not alter the expected open-loop response characteristics in any important respects.

6.5.5 Effect of Internal Loop-gain

The results show that the loop-gain has a strong effect on the stability and spectral characteristics of the response in both closed- and open-loop response feedback modes. It was notable that introducing derivative gain (see Fig. 72) caused improvement in both feedback modes and led to a high-pass gain characteristic with a phase lead in open-loop mode, as observed in the experimental results.

Performance was considerably better in closed-loop than in open-loop, particularly at lower frequencies. This is evidence of the importance of the adaptive feedback loop. The similarity between closed- and open-loop responses was seen to increase as the feedback gain was increased (Fig. 72). This reflects the more accurate inverse formed when a larger feedback gain is employed. The role of the feedback controller is reduced when the inverse is more accurate.

A derivative gain component is particularly effective because the nAMT feedback loop is capable of compensating for low frequency modelling errors. The derivative component provides high gain at those frequencies which the feedback controller is less

capable of compensating for, while maintaining lower gain at low frequencies for overall stability.

The surprisingly low gain of the controller that optimally matches the experimental results (P=0.5, D=1, I = 0.05) is interesting. Keeping the loop-gain as low as possible would be a useful strategy since the inversion loop is more likely to be stable for low loop-gains. Since closed-loop performance is good, this suggests that the adaptive feedback controller is capable of compensating for inaccuracy in the inverse for frequencies within the target bandwidth (0.6 Hz).

The high frequency performance of the simulations in both closed- and open-loop was short of the experimental results due to residual inaccuracies in the forward model at the end of the ten practice runs. This effect may have been caused by the autocorrelated input to the adaptive algorithm, which was shown to distort the learned system (see the pilot study in Appendix II). Finding a neurobiologically plausible solution to this problem is suggested as an area for future research.

6.5.6 Open-loop Model Structures

Of the two model structures investigated open-loop structure 1, in which corrective movements were suspended during blanking (see Fig. 69), showed the behaviour most similar to the experimental results. Structure 1 proved capable of exhibiting good tracking performance in closed-loop while simultaneously showing attenuation and a drop in coherence at low frequencies in its open-loop behaviour. The overall effect was similar to that observed in the experimental results (particularly for $P = 0.5,\ D = 1$).

In contrast, structure 2 (Fig. 70), in which adaptation was maintained during blanking, exhibited tight coupling between closed- and open-loop behaviour which was inconsistent with the experimental results. This tight coupling is also characteristic of standard AMT (Neilson et al., 1992) and feedback-error learning (Bhushan et al., 1999a; Kawato et al., 1992). This result is, perhaps, not surprising given the superior neurobiological plausibility of structure 1 (see the discussion in section 6.2.2.1).

Maintaining adaptation while the nAMT model is in open-loop mode (for open-loop structure 2) appears to introduce behaviour similar to using PD type loop-gain (see Fig. 72). The accompanying degradation of closed-loop performance was, however, impossible to reconcile with the observed results. The implied 'unlearning' of the internal model during blanking is difficult to justify, particularly since closed-loop performance is generally much more important than open-loop performance. This structure, while interesting, was therefore rejected as a likely candidate for the AMT open-loop motor model.

6.5.7 Effect of LRNN Adaptation

Turning off adaptation for the locally-recurrent neural-networks in the nAMT model while controlling a static nonlinear system, and thereby disabling all nonlinear adaptation, caused an increase in RMS error and caused learning at high frequencies to slow (Fig. 83). This is consistent with a decrease in forward model accuracy, the effects of which are visible primarily at higher frequencies due to the action of the feedback controller. This result confirms that the LRNN is able to enhance the control of a nonlinear system.

Conversely, although the presence of the nonlinear learning capacity can improve performance at this task, it appears that it is not essential for producing satisfactory performance. That is, the linear model is surprisingly capable of learning to control this nonlinear system. This is because combining both feedback and feedforward control confers a low-frequency nonlinear control capacity by way of the feedback controller (Astrom et al., 1995). As previously noted, it is likely that the limited bandwidth of the target signal allows the feedback controller to dominate the control effort in this special case, thereby reducing the relative importance of the LRNN.

A systematic study of the extent to which the human motor system needs to and can model nonlinear external systems would be a valuable contribution to our understanding of human motor behaviour (see section 7.2.1). A study of this sort would need to use a higher bandwidth target signal, implying that the mechanical inertia of the external system (which limited the bandwidth of the target for this study) would need to be reduced.

7. Conclusions and Further Research

7.1 Conclusions

A new nonlinear variant of Neilson's Adaptive Model Theory (AMT) (Neilson et al., 1992), *nonlinear Adaptive Model Theory* (nAMT), has been developed and tested in this thesis. nAMT exceeds the capabilities of linear AMT in its capacity to model nonlinear dynamic signals and systems and, consequently, to predict human motor behaviour in a realistic nonlinear environment. nAMT is capable of forming internal inverse models of nonlinear dynamic systems, of predicting signals with nonlinear dynamic statistical characteristics and of performing simultaneous nonlinear adaptive feedback and feedforward control. nAMT also maintains the standard of neurobiological plausibility set in AMT.

7.1.1 nAMT Structural Innovations

nAMT is based firmly on the structure and philosophy of Neilson's linear AMT model. The functional advances over Neilson's model, primarily aimed at generalizing AMT to a nonlinear environment, are considerable. These modifications are summarized below.

7.1.1.1 Nonlinear Modelling Structure and Learning Algorithm

A dynamic, locally-recurrent neural network (LRNN) structure was developed for modelling nonlinear dynamic systems in nAMT. The structure was based on the "dynamic neural unit" structure suggested by Gupta (1992) as a model for the dynamics of a group, or functional unit, of neurons in the brain. This basic unit was then connected into multi-layer networks which proved capable of modelling arbitrary nonlinear dynamic systems. The LRNN structure allowed dynamics of arbitrary temporal depth to be modelled without the a priori specification of a buffer depth. This feature provided an advantage, in terms of neurobiological plausibility, over buffered neural network models (like MLP or CMAC) where the temporal depth of the dynamics must somehow be decided ahead of time.

A novel multi-layer on-line back-propagation adaptation algorithm was also derived from scratch for application in this network structure. The resulting adaptation algorithm, which fits into the Back-Tsoi (1992) class of algorithms due to its approach to online dynamic backpropagation, gives the LRNN the adaptive capacity to act as the modelling element in nAMT.

To bring the online adaptation rate to a level comparable with biological observations, a linear circuit, as employed in AMT, was also included in parallel with the nonlinear LRNN.

7.1.1.2 Nonlinear Stochastic Signal Prediction

A neurobiologically plausible structure was developed for the online prediction of arbitrary target and disturbance (exafference) signals. This was achieved by generalization of the linear predictor structure used in AMT so that signals with nonlinear stochastic properties could be predicted. Superior parsimony was achieved by making an additional move from the moving-average modelling technique used in AMT to a mixed auto-regressive moving-average (ARMA) structure. Consequently, the nAMT model employs adaptive nonlinear auto-regressive moving-average (NARMA) stochastic models for the prediction of target and disturbance signals.

Linear-differential and nonlinear-absolute structures were combined in parallel to form a novel and efficient one-step predictor structure. This combines the excellent performance of the linear model used in AMT with the capacity to model arbitrary nonlinear dynamics. Hence, the newly developed structure facilitates the efficient online learning of NARMA stochastic models in nAMT.

7.1.1.3 Nonlinear Observer Forward Modelling

In nAMT a nonlinear observer forward model replaces the linear input-output forward modelling approach used by AMT for the calculation of exafference and the formation of inverse models. This change enhances the prediction of the consequences of state disturbances. The structure can also be used for adaptive response prediction. The newly developed LRNN network was used as the modelling element in the forward model observer.

7.1.1.4 Nonlinear Adaptive Response Prediction

In linear AMT, response prediction circuitry is unnecessary since the pre-planned responses, in combination with predicted exafference, provide the optimum response prediction. In nAMT, response prediction is necessary since the nonlinear forward and inverse models do not form a precise inverse pair with a unity transfer function as in the linear case. The forward model observer structure was, therefore, employed to efficiently predict the most likely response signal. This effectively adds a deterministic extension to the adaptive stochastic disturbance predictor as used in AMT.

7.1.1.5 Nonlinear Inverse Modelling

An indirect inverse modelling scheme was used for inverse modelling of nonlinear systems. The forward model was placed into an internal feedback loop in which the loop gain is adjusted to maintain stability, thereby defining the characteristics of the inverse model. In simulation this was achieved by using a PID gain which was adjusted manually (the adaptive modification of these few parameters is suggested as an area for future research, see section 7.2.3).

7.1.1.6 Open-loop Modelling Structure

The nAMT model was extended to handle open-loop behaviour (i.e., movements made in the absence of response feedback). This was achieved by turning off the corrective action of the OTG (see Fig. 69) when a loss of response feedback was detected. Simulation results (see section 7.1.3) confirm that this approach is valid.

7.1.2 Experimental Findings

The experimental open-loop tracking study of Chapter 5 looked at some fundamental properties of the human control system. This study provided evidence for the formation of an inverse model of a nonlinear external system in the brain. This important evidence supports the inverse modelling approach on which AMT is based. The study also revealed an unexpected predominance of adaptive feedback control, particularly for difficult dynamic external systems, in the human motor control system.

The experimental study also provided a wealth of data for verification of the nAMT model. In particular an unexpected relationship between closed- and open-loop behaviour was revealed which, to our knowledge, no other motor control models are capable of reproducing.

The key findings from this study are:

- Open-loop learning for a static nonlinear external system demonstrates adaptive feedforward control in the nervous system. This result supports the hypothesis that the brain forms inverse models of external controlled systems.
- The data did not reveal the simple learning transfer from unblanked to blanked runs that would be expected for an adaptive inverse controller, hence suggesting the presence of a strong adaptive feedback control contribution and loose coupling between the forward and inverse models.
- No blanked performance improvement was observed for the dynamic linear external system despite strong improvement during the unblanked runs. This emphasizes the importance of adaptive feedback in the control of difficult dynamic external systems.

- The raw open-loop trajectories and their spectral characteristics indicate a lack of the convergence to the target signal predicted by internal model type motor control models other than nAMT (see section 7.1.3).

7.1.3 Computational Simulation Findings

The primary features of the observed open-loop responses were successfully reproduced in the nAMT simulation. These results were obtained using a single set of parameters across the wide range of conditions studied in the experiment (i.e., both closed- and open-loop control and several different external systems). This supports the claim that an internal feedback loop is used for the inversion of external systems in the human brain (Miall et al., 1996). Paradoxically, the standard AMT model (Neilson et al., 1992), feedback-error learning (Kawato et al., 1992) and, to our knowledge, all other control-systems-type motor control models are incapable of reproducing these results due to the accuracy of the inversion techniques they employ.

It proved possible to generate a high-pass transfer function with a phase lead in the absence of response feedback while retaining acceptable performance in closed-loop. The relative lack of learning in open-loop compared with closed-loop was also reproduced in the simulations while retaining acceptable closed-loop performance. It is notable that both FEL and AMT are incapable of reproducing this disparity between closed- and open-loop results without modification to their structures (see section 6.5.2).

The difference between closed- and open-loop results for the nAMT model emerged from the internal feedback loop used for inversion. The inverse was based on the forward model but was typically less accurate to maintain stability. High-pass trajectories, as observed experimentally, tended to emerge in open-loop since a proportional-plus-differential type characteristic was necessary to stabilize the internal feedback loop.

The internal loop-gain which optimally reproduced the experimental results was surprisingly low (P = 0.5, D = 1, I = 0.05). This was consistent with the poor accuracy of the experimental open-loop response. This low gain may be due to the low target bandwidth used in the study which allows the feedback controller to cope acceptably despite an inaccurate inverse model. Minimizing the loop-gain is advantageous since it improves the stability of the internal feedback loop.

7.2 Further Research

7.2.1 Characterization of Human Nonlinear Modelling Capacity

A careful systematic study aimed at determining the limits of the human ability to adapt to and control nonlinear systems would be of immense benefit in this field of research. Such a study would allow the necessary size, structural and learning

characteristics of the modelling circuits used in simulation to be determined. The work presented here focussed on nonlinear systems that, while challenging, were well within the bounds of human motor learning capacity. By systematically increasing the complexity of the controlled system and looking at the effect that this has on learning and motor accuracy, an upper bound on the representational capacity of human motor models might be determined. This would allow us to judge the necessary size and complexity of the modelling circuitry both in computational models and in the brain.

The primary difficulty with this work would be defining a meaningful indices of complexity for a nonlinear dynamic system. Consequently, it may be necessary to wait until the motor primitives actually employed by the brain are more accurately determined. Knowledge of these primitives would allow systems with a range of complexity to be constructed by specifying certain primitive combinations.

Recent work in a similar area is beginning to bear fruit. Thoroughman and Shadmehr (2000) present evidence that motor primitives resembling the tuning curves of Purkinje cells in the cerebellum underlie the formation of models in the human motor system. Mussa-Ivaldi and Bizzi (2000) also provide experimental evidence of motor primitives at the spinal level in frogs which sum vectorially to generate a movement.

7.2.2 System Identification

The LRNN learning algorithm developed in section 2.4.2.2 performed acceptably for modelling the particular external systems controlled by human subjects in Chapter 5. More complex systems, at the edge of human control capacity, need to be tested to ensure that the algorithm operates acceptably under a wider range of conditions.

The adaptation algorithm was based on an approximation - instantaneous static backpropagation between layers. This limits the accuracy of modelling in higher layers of the network. The modelling efficiency of the algorithm could potentially be improved by using a more accurate dynamic approximation, though this would involve considerable additional work in mathematical development and implementation (Campolucci et al., 1999). There is also room for the investigation of variations in the structure of the locally-recurrent neuron elements. The particular structure in section 2.4.2.1 was selected as it exhibited a suitable trade-off between complexity and dynamic modelling capacity and had previously been proposed as a neurobiological model. More and less complex structures could be constructed and tested. Investigation of other modelling structures, such as an enhanced CMAC structure with Gaussian basis functions and a dynamic RBF network, despite the finite temporal depth issue, might also be worthwhile.

To judge whether such refinements do, in fact, provide a more accurate neurobiological model would require a study like that mentioned in section 7.2.1 to determine the upper limits of modelling complexity in the human brain.

7.2.3 Solving Modelling Bias Caused by Autocorrelation

The highly autocorrelated inputs used for tracking tasks tend to disrupt LMS type adaptation algorithms leading to malformed models (Widrow et al., 1985). This problem has been addressed previously by introducing pre-whitening to the adaptive algorithm (Neilson et al., 1992). In practice, this measure had little impact, probably due to the high level of autocorrelation in the target, and actually reduced performance slightly in simulations. Additional work is required to minimize the observed effect of autocorrelated inputs on the accuracy of internal models, particularly as the simulation work of Chapter 6 highlights that model accuracy at high frequencies does not match human performance.

7.2.4 Adaptive Internal Feedback Loop-gain

The internal feedback loop-gain, as specified in section 4.5, was set manually in the simulations presented here so that the controller was stable at the beginning of learning. The particular value of the gain proved to be critical for determining open-loop characteristics, though less so for closed-loop characteristics. An adaptive algorithm for the tuning of the three parameters in the PID controller, based on minimizing a combination of performance (error) and loop-instability, could be developed so that the correct values are reached automatically. As discussed in Chapter 6, the algorithm would need to impose a stability constraint. The loop-gain should be kept as low as possible to achieve acceptable results.

7.2.5 Experimental Study Suggestions

7.2.5.1 Modifications to the Experimental Study of Chapter 5

Target Bandwidth

Repeating the experimental study with a higher target bandwidth has the potential to consolidate some of the results presented earlier. The target used in this study had a bandwidth of 0.6 Hz to ensure that the biomechanical system could be accurately controlled after practice (as assumption used in the experiment, see 5.2.3.1). At a higher target bandwidth subjects found tracking more difficult due, in part, to the mechanical inertia of the steering-wheel which invalidated the assumption of accurate control. This problem could be remedied by using a smaller input device, such as a joystick so only the fingers need to be moved, and also by reducing the required movement of the limb.

Target Preview

As mentioned in 5.4.4.2, one possible explanation for the unusual response trajectory characteristics observed in the experimental study of Chapter 5 relates to the handling of

the target signal preview by experimental subjects. A pilot study (see Appendix IV), looking at the effects of target preview on open-loop tracking behaviour, suggested that the effect was unlikely to explain the high-pass open-loop response characteristics. This tentative conclusion needs to be confirmed.

The effects of target preview depth could be investigated by varying the preview from none to 8 s.

7.2.5.2 Parallel versus Serial Combined Feedforward / Feedback Control Study

A study aimed directly at differentiating FEL and AMT would be of immense theoretical importance. In this thesis it was explained that the main differences between AMT and FEL is that they employ serial and parallel combinations of feedforward and feedback control respectively. An experiment specifically designed to determine which is used in the human motor system could be devised.

In AMT, feedback corrective movements must pass through the inverse model. In FEL, however, the feedback controller acts independently of the inverse. This action could be tested for in a carefully designed experiment. Subjects could be well trained on a known external system over a period of several days. The external system could then be altered abruptly without the awareness of the subjects. The resulting corrective movements could then be analysed for consistency with a serial or parallel combination of feedforward or feedback control. In the serial case, the corrective movements would be effectively filtered by the existing inverse model, while in the parallel case corrective movements would not be disturbed in this way.

7.2.5.3 Consolidation Study

There is strong evidence that learning a motor task causes neural processes to occur that continue long after the task itself has ended (Brashers-Krug et al., 1996). This process is known as motor *consolidation* (Shadmehr et al., 1997). Skill at a task has been shown to improve when rest periods of up to several hours are given during which no practice occurs. There is a possibility that a rest period between sessions of the experimental study might lead to stronger, more easily detectable inverse model formation. This study has the potential, therefore, to demonstrate that the consolidation process is related to the training of an internal inverse model.

7.2.5.4 Target Prediction Study

The characteristics of the predictive abilities of the human operator could be studied in depth. The ability to predict signals with a variety of statistical characteristics could be compared with the model presented in section 4.1.4. Targets that involve repeating sequences of varying length, wide-band noise multi-choice reaction times could also be studied. The predictive abilities of patients with disorders of the motor system could also be compared with normal subjects (Jones et al., 1989). This study has the potential to confirm some neurobiological aspects of the nAMT model.

7.2.5.5 Applicability of AMT to Eye Movements Control System

The FEL model has been applied to the study of eye movements (for a review of this work see Kawato, 1999). The applicability of the nAMT model to understanding eye movement system could potentially yield useful results, particularly since the eye movement system yields more easily to study than the arm movement system.

7.2.5.6 Source and Extent of Intermittency in the Motor Control System

Intermittency is a phenomenon on which the AMT model places a great deal of importance. Intermittency has been demonstrated in tracking responses (Miall, Weir, & Stein, 1993) and in double-stimulation reaction time experiments (Vince, 1948). The source of intermittency in the motor system has, however, yet to be determined. AMT suggests that intermittency is introduced in response planning through the OTG, which implies intermittency at all levels of the motor system, including feedback and feedforward control pathways. Studies aimed at testing the accuracy of this central idea in AMT could be devised, by separating and testing individual pathways separately for intermittency.

7.2.5.7 Neurological Disorders

The closed-and open-loop experimental paradigm used in Chapter 5, in combination with the nAMT model, could be applied to the study of neurological disorders (Jones et al., 1993). Patients with disorders of the motor system, such as Parkinsons disease, Huntington's disease, cerebellar lesions, and focal lesions (e.g., in the motor cortex, premotor cortex or supplementary motor area) could be compared with normals (Jones et al., 1989). Any deficits in open-loop behaviour might be explained in terms of impairment in the function of specific regions in the nAMT model. This could be used to predict and explain aspects of the multiple symptoms exhibited in certain disorders. It might also provide new insights leading to more effective procedures in rehabilitation. Studies involving comparisons of performance of nAMT with patients with neurological disorders would both provide valuable confirmation of the nAMT model and confirm the neurobiological aspects of the model.

8. Appendix I

Independent Parallel Inverse Model Adaptation in FEL

The feedback error learning (FEL) structure is an appealing motor model for several reasons (see section 3.2.4). One of the disadvantages of the model is its apparent inability to form inverse models independently and in parallel like in AMT. One of the basic tenets of the AMT is that the brain is able to tune a series of adaptive filters in a 'piecemeal' fashion (Neilson et al., 1997). This is equivalent to a parallel modelling process, allowing the re-tuning of an adaptive model without disturbing any other models in the system. If the inverse models are formed in series then adaptation to errors in one inverse (say BM^{-1}) will be distributed through the other two models , thereby rendering them inaccurate for other tasks. A solution to this difficulty was sought.

8.1 Serial FEL

It is possible to combine several FEL modelling subsystems and implement a cascade of inverse models as found in the AMT. The simplest way to cascade the inverse models is to nest the subsystems as shown in Fig. 84. Note that when we refer to a 'subsystem' in this context we mean the inverse modelling structure and the plant it aims to control.

Cascading the FEL subsystems like this results in a serial modelling architecture. A perturbation in one plant will disturb all of the inverse models in the system.

8.2 Parallel FEL

It is possible to modify the serial FEL structure and produce a parallel modelling implementation. A parallel structure is thought essential for modelling the fleeting sensory-motor relationships the central nervous system often encounters. As the response to a perturbation in any plant is local to its own subsystem, a parallel learning structure leads to faster and more efficient adaptation.

The idea is best understood by considering one inverse modelling subsystem at a time. Take, for example, subsystem 1 in Fig. 84. The system error e_s is defined as the

difference between the desired response signal and the actual response signal. This relationship is shown referring to subsystem 1 for convenience:

$$e_{s1} = y_{d1} - y_1 . \tag{17.1}$$

The learning action of the architecture is defined by this relationship. It is possible to arbitrarily choose different desired and actual response signals and modify the function each subsystem learns. The aim, therefore, is to choose desired and actual response signals so that learning in each subsystem only depends on the changing relationship between signals at the input and output of its particular plant, resulting in parallel inverse model adaptation. This can be achieved by defining the desired response signal for a parallel FEL architecture as the difference between the inverse model's input and output, i.e., $y_{d1} - y_{d2}$ in Fig. 84. Thus for subsystem 1,

$$\overline{\overline{y_{d1}}} = y_{d1} - y_{d2} \tag{17.2}$$

Likewise, lets redefine the actual response (output) signal to be the difference between the real system's output and input.

$$\overline{\overline{y_1}} = y_1 - y_2 \tag{17.3}$$

Thus the subsystem is now concerned with the differential action of its particular controlled system. Now, taking the difference between these two quantities as in (17.4):

$$\begin{aligned} \overline{\overline{e_{s1}}} &= \overline{\overline{y_{d1}}} - \overline{\overline{y_1}} \\ &= y_{d1} - y_1 + (y_2 - y_{d2}) \end{aligned} \tag{17.4}$$

Applying this idea we arrive at the structure shown in Fig. 85 where the two modelling subsystems are cascaded in series, but learning occurs in parallel as in standard AMT.

This approach can easily be extended to implement a full AMT parallel modelling structure, as shown in Fig. 86.

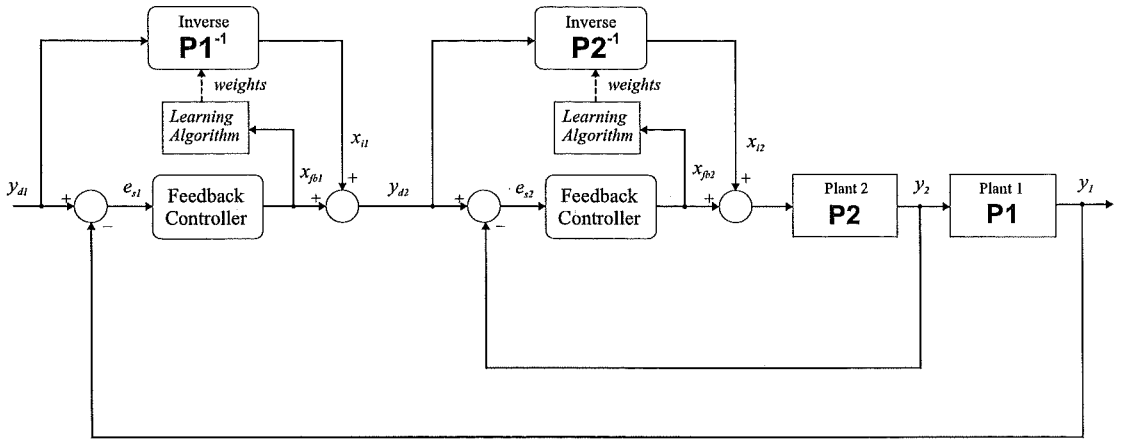

Fig. 84. Serial FEL architecture including two subsystems. Subsystem 2 is nested within the feedback loop of subsystem 1.

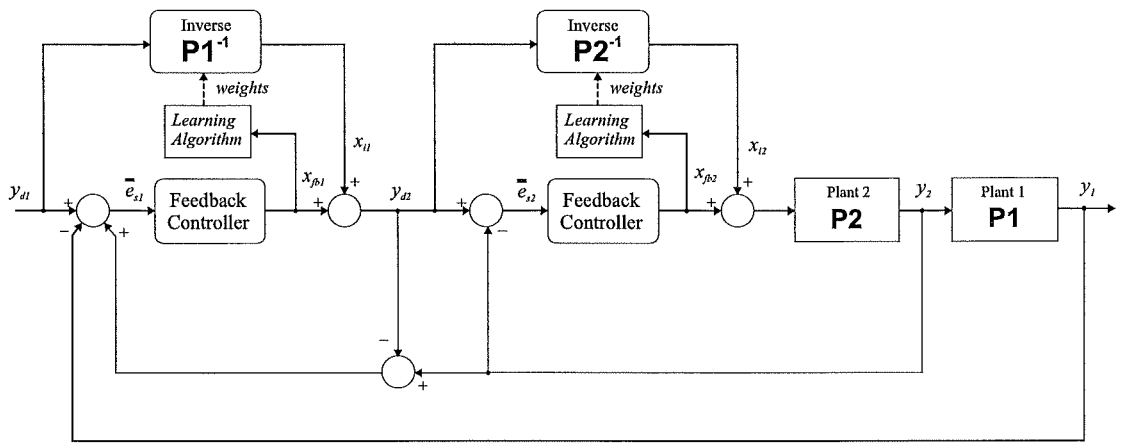

Fig. 85. Parallel FEL structure showing two subsystems. It should be possible to see that this diagram implements (17.4) for the case of subsystem 1.

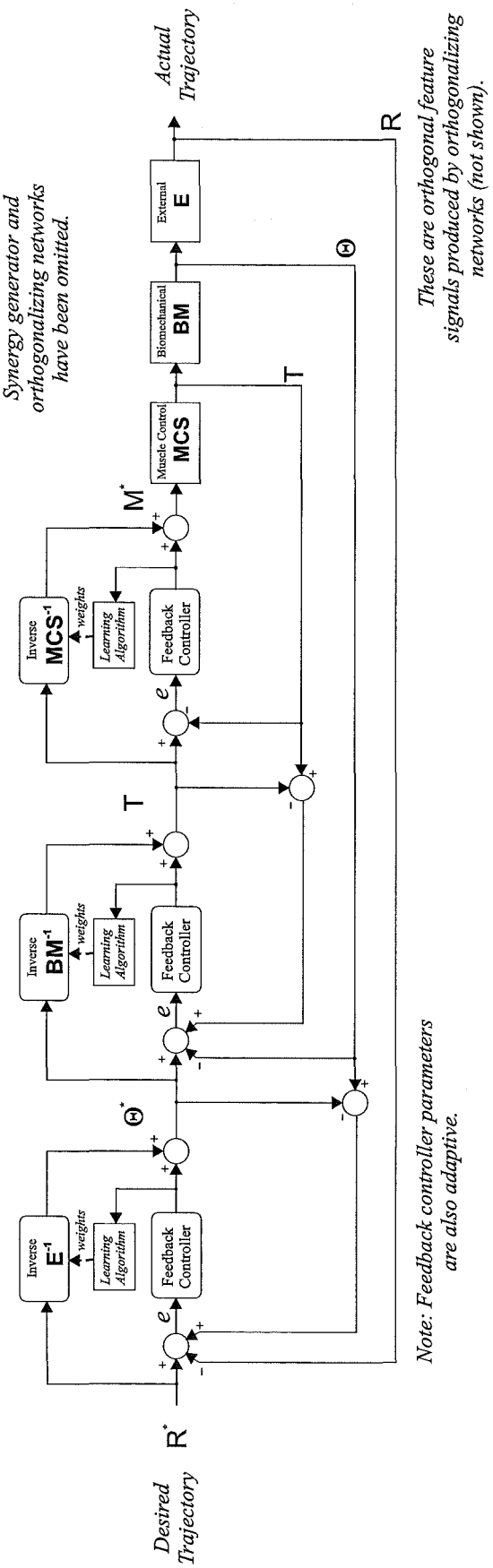

Fig. 86. Full parallel FEL structure applied to AMT

9. Appendix II

Forward Modelling with an Autocorrelated Input Signal

Training an accurate forward model in an AMT system is complicated by the expected level of auto-correlation in the input signal. To better understand the magnitude of this problem an experiment was performed early in this research project to establish the ability of an MLP neural network to form the forward model of a static non-linearity.

After 1000 training samples a network excited with low-pass filtered[6] white noise in the range [-1,1] had not learned the forward characteristics of the plant correctly (see Fig. 87). The same network trained for 1000 samples with a random white noise input in the same range learned the function very accurately. This second system was capable of predicting plant outputs to within a few percent (see Fig. 88).

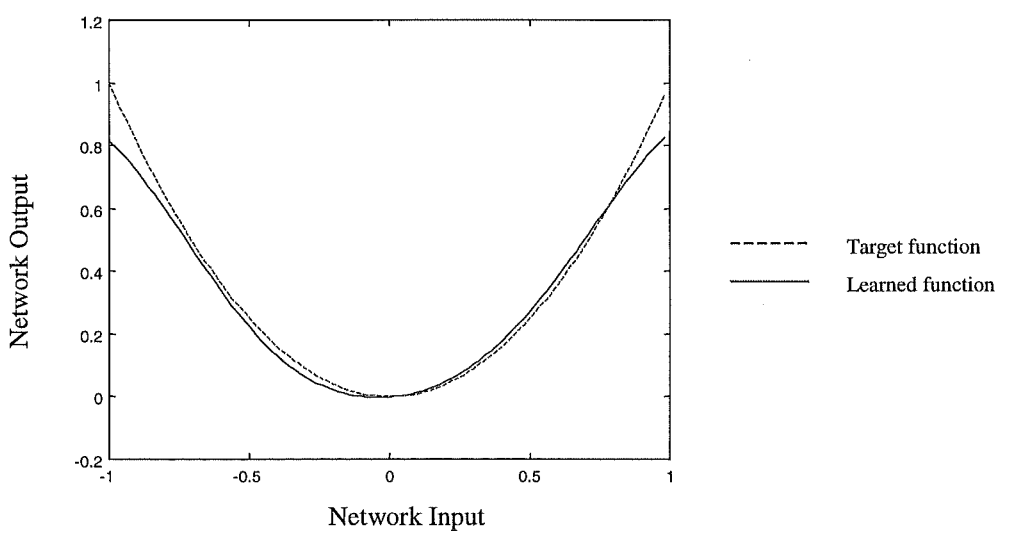

Fig. 87. Forward model trained with a non-white signal (10, 000 samples)

[6] A 32 tap FIR filter with a lower band edge of 0.1 was used in the simulation.

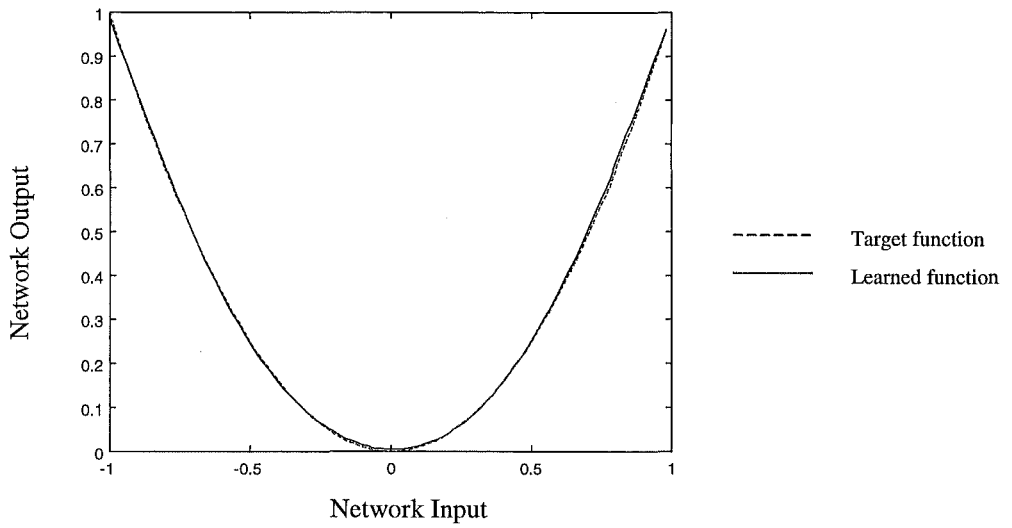

Fig. 88. Forward model trained with white noise signal (10, 000 samples)

It was hypothesized that the difference might be a manifestation of the difficulty LMS type algorithms have in dealing with auto-correlated input signals (Widrow et al., 1985). In this case the forward model is likely to fail to converge correctly even with an extremely long training period. The other possibility is that the forward model simply requires significantly more time to converge when excited with a non-white signal since the input takes longer to cover the input range with the same density. To test these hypotheses the same systems were trained for 10, 000 cycles with white and non-white inputs and the resulting learned functions were compared with the ideal results.

The results confirmed that the system excited with white noise converged almost perfectly to the desired function (not shown), while the system with non-white input showed tolerable performance. The non-white results were inconclusive so a longer training run of 50, 000 samples was performed (see Fig. 89).

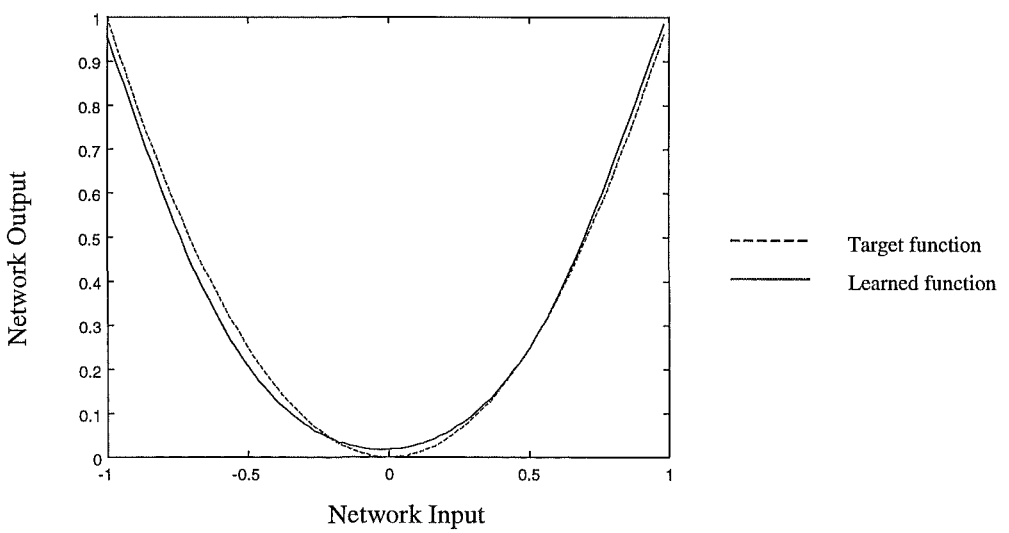

Fig. 89. Forward model trained with a non-white input signal (50, 000 samples)

The resulting learned function here is significantly better than that learned in the 10, 000 cycle run. There is, however, still a residual error which does not exist in the white noise input case. It is still unclear, however, whether the residual error is due to under-training or a training algorithm problem. To answer the question finally a test over 100, 000 samples was performed.

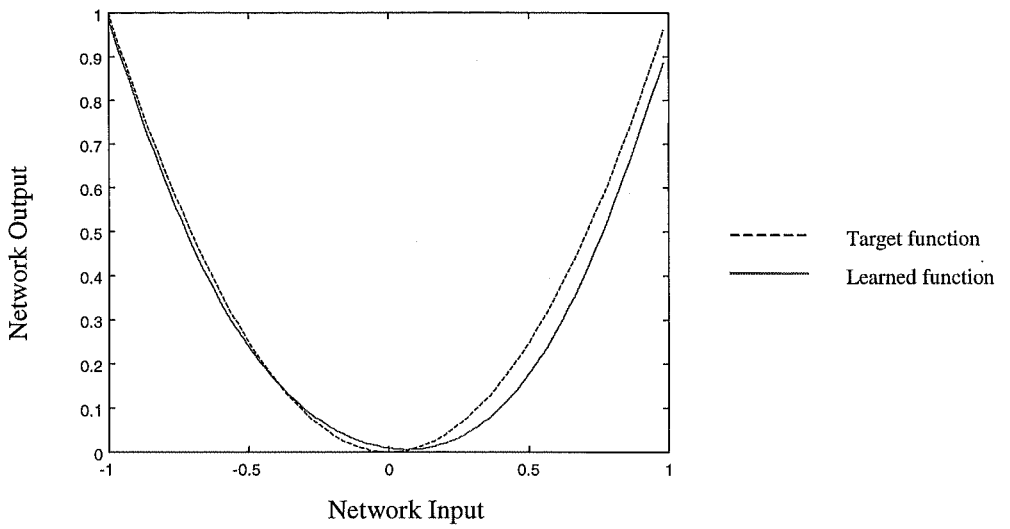

Fig. 90 . Forward model trained with a non-white signal (100, 000 samples)

The resulting function (shown in Fig. 90) was different and less accurate. There is clearly a residual offset of some kind caused by the non-white nature of the input signal. The resulting model would be perfectly capable of acting as an approximation to the forward model, however, for use in AMT. Whether this result can be generalized to all systems, including dynamic ones is an open question. In linear dynamic systems the non-white modelling performance with an LMS algorithm is very poor, so it may be expected that similarly unsatisfactory results might occur in the non-linear dynamic case.

10. Appendix III

Quasi-linear Analysis Results

This section incudes detailed statistical analysis results for the quasi-linear analysis performed in Chapter 5. They provide more detail than the results given within the chapter, but do not reveal any important additional effects. They are presented here for completeness.

10.1 ANOVA Analysis Summary

Gain, phase and coherence were analysed separately. A linear trend analysis at individual frequencies was also performed for all three components of the responses. Mean plots are also provided to assist with the judgement of effect sizes.

Table 7. Analysis of Variance for Gain.

Effect	Unblanked Runs							Blanked Runs						
	Effect		*Error*					*Effect*		*Error*				
	df	*MS*	*df*	*MS*	*F*	*p*		*df*	*MS*	*df*	*MS*	*F*	*p*	
Practise Runs														
R	9	0.06	171	0.00	18.0	0.000	***	9	0.06	171	0.10	0.6	0.801	
F	4	0.08	76	0.00	18.2	0.000	***	4	15.34	76	0.20	76.4	0.000	***
R×F	36	0.01	684	0.00	10.2	0.000	***	36	0.01	684	0.01	1.0	0.526	
Experimental Runs ***(at frequencies within the target bandwidth)***														
G	1	4.97	18	0.11	45.6	0.000	***	1	1.72	18	2.99	0.6	0.458	
R	14	0.03	252	0.01	3.2	0.000	***	14	0.10	252	0.11	0.9	0.546	
F	4	0.37	72	0.02	16.9	0.000	***	4	13.81	72	0.34	40.1	0.000	***
G×R	14	0.04	252	0.01	4.3	0.000	***	14	0.09	252	0.11	0.8	0.621	
G×F	4	0.64	72	0.02	28.9	0.000	***	4	1.07	72	0.34	3.1	0.021	*
R×F	56	0.01	1008	0.00	2.7	0.000	***	56	0.02	1008	0.01	1.6	0.006	***
G×R×F	56	0.01	1008	0.00	5.5	0.000	***	56	0.02	1008	0.01	2.1	0.000	***

*Note: G = Group, R = Run, F = Frequency (in effect column only); p < .05 = *, p < 0.01 = **, p < 0.001 = ****

Table 8. Analysis of Variance for Phase.

Effect	Unblanked Runs							Blanked Runs						
	Effect		*Error*					*Effect*		*Error*				
	df	*MS*	*df*	*MS*	*F*	*p*		*df*	*MS*	*df*	*MS*	*F*	*p*	
Practise Runs														
R	9	291	171	26	11.0	0.000	***	9	80	171	193	0.4	0.926	
F	4	442	76	37	11.9	0.000	***	4	12095	76	500	24.2	0.000	***
R×F	36	29	684	6	5.1	0.000	***	36	28	684	50	0.6	0.983	
Experimental Runs ***(at frequencies within the target bandwidth)***														
G	1	1265	18	1627	0.8	0.390		1	84607	18	14877	5.7	0.028	*
R	14	232	252	73	3.2	0.000	***	14	615	252	357	1.7	0.051	
F	4	1327	72	247	5.4	0.001	**	4	3810	72	1816	2.1	0.090	
G×R	14	71	252	73	1.0	0.495		14	360	252	357	1.0	0.444	
G×F	4	1340	72	247	5.4	0.001	**	4	7736	72	1816	4.3	0.004	**
R×F	56	51	1008	16	3.1	0.000	***	56	94	1008	102	0.9	0.634	
G×R×F	56	25	1008	16	1.5	0.008	**	56	80	1008	102	0.8	0.880	

*Note: G = Group, R = Run, F = Frequency (in effect column only); p < .05 = *, p < 0.01 = **, p < 0.001 = ****

Table 9. Analysis of Variance for Coherence

Effect	Unblanked Runs							Blanked Runs						
	Effect		*Error*					*Effect*		*Error*				
	df	*MS*	*df*	*MS*	*F*	*p*		*df*	*MS*	*df*	*MS*	*F*	*p*	
Practise Runs														
R	9	0.01	171	0.00	13.6	0.000	***	9	0.14	171	0.04	3.3	0.001	***
F	4	0.01	76	0.00	30.0	0.000	***	4	3.20	76	0.05	68.0	0.000	***
R×F	36	0.00	684	0.00	2.6	0.000	***	36	0.01	684	0.01	0.5	0.996	
Experimental Runs ***(at frequencies within the target bandwidth)***														
G	1	0.34	18	0.02	16.9	0.001	**	1	0.93	18	0.42	2.2	0.152	
R	14	0.04	252	0.00	15.9	0.000	***	14	0.06	252	0.04	1.2	0.245	
F	4	0.26	72	0.00	75.5	0.000	***	4	5.86	72	0.13	45.4	0.000	***
G×R	14	0.01	252	0.00	6.0	0.000	***	14	0.05	252	0.04	1.2	0.263	
G×F	4	0.02	72	0.00	6.7	0.000	***	4	0.33	72	0.13	2.6	0.046	*
R×F	56	0.00	1008	0.00	6.7	0.000	***	56	0.02	1008	0.01	1.4	0.028	*
G×R×F	56	0.00	1008	0.00	2.4	0.000	***	56	0.01	1008	0.01	1.0	0.442	

*Note: G = Group, R = Run, F = Frequency (in effect column only); p < .05 = *, p < 0.01 = **, p < 0.001 = ****

Table 10. Gain, phase and coherence linear trend analysis for blanked runs.

	Gain						Phase						Coherence					
	Effect		*Error*				*Effect*		*Error*				*Effect*		*Error*			
	df	*MS*	*df*	*MS*	*F*	*p*	*df*	*MS*	*df*	*MS*	*F*	*p*	*df*	*MS*	*df*	*MS*	*F*	*p*
Practice																		
All f (0-0.6 Hz)	1	0.037	19	0.15	0.2457	0.626	1	537.159	19	349.86	1.535	0.2304	1	0.8942	19	0.0662	13.51	0.0016 **
f = 0 Hz	1	0.001	19	0.056	0.0234	0.88		na					1	0.35801	19	0.0908	3.943	0.0617
f = 0.15 Hz	1	2E-05	19	0.032	0.0007	0.98	1	169.329	19	387.33	0.437	0.5164	1	0.24372	19	0.0396	6.156	0.0226 *
f = 0.3 Hz	1	0.008	19	0.032	0.2598	0.616	1	83.5253	19	162.4	0.514	0.482	1	0.10942	19	0.0117	9.387	0.0064 **
f = 0.45 Hz	1	0.059	19	0.051	1.1569	0.296	1	175.11	19	122.22	1.433	0.246	1	0.07558	19	0.0115	6.59	0.0189 *
f = 0.6 Hz	1	0.018	19	0.083	0.2188	0.645	1	270.271	19	106.05	2.548	0.1269	1	0.17368	19	0.015	11.57	0.003 **
Group A (combined between-groups analysis)																		
All f (0-0.6 Hz)	1	6E-04	18	0.318	0.0019	0.966	1	1530.85	18	764.46	2.003	0.1741	1	0.00035	18	0.0703	0.005	0.9442
f = 0 Hz	1	0.091	18	0.068	1.3465	0.261		na					1	0.01766	18	0.0593	0.298	0.5919
f = 0.15 Hz	1	0.048	18	0.063	0.7714	0.391	1	181.645	18	654.96	0.277	0.6049	1	0.01065	18	0.0401	0.265	0.6127
f = 0.3 Hz	1	7E-05	18	0.07	0.001	0.975	1	606.044	18	249.85	2.426	0.1368	1	0.00094	18	0.014	0.067	0.7985
f = 0.45 Hz	1	0.052	18	0.087	0.5919	0.452	1	463.808	18	395.67	1.172	0.2932	1	0.01107	18	0.0164	0.675	0.4219
f = 0.6 Hz	1	0.128	18	0.101	1.2692	0.275	1	776.004	18	420.94	1.844	0.1913	1	0.04146	18	0.0167	2.484	0.1324
Group B (combined between-groups analysis)																		
All f (0-0.6 Hz)	1	0.06	18	0.32	0.2	0.674	1	3862.87	18	955.58	4.042	0.0596	1	0.21333	18	0.0703	3.035	0.0986
f = 0 Hz	1	0.079	18	0.068	1.1745	0.293		na					1	0.11058	18	0.0593	1.865	0.1889
f = 0.15 Hz	1	0.042	18	0.063	0.671	0.423	1	1270.1	18	654.96	1.939	0.1807	1	0.17651	18	0.0401	4.399	0.0504
f = 0.3 Hz	1	0.014	18	0.07	0.2082	0.654	1	1600.46	18	249.85	6.406	0.0209 *	1	0.07281	18	0.014	5.201	0.035 *
f = 0.45 Hz	1	0.19	18	0.087	2.1816	0.157	1	595.505	18	395.67	1.505	0.2357	1	0.00104	18	0.0164	0.064	0.8037
f = 0.6 Hz	1	0.22	18	0.101	2.1844	0.157	1	588.392	18	420.94	1.398	0.2525	1	0.00049	18	0.0167	0.029	0.8666

$p < .05 = *, p < 0.01 = **, p < 0.001 = ***$

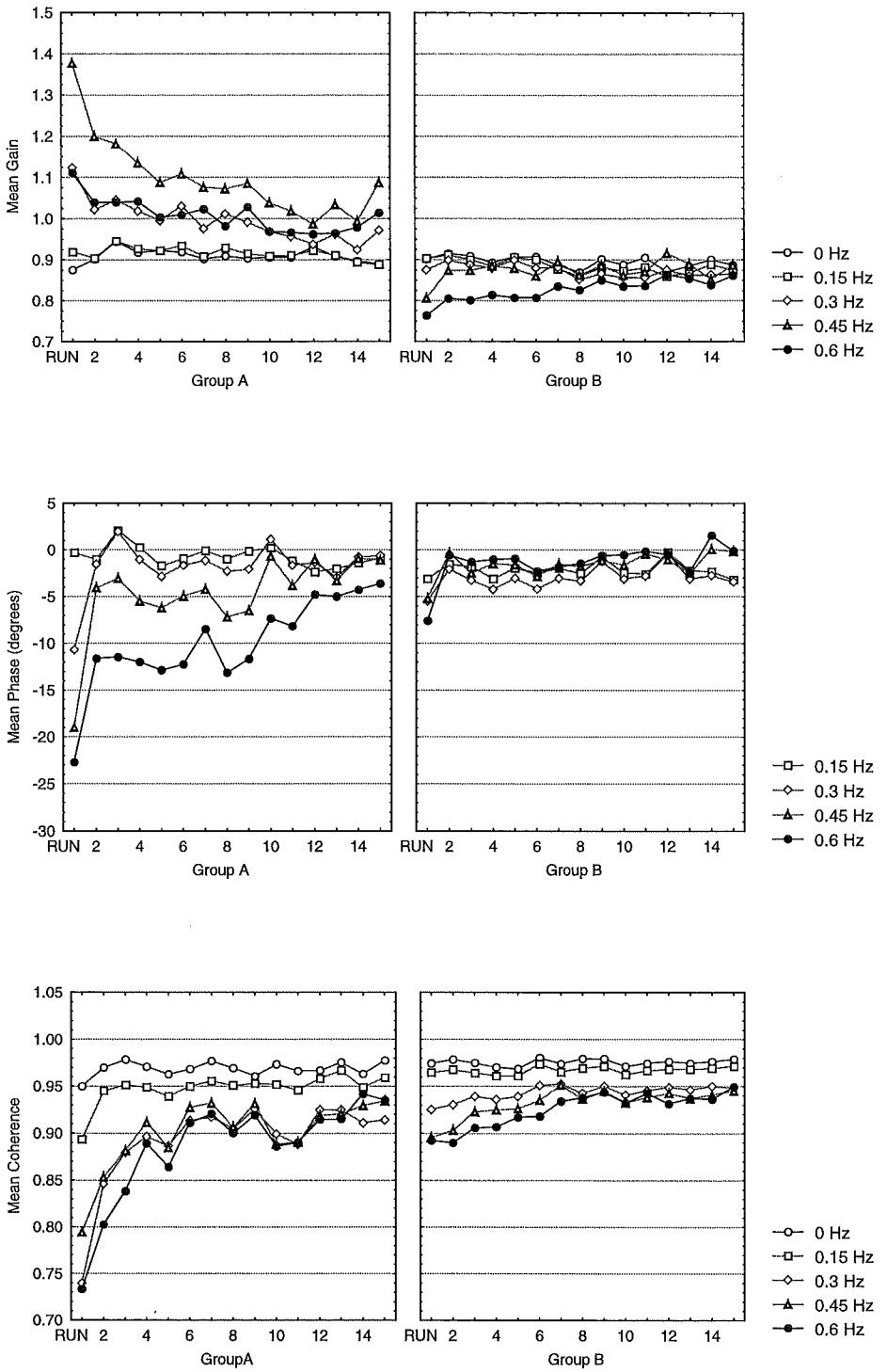

Fig. 91. Mean transfer function for the *unblanked* experimental runs.

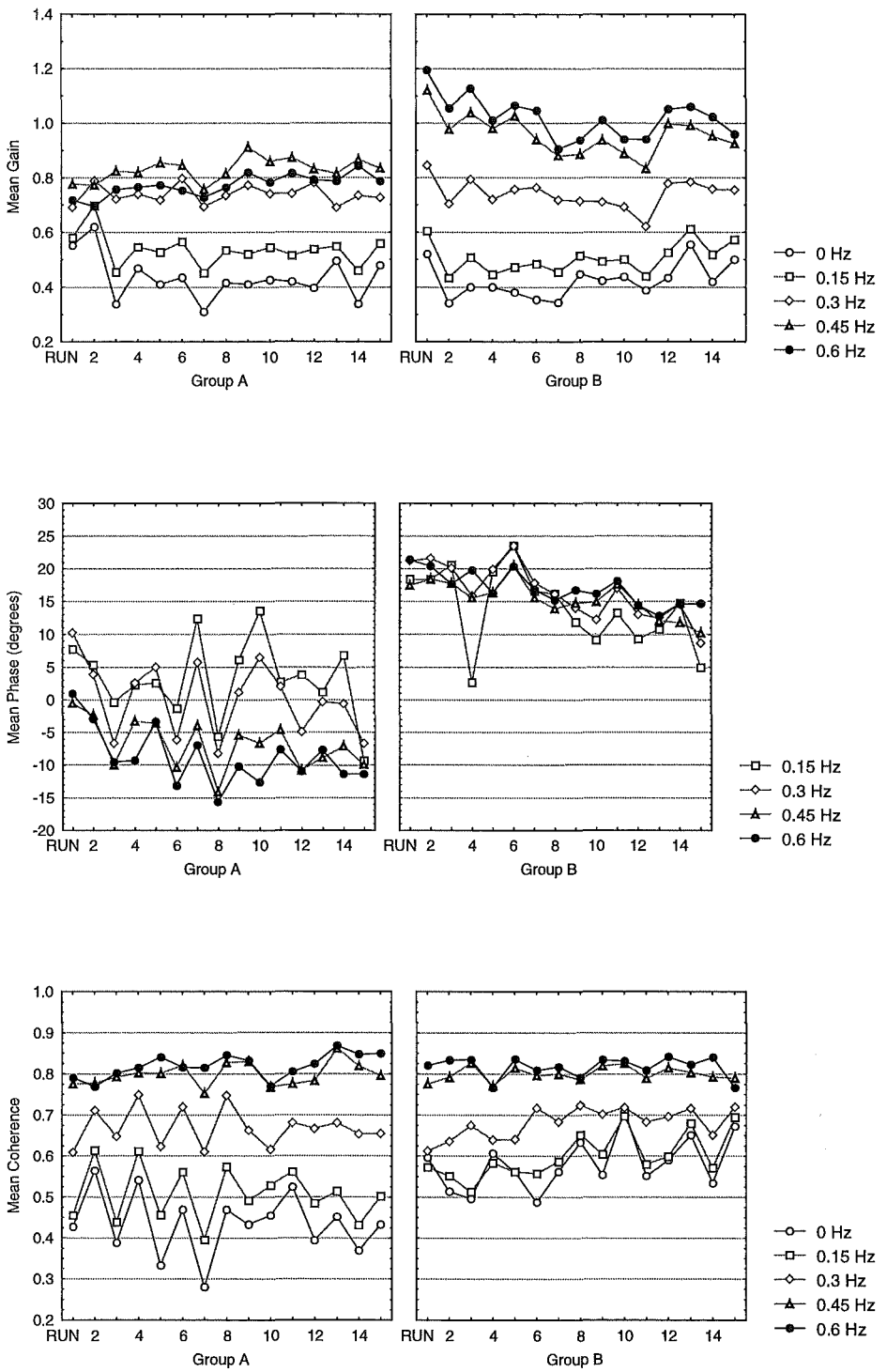

Fig. 92. Mean transfer function for the *blanked* experimental runs.

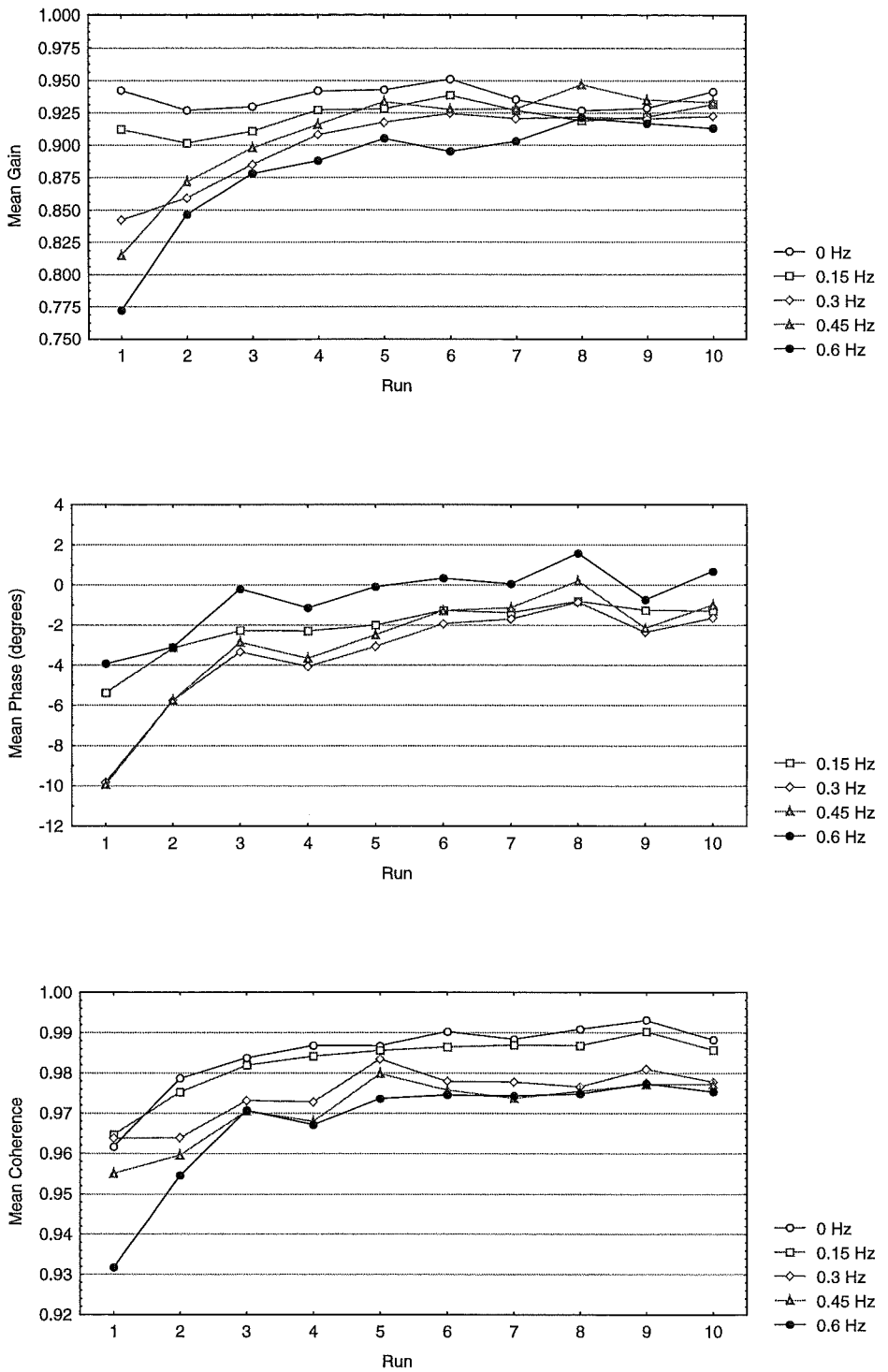

Fig. 93. Mean transfer function for the *unblanked* practice runs.

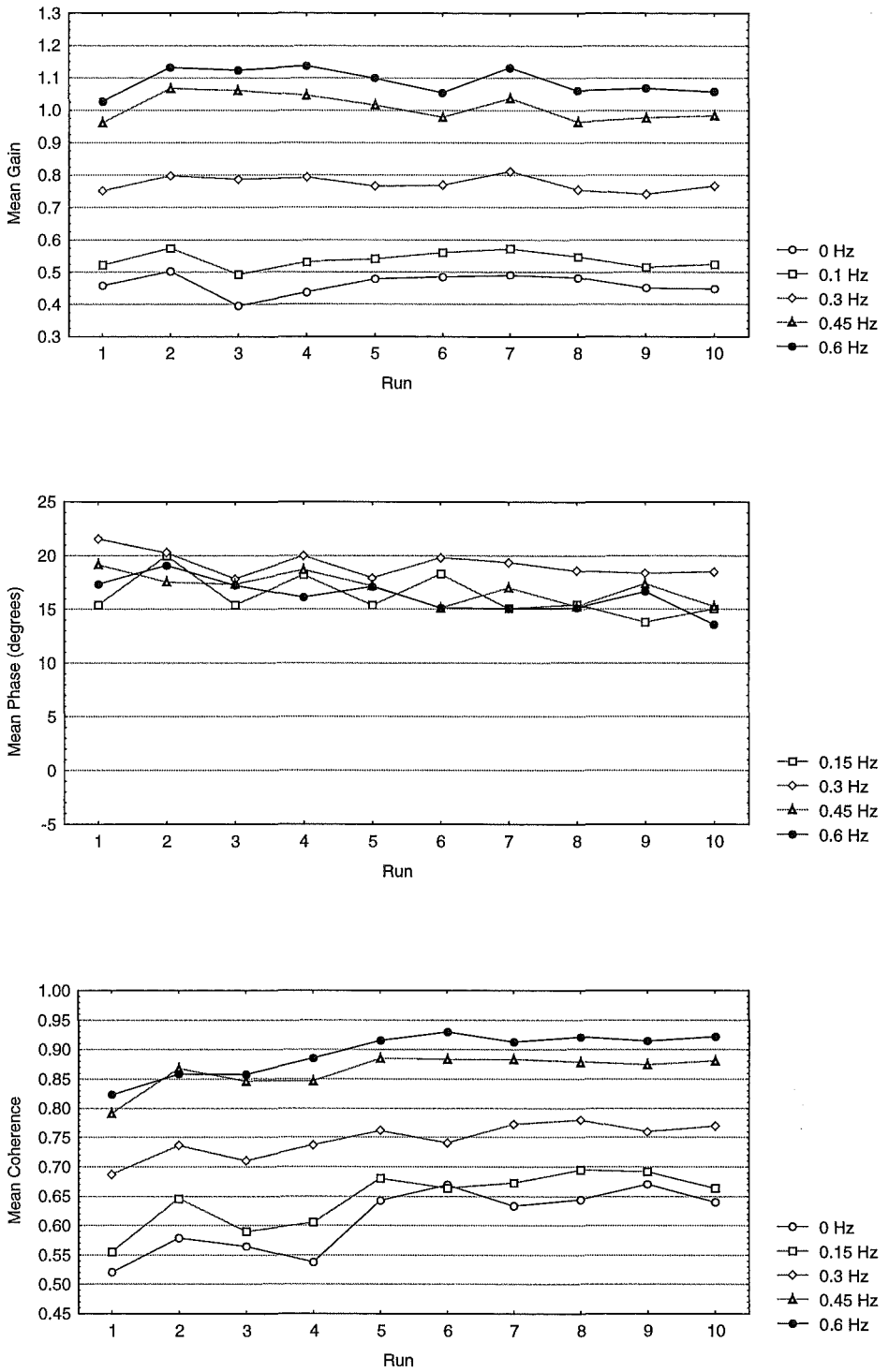

Fig. 94. Mean transfer function for the *blanked* practice runs.

11. Appendix IV

Effect of Target Preview

It was noted in section 5.4.4 that the 8-s target preview provided to subjects in the tracking experiment may have caused the unusual blanked trajectories that were observed. While the possibility seemed unlikely it was important to eliminate it as a confounding source of adaptation in the experiment. A pilot study was carried out aimed at judging the effect of target preview on open-loop tracking.

A well trained subject was asked to duplicate the practice runs of the original 0.6-Hz tracking experiment (as described in Chapter 5) but with the target preview removed. The non-preview quasi-linear transfer function analysis was then compared with the subject's original preview results so that the effect of target preview might be judged.

11.1.1 Results

The quasi-linear transfer function analysis results for the final 5 runs with and without target preview were surprisingly similar, suggesting that target preview has little effect on the open-loop response once a subject has been fully trained (see Fig. 96). The characteristic high-pass gain response is evident in both preview and non-preview responses.

The non-preview responses were slightly more coherent than preview responses (though this effect is unlikely to reach statistical significance, see Fig. 96). The subject exhibited a reduction in coherence at low frequency, as observed in the previous study, though to a lesser degree than average.

Despite the relatively high coherence achieved by the subject, both transfer functions exhibited the behaviour that characterized the previous study. Notably, the idiosyncratic phase response, with a lead at low frequency and a lag at high frequency, appears to be independent of the presence of target preview.

It is acknowledged that this single-case pilot study is insufficient to draw strong conclusions on the effect of target preview on tracking performance. Nevertheless, the results suggest that the use of preview was not the primary cause of the unusual response trajectories exhibited in blanked tracking experiment. Further research is required to confirm this (see section 7.2.5).

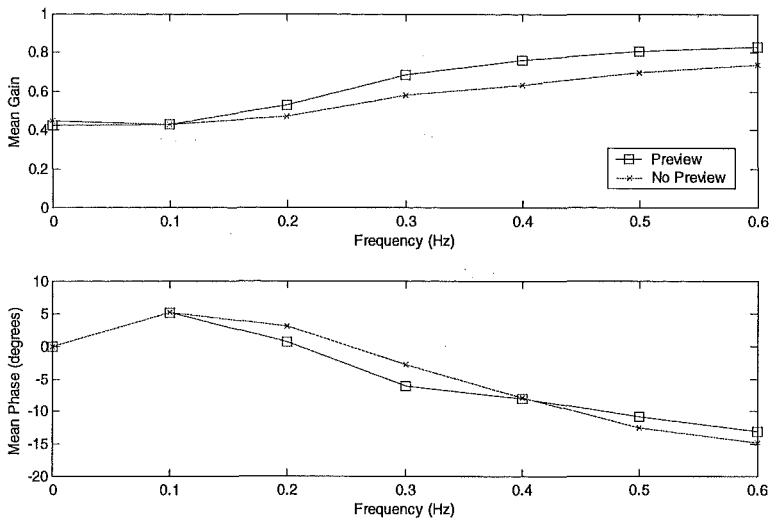

Fig. 95. Gain and phase responses runs 6-10. Responses are very similar with and without preview.

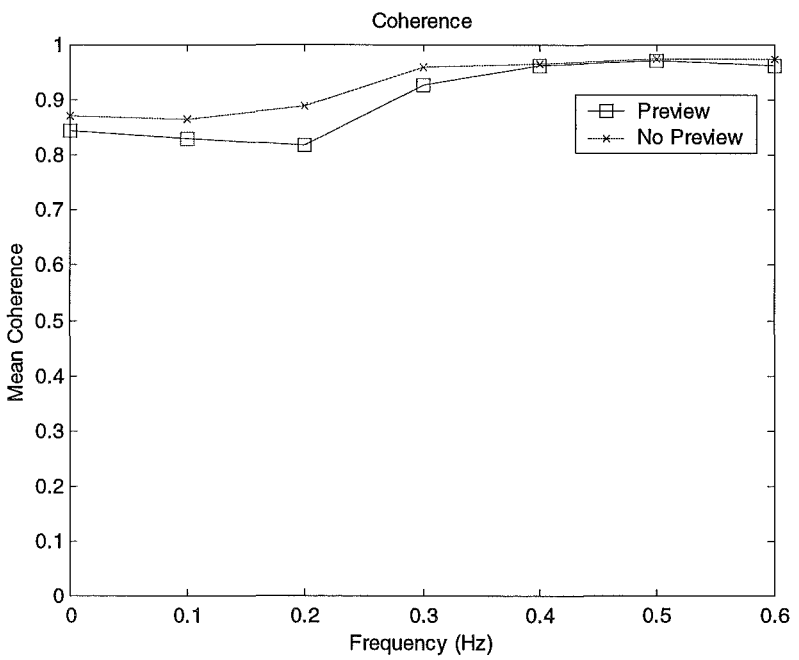

Fig. 96. Mean coherence runs 6-10. This individual exhibited high coherence at low frequencies relative to the mean.

12. References

Abernathy, B., & Sparrow, W. A. (1992). The rise and fall of dominant paradigms in motor behaviour research. In J. J. Summers (Ed.), *Approaches to the study of motor control and learning* (pp. 3-46). Amsterdam: Elsevier.

Adams, J. A. (1971). A closed-loop theory of motor learning. *Journal of Motor Behaviour, 3*, 111-150.

Albus, J. S. (1975). A new approach to manipulator control: The cerebellar model articulation controller (CMAC). *Journal of Dynamic Systems, Measurement and Control, 63*, 220-227.

Albus, J. S. (1979). Mechanisms of planning and problem solving in the brain. *Mathematical Biosciences, 45*, 247-293.

Alexander, G. E., DeLong, M. R., & Crutcher, M. D. (1992). Do cortical and basal ganglionic motor areas use "motor programs" to control movement? *Behavioural and Brain Sciences, 15*, 656-665.

Anderson, J. A. (1995). *An introduction to neural networks.* Massachusetts: MIT Press.

Anderson, R. W. (1998). Biased random-walk learning: A neurobiological correlate to trial-and-error. In O. M. Omidvar & J. E. Dayhoff (Eds.), *Neural networks and pattern recognition* (pp. 221-244). Boston: Academic Press.

Astrom, K. J., & Wittenmark, B. (1995). *Adaptive control.* Reading, Mass: Addison-Wesley.

Back, A. D., & Tsoi, A. C. (1991). FIR and IIR synapses, a new neural network architecture for time series modelling. *Neural Computation, 3*, 375-385.

Back, A. D., & Tsoi, A. C. (1992). *Nonlinear system identification using multilayer perceptrons with locally recurrent synaptic structure.* Proceedings of the IEEE Workshop on Neural Networks for Signal Processing, New York, 444-453.

Baher, H. (1992). *Analog & digital signal processing.* New York: Wiley.

Bear, M. F., Connors, B. W., & Paradiso, M. A. (1996). *Neuroscience : Exploring the brain.* Baltimore: Williams & Wilkins.

Bernstein, N. (1967). *The co-ordination and regulation of movements.* Oxford: Pergamon.

Bhushan, N., & Shadmehr, R. (1999a). Computational nature of human adaptive control during learning of reaching movements in force fields. *Biological Cybernetics, 81*, 39-60.

Bhushan, N., & Shadmehr, R. (1999b). Evidence for a forward dynamics model in human adaptive motor control. In M. S. Kearns & S. A. Solla (Eds.), *Advances in neural information processing systems* (Vol. 11, pp. 3-9). Cambridge MA: MIT Press.

Bizzi, E., Polit, A., & Morasso, P. (1976). Mechanisms underlying achievement of final head position. *Journal of Neurophysiology, 39*, 435-444.

Bliss, T. V. P., & Collingridge, G. L. (1993). A synaptic model of memory: Long-term potentiation in the hippocampus. *Nature*, 31-39.

Bliss, T. V. P., & Lomo, T. (1973). Long-lasting potentiation of synaptic transmission in the dentate area of the anaesthetized rabbit following stimulation of the perforant path. *Journal of Physiology (London), 232*, 331-356.

Bonnet, D., Labouisse, V., & Grumbach, A. (1997). delta-NARMA neural networks: A new approach to signal prediction. *IEEE Transactions on Signal Processing, 45*, 2799-2810.

Box, G. E. P., & Jenkins, G. M. (1970). *Time series analysis : Forecasting and control.* San Francisco: Holden Day.

Boyd, S., & Chua, L. O. (1985). Fading memory and the problem of approximating nonlinear operators with Volterra series. *IEEE Transactions on Circuits and Systems, 32*, 1150-1161.

Brainard, M. S., & Doupe, A. J. (2000). Interruption of a basal ganglia - forebrain circuit prevents plasticity of learned vocalizations. *Nature, 404*, 762-766.

Brashers-Krug, T., Shadmehr, R., & Bizzo, E. (1996). Consolidation in human motor memory. *Nature, 382*, 252-255.

Bray, J. J., Cragg, P. A., Macknight, A. D. C., Mills, R. G., & Taylor, D. W. (Eds.). (1989). *Lecture notes on human physiology* (Second ed.). Oxford: Blackwell Scientific Publications.

Brown, M., & Harris, C. (1994). *Neurofuzzy adaptive modelling and control.* New York: Prentice Hall.

Campolucci, P. (1998). *A circuit theory approach to recurrent neural network architectures and learning methods.* Doctoral Thesis, University of Bologna, Bologna, Italy.

Campolucci, P., Fiori, S., Uncini, A., & Piazza, F. (1997). *A new IIR-MLP learning algorithm for on-line signal processing.* Proceedings of the IEEE International Conference on Acoustics, Speech, and Signal Processing, *4*, 3293 - 3296.

Campolucci, P., & Piazza, F. (1998). *Intrinsically stable IIR filters and IIR-MLP neural networks for signal processing.* Proceedings of the IEEE International Conference on Acoustics, Speech, and Signal Processing, Seattle.

Campolucci, P., Uncini, A., Piazza, F., & Rao, B. D. (1999). On-line learning algorithms for locally recurrent neural networks. *IEEE Transactions on Neural Networks, 10*, 253-271.

Clarke, D. W., Mohtadi, C., & Tuffs, P. S. (1987). Generalized predictive control: Parts I and II. *Automatica, 23*, 137-160.

Connor, J. T., Martin, D. R., & Atlas, L. E. (1994). Recurrent neural networks and robust time series prediction. *IEEE Transactions on Neural Networks, 5*, 240-254.

Cooper, R., McCallum, W. C., & Cornthwaite, S. P. (1989). Slow potential changes related to the velocity of target movement in a tracking task. *Electroencephalography and Clinical Neurophysiology, 72*, 232-239.

Craik, K. J. W. (1943). *The nature of explanation.* London: Cambridge University Press.

Craik, K. J. W. (1948). The theory of the human operator in control systems: II. Man as an element in a control system. *British Journal of Psychology, 38*, 142-148.

Crick, F. (1989). The recent excitement about neural networks. *Nature, 337*, 129-132.

Davidson, P. R., Jones, R. D., Sirisena, H. R., & Andreae, J. H. (in press). Evidence for the formation of inverse motor models in the brain. *International Journal of Neurosciences.*

Dawson, M. R. W., & Shamanski, K. S. (1994). Connectionism, confusion, and cognitive science. *Journal of Intelligent Systems, 4*, 215-262.

Dayhoff, J. E., Hameroff, S. R., Swenberg, C. E., Lahoz-Beltra, R., & Samsonovich, A. (1992). *Biological learning with cytoskeletal signaling.* Proceedings of the International Joint Conference on Neural Networks, Baltimore, Maryland, *2*, 45-51.

Douglas, R. J., & Martin, K. A. C. (1991). Opening the grey box. *Trends In Neuroscience, 14*, 286-293.

Economou, C. G., Morari, M., & Palsson, B. O. (1986). Internal model control. 5. Extension to nonlinear systems. *Industrial & Engineering Chemistry Process Design and Development, 25*, 403-411.

Encyclopaedia Britannica inc. (1990). *The new encyclopaedia britannica* (15th ed.). Chicago, Ill.: Encyclopaedia Britannica.

Fausett, D. W. (1990). *Strictly local backpropagation.* Proceedings of the International Joint Conference on Neural Networks, Washington, DC, *3*, 124-130.

Fel'dman, A. G. (1966). Functional tuning of the nervous system with control of movement or maintenance of a steady posture - II. Controllable parameters of the muscle. *Biophysics, 11*, 565-578.

Ferrier, D. (1876). *The functions of the brain.* London: Smith, Elder.

Finger, S. (2000). *Minds behind the brain : A history of the pioneers and their discoveries.* New York: Oxford University Press.

Fitch, H. L., Tuller, B., & Turvey, M. T. (1982). The Bernstein perspective III. Tuning of coordinative structures with special reference to perception. In J. A. S. Kelso (Ed.), *Human motor behavior* (pp. 271-281). Hillsdale, N.J.: Erlbaum.

Fitts, P. M. (1954). The information capacity of the human motor system in controlling the amplitude of movement. *Journal of Experimental Psychology, 47*, 381-391.

Flash, T., & Hogan, N. (1985). The coordination of arm movements; and experimentally confirmed mathematical model. *Journal of Neurological Science, 5*, 1688-1703.

Foulkes, A. J., & Miall, R. C. (2000). Adaptation to visual feedback delays in a human manual tracking task. *Experimental Brain Research, 131*, 101-110.

Frasconi, P., Gori, M., & Soda, G. (1992). Local feedback multilayered networks. *Neural Computation, 4*, 120-130.

Fritsch, A. H., & Hitzig, E. (1870). Uber die elektrische Errerbarkeit des Grosshirns. *Archiv für Anatomie, Physiologie, und wissenschaftliche Medicin, 37*, 300-332.

Fujita, M. (1982). Adaptive filter model of the cerebellum. *Biological Cybernetics*, 195-206.

Ghez, C. (1991). The control of movement. In E. R. Kandel & J. H. Schwartz & T. M. Jessel (Eds.), *Principles of neural science* (pp. 533-547). Connecticut: Appleton & Lange.

Gibson, J. J. (1979). *An ecological approach to visual perception.* Boston: Houghton-Mifflin.

Gillies, A., & Arbuthnott, G. (2000). Computational models of the basal ganglia. *Movement Disorders, 15*, 762-770.

Gluck, M. A., & Bower, G. H. (1988). Evaluating an adaptive model of human learning. *Journal of Memory and Language, 27*, 166-195.

Gluck, M. A., & Thompson, R. F. (1987). Modelling the neural substrates of associative learning and memory. *Psychological Review, 94*, 176-292.

Gomi, H., & Kawato, M. (1990). *Learning control for a closed loop system using feedback-error-learning.* Proceedings of the 29th Conference on Decision and Control, Honolulu, 3289-3294.

Gomi, H., & Kawato, M. (1996). Equilibrium-point control hypothesis examined by measured arm stiffness during multijoint movement. *Science, 272*, 117-120.

Graybiel, A. M., Aosaki, T., Flaherty, A. W., & Kimura, M. (1994). The basal ganglia and adaptive motor control. *Science, 265*, 1826-1831.

Grossberg, S. (1987). Competitive learning: from interactive activation to adaptive resonance. *Cognitive Science, 11*, 23-63.

Gupta, M. M., & Rao, D. H. (1992). *Dynamic neural units in the control of linear and nonlinear systems.* Proceedings of the International Joint Conference on Neural Networks, Tampa, Florida, 100-105.

Gupta, M. M., & Rao, D. H. (1993). Dynamic neural units with applications to the control of unknown nonlinear systems. *Journal of Intelligent and Fuzzy Systems, 1*, 73-92.

Gupta, M. M., Rao, D. H., & Nikiforuk, P. N. (1993). Neuro-controller with dynamic learning and adaptation. *Journal of Intelligent and Robotic Systems, 7*, 151-173.

Harston, C. T. (1990). Learning background for neural networks. In A. J. Maren & C. T. Harston & R. M. Pap (Eds.), *Handbook of neural computing applications* (pp. 451). San Diego: Academic Press.

Haykin, S. (1994). *Neural networks: A comprehensive foundation.* New York: Macmillan.

Hebb, D. O. (1949). *The organisation of behaviour.* New York: John Wiley & Sons.

Hecht-Nielsen, R. (1989, June 18-22). *Theory of the backpropagation network.* Proceedings of the International Joint Conference on Neural Networks, Washington D.C., *1*, 593-605.

Held, R., & Freedman, S. J. (1963). Plasticity in sensorimotor control. *Science, 142*, 455-462.

Henson, M. A., & Seborg, D. E. (1997). Introduction. In M. A. Henson & D. E. Seborg (Eds.), *Nonlinear process control* (pp. 432). New Jersey: Prentice-Hall.

Hinton, G. E. (1993). How neural networks learn from experience, *Mind and brain* (pp. 113-124). New York: W.H. Freeman.

Hunt, K. J., Sbarbaro, D., Zbikowski, R., & Gawthrop, P. J. (1992). Neural networks for control systems - A survey. *Automatica, 28*, 1083-1112.

Hurley, S. (1998). *Consciousness in action.* Cambridge: Harvard University Press.

Ito, M. (1970). Neurophysiological aspects of the cerebellar motor control system. *International Journal of Neurology, 7*, 162-176.

James, W. (1891). *The principles of psychology.* London: Macmillan and Co.

Jones, R. D. (2000). Measurement of sensory-motor control performance capacities: Tracking tasks. In J. D. Bronzino (Ed.), *The biomedical engineering handbook* (pp. 149.141-149.125). Boca Raton, Florida: CRC Press.

Jones, R. D., & Donaldson, I. M. (1986). Measurement of sensory-motor integrated function in neurological disorders: Three computerised tracking tasks. *Medical and Biological Engineering and Computing, 24*, 536-540.

Jones, R. D., & Donaldson, I. M. (1989). *Tracking tasks and the study of predictive motor planning in Parkinson's disease.* Proceedings of the 11th Annual

International Conference of the IEEE Engineering in Medicine and Biology Society, Seattle, *11*, 1055-1056.

Jones, R. D., Sharman, N. B., Watson, R. W., & Muir, S. R. (1993). *A PC-based battery of tests for quantitative assessment of upper-limb sensory-motor function in brain disorders.* Proceedings of the 15th Annual International Conference of the IEEE Engineering in Medicine and Biology Society, San Diego, USA, *15*, 1414-1415.

Jordan, M. I., & Rumelhart, D. E. (1992). Forward models: Supervised learning with a distal teacher. *Cognitive Science, 16*, 307-354.

Kalveram, K. T. (1999). A modified model of the Hebbian synapse and its role in motor learning. *Human Movement Science, 18*, 185-199.

Kandel, E. R., Schwartz, J. H., & Jessel, T. M. (Eds.). (1991). *Principles of neural science* (3rd ed.). Connecticut: Appleton & Lange.

Kandel, E. R., Schwartz, J. H., & Jessel, T. M. (Eds.). (2000). *Principles of neural science* (4th ed.). New York: McGraw-Hill.

Kawato, M. (1999). Internal models for motor control and trajectory planning. *Current Opinion in Neurobiology, 9*, 718-727.

Kawato, M., Furukawa, K., & Suzuki, R. (1987). A hierarchical neural network model for control and learning of voluntary movement. *Biological Cybernetics, 57*, 169-185.

Kawato, M., & Gomi, H. (1992). A computational model of four regions of the cerebellum based on feedback-error learning. *Biological Cybernetics, 68*, 95-103.

Kawato, M., Uno, Y., Isobe, M., & Suzuki, R. (1988). Hierarchical neural network model for voluntary movement with application to robotics. *IEEE Control Systems Magazine, 8*, 8-16.

Keele, S. W., & Posner, M. I. (1968). Processing of visual feedback in rapid movement. *Journal of Experimental Psychology, 77*, 155-158.

Kelso, J. A. S. (Ed.). (1982). *Human motor behavior: An introduction.* Hillsdale, N.J.: Erlbaum.

Kernell, D. (1965). The adaptation and the relation between discharge frequency and current strength of cat lumbosacral motoneurones stimulated by long-lasting injected currents. *Acta Psychologica Scandinavica, 65*, 65-73.

Lange, W. (1975). Cell number and cell density in the cerebellar cortex of man and other mammals. *Cell Tissue Research, 157*, 115–124.

Lashley, K. S. (1917). The accuracy of movement in the absence of excitation from the moving organ. *The American Journal of Physiology, 43*, 169-194.

Laszlo, J. I. (1992). Motor control and learning: How far do the experimental tasks restrict our theoretical insight? In J. J. Summers (Ed.), *Approaches to the study of motor control and learning* (pp. 47-80). Amsterdam: Elsevier.

Latash, M. L., Aruin, A. S., & Zatsiorsky, V. M. (1999). The basis of a simple synergy: reconstruction of joint equilibrium trajectories during unrestrained arm movements. *Human Movement Science, 18*, 3-30.

Lawrence, A. D. (2000). Error correction and the basal ganglia: similar computations for action, cognition and emotion? *Trends in Cognitive Science, 4*, 365-369.

Ljung, L. (1999). *System identification: Theory for the user* (2nd ed.). Upper Saddle River, N.J.: Prentice Hall PTR.

MacNeilage, P. F. (1970). Motor control of serial ordering of speech. *Psychological Review, 77*, 182-196.

Marr, D. (1969). A theory of cerebellar cortex. *Journal of Neurophysiology, 202*, 437-470.

McClelland, J. L. (1979). On the time relations of mental processes: An examination of systems of processes in cascade. *Psychological Review, 86*, 287-330.

McCulloch, W. S., & Pitts, W. (1949). A logical calculus of ideas imminent in nervous activity. *Bulletin of Mathematical Biophysics*, 115-133.

McDonald, J. D., & Bahill, A. T. (1983). Zero-latent tracking of predictable targets by time-delay systems. *International Journal of Control, 38*, 881-893.

Miall, R. C. (1999). *The cerebellum and visually controlled movements.* Proceedings of the IEE Workshop on Self-Learning Robots III: Brain Style Robotics, London, *2*, 1-5.

Miall, R. C., Weir, D. J., & Stein, J. F. (1993). Intermittency in human manual tracking tasks. *Journal of Motor Behavior, 25*, 53-63.

Miall, R. C., Weir, D. J., Wolpert, D. M., & Stein, J. F. (1993). Is the cerebellum a Smith predictor? *Journal of Motor Behavior, 25*, 203-216.

Miall, R. C., & Wolpert, D. M. (1996). Forward models for physiological motor control. *Neural Networks, 9*, 1265-1279.

Mussa-Ivaldi, F. A., & Bizzi, E. (2000). Motor learning through the combination of primitives. *Philosophical Transactions of the Royal Society of London, 355*, 1755-1769.

Neilson, M. D. (1980). *Stuttering and the control of speech: a systems analysis approach.* Doctoral Thesis, University of New South Wales, Sydney.

Neilson, P. D. (1993). The problem of redundancy in movement control: The adaptive model theory approach. *Psychological Research, 55*, 99-106.

Neilson, P. D., Neilson, M. D., & O'Dwyer, N. J. (1988a). Internal models and intermittency: A theoretical account of human tracking behaviour. *Biological Cybernetics, 58*, 101-112.

Neilson, P. D., Neilson, M. D., & O'Dwyer, N. J. (1988b). Stochastic prediction in pursuit tracking: An experimental test of adaptive model theory. *Biological Cybernetics, 58*, 113-122.

Neilson, P. D., Neilson, M. D., & O'Dwyer, N. J. (1992). Adaptive model theory: Application to disorders of motor control. In J. J. Summers (Ed.), *Approaches to the study of motor control and learning* (pp. 495-548). Amsterdam: Elsevier.

Neilson, P. D., Neilson, M. D., & O'Dwyer, N. J. (1993). What limits high speed tracking performance? *Human Movement Science*, 85-109.

Neilson, P. D., Neilson, M. D., & O'Dwyer, N. J. (1995). Adaptive optimal control of human tracking. In D. J. Glencross & J. P. Piek (Eds.), *Motor control and sensory motor integration: Issues and directions* (pp. 97-140). Amsterdam: Elsevier.

Neilson, P. D., Neilson, M. D., & O'Dwyer, N. J. (1997). Adaptive model theory: Central processing in acquisition of skill. In K. J. Connelly & H. Fossberg (Eds.), *Neurophysiology and neuropsychology of motor development* (pp. 1-43). London: MacKeith Press.

Neilson, P. D., Neilson, M. D., & O'Dwyer, N. J. (1998). Evidence for rapid switching of sensory-motor models. In J. P. Piek (Ed.), *Motor behavior and human skill: A multidisciplinary approach* (pp. 105-126). Champaign, IL: Human Kinetics.

Nie, J., & Linkens, D. A. (1994). FCMAC: a fuzzified cerebellar model articulation controller with self-organizing capacity. *Automatica, 30*, 655-664.

O'Dwyer, N. J., & Neilson, P. D. (1998). Adaptation to a changed sensory motor relation: Immediate and delayed parametric modifications. In J. P. Piek (Ed.), *Motor behaviour and human skill: A multidisciplinary approach.* Champaign, IL: Human Kinetics.

Parent, A., & Cicchetti, F. (1998). The current model of basal ganglia organization under scrutiny. *Movement Disorders, 13*, 199-202.

Pashler, H. (1984). Processing stages in overlapping tasks: Evidence for a central bottleneck. *Journal of Experimental Psychology, 10*, 358-377.

Paulin, M. G. (1993). The role of the cerebellum in motor control and perception. *Brain, Behavior and Evolution, 41*, 39-50.

Pearson, R. K., & Ogunnaike, B. A. (1997). Nonlinear process identification. In M. A. Henson & D. E. Seborg (Eds.), *Nonlinear process control.* New Jersey: Prentice Hall.

Pew, R. W. (1970). Toward a process-oriented theory of human skilled motor performance. *Journal of Motor Behaviour, 2*, 8-24.

Pew, R. W. (1974). Human perceptual-motor performance. In B. H. Kantowitz (Ed.), *Human information processing: Tutorials in performance and cognition.* New York: Erlbaum.

Poulton, E. C. (1952). The basis of perceptual anticipation in tracking. *British Journal of Psychology, 43*, 295-305.

Poulton, E. C. (1957). Learning the statistical properties of the input in pursuit tracking. *Journal of Experimental Psychology, 54*, 295-302.

Rao, D. H., & Gupta, M. M. (1993). *Dynamic neural units and function approximation.* Proceedings of the IEEE Conference on Neural Networks, San Francisco, 743-748.

Rao, D. H., Gupta, M. M., & Wood, H. C. (1993). *Adaptive tracking in nonlinear systems using neural networks.* Proceedings of the 2nd IEEE Conference on Control Applications, Vancouver, B.C., 913-921.

Rashevsky, N. (1960). *Mathematical biophysics* (Vol. 2). New York: Dover.

Rosenbaum, D. A. (1991). *Human motor control.* San Diego: Academic Press.

Rosenblatt, F. (1958). The perceptron: A probabilistic model for information storage and organization in the brain. *Psychological Review, 65*, 386-408.

Rumelhart, D. E., & McClelland, J. L. (1986). Learning representations by back-propagating errors. *Nature, 323*, 533-536.

Sainburg, R. L., Ghez, C., & Kalakanis, D. (1999). Intersegmental dynamics are controlled by sequential anticipatory, error correction, and postural mechanisms. *Journal of Neurophysiology, 81*, 1045-1056.

Sainburg, R. L., Ghilardi, M. F., Poizner, H., & Ghez, C. (1993). Loss of proprioception produces deficits in interjoint coordination. *Journal of Neurophysiology, 70*, 2136-2147.

Schmidt, R. A. (1982). *Motor control and learning.* Champaign, IL: Human Kinetics.

Seong-Wook, P., & Bo-Hyeok, S. (1995). *Design of controller for nonlinear system using dynamic neural unit model.* Proceedings of the IEEE International Conference on Neural Networks, Perth, *4*, 2232-2237.

Shadmehr, R., & Holcomb, H. H. (1997). Neural correlates of motor memory consolidation. *Science, 277*, 821-825.

Shadmehr, R., & Mussa-Ivaldi, F. A. (1994). Adaptive representation of dynamics during learning of a motor task. *Journal of Neuroscience, 14*, 3208-3224.

Sherrington, C. S. (1906). *The integrative action of the nervous system.* New Haven: Yale University Press.

Smith, M. A., Brandt, J., & Shadmehr, R. (2000). Motor disorder in Huntington's disease begins as a dysfunction in error feedback control. *Nature, 403*, 544-549.

Smith, O. J. M. (1959). A controller to overcome dead time. *ISA Journal, 6*, 28-33.

Sriharan, A. (1997). *Mathematical modelling of the human operator control system through tracking tasks.* Master of Engineering Thesis, University of New South Wales, Sydney.

Stork, D. G. (1989). *Is backpropagation biologically plausible?* Proceedings of the International Joint Conference on Neural Networks, Washington D.C., *2*, 241-246.

Sutton, R. S., & Barto, A. G. (1981). Toward a modern theory of adaptive networks: Expectation and prediction. *Psychological Review, 88*, 135-170.

Taub, E. (1976). Movements in non-human primates deprived of somatosensory feedback. *Exercise and Sport Sciences Reviews, 4*, 335-374.

Thoroughman, K. A., & Shadmehr, R. (1999). Electromyographic correlates of learning an internal model of reaching movements. *The Journal of Neuroscience, 19*, 8573-8588.

Thoroughman, K. A., & Shadmehr, R. (2000). Learning through adaptive combination of motor primitives. *Nature, 407*, 742-747.

Turvey, M. T., Fitch, H. L., & Tuller, B. (1982). The Bernstein perspective: I. The problems of degrees of freedom and context-conditioned variability. In J. A. S. Kelso (Ed.), *Human motor behavior : An introduction.* Hillsdale, N.J.: Erlbaum.

van Ingen Schenau, G. J., van Soest, A. J., Gabreels, F. J. M., & Horstink, M. W. I. M. (1995). The control of multi-joint movements relies on detailed internal representations. *Human Movement Science, 14*, 511-538.

Vince, M. A. (1948). The intermittency of control movements and the psychological refractory period. *British Journal of Psychology*, 149-157.

Welford, A. T. (1952). The psychological refractory period and the timing of high-speed performance - A review and a theory. *British Journal of Psychology, 43*, 2-19.

Welford, A. T. (1959). Evidence of a single-channel decision mechanism limiting performance in a serial reaction task. *Quarterly Journal of Experimental Psychology, 11*, 193-210.

Welford, A. T. (1980). The single-channel hypothesis. In A. T. Welford (Ed.), *Reaction times* (pp. 215-252). London: Academic Press.

Werbos, P. J. (1990). Backpropagation through time: What it does and how to do it. *Proceedings of the IEEE, 78*, 1550-1560.

Widrow, B. (1996). *Adaptive inverse control.* Upper Saddle River, N.J.: Prentice-Hall.

Widrow, B., & Plett, G. L. (1996). *Adaptive inverse control based on linear and nonlinear adaptive filtering.* Proceedings of the International Workshop on Neural Networks for Identification, Control, Robotics, and Signal / Image Processing, Venice, 30-38.

Widrow, B., & Stearns, S. D. (1985). *Adaptive signal processing* (1st ed.). New Jersey: Prentice-Hall.

Winer, B. J. (1971). *Statistical principles in experimental design* (2nd ed.). New York: McGraw-Hill.

Wolpert, D. M., Ghahramani, Z., & Jordan, M. I. (1995). An internal model for sensorimotor integration. *Science, 269*, 1880-1882.

Wolpert, D. M., Miall, R. C., & Kawato, M. (1998). Internal models in the cerebellum. *Trends in Cognitive Science, 2*, 338-347.